UNIVERSITY OF NOTTINGHAM

SCHOOL OF BIOSCIENCES
PhD in Agriculture & Food Security

A Mutagenomic Dissection of Virulence in the Fungal Wheat Pathogen *Zymoseptoria tritici*

PhD
Academic Year 2017 - 2022

Hannah Ruth Blyth, MSci(Hons)

Supervisor: Dr Jason Rudd, Rothamsted Research

Associate Supervisors:
Dr Kostya Kanyuka, NIAB,
Professor Rumiana Ray, University of Nottingham

April 2022

No part of this publication may be reproduced without
the written permission of the copyright owner.

ABSTRACT

Zymoseptoria tritici is the causal agent of Septoria tritici leaf blotch (STB), an economically significant disease that can reduce wheat (*Triticum aestivum*) yields. Due to this fungus' *in vitro* growth capabilities, functional genomics studies can isolate morphogenic switching genes that play a crucial role in fungal virulence. Depending on *in vitro* nutrient availability and temperature, *Z. tritici* can grow and switch between a “yeast-like” budding form or a hyphal form. As no specialised infection structures have been identified in *Z. tritici* infection, the genes involved in morphogenic switching and successful hyphal extension are essential for virulence, enabling leaf penetration through stomatal openings or wounds. “Mutagenomics” is a combination approach of mutagenesis, phenotypic screening, and whole-genome re-sequencing. Advancements in genomic sequencing technologies have eased the process of identifying candidate virulence and morphogenic switching associated genes in *Z. tritici*.

The mutagenomic study described herein identified strains impaired in full virulence through *in planta* and *in vitro* screening of two independent mutant libraries, one generated by restriction enzyme-mediated integration and the other by *Agrobacterium*-mediated T-DNA mutagenesis. From the nineteen re-sequenced mutant strains, a list of nearly 100 genes affected either by plasmid/T-DNA integration or untagged variation have been identified and prioritised using a combination of approaches and datasets. Functional complementation assays on three candidate genes resulted in restored hyphal growth and restoration of full virulence. These genes include one involved in the purine biosynthesis pathway, a mitogen-activated protein kinase kinase kinase (MAPKKK) which functions upstream of HOG1 MAPK, and a predicted cell cycle control protein involved in pre-mRNA splicing. The data presented support the use of mutagenomics approaches to identify new genes implicated in fungal plant pathogen virulence and identify new Achilles heels in the infection biology of *Z. tritici*.

Keywords:
Zymoseptoria tritici, fungus, morphogenic switch, hyphal growth, spliceosome, virulence

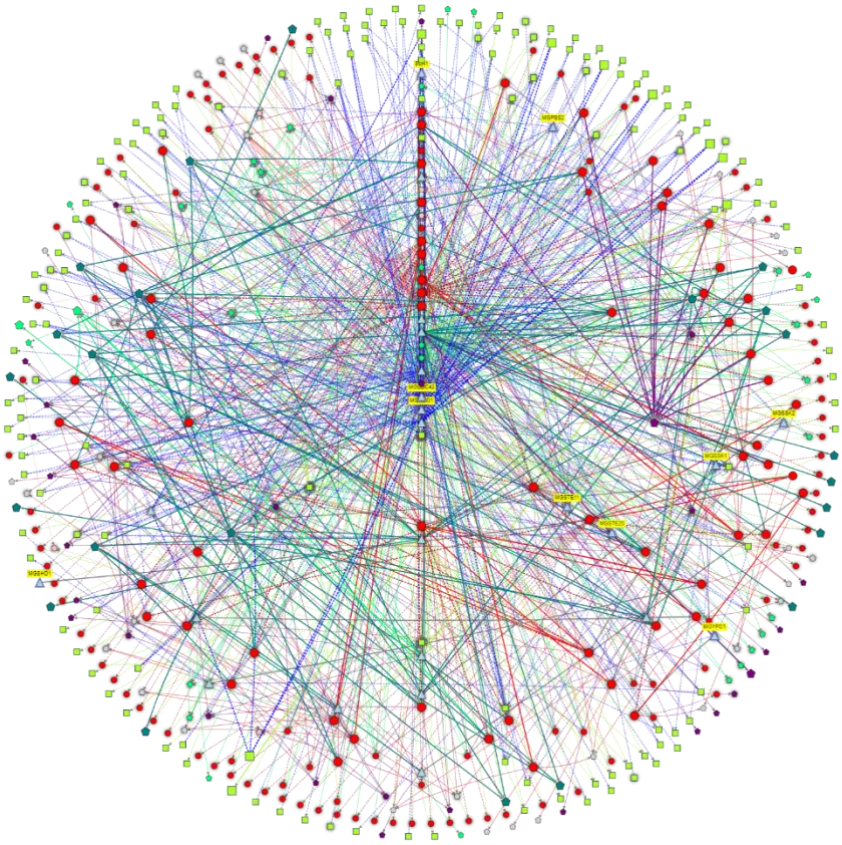

Zymoseptoria KnetMiner HOG1 Pathway Knowledge Graph

ACKNOWLEDGEMENTS

I am grateful for the support, patience, and invaluable advice from my supervisor, Jason Rudd, throughout my PhD. I also deeply appreciate the inputs from the Wheat Pathogenomics Team at Rothamsted Research, from the constructive criticisms and thoughts from Kostya Kanyuka, Javier Palma-Guerrero and Kim Hammond-Kosack to the laughs in Bay B with Mike Hammond-Kosack and George Lund. They have been instrumental in helping me develop as a researcher. I greatly appreciated the insights and additional annual motivation boosts following reviews with Martin Urban and Mark Wilkinson. Many thanks to all the support staff at the University and Rothamsted Research. Carlos Bayon and Hongxin Chen, I cannot fathom getting this work going without your guidance. Rob King for laying down the early bioinformatic groundwork, followed by Dan Smith for his bioinformatics analyses and endless support for my attempts. I feel lucky to have had Donna Fellowes and Sandra Rose as compassionate advocates for my mental health.

I am immensely thankful for my entire cohort, the Manor Ghosts (too many to name). They made these years some of the best, but especially grateful to my fellow Rothamsted-based University of Nottingham students, Tania Chancellor, Chris Stephens, and Darwin Hickman. You all have been truly inspirational and wonderful people to work alongside, as were the older and newer cohorts I had the joy of getting to know. Thanks to my climbing and gymnastics buddies for (physically) lifting me and (metaphorically) my spirits. Samantha Ashton, my Harpenden local Pokémon GO friend, thanks for listening to my coffee-fueled rants. To my university-based cohort, thank you for the spring school memories. Alexandra Batchelor, we've come a long way from that introductory undergraduate lecture to the end of our PhD studies. DFTBA.

Last but not least, with all my heart, thanks, Mum, Dad, Tom and Lucy.

TABLE OF CONTENTS

ABSTRACT i
ACKNOWLEDGEMENTS iii
TABLE OF CONTENTS iv
LIST OF FIGURES ix
LIST OF TABLES xiii
LIST OF APPENDIX TABLES xiv
LIST OF ABBREVIATIONS xv
1 Introduction 1
1.1 Phytopathogenic Fungi and Food Security 1
1.2 Fungal phytopathogen lifestyles 2
1.3 Plant host inducible defences against fungi 3
1.4 Importance of wheat in global food systems 5
1.5 *Zymoseptoria tritici* and its pathogen genomics 5
1.6 Septoria Tritici Blotch disease (STB) 8
1.6.1 Control Methods for STB 9
1.6.2 Life and Infection Cycle of *Z. tritici* 10
1.6.3 Germination and Penetration in *Z. tritici* infection 12
1.6.4 Early colonisation by *Z. tritici*: a biotrophic phase or latency? 13
1.6.5 Necrotrophic Growth and Pycnidia Formation in *Z. tritici* infection 14
1.7 *Zymoseptoria tritici* cell biology 15
1.8 The genetic tools available for understanding the biology of *Z. tritici* 16
1.9 Pathogenicity and Virulence Associated Genes in *Z. tritici* and other Fungal Phytopathogens 17
1.9.1 Proteins and processes implicated in signal transduction pathways 18
1.9.2 Proteins and processes involved in morphogenic switching 20
1.9.3 Proteins and processes involved in sporulation 21
1.9.4 Proteins and processes controlling fungal melanisation 22
1.9.5 Extracellular hydrolytic enzymes 22
1.9.6 Secondary metabolites 23
1.9.7 Putative *Z. tritici* toxins 24
1.9.8 Transport processes 25
1.9.9 Virulence and avirulence effectors 26
1.10 Research Objectives 28
2 Materials and Methods 29
2.1 Acknowledgements 29
2.2 Materials and Chemicals 29
2.2.1 Growth media 29
2.2.2 Fungal strains 30

2.2.3 Bacterial strains 30
2.2.4 DNA plasmids 31
2.2.5 Antibiotics 31
2.3 Growth and Inoculation of Plants 31
2.3.1 Wheat cultivar and growth conditions 31
2.3.2 Attached wheat leaf bioassay 32
2.3.3 *In planta* inoculation for scanning electron microscopy (SEM) .. 32
2.4 Molecular Methods 33
2.4.1 DNA extraction and quantification 33
2.4.2 RNA extraction and quantification 33
2.4.3 PCR 34
2.4.4 DNA gel electrophoresis 35
2.4.5 RNA integrity gel 36
2.4.6 Cloning and Gibson Assembly 39
2.5 Transformation and Mutagenesis 39
2.5.1 Transformation of *Escherichia coli* for vector construct bulking 39
2.5.2 Construct miniprep 39
2.5.3 Transformation of *Agrobacterium tumefaciens* 40
2.5.4 *Agrobacterium*-mediated transformation of *Zymoseptoria tritici* 40
2.6 Protein analysis 42
2.6.1 Protein extraction 42
2.6.2 SDS-PAGE 42
2.6.3 Western blotting 43
3 “Resurrection” and phenotypic screening of mutagenised *Zymoseptoria tritici* libraries for reduced virulence strains 46
3.1 Introduction 46
3.2 Materials and Methods 49
3.2.1 Strain collections 49
3.2.2 *In vitro* culture conditions and fungal strains 49
3.2.3 *In planta* infection assays 50
3.2.4 *In vitro* assays for hyphal growth and stress sensitivity 50
3.3 Results 51
3.3.1 Identification of reduced virulence REMI mutants of *Z. tritici* through strain reconstitution and *in planta* infection assays 51
3.3.2 Screening the REMI mutants for defective dimorphic switching phenotypes 57
3.3.3 Further characterisation of the REMI mutant isolates for *in* vitro growth and stress defects 61
3.3.4 *In planta* characterisation of selected *Agrobacterium tumefaciens* mediated (ATMT) transformants 63

3.3.5 Further characterisation of the random T-DNA mutant isolates for *in vitro* growth and stress defects 66
3.4 Discussion 68
3.4.1 Twenty years at -80℃: the viability of fungal mutant libraries in long term storage 68
3.4.2 *In planta* assay methodologies: spraying, wounded droplet and swab techniques 69
3.4.3 Utilising stress screening to help identify and select for mutant isolates of interest 70
4 Exploring “mutagenomic” landscapes through next-generation genome re-sequencing to identify candidate virulence genes. 73
4.1 Introduction 73
4.2 Materials and Methods 76
4.2.1 Sequencing and assembly of a gapless reference genome assembly for *Z. tritici* strain L951 76
4.2.2 Identifying plasmid integration, T-DNA insertion sites and off-target mutations in mutant strains 76
4.2.3 Detection of non-plasmid and non-T-DNA insert associated variants in the mutant isolate genomes 78
4.3 Results 79
4.3.1 Assembly and analysis of the genomic sequence for *Z. tritici* strain L951 79
4.3.2 Identification and analysis of non-plasmid associated ‘untagged’ sequence variants in the fifteen REMI *Hin*dIII isolates 81
4.3.3 Identification and characterisation of eighteen plasmid integrations identified in the *Z. tritici* L951 *Hin*dIII REMI mutant genomes 93
4.3.4 Positional analysis confirms a trend towards REMI plasmid integration “near” *Hin*dIII restriction sites 102
4.3.5 Detection of T-DNA insertion sites in the five IPO323 derived random ATMT mutant isolates 107
4.3.6 Detection of untagged variants in the T-DNA insertion mutants 110
4.3.7 Prioritisation pipeline for best candidate genes affecting virulence in REMI and T-DNA mutant isolates 113
4.3.8 Whole-genome resequencing confirms the genetic instability of *Z. tritici* genomes 119
4.3.9 The power of casting a genome-wide net in fishing for untagged variants generated by mutagenesis 120
4.3.10 Prioritisation of candidates: pros and pitfalls of the pipeline .. 122
5 Functional complementation and characterisation of genes arising from the REMI dataset 123

5.1 Introduction 123
5.2 Materials and Methods 127
5.2.1 Complementation of select candidate genes into the *Z. tritici* REMI mutants 127
5.2.2 *In planta* and *in vitro* screening 129
5.2.3 Scanning electron microscopy (SEM) 129
5.3 Results 129
5.3.1 *De novo* purine biosynthesis pathway impacted in REMI L/121 by a frameshift mutation in *ZtADE6* 129
5.3.2 Complementation with *ZtADE6* restored WT virulence phenotype to REMI L/121 134
5.3.3 Inactivation of *ZtADE6* resulted in adenine auxotrophy in REMI L/121 136
5.3.4 *In silico* and phylogenetic analysis of the *Z. tritici* orthologue of the crooked neck-like factor (*ZtCLF1*) 139
5.3.5 Restoration of virulence to L951 *Z. tritici* REMI B/6 via complementation with *ZtCLF1* 142
5.3.6 Reintroduction of *ZtCLF1* restores *in vitro* hyphal growth switching 143
5.4 Discussion 147
5.4.1 The diversity of tools now available to explore putative biological function/ pathways affected by gene mutations 147
5.4.2 *De novo* metabolite biosynthesis in fungal pathogenicity 148
5.4.3 Complex networks integrating spliceosome complex, hyphal growth, and the cell cycle 149
6 Functional characterisation of the MAPKKK SSK2, impacted in two independent random ATMT *Z. tritici* mutants 152
6.1 Introduction 152
6.2 Materials and Methods 156
6.2.1 Constructs 156
6.2.2 *In planta* and *in vitro* screening 156
6.2.3 Protein work 157
6.2.4 RNA Sequencing 157
6.3 Results 158
6.3.1 Further analysis of the T-DNA and SNP mediated mutations in *ZtSSK2* in mutants 4-124 and 4-158 158
6.3.2 KnetMiner and phylogenetics analysis confirm *ZtSSK2* as a likely true orthologue of yeast and fungal SSK2 MAPKKKs 159
6.3.3 Complementation with WT *ZtSSK2* restored full *in planta* disease symptom development 162
6.3.4 Hyphal growth assays on *ZtSsk2* mutants and complemented *ΔZtSsk2*/ZtSSK2 isolates 164

6.3.5 Scanning electron microscopy shows germination of hyphae on the wheat leaf surface in the *ZtSsk2* defective mutants 165
6.3.6 Stress sensitivity assays on the *ZtSsk2* defective mutants and *ΔZtSsk2*/*ZtSSK2* complemented strains 167
6.3.7 Fungicide sensitivity assays place ZtSsk2p upstream of ZtHog1p 168
6.3.8 Analysis of early gene expression of *ZtSSK2* 'KO' mutant *in planta* through global RNA sequencing 169
6.3.9 *ZtSSK2* is required for the post-translational modification and activation of the ZtHog1 MAPK in response to oxidative stress 179
6.4 Discussion 181
6.4.1 Efficient stress responses are necessary for fungal virulence and hyphal growth 181
6.4.2 *HOG1*-dependent gene expression 182
7 General Discussion 184
7.1 Thawing information in deep freeze: what mysteries at the back of the freezer can we solve today 185
7.2 Dimorphic switching: An important component of fungal virulence 186
7.3 Escaping guilt by sequence similarity: *Z. tritici* as a new model for foliar fungal plant pathogens? 188
7.4 Future work 189
REFERENCES 191
Professional Internships for PhD Students reflection form. 220
APPENDICES 223
Appendix Chapter 4 223
Appendix Chapter 6 224

LIST OF FIGURES

Figure 1.1 Zig-zag co-evolutionary plant immunity model. 4

Figure 1.2 Overview of *Z. tritici* infection stages upon landing on susceptible wheat cultivar. 12

Figure 3.1 Overview of the restriction enzyme-mediated integration (REMI) collection and screening process. 52

Figure 3.2 A selection of *in planta* phenotypic screening photographs from the *Z. tritici* L951 *Hin*dIII REMI mutant isolates on wheat cv. Riband.. 56

Figure 3.3 The REMI fifteen shows the different hyphal growth phenotypes observed within the 196 screened *Z. tritici* L951 REMI mutant isolates. 58

Figure 3.4 Visual inspection of dense/hyperbranched *in vitro* hyphal growth mutants from the REMI fifteen at four dpi. 60

Figure 3.5 *In vitro* 'spotting' REMI mutant screen on YPD agar amended with fungal growth stressors including sorbitol, calcofluor white (CFW) and hydrogen peroxide. 62

Figure 3.6 *In planta* screening photographs from the *Z. tritici* IPO323 random ATMT mutant isolates on wheat cv. Riband. 65

Figure 3.7 *In vitro* 'spotting' stress tests for the five random ATMT *Z. tritici* IPO323 mutants. 66

Figure 3.8 *In vitro* hyphal growth assay of random ATMT *Z. tritici* IPO323 mutant isolates on low nutrient tap water agar (TWA). 68

Figure 4.1 Representation of the pAN7-1 and T-DNA plasmids used for transformation by REMI and ATMT, respectively. 79

Figure 4.2 The SNPeff assessed impacts in coding sequences of 'non-plasmid' associated variants identified in the *Z. tritici* L951 *Hin*dIII REMI mutant isolates. 84

Figure 4.3 SNPeff predicted a moderate impact predicted non-synonymous resulting in an amino acid change near a binding site in a predicted cyclin protein in all REMI mutants, including those with WT pathogenicity. .. 86

Figure 4.4 Number of untagged variants detected in the fifteen sequenced REMI mutagenised *Z. tritici* L951 isolates by chromosome. 91

Figure 4.5 Distribution of putative IPO323 orthologues and 'untagged' untagged variants in the L951 genome. 92

Figure 4.6 Number of detected pAN7-1 plasmid integration events detected in each *Z. tritici* L951 *Hin*dIII REMI mutant isolates above the higher (≥10 coverage) and lower (≥5 coverage) pile-up depth threshold. 94

Figure 4.7 Number of plasmid integration events detected in the fifteen sequenced REMI mutagenised *Z. tritici*, L951, isolates by chromosome. 97

Figure 4.8 Distribution of genes potentially impacted by pAN7-1 plasmid integrations in the L951 REMI mutant isolates genomes showing the relative positions of putative IPO323 orthologues. 99

Figure 4.9 pAN7-1 plasmid integration and an untagged variant in the L951 gene, ZtritL951_01g13791, on the reverse strand of chromosome two. 100

Figure 4.10 Examples of plasmid pile-ups in the *Z. tritici* L951 *Hin*dIII REMI mutant isolates in Geneious. 103

Figure 4.11 Planned contrasts in Log10 transformed base pair distances to the nearest identified *Hin*dIII cut site the sequenced L951 and IPO323 mutants. 106

Figure 4.12 Display of the relative chromosomal locations of the T-DNA and untagged variants in the five random ATMT *Z. tritici* IPO323 mutants. 108

Figure 4.13 Flow diagram showing the stages of the candidate gene elimination process used to arrive at a shortlist of candidates. 115

Figure 5.1 *S. cerevisiae* Clf1 and Prp19 C* complex in Catalytic Step II spliceosome complex and functions in the spliceosome. 126

Figure 5.2 pCGEN and an example complementation construct design, *ZtADE6*. 128

Figure 5.3 A predicted schematic representation of the *de novo* purine biosynthesis pathway in *Z. tritici*. 130

Figure 5.4 *Zymoseptoria tritici* L951 ZtAde6p alignment with *S. cerevisiae* and *Homo sapiens* homologue showing domains. 131

Figure 5.5 Phylogenetic analysis of the L951 *Z. tritici* Ade6p sequence with 35 orthologous proteins. 133

Figure 5.6 *In planta* screening results for the *ZtADE6* complements at 21 days post-inoculation. 135

Figure 5.7 *In vitro* spotting of Δ*ZtAde6* mutant and Δ*ZtAde6/ZtADE6* complement on tap water agar under purine auxotrophic conditions. 136

Figure 5.8 Scanning electron microscopy shows little differences at 24 h post-inoculation in spore germination and filament extension in the *ZtADE6* defective strain compared to complements and L951 control. 138

Figure 5.9 Zymoseptoria KnetMiner knowledge graph showing a selection of information on *ZtCLF1* 140

Figure 5.10 *CLF1* phylogenetic analysis reflects the known evolutionary relationship in fungal taxa. 141

Figure 5.11 *In planta* screening results for the *ZtCLF1* complements at 21 days post-inoculation..... 143

Figure 5.12 Complmentation of *ZtCLF1* restored *in vitro* hyphal growth on TWA. 144

Figure 5.13 Scanning electron microscopy shows no apparent visual differences at 24 h post-inoculation in spore germination and filament extension in the *ZtClf1* defective strain compared to complements and L951 control. 146

Figure 6.1 The currently known/predicted orthologues in the *Z. tritici* stress-activated protein kinase HOG1 pathway. 154

Figure 6.2 pCGEN+ZtSSK2 construct for ATMT for complementation approach to restore functional copy to mutant isolates 4-124 and 4-158. 156

Figure 6.3 Two independent *ZtSsk2* defective strains arising from different mutation events. 159

Figure 6.4 KnetMiner knowledge graph on the ZtSsk2 gene..... 160

Figure 6.5 Maximum Likelihood *SSK2* kinase domain nucleotide sequence tree. 161

Figure 6.6 *In planta* assessment of disease progression comparing WT IPO323, two *ZtSsk2* defective mutant isolates and *ZtSSK2* complements at 21 dpi. 163

Figure 6.7 *In vitro* spotting on tap water agar (TWA) demonstrates restoration of typical hyphal growth in two independent defective *ZtSsk2* mutant isolates. 165

Figure 6.8 Scanning electron microscopy of wheat leaf surface in the *ZtSsk2* defective mutants at nine days post-inoculation..... 166

Figure 6.9 *In vitro* fungal growth stressor assays with the *ΔZtSsk2* mutant isolates and *ΔZtSsk2*/*ZtSSK2* complementation strains. 168

Figure 6.10 *In vitro* fludioxonil sensitivity assay on IPO323, two independent *ZtSsk2* mutant isolates and representative *ΔZtSsk2*/*ZtSSK2* complementation strains. 169

Figure 6.11 Principal component analysis revealed separation of *Z. tritici* IPO323 and *ZtSsk2* defective mutant RNA samples by strain and time. 171

Figure 6.12 Differential expression of *ZtSSK2* and *ZtHOG1* in the *Z. tritici* mutant 4-124 was not statistically significantly different in 4-124 compared to IPO323. 172

Figure 6.13 Numbers of differentially expressed genes identified in the contrasts between *Z. tritici* Ssk2 mutant and IPO323 (WT). 173

Figure 6.14 Heatmap of the 252 differentially expressed genes in *Z. tritici* IPO323 and *ZtSsk2* deficient strains. 175

Figure 6.15 Functional categories of the 252 differentially expressed genes across strain contrasts at 6 h and 24 h. 177

Figure 6.16 Western blot shows oxidative stress activated p38 MAPK Hog1 in a complemented *ΔZtSsk2*/SSK2 mutant isolate. 180

LIST OF TABLES

Table 2.1 Antibiotics used in this study..... 31

Table 2.2 PCR conditions used in this study..... 35

Table 2.3 Primers used in this study..... 37

Table 2.4 A list of buffers and stock materials used in this work. 44

Table 3.1 Fifteen REMI mutants selected for further detailed characterisation from the primary two leaf screen..... 54

Table 3.2 Summary of the *in planta* and *in vitro* filamentous growth phenotypes of the fifteen REMI mutagenised isolates. 63

Table 4.1 L951 vs. IPO323 genome assembly statistics and chromosome. lengths. 80

Table 4.2 The total number of variants detected in the fifteen *Z. tritici* L951 *Hin*dIII restriction enzyme-mediated integration mutant isolates. 82

Table 4.3 Common untagged effects in fifteen *Z. tritici* L951 *Hin*dIII restriction enzyme-mediated integration mutant isolates. 87

Table 4.4 Isolate specific untagged variants present in the fifteen *Z. tritici* L951 *Hin*dIII REMI mutant isolates. 90

Table 4.5 Nine REMI isolates with single identified pAN7-1 plasmid integration event above the depth threshold (≥10 coverage). The likely impact of the integration event for the listed genes with any known predicted functions are shown. 95

Table 4.6 Three REMI isolates with multiple pAN7-1 plasmid integration events detected above the depth threshold (≥10 coverage)..... 98

Table 4.7 Putative pAN7-1 integration events detected in four REMI mutant isolates detected above the lower depth threshold (≥5 coverage) 101

Table 4.8 Estimating the likely distances to the nearest *Hin*dIII site on each chromosome in the L951 genome. 104

Table 4.9 The sites of random T-DNA insertion in the four explored IPO323 mutant isolates and the genes with putatively impacted function. 109

Table 4.10 Identified variants in the *Z. tritici* IPO323 random ATMT mutant collection. 112

Table 4.11 Final list of prioritised candidate virulence and morphogenic switching associated genes identified in L951 REMI mutant library.. 117

Table 4.12 Final list of prioritised candidate virulence and morphogenic switching associated genes identified in the IPO323 random ATMT mutant library. 118

LIST OF APPENDIX TABLES

Table A4.1 Top five BLAT hits for the low impact common mutations linked to transposable elements. 223

Table A4.2 Planned contrast distances to *Hin*dIII Summary Statistics..... 223

Table A6.1 RNA and RNA sequencing quality control measures. 224

Table A6.2 DE genes identified in the individually carried out contrasts between strains at 6 h and 24 h. 225

Table A6.3 Number of differentially expressed genes present in the functional categories in this study. 243

LIST OF ABBREVIATIONS

aa	amino acid
ABC	ATP-binding cassette
Ade	Adenine
ANOVA	Analysis of Variance
AspMM	*Aspergillus nidulans* minimal media
At	*Agrobacterium tumefaciens*
ATMT	*Agrobacterium tumefaciens* mediated transformation
ATP	Adenosine triphosphate
BLAST	Basic local alignment search tool
BLASTp	Protein BLAST
bp	Base pair
cDNA	Complementary DNA
DEG	Differentially expressed genes
dH2O	Distilled water
DMSO	Dimethyl sulphoxide
DNA	Deoxyribonucleic acid
DPI	Days post-inoculation
EC	Evidence code
EDTA	Disophium ethylenediaminetetraacetate
ETI	Effector triggered immunity
FAO	Food and Agriculture Organisation
Fg	*Fusarium graminearum*
FPKM	Fragments per kilobase of exon per million fragments mapped
gDNA	Genomic DNA
GO	Gene Ontology
h	Hours
hph	Hygromycin phosphotransferase
HST	Host selective toxin
LFC	Log2 fold change
LSD	Least significant difference
M	Molar
MAPK	Mitogen-activated protein kinase
Mb	Mega base
MES	2-[N-morpholino]ethanesulphonic acid

MFS	Major facillitator superfamily
Mg	*Mycosphaerella graminicola* (previous name for *Zymoseptoria tritici*)
min	Minute(s)
NCBI	National Centre for Biotechnology Information
NE	Normalised expression
NRP	Non-ribosomal peptide
NRPS	Non-ribosomal peptide synthase
OD	Optical density
PAGE	Polyacrylamide gel electrophoresis
PAMP	Pathogen-associated molecular pattern
PCR	Polymerase chain reaction
PEG	Polyethyleneglycol
PTI	Pathogen-triggered immunity
REMI	Restriction enzyme-mediated integration
RNA	Ribonucleic acid
RNA-seq	RNA sequencing
ROS	Reactive oxygen species
RPM	Rotations per minute
SDS	Sodium dodecyl sulphate
SDW	Sterile distilled water
SEM	Scanning electron microscopy
SNP	Single nucleotide polymorphism
SOC	Super-optimal broth with catabolite repression
T-DNA	Transfer DNA
TBE	Tris borate EDTA
TEMED	Tetramethylethylenediamine
TWA	Tap water agar
UV	Ultraviolet light
WT	Wild type
YPD	Yeast peptone dextrose
Zt	*Zymoseptoria tritici*

1 Introduction

1.1 Phytopathogenic Fungi and Food Security

Though only a tiny percentage of an estimated five million fungal species can cause disease, in either animals or plants, they have the potential for enormous impacts on human welfare (Almeida *et al.,* 2019; Köhler *et al*., 2015). Approximately 50 fungal species pose threats directly to human health, causing over 1.6 million deaths annually. Fungal diseases are also recognised as a threat to biodiversity, with severe declines observed in multiple amphibian populations that have been linked to chytrid fungi (Scheele *et al*., 2019). In addition, more than 10,000 known phytopathogenic fungi, which are fungi that cause plant diseases, pose a threat to global food security (Agrios, 2005; Meyer *et al*., 2016). The combined challenges of maintaining global food security whilst protecting biodiversity and preserving the environment with a growing global population are among the most significant issues facing humankind today. The global population has been projected to reach over 9 billion by 2050, and the increased food production needed to feed that population is estimated to be 70% (FAO, 2009).

Statistics recently released by the Food and Agriculture Organization of the United Nations (FAO) show the prevalence of undernourishment increased by 1.5% in just one year due to the COVID-19 pandemic. Despite remaining unchanged for the five years prior, highlighting the fragility of our current global food production systems and the devastating impacts of ‘human’ pandemics on food security. Malnutrition is projected to affect 700-800 million people worldwide through hunger in 2020 (FAO, 2021). Complex socioeconomic factors significantly contribute to overall food security. On top of these, food production faces an increasing risk from emerging crop diseases, climate change, soil exhaustion, the plateauing of crop yields and diminishing natural resources (Fones *et al*., 2020; McCarthy *et al*., 2018). Some of the significant fungal phytopathogens that threaten agricultural ecosystems worldwide include *Botrytis*, *Fusarium*, *Magnaporthe*, *Ustilago*, *Puccinia* and *Zymoseptoria* species (Dean *et al*., 2012). Collectively fungal

phytopathogens and Oomycetes, once considered lower fungi, are estimated to be responsible for the loss of approximately a third of food crops annually. These losses can occur during the growing season and post-harvest (Almeida *et al.,* 2019).

1.2 Fungal phytopathogen lifestyles

The fungal kingdom contains diverse taxa with a range of ecologies and morphologies. Most phytopathogenic fungi are filamentous ascomycetes or basidiomycetes. Fungal phytopathogens differ in hosts and the types of host tissue they can infect. For example, there are fungal phytopathogens capable of infecting floral tissue, leaf tissue, stem tissue, root tissue, or even a combination. Each has evolved differing strategies for feeding on plant tissues or plant-derived substrates for reproduction and dispersal (Agrios, 2005). Plant pathogens are described broadly as having three nutrient acquisition strategies related to how the microorganism interacts with its host(s).

Biotrophs colonise and feed off the living tissues of their host, using specialised feeding structures such as haustoria. The rust fungi *Puccinia graminis* f. sp. *tritici* is an obligate biotroph and a basidiomycete that infects wheat stems, producing characteristic masses of yellow-to-red asexual urediniospores that are airborne (Figueroa *et al*., 2018). The strategy of necrotrophs is considered more destructive, involving the secretion of toxins and enzymes to kill host cells and take up the released nutrients or co-opting host programmed cell death mechanisms. For example, *Fusarium graminearum* is one species responsible for fusarium head blight (FHB) disease, causing significant yield losses through reduced grain production and toxin contamination. Meanwhile, *F. culmorum* is one of the several *Fusarium* species responsible for Fusarium foot and root rot disease (also known as Fusarium crown rot) and a causal agent of FHB (Figueroa *et al*., 2018*).*

Hemibiotrophs employ a combination of these strategies, starting as a biotroph and then transitioning into a necrotrophic phase (Möller &

Stukenbrock, 2017). A typical example is *Magnaporthe oryzae* which causes wheat and rice blast diseases resulting in *partially* bleached spikes with shrivelled grain or no grain (Fernanez & Orth, 2018).

1.3 Plant host inducible defences against fungi

Figure 1.1 represents the widely accepted zig-zag model of plant immunity proposed by Jones & Dangl (2006). Broadly, hosts can detect fungal phytopathogens by recognising conserved molecular patterns. These are pathogen-associated molecular patterns (PAMPS) or microbe-associated molecular patterns (MAMPS). As displayed in Figure 1.1, the classic example of a PAMP is chitin, a major component of fungal cell walls, which can be recognised by membrane-localised pattern recognition receptors (PRRs) of host cells. Recognition triggers PAMP-triggered immunity (PTI) (Boller & Felix, 2009). Plant PRRs can also recognise host-derived damage-associated molecular patterns (DAMPs); these can be generated from herbivore attacks and invading pathogens (Li *et al*., 2020; Pontiggia *et al*., 2020). Upon recognition by host plant PRRs, the resulting signalling leads to the accumulation of antimicrobial compounds, including reactive oxygen species (ROS) and transcriptional reprogramming of the host. Therefore, for a pathogen to cause disease, it must either avoid triggering PTI or suppress it. Fungal pathogens are capable of this suppression via secretion of ‘effectors’ to protect the fungus, suppress the plant immune response or produce secondary metabolites and proteins that can kill the host plant cells instead of masking or suppressing (Lo Presti *et al*., 2015). In Figure 1.1, I use the example of the chitin-binding LysM domain-containing effector that fungi, such as *Z. tritici* (3LysM) and *Cladosporium fulvum* (Ecp6), use to sequester chitin from host receptors. Thereby effectively suppressing a chitin-induced ROS burst and protecting the fungal hyphae against chitinase hydrolysis (Tian *et al*., 2021). Effector-triggered susceptibility occurs when these effectors successfully prevent the mounting of defence response. However, as part of the evolutionary ‘arms race’ between pathogens and their hosts, some plants evolved to detect effectors through resistance proteins (R-

proteins). Examples include conserved intracellular receptors of the nucleotide-binding leucine-rich receptor (NB-LRR) class or receptor-like proteins (Deller *et al*., 2011). Effectors that activate host R-proteins are called avirulence (avr) proteins, and these trigger the hosts' second layer of defence known as effector-triggered immunity (ETI). ETI results in host resistance to disease and, typically, a hypersensitive (HR) cell death response at the site of pathogen attack (Jones & Dangl, 2006). This mechanism is beneficial for obligate biotrophic pathogens, which require living plant cells to thrive.

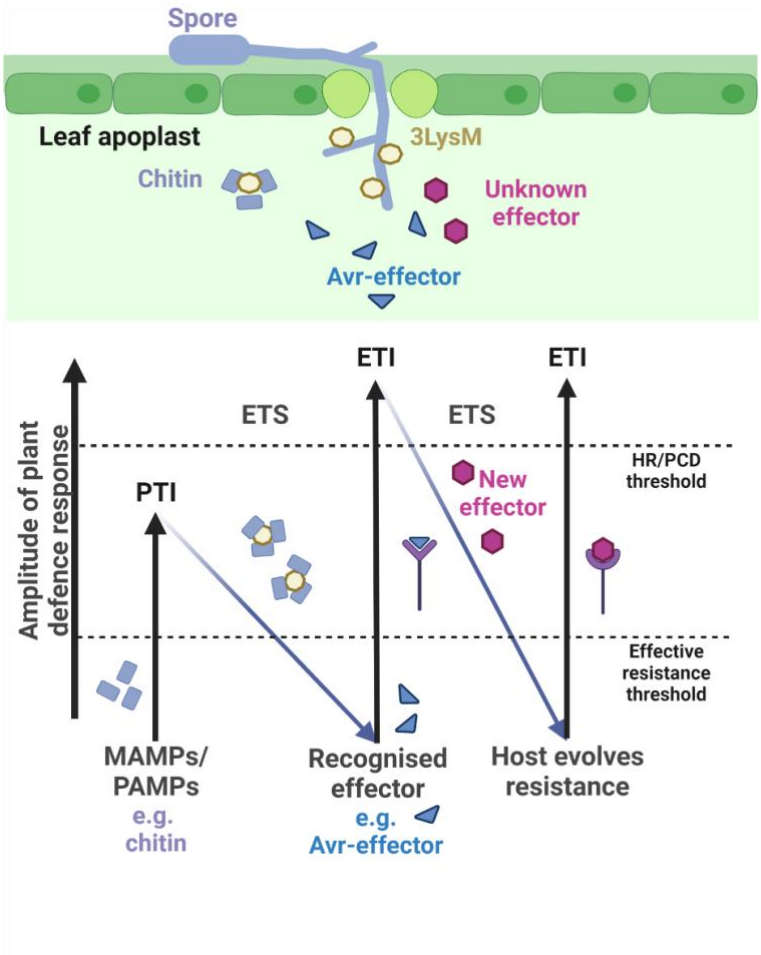

Figure 1.1 Zig-zag co-evolutionary plant immunity model.

A modified version of Jones and Dangl (2006) zig-zag plant immunity model, including a representation of an invading fungal hypha on a leaf surface. Co-evolutionary pathogenicity mechanisms and immune response in plants result in either disease susceptibility or disease resistance. MAMP: microbe-associated molecular patterns, PAMP: pathogen-associated molecular patterns, ETS: effector-

triggered susceptibility, ETI: effector-triggered immunity, HR: hypersensitive response, PCD: programmed cell death. Figure created using BioRender.com.

1.4 Importance of wheat in global food systems

Second only to rice (*Oryza* sp.), wheat (*Triticum aestivum*) is one of the most important cereal crops worldwide. Humans have cultivated wheat for approximately 10,000 years, beginning with the domestication in South-eastern Turkey of the grass species *Triticum monococcum* (Heun *et al.*, 1997). Modern hexaploid (AABBDD) bread wheat is the product of several hybridisations between grass species (Shewry, 2009). The current levels of distribution and production of wheat were made possible by achievements during the so-called "Green Revolution" of the 1950s and 1960s, which refers specifically to the development of high yielding, semi-dwarfing cultivars responsive to fertilizer (Shiferaw *et al*., 2013). With over 850 million tonnes of grain harvested in 2018 (www.fao.org/faostat/en/#data), wheat provides around 20% of human caloric intake globally. However, in regions such as the UK, wheat yields have not experienced significant improvements since 1984 (FAOSTAT, 2018). Furthermore, modern wheat varieties are more susceptible to biotic stresses caused by pests and pathogens than their ancestral progenitor species (Pour-Aboughadareh *et al*., 2021).

Therefore the growing demand alongside the apparent plateau in yields has prompted efforts to address the gap between potential theoretical yields and actual yield levels. For future-proofing production, wheat cultivars should be bred for yield and resilience to both biotic and abiotic stresses. Therefore, research into understanding and controlling the pests and pathogens (such as *Zymoseptoria tritici*) that cause wheat yield reductions also plays a role in global food security.

1.5 *Zymoseptoria tritici* and its pathogen genomics

Zymoseptoria tritici (formerly *Mycosphaerella graminicola*; anamorph, *Septoria tritici*) is a filamentous ascomycete in the class *Dothideomycetes*. The genus *Zymoseptoria* was proposed following realisations detailed in

Quaedvlieg *et al*., (2011), that the genus *Mycosphaerella* was polyphyletic. Since this reclassification, seven *Zymoseptoria* species have been described, including *Z. tritici,* the causal agent of Septoria tritici blotch (STB) and synonym septoria leaf blotch (Crous *et al*., 2012; Eyal *et al*., 1987; Quaedvlieg *et al.*, 2011). Furthermore, several "reference" strains of *Z. tritici* have had their genomes sequenced. A Dutch isolate IPO323, initially isolated in 1981 from a wheat variety *Triticum aestivum cv.* Arminda (Kema & van Silfhout, 1997) and ST99CH_1A5, ST99CH_1E4, ST99CH_3D1 and ST99CH_3D7, all isolated in 1999 from infected wheat fields in Switzerland. In addition, several closely related species have been identified, including *Z. brevis*, *Z. pseudotritici* and *Z. ardabiliae* (Croll *et al*., 2013; Grandaubert *et al*., 2015; Plissonneau *et al*., 2018; Zhan *et al*., 2002). These resources have fuelled genomic sequencing-based efforts to understand speciation and specificity in the Zymoseptoria species.

Z. tritici is a wheat leaf-specific pathogen and is not known to cause disease on other plant species or alternative wheat tissues. However, *Z. tritici* has extensive and diverse populations structures, and different isolates often display race-specific (isolate vs cultivar) virulence on differential hexaploid wheat. Studies have placed the centre of origin of *Z. tritici* in the Middle East, likely emerging as a pathogen 10-11,000 years ago alongside the domestication of wheat (Banke & McDonald, 2005; Stukenbrock *et al.*, 2010). *Z. tritici* has both asexual and sexual life stages driven by its heterothallic bipolar mating system, with two identified mating types, MAT1-1 and MAT1-2 (Kema *et al*., 1996; Quaedvlieg *et al*., 2011). Ascospores released from sexual fruiting bodies, known as pseudothecia, are a source of primary inoculum released from wheat debris. Whilst pycnidiospores, released from asexual fruiting bodies (pycnidia), primarily drive disease progress during the growing season propagated by "splashy" rainfall (Eyal *et al*., 1987). Though ascospores are formed year-round, the long latent period for pseudothecia compared to pycnidia results in the asexual spores having a higher production rate during the growing season (Eriksen *et al.*, 2001).

Z. tritici is considered a rapidly evolving pathogen due to its active sexual lifestyle; frequent sexual recombination has resulted in highly diverse natural populations with high genome plasticity (Goodwin *et al.*, 2011; Mohammadi *et al.*, 2017; Wittenberg *et al.*, 2009). The 39.7 Mb genome of *Z. tritici* reference strain IPO323 was fully sequenced by the US Department of Energy's Joint Genome Institute. The project revealed the complete sequences of the 21 chromosomes found in this strain, of which the shortest eight were found to be dispensable for full virulence (Goodwin *et al*., 2011). These smaller, highly variable chromosomes have high repeat content, and a presence/absence variation is observed in both field strains and progeny of crosses between *Z. tritici* isolates (Grandaubert *et al.*, 2015; Wittenberg *et al.*, 2009). Goodwin *et al.*, (2011) proposed the origin of these dispensable or accessory chromosomes through horizontal transfer from an unknown donor, followed by extensive recombination. However, Croll *et al.*, (2013) suggest that these accessory chromosomes may have formed through ancient core chromosomal duplications (non-disjunctions) followed by degradations, breakage fusion bridge cycles, and a genomic defence mechanism activity known as Repeat-Induced Point mutation.

Accessory chromosomes have been identified in numerous fungal plant pathogens, and in some have been associated with pathogenicity (Coleman *et al*., 2009; Han *et al.*, 2001; Hatta *et al.*, 2002; Ma *et al*., 2010; Plaumann *et al.*, 2018; Wang *et al.*, 2003). However, the role these dispensable chromosomes of *Z. tritici* play. There are limited studies supporting the role of the *Z. tritici* accessory chromosomes in virulence. The *Z. tritici* dispensable chromosomes make up 12% of IPO323 genome but were found to only contain 6% of the genes, of which only 10% were able to be annotated (Goodwin *et al*., 2011). Two further studies indicated cultivar dependent effects and 2-3% increases in virulence traits associated with the accessory chromosomes (Habig *et al*., 2017; Stewart *et al*., 2018). However, the accessory chromosomes are lowly expressed during infection and to date, there are no known pathogenicity or fitness associated genes located to the

Z. tritici accessory chromosomes (Goodwin *et al.*, 2011; Kellner *et al.*, 2014; Rudd *et al.*, 2015).

With the development of faster, more accurate and cheaper DNA sequencing technologies, many more isolates of *Z. tritici* have been fully sequenced, and several groups have reported on 'pangenomes' (Badet *et al*., 2020; Badet *et al*., 2021; Curran *et* al., 2019; Plissonneau *et al*., 2018). Pangenomes aim to describe as much genetic variation within a species as possible, requiring the whole genome sequences of many isolates to be compared. In addition, a pangenome enables easy identification of and can fully distinguish between core, unique and dispensable genes (McCarthy & Fitzpatrick, 2019; Vernikos *et al*., 2015). For *Z. tritici* and other pathogens, pan-genomics could facilitate recognition of key pathogenicity determinants through quick elimination of genes unlikely to be involved in virulence (i.e. absence of a gene in disease-causing field isolates). Furthermore, it may pinpoint intraspecies-specific determinants, such as the genetics behind bread wheat infecting versus durum wheat infecting isolates (Torriani *et al*., 2011). In one *Z. tritici* pangenome, Plissonneau *et al*., (2018) found that up to 40 % of genes in the total were either lineage or strain-specific. If historical collections are added to the pangenome of *Z. tritici,* an evolutionary/time dimension could provide further insights into the pathogen populations.

1.6 Septoria Tritici Blotch disease (STB)

STB is widely considered to be the most economically important foliar disease of both bread wheat (*Triticum aestivum* L.) and durum wheat (*T. turgidum* ssp. *durum* L.). First described in Europe by Desmazières (1842), STB was not linked to *Z. tritici* until the 1970s. Necrotic blotches containing pycnidia that form on the leaf in the late stages of infection are the characteristic symptoms of STB (Ponomarenko *et al*., 2011). However, it is a persistent threat to wheat yields in temperate climates across the globe and becoming increasingly more difficult to control due to current intense farming practices, lack of widespread wheat genetic resistance and emerging

resistances to multiple fungicides already observed (Fones & Gurr, 2015; Torriani *et al*., 2015).

1.6.1 Control Methods for STB

As with many fungal phytopathogens, the primary control method against STB is fungicide application. While yield losses of up to 50% have been reported due to STB on untreated fields growing susceptible cultivars, even on treated fields and using more resistant cultivars, losses of 5-10% are still typical. In the European Union, approximately 70% of annual cereal fungicide usage is targeted against STB, supporting a market with an estimated worth of $1.2 billion per annum (Fones & Gurr, 2015; Torriani *et al*., 2015).

The breeding of STB resistant lines of wheat is considered necessary for disease control, yet all currently available commercial wheat varieties display some susceptibility to this pathogen (AHDB, 2019). There are currently 21 major genes known to contribute to qualitative resistance against STB that have been mapped and some sources of quantitative resistance. While fungicides are successfully used against *Z. tritici*, there has been a decline in effectiveness observed for two main chemical groups, triazoles and QoIs, also known as strobilurin (Fraaije *et al*., 2011; Fraaije *et al.*, 2012).

Farming systems are more intensive, and older prevention practices are less profitable or banned in the United Kingdom due to regulations (e.g. burning stubble). In their study, Bankina *et al.*, (2018) concluded that while crop rotation and tillage practices affected tan spot disease (caused by *Pyrenophora tritici-repentis*), STB was affected more by meteorological conditions. Typically, airborne pathogens such as *Z. tritici,* whose ascospores can disseminate over 10-200 kilometres, can circumvent such practices (Linde *et al.*, 2002). Late sowing practices have been shown to reduce STB incidence, though this comes at a cost to yield (Eyal, 1981; Green & Ivins, 1985).

A novel method of control that gained attention with some promising results against select phytopathogens and insect pest species is RNA silencing, also

known as RNAi (RNA interference) (de Andrade & Hunter, 2016; Baum *et al*., 2007; Head *et al*., 2017; McLoughlin *et al*., 2018). The RNAi machinery includes double-stranded RNA endonucleases (Dicer or Dicer-like), RNA binding protein(s) (Argonaute), and, in some species, RNA-dependent RNA polymerases. RNAi has been linked to diverse functions, ranging from defence against viral or transposon invasion to regulating developmental processes and epigenetic modifications (Holoch & Moazed, 2015; Torres-Martínez & Ruiz-Vazquez, 2017). However, an in-depth study by Kettles *et al*., (2019) casts doubt on using the possible 'next-generation RNA fungicides' and transgenic wheat lines for 'cross-kingdom' RNAi to control *Z. tritici*. Targeted deletion strains of key RNAi machinery genes Dcl, Ago1, and Ago2 were fully pathogenic on the wheat cultivar Bobwhite. Recently Habig *et al*., (2021) confirmed observations of full pathogenicity for targeted deletion strains Dcl, Ago2, and Ago3 against a different wheat cultivar (Obelisk). However, their results indicate that Ago1 may have a role in pathogenicity. Deletion strains were statistically significantly attenuated in their ability to produce pycnidia, and complementation with *AGO1* restored typical pycnidiation.

1.6.2 Life and Infection Cycle of *Z. tritici*

Figure 1.2 shows an overview of the known events in *Z. tritici* infection of wheat, breaking the infection cycle down into six stages from Fantozzi *et al*., (2021). A complete infection cycle begins with a compatible interaction between a viable spore and a susceptible host. Both airborne ascospores and rain-splash dispersed pycnidiospores are pathogenic to wheat (Eyal *et al*., 1987). Temperature and relative humidity are considered the most important conditions for establishing infection. Temperatures of 20-25 °C promote disease, with the optimal relative humidity at higher than 85% for pycnidia production (Holmes & Colhoun, 1974; Kema *et al*., 1996). Regardless, Shaw & Royal (1993) reported that even under suboptimal field conditions, which delay the appearance of disease symptoms, damage to susceptible cultivars is not significantly reduced.

Field grown wheat contends with mixed infections involving multiple strains and pathogens on any leaf. Recent studies have shown that individuals in a ‘population’ of mixed *Z. tritici* strains can help and hinder one another through competition for the same resources. Similarly, when avirulent and virulent strains are mixed on a single cultivar, pycnidia are still produced, albeit later than with a single strain infection (Barrett *et al*., 2021; Kema *et al.,* 2018). Attention has also recently been drawn to the asynchronous development through the infection stages by the *Z. tritici* population upon landing on a leaf surface (Fantozzi *et al*., 2021), which makes the exact timing of specific infection events difficult.

Nevertheless, the timings of “events” in the biphasic (first symptomless then necrotrophic) infection cycle of *Z. tritici* differ slightly between studies. The ranges shown in Figure 1.2 include the considerations for asynchronous development and broadly represent the infection timings. There is an extended initial symptomless phase followed by a switch to a necrotrophic phase of infection with a rapid increase of fungal biomass inside the plant; as such, *Z. tritici* was commonly initially referred to as a hemibiotroph (Palmer & Skinner, 2002; Deller *et al*., 2011; Rudd *et al*., 2015). However, Sánchez-Vallet *et al.* (2015) put forward an argument for using the term “latent necrotroph”, which I shall discuss in the following relevant sections on the infection cycle.

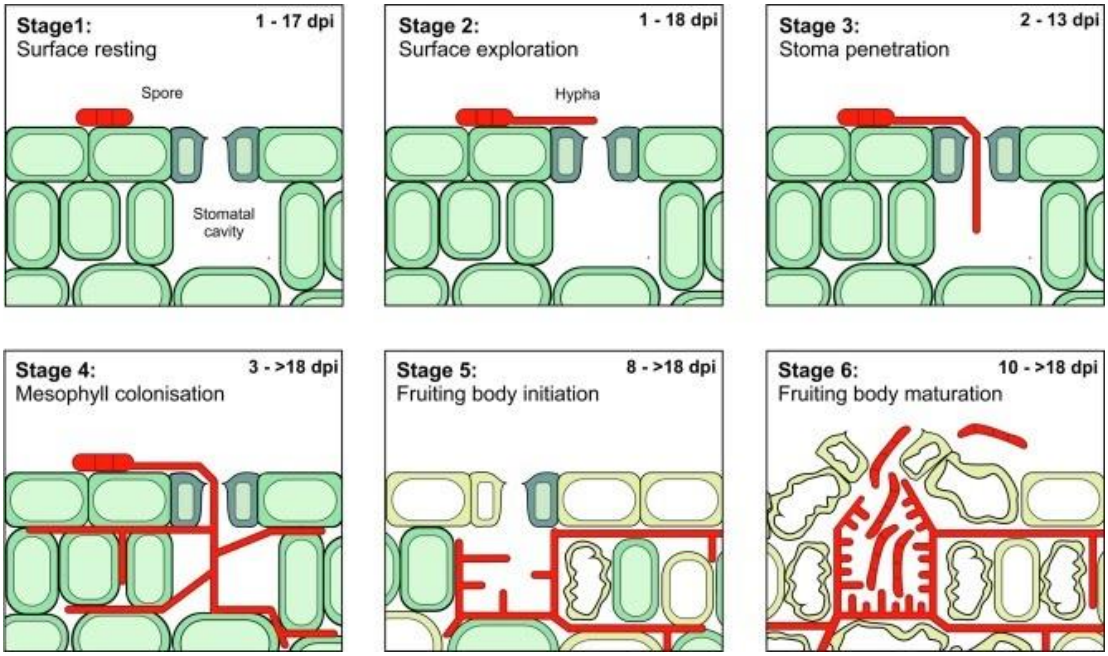

Figure 1.2 Overview of *Z. tritici* infection stages upon landing on susceptible wheat cultivar.

From Fantozzi *et al*., (2021) shows the *Z. tritici* infection cycle, broken into six stages. Individual hyphae can go from one stage to the next, but as the population is not synchronized, up to five stages can co-occur in infected wheat leaves at a given time.

1.6.3 Germination and Penetration in *Z. tritici* infection

Stages 1 through 3, shown in Figure 1.2, are described here. Within hours of landing on a wheat leaf, spore germination can occur. Spores develop germ tubes that grow and differentiate to form hyphae. These hyphae spread short distances across the leaf surface, searching for natural openings, namely stomata (Goodwin *et al*., 2011). However, Fantozzi *et al*., (2021) observed the randomness of this process resulting in individual hyphal germination and exploration as late as 18 days post-inoculation.

Evidence that *Z. tritici* hyphae grow directly towards stomatal openings is limited. There is also no convincing evidence that *Z. tritici* can invade the epidermis directly without using natural openings or surface wounds. Duncan & Howard (2000) reported observing germ tubes extending towards stomata, suggesting this was a response to a ‘thigmotropic’ signal. However, there is

limited evidence elsewhere to support this observation of non-random growth of hyphae in *Z. tritici*. In one study, mutant isolates with a knockout of MAP kinase, MgFus3, were described as unable to recognise substomatal openings (Cousin *et al.*, 2006). Others have observed hyphae in varied *Z. tritici* isolates frequently growing across stomata without entering the leaf, suggesting that stomatal penetration is somewhat stochastic (Kema *et al.*,1996; Shetty *et al.*, 2003).

Penetration of the leaf via stomata was initially observed between twelve hours to three days of the spore landing on the leaf surface, though a recent study extends this up to thirteen days post-inoculation (dpi) (Eyal *et al*., 1987; Fantozzi *et* al., 2021; Kema *et al*., 1996; Steinberg, 2015). Despite studies reporting appressorium-like swellings present at the tip of invading *Z. tritici* hyphae, its genome lacks many genes associated with appressoria formation (Goodwin *et al*., 2011). Steinberg (2015) suggested a possible explanation for conflicting reports on this could reflect the differences in experimental conditions or inoculation methods involved, which may create wounds in the leaf tissue through which *Z. tritici* can begin colonisation.

1.6.4 Early colonisation by *Z. tritici*: a biotrophic phase or latency?

Following penetration, in Figure 1.2, from stage 3 onwards, as early as two dpi, hyphae begin colonisation of the substomatal cavity invading the intercellular spaces within the mesophyll (Kema *et al*., 1996). This is followed by an extended asymptomatic phase, in which the fungus grows slowly in the apoplast. The fungal growth of *Z. tritici* during colonisation is relatively slow (Keon *et al.*, 2007). The network of hyphae becomes increasingly dense inside the substomatal cavity towards the time that visible symptoms can be observed. Kema *et al. (1996)* observed that mesophyll cell walls had wrinkled appearances by eight dpi and occasionally were collapsed.

How *Z. tritici*, restricted to the apoplast, gains nutrients for growth during the asymptomatic phase is the crux behind whether the fungus should be considered a hemibiotroph. Evidence supports the evasion and suppression

of plant defences through the secretion of effectors during the asymptomatic phase of infection (Marshall *et al*., 2011; Shetty *et al.*, 2009; Lee *et al.*, 2014; Yang *et al*., 2013). However, *Z. tritici* has not been observed to form specialised feeding structures. Sánchez-Vallet *et al.*, (2015) argued that the fungus requires the death of host cells for growth and sporulation, releasing nutrients from collapsed tissues. A widely accepted suggestion is that *Z. tritici* obtains its nutrients from breaking down reserves stored in germinating spores themselves and nutrients that happen to be present in the apoplast. RNA sequencing and metabolomics experiments indicated that genes involved in beta-oxidation of fatty acids and lipids are specifically up-regulated at one dpi, decreasing by 9-14 dpi, suggesting these enzymes might provide an early source of nutrients (Rudd *et al.*, 2015). It is also hypothesised that cell wall degrading enzymes (CWDEs) could be used to degrade components of the host cell wall to release nutrients (Brunner *et al.*, 2013; Keon *et al.*, 2005; Goodwin *et al.*, 2011; Siah *et al.*, 2010).

In their study, Rudd *et al.*, (2015) agree with Sánchez-Vallet *et al.*, (2015), suggesting that *Z. tritici* is a relatively poor biotroph being unable to significantly reprogram host physiology to gain nutrients during its 'biotrophic' latent phase. Lee *et al*., (2015) reported that silencing the TaR1 protein in *Z. tritici,* which binds to chromatin, enabling chromatin remodelling, resulted in a truncated latent phase and noted a reduced asexual fecundity. Plus, the over-representation of transcripts attributed to sexual reproduction including meiosis and sporulation (sexual or asexual), was reported during this phase (3-7dpi; Palma-Guerrero *et al.*, 2016). In their review, Brennan *et al.* (2019) suggest that instead of nutrient acquisition, the latent phase could boost the effectiveness of the approaching reproductive stages. However, the latent phase of *Z. tritici* infection remains enigmatic.

1.6.5 Necrotrophic Growth and Pycnidia Formation in *Z. tritici* infection

Stages 5 and 6 in Figure 1.2 illustrate necrotrophic growth and asexual sporulation phases. In studies before Fantozzi *et al.*, (2021), the earliest 'pre-

pycnidia' (pycnidial initials) begin forming inside the substomatal cavity at 5-9 dpi, therein marking the transition from the latent to the necrotrophic phase (Steinberg, 2015). The onset of necrotrophy coincides with an up-regulation of proteases, plant cell wall-degrading enzymes (CWDEs) and lipases (Palma-Guerro *et al.*, 2016; Rudd *et al*., 2015).

Plant cells appear to undergo programmed cell death (PCD) during this phase, which coincides with releasing nutrients from dying host cells into the apoplast, enabling rapid fungal growth and proliferation (Keon *et al.*, 2007). After ~10-21 days, 'pre-pycnidia' mature into pycnidia, producing the multi-cellular pycnidiospores that, when released by water splash, continue the spread of infection (Steinberg, 2015).

1.7 *Zymoseptoria tritici* cell biology

Fungi show much morphological diversity, and many have several different growth forms. *Z. tritici* is considered a pleomorph, having more than one distinct growth form (Rossman *et al.*, 2015). Depending on the nutrients available and temperature, *Z. tritici* can be grown *in vitro* on agar plates in a "yeast-like" blastospore form or a hyphal form, extending true hyphal filaments (Francisco *et al*., 2019). On solid nutrient-rich agar, such as yeast extract peptone dextrose (YPD), wild-type (WT) *Z. tritici* spores produce a mass of blastospores at lower temperatures (e.g.~16˚C). Blastospores are unicellular structures that form by lateral budding, also known as micropycnidiospores which are ~1 µm wide and 5-10 µm long (Eyal *et al*., 1987). Increasing the incubation temperature to 25 °C leads to extensive networks of melanised aerial hyphae above the colony in WT *Z. tritici* (King *et al.*, 2017; Yemelin *et al.*, 2017). When nutrients are limited, mimicking the nutrient availability on leaf surfaces, the hyphal growth form is also observed (King *et al.*, 2017; Yemelin *et al.*, 2017). *Z. tritici* also produces macropycnidiospores, multicellular structures formed of 4-8 elongate cells, ~1.5-3.5 µm wide and up to ~40-100 µm in length (Eyal *et al.*, 1987; Steinberg, 2015). Macropycnidiospores can also germinate to form thin

hyphae, which are elongated cells extending by polar tip growth (Steinberg, 2015).

1.8 The genetic tools available for understanding the biology of *Z. tritici*

Understanding the genomics underpinning fungal phytopathogenicity is key to developing novel methods to protect against attack. Mutagenesis methods, including stable genetic transformations, have been key in identifying and functional characterisation of genes involved in pathogenesis.

There are multiple iterations on the type and use of different fungal transformation methods. Random mutagenesis, where there is no prior knowledge of genes involved, is used in forward genetics-based approaches. These studies seek the genetic basis of an observed altered phenotype (Nurse & Hayles, 2019). This approach has led to many advances in understanding fungal virulence mechanisms and development. Mutagenic agents used to achieve 'random' mutational changes to genomes include physical mutagens, such as ultraviolet light, and chemical mutagens, such as alkylator ethyl methanesulfonate (EMS) (Hodgens *et al*., 2020; Maier & Schäfer, 1999). There are also random insertional mutagenesis methods, such as restriction enzyme-mediated integration (REMI) and horizontal gene transfer using *Agrobacterium tumefaciens*-mediated transformation (ATMT) (Jiang *et al*., 2013; Weld *et al*., 2006). The advantages of these methods are that transformed strains can be maintained using antibiotic selection, and they frequently are thought to involve fewer genomic insertion (mutation) events.

In contrast to forward genetics, targeted mutagenesis approaches are used in reverse genetics-based strategies. It typically involves prior knowledge (or a hypothesis) of candidate genes likely to be involved in a particular phenotype. ATMT is a commonly used method for targeted mutagenesis in *Z. tritici*. Many of the genes described in the current literature involved using ATMT to perform genes' targeted interruptions (deletions or disruptions). Targeted gene interruption works by homologous recombination of the T-

DNA into the genome mediated through homologous flanking sequences within the binary vector (Michielse *et al*., 2005). Using an IPO323Δ*KU70* mutant, engineered to block non-homologous recombination (neighbour end-joining machinery), increases the efficiency of getting targeted transformants (Bowler *et al*., 2010; Fell & Schild-Poulter, 2012). Developments in the CRISPR-Cas9 gene-editing systems since 2013 have enabled the efficient introduction of point mutations into many different organisms, from fungi to crop plants (DiCarlo *et al*., 2013; Mikami *et al*., 2015; Nødvig *et al*., 2015; Schuster *et al*., 2016; Zhang *et al*., 2019). However, there is currently no working protocol for *Z. tritici*. Furthermore, it is unclear how useful this would be as a tool in an organism that is very amenable to other forms of transformation (Khan *et al*., 2019).

1.9 Pathogenicity and Virulence Associated Genes in *Z. tritici* and other Fungal Phytopathogens

Key 'housekeeping genes' are generally defined as those involved in basic cellular metabolism and are not generally considered pathogenic determinants. However, if the loss of such a gene can be shown to attenuate virulence without impacting the growth of the fungus, it could be considered virulence associated (Wassenaar & Gaastra, 2001). Pathogenicity determinants are genes that affect the virulence of a pathogen. These include regulatory genes involved in transcriptional responses or signalling pathways controlling several vital processes such as sporulation, melanisation and morphogenic switching. Additionally, the following can interfere with host cellular functions proteins, peptides, or small molecules such as secondary metabolites, extracellular enzymes, transporters, and effectors (Wassenaar & Gaastra, 2001; Perez-Nadales *et al*., 2014). The following sections will summarise some of the critical functional categories (proteins and processes) contributing to the fungal pathogenesis of plants.

1.9.1 Proteins and processes implicated in signal transduction pathways

Signalling plays a vital role in regulating all processes within any living cell, and several well-established signalling pathways in fungi have been shown to regulate plant pathogenic interactions by transducing extracellular changes into intracellular transcriptional. Mitogen-activated protein kinases (MAPKs) are a family of highly conserved proteins involved in multiple aspects of fungal development, including the transduction of extracellular signals (Jiang *et al*., 2018). For example, in *Saccharomyces cerevisiae* there are five MAPK pathways, four of which are conserved in ascomycete plant pathogens.

Filamentous ascomycetes tend to have a single orthologue of yeast *FUS3*/*KSS1*. The equivalent functional orthologue in the rice (*Oryza sativa*) blast ascomycete *Magnaporthe oryzae*, pathogenicity MAP kinase 1 (*PMK1*), is essential for appressorium formation and invasive growth (Jiang *et al*., 2018). In *Fusarium graminearum,* the *FUS3* orthologue also acts to synthesise the deoxynivalenol (DON) toxin, a secondary metabolite. In other non-appressorium-forming pathogens, including *Z. tritici*, this pathway is necessary for plant penetration and infectious growth. For example, in *Z. tritici,* deletion strains lacking *ZtFUS3* (published as MgFus3) failed to colonise mesophyll tissue, and microscopic analysis indicates that they appeared to no longer recognise substomatal openings (Cousin *et al.*, 2006).

The *SLT2* cell wall integrity associated pathway is also conserved in filamentous ascomycetes. Its role in the penetration of the host in fungi varies, being required for early appressorium development in *Colletotrichum gloeosporioides,* but in *M. oryzae,* the orthologue was dispensable for virulence (Jiang *et al*., 2018). In *Z. tritici,* the orthologue *ZtSLT2* (published as MgSlt2) was required for virulence in the post stomatal penetration phase. *ZtSlt2* mutant is also hypersensitive to azole fungicides. (Mehrabi *et al*., 2006a).

Finally, the ‘osmoregulation’ MAPK pathway is not essential for virulence across all fungal phytopathogens. In *S. cerevisiae,* this pathway activates HOG1 (with threonine-glutamate-tyrosine phosphorylation sites). The *M. oryzae* equivalent *OSM1* (threonine-glycine-tyrosine phosphorylation sites) is dispensable for virulence. MAPK-encoding gene *ZtHOG1* (published as MgHOG1) was required for virulence, regulating the morphogenic transition from blastosporulation (“yeast-like”) to filamentous growth (Mehrabi *et al*., 2006b). Yemelin *et al*. (2017) identified a mutant with a defective Ssk1 orthologue. *SSK1* is a known upstream regulator within the HOG1-pathway in *S. cerevisiae*. The *Z. tritici* mutant displayed altered morphology, forming swollen conidia and reduced virulence and tolerance to osmotic and oxidative stress conditions.

A group of highly conserved regulatory proteins known as heterotrimeric guanine nucleotide-binding proteins (G proteins) are essential for signal transduction (Yu & Keller, 2005). Individual mutations in *Z. tritici* Gα subunits encoded by *ZtGPA1* and *ZtGPA3* (published as MgGpa1 and MgGpa3), and Gβ subunit encoded by *ZtGPB1* (published as MgGpb1), all resulted in an inability to form mature pycnidia *in planta* and reduced pathogenicity (Mehrabi *et al.*, 2009). The latter regulates the cyclic adenosine monophosphate (cAMP) pathway. The cAMP signalling pathway is another conserved signal transduction pathway that supports numerous processes, including virulence in pathogenic fungi (Xu, 2000; Yu & Keller, 2005). In their study, Mehrabi & Kema (2006) investigated the role of the catalytic (*ZtTPK2*, previously published as MgTpk2) and regulatory (*ZtBCY1*, previously MgBcy1) subunits of a cAMP-dependent protein kinase A (PKA) in *Z. tritici*. PKA is a major downstream component of the cAMP signalling pathway (Xu, 2000). Interruption of these genes in *Z. tritici* resulted in reduced virulence, and both mutants were unable to produce pycnidia (Mehrabi & Kema, 2006). The transcription factor *ZtWOR1* acts downstream of the cAMP family, is an orthologue of *WOR1* in the human fungal pathogen *Candida albicans*. It regulates phase-specific gene expression and controls the white–opaque

switch, a change in morphology associated with pathogenicity (Mirzadi Gohari *et al*., 2014).

1.9.2 Proteins and processes involved in morphogenic switching

In many eukaryotic pathogens, morphological changes are thought to be important for disease. The human opportunistic fungal pathogen that requires morphogenic switching is the ascomycete *Candida albicans* (Kornitzer, 2019). This change from yeast to a hyphal form is associated with *C. albicans* lifestyle transition from commensal (yeast) to pathogenic (hyphal). For many phytopathogenic fungi, hyphal growth is understood to be critical for the establishment and completion of infection. An example of a phytopathogenic ascomycete that undergoes multiple morphotype switches is *M.oryzae*. Conidia land on and attach to a rice leaf then germinate. The tip of the germ tube that forms then differentiates into a specialized infection structure called an appressorium which generates turgor pressure to allow for direct physical cell penetration (Deng *et al*., 2019; Wang & Lin, 2012). Another example is *Ustilago maydis*, the corn smut disease-causing basidiomycete, which can grow *in vitro* in a haploid yeast form. However, unlike *Z. tritici*, it requires mating between two compatible haploid strains to produce a dikaryotic hyphal form to be capable of causing disease (Brefort *et al.*, 2009; Wang & Lin, 2012).

For *Z. tritici* to switch between “yeast-like blastosporulation” and hyphal growth *in vitro* is a unique aspect of its biology, enabling easier identification of genes involved in morphological switching. The essentiality of switching to a hyphal form for pathogenicity has been demonstrated in *Z. tritici*, as defective morphogenic switching mutants typically display limited capability in infecting wheat. Mutagenised isolates with defective mitogen-activated protein (MAP) kinase, *ZtHOG1* (previously MgHog1), or defects in N-glycosylation through the alpha 1,2 mannosyltransferase, *ZtALG2* (previously MgAlg2), were among the first to show the essentiality of the hyphal form for infection (Merhabi *et al.*, 2006a; Motteram *et al.*, 2011; Steinberg, 2015). Both mutant strains were able to grow as blastospores on

rich media agar plates but did not cause full infection of wheat leaf tissue attributed to impaired transitions to hyphal growth (Merhabi *et al.*, 2006a; Motteram *et al.*, 2011). Another recent example of a protein required for a successful transition is a predicted type-two glycosyltransferase, *ZtGT2*. King *et al.*, (2017) suggest that *ZtGT2* may be functioning to create an extracellular matrix, which may act as either a lubricant, reducing surface friction and allowing hyphae to spread across the leaf or as simply a structural component in the hyphal cell wall. Interruption of the orthologous gene in *Fusarium graminearum*, a taxonomically distant pathogen that causes Fusarium head blight in wheat, also displayed an impaired ability to form hyphae on solid agar reduced virulence on wheat ears (King *et al.*, 2017). In a recent study, Deng *et al*., (2019) also identified and characterized a type 2 glycosyltransferase, *MoGT2*, in *M. oryzae*. Gene deletion mutants (Δ*MoGt2* strains) were non-pathogenic and displayed impaired vegetative growth, conidiation, and appressorium formation at hyphal tips suggesting that the *GT2* function may be quite widespread and important in plant pathogenic fungi.

1.9.3 Proteins and processes involved in sporulation

Sporulation is an essential final part of a fungal pathogens lifecycle, tightly regulated by several genes and pathways. Tiley *et al.*, (2018) investigated asexual sporulation in *Z. tritici* through comparison to the well-defined genetic mechanisms of a model ascomycete fungus, *Aspergillus nidulans*. Deletion of *ZtFlbC* and *ZtBrlA2* resulted in reduced pycnidiospore production, while deletion of *ZtStuA* caused non-pigmented mutants to be unable to produce asexual spores or cause infection (Tiley *et al.*, 2018). In a later study, Tiley *et al.*, (2019) targeted the velvet B gene, velB, which has conserved roles in pathogenicity, development and secondary metabolism and is also well characterised in *A. nidulans*. The targeted deletion of this gene's orthologue in *Z. tritici* indicated that *ZtvelB* is required in both yeast-like growth and asexual sporulation.

1.9.4 Proteins and processes controlling fungal melanisation

Melanin is a pigment composed of complexes of various phenolic or indolic monomers, often with carbohydrates and proteins (Jacobson, 2000). Most fungi produce melanin, and it is thought to play an essential role in adapting to changing environments providing a defensive barrier to external conditions, to UV light (Jacobson, 2000; Krishnan *et al.*, 2018). For some phytopathogenic fungi, melanisation is essential for invasion allowing the build-up of turgor pressure within appressoria for directly penetrating through the leaf surface (Jacobson, 2000). However, *Z. tritici* is lacking many of the genes considered necessary for appressoria formation (Goodwin *et al.*, 2011). While *Z. tritici* does not appear to form an appressorium, it does produce melanins (Cairns & Meyer, 2017; Krishnan *et al.*, 2018; Lendenmann *et al*., 2014). Lendenmann *et al.*, (2014) identified 16 candidate genes, via a QTL analysis on progeny from a cross between low and high pigmented parental isolates, likely to affect melanisation. One of these was polyketide synthase 1 (*Pks1*), a gene known to play a role in synthesising dihydroxynaphthalene (DHN) melanin. Krishnan *et al*., (2018) studied the identified *Pks1* gene cluster in *Z. tritici* and observed differential regulation of the transcription factor *Zmr1,* which controlled the expression of the melanin biosynthetic gene cluster. Although pycnidia are melanised structures, DHN melanin production was not essential for virulence, as ΔZtPks1 was shown to generate non-melanised pycnidia at the end of its otherwise normal infection cycle (Krishnan *et al.*, 2018; Derbyshire *et al*., 2018).

1.9.5 Extracellular hydrolytic enzymes

The *Z. tritici* genome reveals a reduced overall number of genes encoding cell wall degrading enzymes (CWDEs) genes than would be expected for typical hemibiotrophic or necrotrophic fungi (Goodwin *et al.*, 2011). The reduced number of genes encoding carbohydrate-active enzymes (CAZymes) highlighted that *Z. tritici* has only a few cellulases, xylanases or xyloglucanses compared to other cereal pathogens (e.g. *Parastagonospora nodorum* and *M. oryzae*). It has been suggested that this might reflect its

apparent intercellular, rather than intracellular, lifestyle (Goodwin *et al.*, 2011; Orton, 2012). Goodwin *et al.*, (2011) posit that this may be an evolutionary adaptation that allowed the fungus to avoid detection and thus evade plant defences during the latent phase by preventing the generation of DAMPs. Furthermore, Goodwin *et al.*, (2011) point to a similar reduction of CWDEs in *Laccaria bicolor*, an ectomycorrhizal fungus suggesting that the nutritional lifestyle of *Z. tritici* may have initially been endophytic.

Conversely, compared to other fungal pathogens of wheat, *Z. tritici* has a larger repertoire of predicted secreted protease encoding genes (Goodwin *et al.*, 2011). It is thought that this is also part of the 'stealth' pathogenicity of *Z. tritici*, enabling the fungus to use alternative nutrition sources that do not require cell wall attack (Rudd *et al.*, 2015). In support of this idea, RNA-seq data displayed an increase in the expression of protease encoding genes peaking in the transitory phase at the onset of necrotrophy. Levels then began to fall into this category and were finally replaced by a limited set of CWDEs, then upregulated (Goodwin *et al.*, 2011; Rudd *et al.*, 2015). These data suggest different nutrient source acquisition and mobilisation, spanning and extending into the necrotrophic growth phase.

1.9.6 Secondary metabolites

Fungal secondary metabolites can be divided into four main classes: polyketides, non-ribosomal peptides (NRPs), terpenoids and tryptophan derivatives (Muria-Gonzalez *et al*., 2015; Pusztahelyi *et al*., 2015). These compounds are typically low molecular weight, have many different functions and are not generally regarded as essential for life per se. However, certain toxins and secondary metabolites are critical for certain fungal pathogens to cause disease. Toxins can, therefore, be considered virulence factors if the toxin is required for the invasion and induction of disease in the host (Yoder, 1980). For example, *Fusarium graminearum* is a major global fungal phytopathogen that produces several mycotoxins. These include trichothecene derivatives (e.g., DON) which are responsible for reducing crop yield and quality, as well as polyketides such as zearalenone (ZEA) and

fusarin C (Marasas *et al*., 1984; Desjardins, 2006; Summerell & Leslie, 2011). Phytopathogenic fungi produce toxins defined as either host selective (HST) or nonspecific toxins. HSTs are toxic only to host plants (or select host plant cultivars) of the toxin-producing fungus, while nonspecific toxins can affect even non-host plants when applied exogenously.

Very few specific secondary metabolites have been determined for *Z. tritici* though many putative gene clusters likely to generate metabolites have been identified (Muria-Gonzalez *et al*., 2015; Duba *et al.*, 2018). Cairns & Meyer (2017) carried out comparative genomic experiments that identified three putative phytotoxin biosynthetic clusters in the genome of strain IPO323. This indicated that *Z. tritici* might produce an epipolythiodioxopiperazine, a polyketide (PKS) with structural similarities to fumonisin, and a non-ribosomal peptide (NRPS) with similarities to another Dothideomycete fungus *Alternaria alternata* AM-toxin. Expression studies on infected plants have identified several upregulated secondary metabolite clusters that coincide with lesion formation; however, functional studies have failed to provide evidence for them producing molecules that evoke the disease transition (Derbyshire *et al*.,2018).

1.9.7 Putative *Z. tritici* toxins

Other candidate molecules exist for potential plant cell death-inducing toxins above and beyond secondary metabolites. A family of proteins that cause plant necrosis have been identified and characterised in several plant pathogens, including *Z. tritici*, which are now referred to as the Necrosis and Ethylene-inducing Peptide 1 (NEP1)-like (NLP) proteins (Kettles & Kanyuka, 2017; Gijzen & Nürnberger, 2006). While NLPs usually occur in large families in oomycetes and as smaller multigene families in many pathogenic fungi, *Z. tritici* has only a single NEP1-like protein, ZtNLP (published as MgNLP). This protein induced typical defence-related responses and cell death on the leaves of dicotyledonous plants. However, it could not elicit this response in wheat and KO strains were able to cause disease (Motteram *et al.*, 2009). The function of this protein in *Z. tritici* is thus a mystery though Motteram *et*

al., (2009) point out that, as for all NLP's, there is no evidence for their ability to cause cell death in monocots suggesting that they may target other organisms in the infection zone. Two other putative necrosis-inducing "toxic" proteins, ZtNIP1 and ZtNIP2, were identified by Ben M'Barek *et al.*, (2015). These effectors induced chlorosis and necrosis, seemingly dependent on the wheat cultivar, suggesting an interaction with host susceptibility factors which agrees with observations made in *P. nodorum* and *P. tritici-repentis* (Ben M'Barek *et al.*, 2015; Kettles & Kanyuka, 2016; Tan *et al.*, 2015). Mirzadi Gohari *et al.* (2015) identified a cerato-platanin protein, ZtCP (SSP70), previously implicated in other fungal phytopathogens as either a phytotoxin or PAMP that triggers host defence mechanisms. However, knock-out strains of ZtCP did not display attenuated pathogenicity (Mirzadi Gohari *et al.*, 2015). Overall, combined with the analysis of secondary metabolite clusters, there are still no compelling leads on toxins' identity (or existence) that might affect the switch to necrotrophic colonisation of wheat leaves.

1.9.8 Transport processes

Transporters are essential proteins that enable living cells to control molecules that move between their cytoplasm and the external environment (Law *et al*., 2008). Fungi can use these proteins to accumulate nutrients from the environment, secrete compounds that can manipulate their local environment or interact with neighbouring microbes. For fungal pathogens capable of producing toxins, transporters provide a mechanism of delivery out of the cell into the environment (Cavalheiro *et al*., 2018; Del Sorbo *et al*., 2000; Schoonbeek *et al*., 2002).

ATP-binding cassette (ABC) superfamily transporters are a large protein family known to transport a variety of hydrophobic compounds against concentration gradients, the energy for which comes from ATP hydrolysis (Schoonbeek *et al.*, 2002; Stergiopoulos *et al.*, 2003). Due to the requirement for ATP for transport, ABC transporters are classed as active transporters. Five ABC transporter genes were characterised and cloned from *Z. tritici* are coded ZtAtr1, ZtAtr2, ZtAtr3, ZtAtr4, and ZtAtr5 (published as MgAtr1,

MgAtr2, etc.). Stergiopoulos *et al.*, (2003) demonstrated that disruption of *MgAtr4* resulted in a significantly reduced virulence on susceptible wheat cultivars compared to control strains. ZtAtr4 was involved in protecting the fungus against fungitoxic compounds produced by the host. High homology between Abc1 in *M. oryzae* and ZtAtr4 and the similar phenotypic effects of disruption suggest a similar function in other cereal infecting fungi (Stergiopoulos *et al.*, 2003; Urban *et al.*, 1999).

Major facilitator superfamily (MFS) transporters are linked to the movement of small molecules in response to ion gradients (Law *et al*., 2008). These transporters play an essential role in toxin export and multidrug resistance (MDR) and growth under stress conditions in many fungi (Law *et al*., 2008; Vela-Corcía *et al*., 2019; Wang *et al*., 2018; Wirsching *et al*., 2000)**.** In *Z. tritici* Roohparvar *et al*., (2007) and (2008) identified and analysed the function of ZtMfs1 (published as MgMfs1). This MFS transporter was found to share homology to DHA14 configuration transporters implicated in toxin export and MDR. Furthermore, their results indicated that ZtMfs1 was not involved in virulence against wheat but does act as a multidrug transporter, particularly against strobilurin fungicides.

1.9.9 Virulence and avirulence effectors

Currently characterised effectors in phytopathogenic fungi share some structural features. These have been used to identify other candidate effectors, spinning a new analysis pipeline called “effectoromics” (Domazakis *et al*., 2017; Mirzadi Gohari *et al*., 2015). They are generally considered virulence factors, although single-gene deletions often fail to reveal these functions, perhaps due to functional redundancies. Fungal effectors are often small proteins containing numerous cysteine residues and an N-terminus signal peptide to allow extracellular secretion. They are generally thought to, and have in some cases been shown to, can modify host plant physiological and morphological processes to assist infection (Lo Preseti *et al.*, 2015). However, some effectors can be recognised by plant disease resistance

genes, thereby protecting plants, and in this case, they are considered to be avirulence genes

An example of a ‘virulence’ effector that allows *Z. tritici* to evade host recognition is the broadly conserved Lysin domain-containing (LysM) effector proteins, 3LysM which, as previously mentioned, functions to sequester chitin fragments of fungal cell walls (Marshall *et al.*, 2011). 3LysM shares homology with other secreted LysM effectors, such as Slp1 in *M. oryzae* and Ecp6 in *Cladosporium fulvum* (de Jonge *et al.*, 2010; Mentlak *et al.*, 2012). In their study, Marshall *et al.*, (2011) identified a novel function in two candidate-secreted LysM proteins of *Z. tritici*, Mg1LysM and Mg3LysM, not observed in the homologs CfEcp6 and MoSlp1, in protecting developing fungal hyphae against plant-derived chitinases.

Zhong *et al.*, (2017) identified *AvrStb6* as the first validated avirulence gene with a gene-for-gene interaction against wheat cultivars in *Z. tritici*. This was achieved by combining quantitative trait locus mapping with a genome-wide association study. AvrStb6 is a small, cysteine-rich, secreted protein that, by some currently unknown process, interacts and triggers host-resistance in wheat cultivars containing Stb6, a conserved wall-associated receptor kinase (WAK)-like protein (Saintenac *et al.*, 2018; Zhong *et al.*, 2017). Stb6 recognition strongly hinders infection progress, effectively preventing the induction of necrosis (Kema *et al.*, 2000; Zhong *et al.*, 2017). AvrStb6 is highly polymorphic, located near telomeres which are genomic hotspots of recombination, and is under strong diversifying selection, likely due to the widespread use of *Stb6* containing wheat lines (Brunner & McDonald, 2018; Zhong *et al.*, 2017). However, the function of this Avr remains elusive as it does not appear to interact with Stb6 directly, and it is also not a significant virulence determinant when deleted.

A second avirulence gene, *Avr3D1*, identified by Meile *et al.*, (2018), is also described as highly polymorphic and recognised by wheat cultivars with either *Stb7* or *Stb12* resistance genes. However, Avr3D1 recognition does not prevent lesion formation or pathogen reproduction though there is a

dramatic reduction in infection, suggesting it confers a quantitative rather than qualitative resistance (Meile *et al.*, 2018). Finally, another *Avr* gene, *AvrStb9*, was recently cloned by Marcel *et al*., (2019). *AvrStb9* encodes a putative secreted protease containing ClpP/crotonase-like domain and was found by a genome-wide association study (GWAS) with *Z. tritici* isolates pathotyped on the wheat cultivar Soissons. Marcel *et al*., (2019) observed a gene-for-gene relationship between *AvrStb9* and *Stb9* by phenotyping using *Z. tritici* transformants, with either the virulent or avirulent *Avr* allele, on near-isogenic wheat lines carrying a resistant or susceptible allele at *Stb9*.

1.10 Research Objectives

It is clear from the above sections that the full repertoire and diversity of genes and processes which underpin the virulence of *Z. tritici* on wheat remain relatively poorly understood. This research aims to build upon this knowledge base and identify novel genes that underpin virulence in the fungal wheat pathogen *Z. tritici*. I will describe results from a “mutagenomics” forwards genetics-based approach. To recap, a mutagenomics approach involves identifying a phenotype of interest from a mutagenised library of isolates, which can reveal the genetics putatively behind said phenotype upon whole-genome re-sequencing. This approach was first mentioned in literature by Penna & Jain (2017) and was recently utilised in the model plant *Arabidopsis thaliana* (Hodgens *et al*., 2020).

The specific objectives of this research are:

1. To test existing mutagenised collections of *Zymoseptoria tritici* strains to identify individuals affected in pathogenicity on wheat and/or with any associated hyphal growth and stress defects.

2. To re-sequence the genomes of the strains identified in (1) and to determine the global mutational landscape, and identify and prioritise candidate genes.

3. To functionally validate the best candidates arising from (2) and to provide new insights into key elements of the pathogens' ability to cause STB disease on wheat.

2 Materials and Methods

2.1 Acknowledgements

Wendy Skinner produced the *Z. tritici* restriction enzyme mediated-integration mutant collection. Juliette Motteram generated the random *Agrobacterium tumefaciens* mediated-transformation mutant library. Hongxin Chen and Jason Rudd gave access to pangenome resources utilised during the bioinformatic analyses. Chris Stephens assisted in the initial *in planta* and *in vitro* screening of the REMI mutant isolates whilst undertaking a rotation in the Rudd laboratory. The bioimaging team, Eudri Venter and Hannah Walpole, prepared the samples for imaging and generated the scanning electron microscopy (SEM) images.

The statistical analyses and bioinformatics work was performed with resources and support from the teams at Rothamsted Research. Suzanne Clarke, consulted on the statistical analysis of pAN7-1 plasmid integration sites in Chapter Four. Rob King assembled the L951 reference genome before the onset of this work (unpublished) in Chapter Four. In the REMI mutant re-sequencing project, Dan Smith performed the genome mapping and identified the integration sites of the pAN7-1 plasmid and the untagged effects. Rob King performed a similar analysis for determining the location of T-DNA insertions in the IPO323 random ATMT mutant library before the onset of my work. Dan Smith also aided in the analysis of an RNA sequencing experiment detailed in Chapter Six.

2.2 Materials and Chemicals

2.2.1 Growth media

Depending on experimental requirements, bacterial and fungal cultures were grown either on agar media or in liquid broth. All growth medium was sourced from Formedium (UK) unless stated otherwise. Luria-Bertani (LB) broth/agar were used to culture bacterial strains; LB Miller for *Escherichia coli* and LB Lennox for *Agrobacterium tumefaciens*.

Yeast peptone dextrose (YPD) broth/agar was used to culture *Zymoseptoria tritici* for complete nutrition. Tap water agar (TWA), made using 1% w/v agarose in distilled water and autoclaved, was used to grow *Z. tritici* on a minimal media.

In fungal growth stress assays H_2O_2 (Sigma Aldritch), Sorbitol (Sigma Aldritch), and Calcofluor White (Cyanamid).

2.2.2 Fungal strains

Stocks of fungal strains were stored as conidial suspensions in 50% glycerol at -80°C. All strains are cultured in darkness except when stated otherwise.

The parental *Z. tritici* strain for the random ATMT mutant library was IPO323, and an IPO323Δ*KU70* isolate was used for the targeted knockout experiments. The parental strain for the REMI mutant library was L951. The relevant strains/isolates were used as controls to test mutants against.

A range of media was used to compare *in vitro* growth phenotypes of *Z. tritici*. For yeast-like growth, yeast peptone dextrose (YPD) agar for 4-7 days at 16˚C. *In vitro* conidial spores were suspended in 0.01% tween20 water and spot-inoculated onto tap-water agar (TWA) plates for inducing filamentous growth. To yield higher quantities of tissue for DNA/RNA extraction, *Z. tritici* isolates were inoculated into shake flask cultures containing YPD broth. Leurin broth (LB) Miller, LB Lennox, and *Aspergillus nidulans* minimal medium were used during fungal transformation experiments.

2.2.3 Bacterial strains

Electrocompetent *Agrobacterium tumefaciens* strain AGL-1 was used in fungal transformations by ATMT. Incubation of *Agrobacterium* strains on agar plates was carried out at 28˚C, unless otherwise stated.

Chemically competent NEB® 5-alpha Competent *E. coli* (High Efficiency) produced by New England Biolabs (UK) were used to bulk experimental plasmids. All *E. coli* strains were incubated at 37˚C unless otherwise stated.

2.2.4 DNA plasmids

pCHYG and pCGEN – both ATMT Ti plasmids (binary vectors) with multi-cloning sites (MCS) were used in this work.

Another relevant plasmid involved in this study is the pAN7-1 plasmid used to generate the restriction enzyme-mediated integration mutants by Wendy Skinner. This plasmid confers hygromycin resistance to stably transformed *Z. tritici* mutant isolates. Diagram and more details in Chapter Four.

2.2.5 Antibiotics

Antibiotics were used to select bacterial and fungal strains with resistance conferred by the resistance markers in the transformed plasmid. See Table 2.1 for antibiotics used and their working concentrations.

Table 2.1 Antibiotics used in this study.

Antibiotic	Working concentration (µg ml^{-1})
Fludioxonil (Fluka)	30
Geneticin (G418) (Sigma Aldritch)	200
Hygromycin (Invitrogen)	100
Kanamycin (Melford)	50
Timentin (Merck)	100

2.3 Growth and Inoculation of Plants

2.3.1 Wheat cultivar and growth conditions

Wheat cultivar cv. Riband was used in inoculation bioassays; approximately 20-30 seeds were sown in seed trays (220 mm x 170 mm) filled with Levington F2+S compost, approximately 1 cm beneath the surface and 1 cm from the long side wall of the tray. Greenhouse conditions were kept at 18˚C with a 16 h light cycle. Experiments were also carried out in a light cabinet (Sanyo MLR 350 Environmental test chamber) maintained with the same

temperature and light cycle conditions. An indication is made as to which was used for each experiment in the relevant section.

2.3.2 Attached wheat leaf bioassay

Wheat leaf inoculation bioassays were carried out as described in Keon *et al.* (2007). All wheat leaf assays used the second leaves of 17–21-day-old wheat seedlings taped adaxial side-up to metallic platforms. Before inoculation, *Z. tritici* spores were grown on YPD agar as described, and suspensions of 1×10^7 spores ml^{-1} were made in 0.01% Tween20 water and applied to the leaf surface using cotton buds with care to avoid accidental wounding of the leaves. After inoculation, the wheat plants were incubated for 72 hours inside clear perspex boxes. This creates a high humidity environment and encourages *Z. tritici* spore germination. They were maintained for 21 days, and symptom development was observed from 10-21 days post-inoculation (dpi) with photographs taken at 14 and 21 dpi.

2.3.3 *In planta* inoculation for scanning electron microscopy (SEM)

To prevent damage to the leaf surface by inoculation with a cotton bud, a different approach was used from the standard attached wheat leaf bioassay. A 0.1% Tween20-water solution with a spore concentration of 1×10^7 spores ml^{-1} was instead paint brush inoculated onto leaf surfaces.

The Rothamsted Research bioimagers, Eudri Venter and Hannah Walpole, performed the scanning electron microscopy following a method used in King *et al*., (2017). Approximately 5mm square regions were cut from samples and attached to aluminium stubs using a 50:50 mixture of graphite:TissueTek. The samples were plunge frozen in liquid nitrogen and transferred to the GATAN ALTO 2100 cryo prep system. Samples were etched and coated in a thin layer of gold. Micrographs were collected using a JEOL 6360 scanning electron microscope at 5kV.

2.4 Molecular Methods

2.4.1 DNA extraction and quantification

2.4.1.1 Genomic DNA from *Z. tritici*

Genomic DNA (gDNA) was extracted from *Z. tritici* using the following protocol. *Z. tritici* blastospores from glycerol stocks were streaked onto YPD plates and incubated for 7 days at 15˚C. Cells were then streaked into a suspension of 50 mls of YPD broth and allowed to grow up to near saturating densities in flasks after 5 days at 20C at 180 rpm. Fungal materials were collected by vacuum filtration, snap frozen and freeze-dried. Next, materials were lysed by adding a small ball bearing and using a Fast Prep-24 homogeniser (4.0 m/sec for 20 sec; MP Biomedicals). 1 ml DNA extraction buffer (Table 2.4) was added to the lysed cells and incubated at 65˚C for 20 min. Next, 350 µl ice-cold ammonium acetate (7.5 M) was added and mixed before incubation on ice for 20 min. Tubes were centrifuged (16,000 g, 15 min), and the supernatant was added to a fresh tube with 900 µl isopropanol. Tubes were incubated (room temperature (RT), 15 min) before centrifugation (16,000 g, 15 min). Finally, the DNA pellet was washed with 400 µl 70% ethanol, recentrifuged (16,000 g, 15 min), and the pellet air-dried and resuspended in 50-100 µl nuclease-free water.

2.4.1.2 Vector constructs bulked in *E. coli*

Binary vector constructs (pCHYG or pCGEN) were bulked up in *E. coli*, and extracted for subsequent use. Colony PCR positive *E. coli* colonies were picked with a sterile pipette tip, transferred to 2 ml LB broth (supplemented with kanamycin), and incubated overnight (180 rpm). Vector extraction from overnight culture was performed using QIAprep Spin Miniprep Kit (Qiagen). Minipreps were carried out using 50 ml overnight bacterial cultures. Protocols described in the Qiagen Plasmid Mini Kits Handbook were followed.

2.4.2 RNA extraction and quantification

For RNA extraction, five inoculated wheat leaves were cut and placed in sterile Falcon Round-Bottom Tubes (14 ml) and snap-frozen in liquid

nitrogen. Total RNA was later isolated from these samples using TRIZOL procedure (Invitrogen) and a polytron homogeniser to disrupt the tissue. The resulting solution was then transferred to 2 ml tubes, vortexed and centrifuged (12,000 g, 10˚C, 10 min). Next, the supernatant was transferred to a fresh 2 ml tube with 150 µl 1–bromo–3–chloropropane (BCP) phase separation reagent (Molecular Research Centre, Inc.) vortexed and centrifuged (12,000 g, 4˚C, 10 min). Finally, the aqueous layer on top was carefully pipetted off into a fresh 2 ml tube, and mixed 1:1 with isopropanol, and samples were vortexed. The RNA samples were incubated at room temperature for 10-15 minutes and once again centrifuged (12,000 g, 4˚C, 10 min) to precipitate. Next, the supernatant was removed, and the pellet was washed in 1 ml 70% Ethanol before re-centrifugation (7500 g, 4˚C, 5 min). This washing step was repeated twice. Afterwards, the supernatant was removed, and the pellet was air-dried before resuspension in 100 µl nuclease-free water. RNA solutions quality was estimated and quantified using a Nanodrop 2000c (ThermoFisher) for samples that required additional clean-up Qiagen RNeasy Mini Kit.

2.4.3 PCR

Primers for polymerase chain reaction (PCR) amplification were designed using Geneious version 10.3.2 (https://www.geneious.com primer design function), and BLASTs were carried out to establish sequence specificity. See Table 2.3 for all primers used in this study. All primers were synthesised by Eurofins Genomics (UK). DNA solutions were quantified using a Nanodrop 2000c (ThermoFisher). PCRs were carried out using a BioRad T100 thermocycler for PCR conditions and reagents (see Table 2.2).

Colony PCR was used to confirm the transformation of *E. coli*, *A. tumefaciens* and *Z. tritici* colonies with correctly assembled vector constructs or check for the insertion of the T-DNA, respectively, following antibiotic selection. A small portion of a colony was picked using a sterile pipette tip and transferred to the PCR mix. PCR products for subsequent analysis by sequencing were purified either using a QIAquick PCR purification kit or QIAquick gel

extraction kit, following the manufacturer's protocol. PCRs for Gibson Assembly reactions were carried out using either Phusion High-Fidelity DNA Polymerase (ThermoFisher), whilst colony PCRs were carried out using Green PCR Master Mix (ThermoFisher).

Table 2.2 PCR conditions used in this study

PCR programme			PCR reaction mix	
Stage	**Temperature (˚C)**	**Time (s)**	**Component**	**Volume (µl)**
Colony PCR				
1	95	300	DreamTaq Green PCR Master Mix	10.0
2	95	30	F primer (10 µM)	1.0
3	55[1]	30	R primer (10 µM)	1.0
4	72	60[2]	Nuclease free water	8.0
5	Return to Stage 2 (X34 repeat)			
Phusion polymerase PCR				
1	98	30	5X Phusion HF Buffer	10.0
2	98	10	10mM dNTPs	1.0
3	68[1]	20	F primer (10 µM)	2.5
4	72	30[2]	R primer (10 µM)	2.5
5	Return to Stage 2 (X34 repeat)		Phusion DNA polymerase	0.5
			Nuclease free water	31.0
			gDNA (>20ng/µl)	2.5

[1]Varies depending on primer T_m. [2]Varies depending on PCR product length (DreamTaq Green, 60 s per kb; Phusion DNA polymerase, 15-30 s per kb).

2.4.4 DNA gel electrophoresis

Gel electrophoresis was used to assess PCR, isolate and purify DNA fragments for use in subsequent protocols, check restriction enzyme digest banding patterns, and determine the presence/absence of specific DNA sequences. In addition, GeneRuler 1 kb DNA Ladder (ThermoScientific) was used to check the fragment sizes.

The typical 1% (w/v) agarose gels were prepared by dissolving agarose powder in 1X Tris/Borate/EDTA (TBE) buffer (National Diagnostics}. Before casting, ethidium bromide (5 µg ml^{-1}) was added to the cooled gel solution.

Cast gels were transferred to a BioRad Mini-Sub Cell GT chamber filled with 1X TBE buffer. DNA was mixed with 6X loading dye (ThermoFisher) and added to wells in the agarose gel. Gels were run at 75-100 volts (V) for 1 h, or until the dye front reached the bottom of the gel. Gels were then imaged using a UVP UVsolo touch imager (Analytik Jena AG, Germany). For gel extraction, gels were observed on a UV transilluminator (Clare Chemical), and DNA bands were cut out of the gel using a scalpel blade. DNA bands were then purified using a QIAquick gel extraction kit (QIAGEN), following the manufacturer's protocol.

2.4.5 RNA integrity gel

RNA integrity was tested on a 1.2% agarose gel with agarose powder dissolved in 1X TBE buffer. An aliquot of 4 µl RNA was added to 13 µl formamide solution, 1 µl ethidium bromide and 2 µl 6X loading dye, and incubated in a thermocycler at 65˚C for five minutes, then placed on ice for two minutes before loading into the agarose gel. The gels were run for 60 minutes at 80 V, then imaged using a UVP UVsolo touch imager.

Table 2.3 Primers used in this study.

Primer name	DNA Sequence (5' > 3')	Experimental use
cSSK2-Fwd	aattcctaggccaccatgttgggccTAAAAGTGCCCAAAGTCC	Complementation construct for SSK2 in 4-124 and 4-158
cSSK2-Rev	ggtggagtgaggggtaccgagctcgGTCCTGTCTCTCTTGTGAGAC	
87913_Fwd	aattcctaggccaccatgttgggccGAATCCTTGCATGAAACC	Complementation construct for "87913" in 15-120
87913_Rev	ggtggagtgaggggtaccgagctcgAGCATGTGAAGTGGAGTG	
76651_Fwd	aattcctaggccaccatgttgggccGCCTGTTGGATATCTGCAG	Complementation construct for "76651" in 5-51
76651_Rev	ggtggagtgaggggtaccgagctcgCTTGGCGATTGATTCCTC	
36895_Fwd	aattcctaggccaccatgttgggccAAGGTTCGGTATCCCATCG	Complementation construct for "36895" in 15-120
36895_Rev	ggtggagtgaggggtaccgagctcgAAATACAAGCTGCGCCGC	
cL951_01t07445-Fwd	aattcctaggccaccatgttgggccAGCTCATGTAGCTCTGTCG	Complementation construct for L951_01g07445 in REMI A
cL951_01t07445-Rev	ggtggagtgaggggtaccgagctcgTCTATGGACATGCACTGG	
cL951_01t03851-Fwd	aattcctaggccaccatgttgggccTGGCAGGTCGTACTTAACAG	Complementation construct for L951_01g03851 in REMI B
cL951_01t03851-Rev	ggtggagtgaggggtaccgagctcgGTTGTTCCGTGATCGCTG	
cL951_01t027137-Fwd	aattcctaggccaccatgttgggccACCATTCCAGGCCAGCCG	Complementation construct for L951_01g027137 in REMI C
cL951_01t027137-Rev	ggtggagtgaggggtaccgagctcgCACAGTGGTAATGTGCAAAGATCTG	
cL951_01t06093-Fwd	aattcctaggccaccatgttgggccGGGTGATGAGAAGAAGATG	Complementation construct for L951_01g06093 in REMI D
cL951_01t06093-Rev	ggtggagtgaggggtaccgagctcgTAGCAACTACCGTGGCAAC	
cL951_01t20577-Fwd	aattcctaggccaccatgttgggccGACATGAGGAGAGCGAAG	Complementation construct for L951_01g20577 in REMI E
cL951_01t20577-Rev	ggtggagtgaggggtaccgagctcgGAATAGATGACAGACCCTATCG	
cL951_01t08983-Fwd	aattcctaggccaccatgttgggccCACTGTCTACTCATACACAGCC	Complementation construct for L951_01g08983 in REMI F
cL951_01t08983-Rev	ggtggagtgaggggtaccgagctcgGCTGCCGTATATCTTGAG	
cL951_01t26261-Fwd	aattcctaggccaccatgttgggccTCCATTCTAGGTTCCTCTCACATC	Complementation construct for L951_01g26261 in REMI I
cL951_01t26261-Rev	ggtggagtgaggggtaccgagctcgCTGTCCCCGGTTTCTTGC	

Primer name	DNA Sequence (5' > 3')	Experimental use
cL951_01t25689-Fwd	aattcctaggccaccatgttgggccTCAGGGTATCAACCACGC	Complementation construct for L951_01g25689 in REMI J
cL951_01t25689-Rev	ggtggagtaggggtaccgagctcgCGACTATGTACTGGGATTCG	
cL951_01t25589-Fwd	aattcctaggccaccatgttgggccGCCGCTTCTATTTGTGCTC	Complementation construct for L951_01g25589 in REMI L
cL951_01t25589-Rev	ggtggagtaggggtaccgagctcgCAATTCGCATTTGCAACAG	
cL951_01t04653-Fwd	aattcctaggccaccatgttgggccGCCCTGCGGCTGTTGGAG	Complementation construct for L951_01g04653 in REMI M
cL951_01t04653-Rev	ggtggagtaggggtaccgagctcgGTCTGCTCCTTCTGGCAACCC	
cL951_01t02957-Fwd	aattcctaggccaccatgttgggccGTGGAACTTGCCGACGTC	Complementation construct for L951_01g02957 in REMI N
cL951_01t02957-Rev	ggtggagtaggggtaccgagctcgATTGGCGTTAGGTTTCCTTC	
Mini-01t07445-Fwd	TCGTATCTCCGGACCCAAGT	Mini-prep test primers for 01t07445
Mini-01t07445-Rev	CCGGTCGCTCTCATCTCTTC	
Mini-01t08983-Fwd	TGTTGTCCATAGCCACCACC	Mini-prep test primers for 01t08983
Mini-01t08983-Rev	GCAAACGCAAACACACAAGC	
Mini-01t26261-Fwd	ACCTCACTCTCCTACGCCTT	Mini-prep test primers for 01t26261
Mini-01t26261-Rev	ACCATCCCTTCGTCCTCTCA	

2.4.6 Cloning and Gibson Assembly

Gibson assembly is a robust exonuclease-based method to assemble DNA in a specified order based on sequence overlaps between fragments. The ATMT compatible plasmid vectors are cut with a pair of restriction enzymes to linearise and create a set of differing overhangs. Then, each required fragment is amplified by PCR using primers containing 5' overhangs overlapping with the neighbouring fragments from gDNA. Primers used in construct building for Gibson assembly were designed using the NEBuilder tool (https://nebuilder.neb.com/), listed in Table 2.2. The plasmid was assembled following the Gibson Assembly® Protocol (E5510) and reagents produced by NEB. The generated transformation plasmid was verified by restriction digest using colony PCR of transformed *E. coli* ahead of miniprep.

2.5 Transformation and Mutagenesis

2.5.1 Transformation of *Escherichia coli* for vector construct bulking

The manufacturer's protocol for transforming chemically competent cells NEB® 5-alpha Competent *E. coli* (High Efficiency, DH5α) was followed. 200µl of DH5α were thawed on ice (20 minutes) before the addition of 1µl of the vector. The cells were then heat shocked at 42˚C for 30 seconds before placing on ice. 250µl of S.O.C. medium (Super Optimal broth with Catabolite repression) was added and incubated with shaking at 37˚C for 1 hour. The cells were then spread onto LB Miller agar plates containing the appropriate antibiotic for the vector (50 µg ml^{-1} of kanamycin) and left overnight to incubate at 37˚C.

2.5.2 Construct miniprep

In 10 ml of LB with 50 µg ml^{-1} of kanamycin, an *E. coli* colony picked from the LB Miller agar, was grown overnight at 37˚C. First, the culture was spun down for 2 minutes at 3,000 g; then, the supernatant was discarded, leaving the bacterial pellet. The vector was then isolated from the bacteria using QIAprep

spin miniprep kit (Qiagen) eluting in 30 µl of nuclease-free water. The concentration of the vector was measured and then stored at -20˚C.

2.5.3 Transformation of *Agrobacterium tumefaciens*

To transform the electrocompetent AGL-1 cells, 1 µg plasmid DNA was pipetted into a 50 µl aliquot of AGL-1 cells and added to cool electroporation cuvettes. The mix was electroporated on the default Agro setting on a BioRad Micropulser. 1000 µl LB Miller broth if added to the cuvettes and pipetted up and down to mix before transfer to a 15 ml falcon tube. They were then incubated at 28˚C for one hour in a shaker incubator at 220 rpm. 100 µl was then spread onto LB Miller agar amended with Kanamycin to select for successfully transformed *A. tumefaciens*, plates sealed with parafilm and incubated at 28˚C for three days. Stocks in 50% glycerol are stored at -80˚C.

2.5.4 *Agrobacterium*-mediated transformation of *Zymoseptoria tritici*

Agrobacterium-mediated transformation of *Z. tritici* was carried out following a protocol first described by (Zwiers & De Waard, 2001). Stock solutions labelled A-D are listed in Table 2.4 (page 46). First, 50 ml of stocks A-C and 1 ml of stock D were added to 800 ml distilled water (dH_2O), and the volume of the resulting solution volume was adjusted to 1 L with dH_2O; this solution is referred to as completed stock. Additionally, “20X salts” and “trace elements” are made (Table 2.4).

To obtain enough bacterial cells for fungal transformation, *A. tumefaciens* strains were grown for 24 hours in LB mannitol. Immediately preceding transformation *A. tumefaciens* strains were grown in an induction medium (IM). IM was amended with kanamycin and acetosyringone. During transformation, *Z. tritici* spores and *A. tumefaciens* cells are co-cultivated on IM agar with acetosyringone added after autoclaving atop cellophane discs. In the complementation, of an adenine auxotrophic mutant, 0.1 mM adenine solution was added to the IM agar. After co-cultivation, *A. tumefaciens* and *Z. tritici* cultures, the discs were transferred to *Aspergillus nidulans* minimal

medium (AspMM) agar, which was amended with hygromycin, geneticin and timentin to select for transformant *Z. tritici* colonies and kill the remaining *A. tumefaciens* cells respectively.

The *Z. tritici* mutant to be transformed was inoculated onto YPD plate amended with hygromycin six days before the transformation; from these cultures a spore suspension of between 10^6 and 10^7 spores ml^{-1} was prepared in IM. *A. tumefaciens* strains harbouring the constructs were inoculated from glycerol stocks onto kanamycin-selective LB plates and incubated for three days before transformation. Cells from these plates were used to inoculate 40 ml kanamycin-amended LB. After incubating for 18 h, 2 ml of the overnight cultures were centrifuged at 10,161 x g for two minutes. The resulting bacterial pellets were washed in 400 µl IM + acetosyringone. After re-pelleting, cells were suspended in 1 ml IM + acetosyringone and kanamycin. The resulting bacterial suspensions were diluted with the amended IM to obtain an OD_{600} of 0.15. Bacterial cultures were then left to grow typically for 3 h until they reached an OD_{600} of 0.2-0.24.

Whilst bacterial cultures were growing; sterile cellophane discs were placed onto IM plates amended with acetosyringone. To spread discs flat to the surfaces of plates, an empty plate containing IM+acetosyringone was used to dip the cellophane disc into using sterile forceps and spreaders to place and adjust the position of the disc. These plates were allowed to dry before the next steps. 100 µl *A. tumefaciens* culture and 100 µl *Z. tritici* spore suspension per IM plate were mixed, and an additional 1 µl acetosyringone stock solution was added. 100 µl of the mixtures were then plated out five plates per strain and incubated for 72 h. In addition to the *A. tumefaciens* co-cultivations, a single plate was spread with 100 µl *Z. tritici* spore suspension mixed with 100 µl induction medium and 1 µl acetosyringone used as a negative control and allowed for assessment of background *Z. tritici* growth.

AspMM plates were amended with hygromycin and timentin. Cellophane discs were transferred from IM plates using sterile forceps to AspMM plates after co-cultivation for 48 hours. Before the transfer of discs 300 µl SDW was

spread onto AspMM plates to allow for better adhesion of discs to the plate surfaces. Putative transformant colonies were identified on the surfaces of the discs covering the AspMM plates after 14 days. First, colonies were picked with sterile cocktail sticks onto YPD agar plates amended with hygromycin, geneticin and timentin. Next, glycerol stocks were made from colonies that grew back fully within two weeks of harvesting.

2.6 Protein analysis

To test for the activation of p38 MAPK Hog1 in *Z. tritici* isolates after 6-days post-inoculation in YPD broth with a single 10 µl loop of blastospores from YPD agar (amended with antibiotics where necessary). This step was done to ensure a similar starting level of inoculum through OD measurement using the Nanodrop 2000c (ThermoFisher). After 6-days growth in fresh YPD broth culture, the fungi were spiked with 25 mM H_2O_2. The samples at 30 and 60 minutes after exposure were extracted using vacuum flasks and were snap-frozen, stored at -80˚C ahead of protein extraction.

2.6.1 Protein extraction

A portion of the frozen disc is broken off and transferred to 2 ml tubes with two small ball bearings and freeze-dried using LyoDry Compact Benchtop Freeze Dryer (MechaTech Systems) overnight. To lyse the samples Y-PER™ Yeast Protein Extraction Reagent (ThermoScientific) was added (for 150 mg protein material, 1.5 ml) with Protease Inhibitor Cocktail (100X) (ThermoScientific). A TissueLyserII was used to agitate and homogenise the mixture for 5 min at 20 Hz. The samples were then spun in a centrifuge (14,000 g, 10 min), and the supernatant was transferred to a fresh tube. For storage, 200 µl protein extracts were added to 50 µl 5X SDS loading buffer (see Table 2.4) and kept at -20˚C.

2.6.2 SDS-PAGE

Sodium dodecyl sulphate-polyacrylamide gel electrophoresis (SDS-PAGE) gels separates proteins based on their size. Gels were cast in a Mini-Protean system using 1 mm spacers and glass plates (BioRad). Resolving gels were

prepared at 10% acrylamide, and 4% acrylamide in stacking gel. Cast gels were transferred to a Mini Protean Tetra Cell (BioRad), filled with 1X Tris-buffered saline (TBS) running buffer (Table 2.4). Protein extract was stored mixed with protein loading buffer at -20˚C as described and incubated (70˚C, 10 min). Protein marker ladder (10 µl) or protein sample (25-40 µl) were added to wells of SDS-PAGE gel. Benchmark ladder and MagicMark XP ladder (ThermoFisher) were used.

2.6.3 Western blotting

Following electrophoresis, proteins were transferred from SDS-PAGE gel to nitrocellulose (GE Healthcare, 0.1 µm pore size). A wet transfer method was used with a Mini Trans-Blot cell (BioRad), with transfer at 100 V for 40 min (at 4˚C). Correct transfer to the membrane was assessed by staining with ponceau S solution (0.5% ponceau S, 1% acetic acid) and de-stained with D.I. water. The membrane was washed three times (5 min, RT) in TBS buffer (Table 2.4), before blocking in 5% non-fat milk (Marvel Skimmed Milk Powder) in TBS-Tween buffer (1 h, RT). The membrane was rewashed three times (5 min, RT) in TBS-Tween, before primary antibody blotting (overnight, 4˚C). Anti-p44/42 and p38 blotting was carried out with a 1:1000 dilution of rabbit Anti-p44/42 and p38 antibodies (Cell Signalling) in 5% BSA TBS-Tween buffer. The membrane was rewashed as above in TBS-Tween buffer, before secondary blotting with a 1:10,000 dilution horseradish peroxidase-conjugated goat anti-rabbit antibody (Invitrogen), in 5% non-fat milk TBS-Tween buffer (1 h, RT). The membrane was rewashed as above in TBS-Tween buffer, then dried on a paper towel and treated with a 1:1 ratio mix of ECL reagents (GE Healthcare). The membrane was incubated in the dark (5 min, RT), before removal of excess ECL reagent and imaging using an Odyssey Fc imager (Li-Cor), with a 10 min exposure time. Images were optimised and saved using Image Studio 5.2. Protein loading control was stained using Napthol blue black (also known as Amido Black).

Table 2.4 A list of buffers and stock materials used in this work.

Buffer Name	Components
Extraction buffers	
Z. tritici DNA extraction buffer	250 mM NaCl, 200 mM Tris-HCl, 25 mM EDTA (pH 8.0), 2% sodium dodecyl sulphate (SDS), 5 mM Phenanthroline (PT), 2% Polyvinylpyrrolidone (PVP), 0.5% β-mercaptoethanol[1]
Transformation	
Stock A	Per litre - 10 g $MgSO_4$, 29 g KH_2PO_4, 3 g NaCl
Stock B	Per litre - 40.5 g K_2HPO_4, 10 g $(NH_4)_2SO_4$
Stock C	Per litre - 2 g $CaCl_2$
Stock D	2.5 mg ml^{-1} $FeSO_4$
20X salts	120 g $NaNO_3$, 24 g KCl, 10.4 g $MgSO_4.7H_2O$, 30.4 g KH_2PO_4
Trace elements	22 g $ZnSO_2.7H_20$, 11g H_3BO_3, 5 g $MnCl_2.4H_2O$, 5 g $FeSO_4.7H_2O$, 16 g $CoCl_2.5H_2O$, 11 g $(NH_4)_6Mo_7O_{24}.4H_2O$, 50 g Na_4EDTA. Added to 800 ml dH_20, each dissolved before the addition of next. The resulting mixture was then boiled and left to cool and adjusted to between pH 6.5 and 6.8 with 5M KOH.
Induction Medium (IM)	Per 100 ml - 0.9 ml 20 % glucose, 4 ml 1 M 2-(N-Morpholino) ethanesulfonic acid (MES) pH 5.3, 5 ml 50 % glycerol, remaining volume composed of complete stock.
Induction Agar	Per 500 ml - 2.25 mt 20 % glucose, 20 ml MES, 5 ml 50 % glycerol, 6.5 g agar, remaining volume completed stock. IM plates were amended with 500 µl acetosyringone [200 mM in DMSO] (Sigma Aldritch)
Induction Medium + Acetosyringone	Added 100 µl 200 mM acetosyringone per 100 ml IM
Aspergillus nidulans mimimal media	Per litre - 50 ml 20X salts, 1 ml trace elements, 10 g glucose, adjusted to pH 6.5 with 5M KOH and 1 % agar.
Western running & washing buffers	
5x SDS loading buffer	250 mM Tris-HCl (pH 6.8), 30% glycerol, 10% SDS, 5% β- mercaptoethanol, pinch of bromophenol blue
5X TBS-Tween buffer (pH 7.3)	2 mM Tris-HCl (pH 7.3), 140 mM NaCl, 0.1% Tween-20
10% Resolving gel (10 ml)	3.3 ml ready-made 30% acrylamide soln (Protogel), 2.5 ml 1.5M Tris-HCl pH 8.8, 4.0 ml MQ H2O, 100 µL 10% w/v SDS, 100 µL 10% Ammonium persulphate (APS)[1], 10 µL Temed (SigmaAldritch)[1]
4% Stacking gel (5 ml)	650 µL acrylamide, 1.25 ml 0.5M Tris-HCl pH 6.8, 3 ml MQ H_2O, 50 µL APS[1], 50 µL 10%SDS, 5 µL Temed[1]

Buffer Name	Components
Running Tank buffer (pH 8.3)	6 g Tris base, 28.8 g Glycine, 2 g SDS
Transfer buffer (pH 8.3)	6 g Tris base, 28.8 g Glycine, 2 g SDS, 400 ml Methanol

[1]Added shortly before use.

3 “Resurrection” and phenotypic screening of mutagenised *Zymoseptoria tritici* libraries for reduced virulence strains

3.1 Introduction

The fungus *Zymoseptoria tritici* causes the disease Septoria Tritici Blotch (STB) in wheat (*Triticum aestivum*) and is responsible for major economic losses worldwide. *Z. tritici* has a biphasic infection cycle with an extended symptomless growth phase followed by a switch to a necrotrophic phase when the symptoms of infection begin to show (Goodwin *et al.*, 2011; Steinberg, 2015). The timing of symptom development on susceptible wheat varieties differs slightly between studies. However, the differences between studies may be due to multiple factors, including application technique, experimental conditions, individual *Z. tritici* isolates virulence and wheat host cultivar, and the recently elucidated asynchronous hyphal development (Fantozzi *et al*., 2021).

Z. tritici is a filamentous ascomycete that is strictly apoplastic and is not known to invade host cells. While interactions between the invading fungus and wheat leaf cells are not fully understood, hyphal filament extension from “yeast-like” spores is considered essential for successful leaf infection predominantly through leaf stomates (Mehrabi *et al.,* 2006b; Motteram *et al*., 2011; King *et al*., 2017; Yemelin *et al*., 2017)**.** This switch between growth forms is typical of “dimorphic” fungi, and for *Z. tritici*, it is dependent on nutritional sources and temperature *in vitro* (Rossman *et al.*, 2015). Among the filamentous ascomycetes, this is a unique aspect of *Z. tritici* biology, enabling studies targeting the critical yeast-hyphal growth state switch. Mutations that affect hyphal growth are lethal to most filamentous fungal pathogens, but in *Z. tritici,* these mutants are culturable in their “yeast-like” form on high nutrient media. The failure of yeast-like cells to transition into hyphae, or reduction of overall filamentation, results in reduced virulence on leaves due to less frequent (to no) stomatal penetrations. This limits the capacity for intercellular colonisation or severely delays virulence due to

reduced efficiency (King *et al*., 2017; Mohammadi *et al*., 2020). For this reason, assays that easily identify “switching” mutants are a quick valuable screen for putatively identifying reduced virulence mutants. For *Z. tritici,* the hyphal growth from yeast-like blastospores spores can be induced and monitored following inoculation on the poor nutrient tap water agar (TWA) (King *et al*., 2017).

“Mutagenomics” we define as the combination approach of first introducing random DNA mutations followed by phenotypic screening and whole-genome re-sequencing to identify the causative genetic changes behind an observed mutant phenotype. The use of *Z. tritici* in mutagenomic screening is aided by the ease of its culture *in vitro*, adaptive morphologies and reproducible bioassays *in planta* and *in vitro*. Furthermore, this fungus’ haploid genome is fully sequenced (for IPO323) and, most crucially, is amenable to several mutagenesis methods (Steinberg, 2015). The two mutant libraries, which form the basis of the forward genetic screens described here, were produced using two different methods of fungal transformation. Library **(1)** random *Agrobacterium tumefaciens*-mediated transformation introducing T-DNA (ATMT) in strain IPO323 and **(2)** restriction enzyme-mediated integration (REMI) of plasmid DNA in a previously un-sequenced strain, L951 (described in Chapter Four).

Agrobacterium tumefaciens is a soil phytopathogen that naturally infects plant wound sites and causes crown gall disease via delivery of ‘Transfer DNA’ (T-DNA) into host plant cells through a bacterial type IV secretion system (Michielse *et al*., 2005). During the infection process, the T-DNA, which is localised in a ~200 kb ‘Tumour inducing’ (Ti) plasmid inserts randomly into the host genome and is expressed. ATMT has also been used to transform fungi by co-cultivation in the presence of a phenolic inducer, acetosyringone (Zwiers & De Waard, 2001). A random T-DNA insertion mutant library previously produced in our group by ATMT generated 1,316 stable transformants in the reference genotype IPO323. Initial screening of these suggested that fourteen were in reduced virulence, and four displayed

aberrant hyphal growth. Two mutants from this collection, and the underlying causative genes, have previously been investigated and published. ZtALG2 (published as MgALG2) and ZtGT2 affected fungal transitions into hyphae whilst not impacting yeast-like growth (Motteram *et al*., 2011; King *et al*., 2017). However, previous work has established that, typically, ATMT introduces only one T-DNA per fully sequenced strain (Choi *et al*., 2007; Zwiers & De Waard, 2001).

REMI is based on a PEG–protoplast system. The transformation is performed using a linearised plasmid vector with a restriction enzyme that is thought to enable the plasmid integration into the host genome. The vector integrates into restriction sites in the genome, simultaneously mutating and tagging the affected genomic locus (Mullins & Kang, 2001). This method of fungal transformation was initially established in *Saccharomyces cerevisiae* (Schiestl & Petes, 1991) and has been successfully applied to several fungal pathogens. For example, in the rice blast fungus, *Magnaporthe oryzae*, a collection of 5,538 REMI transformants were generated. Of these, eighteen contained mutations co-segregated with the hygromycin resistance marker (i.e. were tagged), and seven PTH genes were cloned that played a role in pathogenicity (Sweigard *et al*., 1998). In the late 1990's a former PhD student, Wendy Skinner, generated a REMI library of L951 strain *Z. tritici* at the Long Ashton research station using a modified *Ustilago maydis* transformation method described by Hargreaves & Turner (1992) (Skinner, 2001). The REMI procedure requires the generation of fungal protoplasts, which was done using Novozyme 234 (InterSpex Products Inc., California, USA), which is no longer commercially available. The fungal protoplasts were transformed with the pAN7-1 plasmid carrying hygromycin resistance and co-incubation with one of four restriction enzymes (*Bgl*II, *Hin*dIII, *Xba*I and *Xho*I). Skinner performed initial characterisations of the pathogenicity and metabolic capabilities of the *Z. tritici* REMI mutants, but records of which specific isolates exhibited limited pathogenicity were lost. Furthermore, due to the age of these samples, it was unclear whether they would still be viable and suitable for re-examination.

This chapter describes results from the first step in a “Mutagenomic” pipeline, which is the phenotypic characterisation of mutagenized fungal strains. Here I report on the REMI mutant collection's regeneration and characterisation through both *in vitro* and *in planta* screening. A similar process of additional characterisation and validation for the random ATMT mutant library subset. The results presented herein demonstrate that multiple strains were identified from both libraries to have delayed or total loss of virulence on susceptible wheat plants. Some also exhibited hyphal growth defects and altered sensitivity to different stresses. Further characterisation of these strains may enable the identification of specific genes responsible for reduced virulence observed on wheat plants.

3.2 Materials and Methods

3.2.1 Strain collections

Wendy Skinner generated the L951 REMI mutant library and Juliet Motteram generated the IPO323 random ATMT library using vector pCHYG (Motteram *et al.*, 2011). Both libraries are made of strains that should be resistant to the selective agent, Hygromycin B.

3.2.2 *In vitro* culture conditions and fungal strains

The parental *Z. tritici* strain of the restriction enzyme mediated-integration mutants produced by Wendy Skinner is L951, isolated in 1995 from an unsprayed wheat cultivar, Longbow (Skinner, 2001). The L951 strain was provided to Skinner by Hunter *et al*., 1999. The commonly used genomic reference strain *Z. tritici* IPO323, isolated in the Netherlands, is the parental strain for the ATMT collection. Both strains are virulent towards the wheat cultivar Riband.

For all experiments, fungal spores were harvested from 5-6 days old cultures on Yeast extract peptone dextrose (YPD) plates at 16°C. Hygromycin B resistance was conferred for isolates from both the REMI and ATMT mutant libraries by introducing a hygromycin resistance gene cassette as a selectable marker. To ensure that the mutant isolates transformations were

stable YPD was amended with hygromycin at a concentration of 200 µg ml^{-1}.

3.2.3 *In planta* infection assays

Secondary leaves of wheat cv. Riband seedlings grown for 21 days were inoculated with spores of mutant isolates collected from YPD cultures, washed and re-suspended in dH_2O+0.01% Tween 20 to a density of $1x10^7$ spores ml^{-1}. In the initial high throughput screening, two leaves from independent seedlings were attached adaxial side up to metal trays using double-sided tape and rubber bands and inoculated with each strain. A wild type (WT) parental strain was used on each tray to compare the rate of disease symptom development. The later in-depth attached leaf screening with three replica leaves follows the methods listed in Chapter Two.

3.2.4 *In vitro* assays for hyphal growth and stress sensitivity

A range of media was used to compare *in vitro* growth phenotypes of *Z. tritici* mutants. For the following assays *in vitro,* blastospores were grown from glycerol stocks and then collected from 5–6-day YPD amended with hygromycin plates incubated at 16˚C. From these plates approximately $1x10^7$ spores ml^{-1} were suspended in dH_20+0.01% Tween20, spotted as drops of 5 µl and allowed to air dry before being sealed with parafilm.

For yeast-like growth rate assays, growth on YPD agar for 5-6 days at 16˚C, as well as YPD amended with antibiotics, was performed to demonstrate that the transformants were stable. Spore suspensions were spot-inoculated onto 1% tap-water agar (TWA) plates for filamentous growth assays. TWA plates were sealed and kept at room temperature for ten days. Growth was monitored on 2-, 5- and 8-days post-inoculation (dpi). Final photos of hyphal development were taken after ten days.

YPD media was amended with a range of stressors at concentrations used in previous literature for the stress sensitivity assays. A concentration of 200 µg ml^{-1} of calcofluor white was used to induce cell wall integrity stress. To cause oxidative stress, YPD media containing hydrogen peroxide at a

concentration of 5 mM. Finally, for osmotic stress conditions, a concentration of 1 M sorbitol. Both spot inoculated YPD and YPD amended plates were sealed and kept at 16˚C for 5 days. Growth was monitored from 2 dpi, and final photos were taken 5 days post-inoculation (dpi).

3.3 Results

3.3.1 Identification of reduced virulence REMI mutants of *Z. tritici* through strain reconstitution and *in planta* infection assays

Of the 493 REMI L951 mutants generated by Skinner in ~2000, attempts were made to subculture and restock 231 of the *Hin*dIII transformants from their original glycerol stocks. The focus on strains generated using this restriction enzyme was due to the proportion of mutants with disease scores between 0-2 (indicating strongly reduced virulence), initially identified in the first study (see Figure 3.1A). Therefore, I aimed to re-identify the fourteen non-pathogenic (Skinner's disease scores 0) and eight reduced virulence mutants (across Skinner's disease scores 1 and 2) from this collection using *in planta* screening and associated *in vitro* growth tests.

For definitions of non-pathogenic, "reduced" and delayed virulence, and wild type virulence, the following criteria were used. Non-pathogenic isolates did not show any symptoms at 21 days post-inoculation (dpi) on inoculated leaves. Delayed virulence refers to the observation of delayed symptom development compared to the wild type (WT) strain. For example, in the case of some isolates, you may see extensive chlorosis at 21 dpi but little to no necrosis on the leaves. WT virulence isolates are those whose symptom development progresses closely with the control WT strain. Examples of these phenotypes are shown in Figure 3.1B, with the photographs representative of symptoms seen at 21 dpi. Of the 231 mutants I attempted to subculture, 196 were deemed sufficiently viable to be taken forward and were re-screened for altered virulence *in planta*, see Figure 3.1B. In contrast, mutant isolates that would not grow on hygromycin amended media, or generally grew extremely slowly, or melanised early into small hard colonies and were unable to be screened *in planta*.

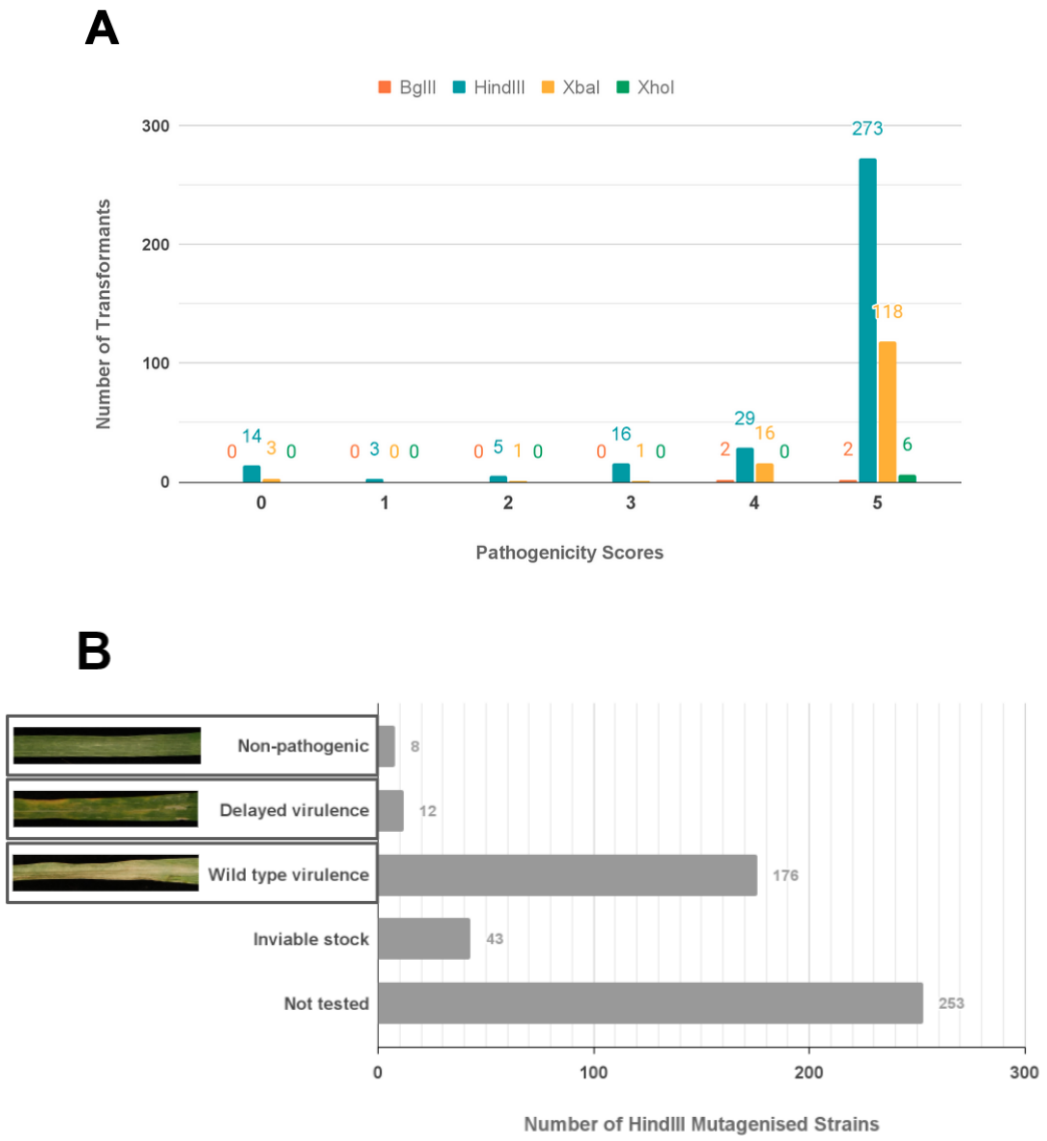

Figure 3.1 Overview of the restriction enzyme-mediated integration (REMI) collection and screening process.

[A] A graph showing the number of REMI mutagenised transformants produced with four different restriction enzymes and their pathogenicity scores as tested against bread wheat cultivar Riband. Scores represented the following, 0 - no symptoms observed, 1 – limited lesions, 2 – large lesions, limited chlorosis, 3 – large lesions, with chlorotic haloes, 4 – senescent leaf, no pycnidia, and finally, 5 – senescent leaf, pycnidia formation (adapted from Skinner, 2001). **[B]** The number of *Hin*dIII REMI mutants re-screened in the current study and their virulence data (where applicable). A high proportion of the mutants tested were culturable, 196 of 231 transformants. The vast majority (176), as expected from the results of Skinner (2001) original screen, were fully virulent against wheat cv. Riband. From the original screen, I was

looking for 22 non-pathogenic or reduced virulence strains. I identified twenty mutants from the high-throughput initial screen, eight non-pathogenic and twelve delayed virulence mutants.

A total of 43 isolates failed to sub-culture on Hygromycin amended agar indicating that they were either inviable (likely due to long term storage) or not genuine stable transformants. Even for those successfully sub-cultured, growth from many stocks varied, and in some cases, mutants were successfully recovered from only a few colonies over long periods. I successfully subcultured 196 isolates, which are now stored at -80˚C as new glycerol stocks. Compared to the control WT strain, visual assessment of the symptom development was used to identify non-pathogenic, delayed virulence and WT virulent *Z. tritici* L951 REMI mutant isolates. In the initial *in planta* screen, 196 strains were tested each against two leaves for their ability to induce STB symptoms. Of the 196, eight were non-pathogenic by 21 dpi, and twelve were delayed in virulence compared to the WT *Z. tritici* strain L951 (Figure 3.2). In addition, a range of disease phenotypes was observed for collecting and photographs of a selection taken at 14 and 21 dpi.

A final number of fifteen isolates were taken for a more detailed study, including replicated plant infection assays. The fifteen were selected from the original 20 based on the most interesting phenotypes (including *in planta* and *in vitro*, described subsequently) and according to the available genomic sequencing budget. This set included strains with a range of delayed and non-pathogenic phenotypes listed in Table 3.1. Figure 3.2, shows the results of the later rounds of *in planta* screening of the fifteen selected mutant isolates against three leaves. These assays generated a range of symptom development phenotypes (Figure 3.2), including two (REMI-161/M and REMI-166/N) that were subsequently reclassified as delayed virulence in addition to the WT REMI-23/E. Aside from providing a transformed mutant control alongside L951 non-transformed control, the ‘WT’ mutant strain was further characterised due to its limited hyphal growth phenotype described in the next section.

Table 3.1 Fifteen REMI mutants selected for further detailed characterisation from the primary two leaf screen.

L951 Mutant Number	Skinner (2001) Original ID	Chp4 Sequencing ID	Virulence on wheat cv. Riband
2	1HR.202	A	Non-pathogenic, 21 dpi
6	1HR.206	B	Non-pathogenic, 21 dpi
10	1HR.210	C	Delayed virulence
11	1HR.211	D	Non-pathogenic, 21 dpi
23	1HR.223	E	WT symptoms
44	1HR.244	F	Non-pathogenic, 21 dpi
45	1HR.245	G	Delayed virulence
67	1HR.117	H	Delayed virulence
89	1HR.139	I	Delayed virulence
90	1HR.140	J	Delayed virulence
109	1HR.159	K	Chlorotic symptoms
121	1HR.171	L	Non-pathogenic, 21 dpi
161	1HR.261	M	Non-pathogenic, 21 dpi
166	1HR.266	N	Non-pathogenic, 21 dpi
169	1HR.269	O	Delayed virulence

Highlighted are the two mutants that were more virulent in subsequent *in planta* screens. This could result from tray-specific effects or increased fitness between the original and later bulked glycerol stocks.

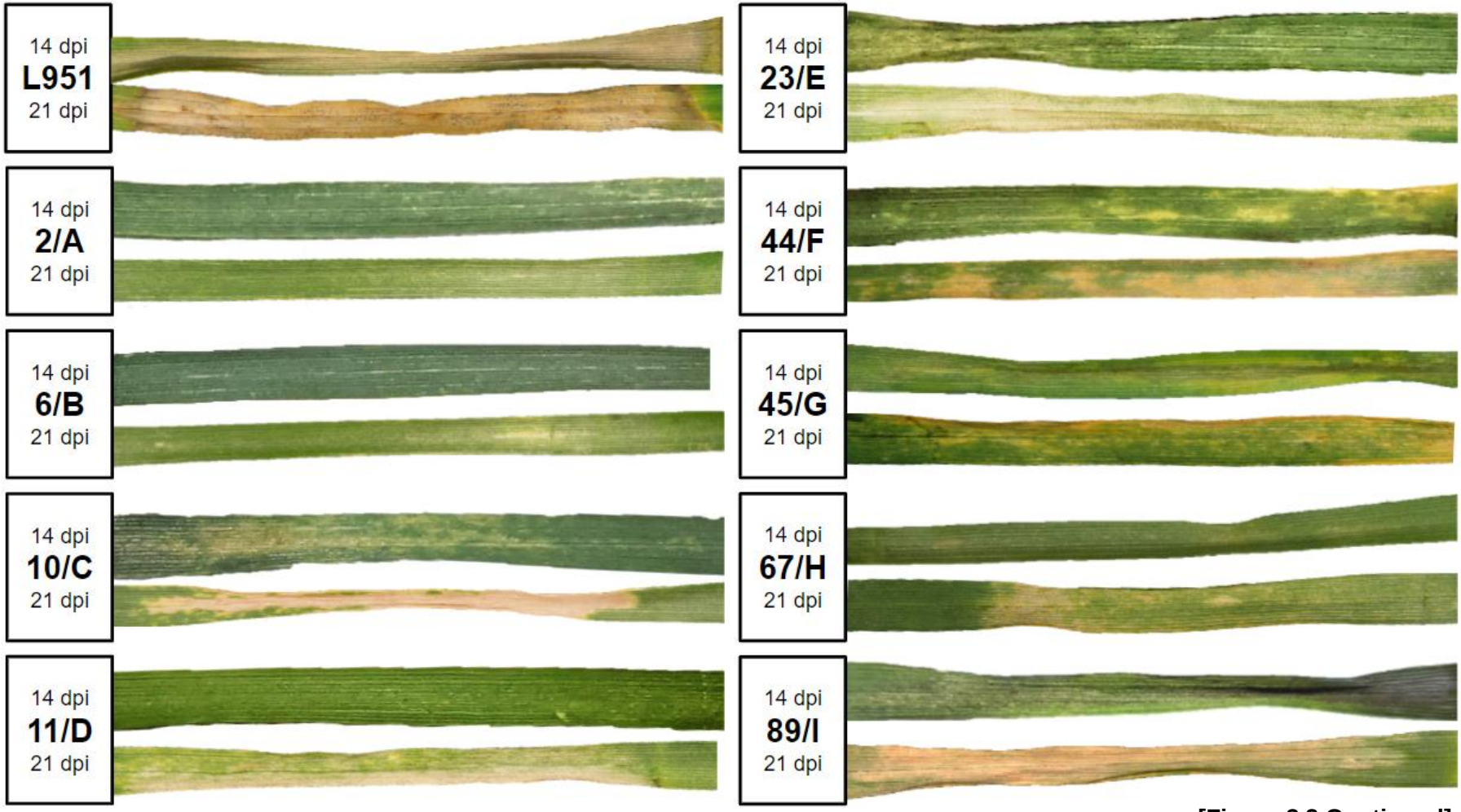

[Figure 3.2 Continued]

[Figure 3.2 Continued]

Figure 3.2 A selection of *in planta* phenotypic screening photographs from the *Z. tritici* L951 *Hin*dIII REMI mutant isolates on wheat cv. Riband.

Images show a representative wheat leaf with typical symptoms from the three replicate inoculated leaves at 14 days post inoculation (dpi) and 21 dpi. The entire leaf surface shown was inoculated via cotton swab with $1x10^7$ spores ml^{-1} solution. Each mutant isolate displayed here were tested a minimum of three times *in planta* on wheat cv. Riband.

3.3.2 Screening the REMI mutants for defective dimorphic switching phenotypes

The importance of the yeast-to-hyphal transition in *Z. tritici* virulence was previously discussed. All fifteen preselected mutant isolates mentioned above were screened for altered hyphal growth switching by spotting 5 µL spore suspensions (1×10^7 spores ml^{-1}) onto solid tap water agar (TWA) at 25˚C. These conditions used in multiple previous studies are believed to mimic the nutrient-poor conditions encountered on the wheat leaf surface (King *et al.*, 2017). In WT strains, the 'spotted' spore suspensions subsequently germinate hyphae that extend radially out from the droplet. Hyphal growth patterns vary between spots, even on the same plate where conditions are consistent. Each mutant isolate described herein was spotted on TWA a minimum of three times, and each plate had a wild type strain to compare with.

The fifteen REMI mutants selected for analysis displayed a range of switching hyphal growth phenotypes, as shown in Figure 3.3. As in previous *Z. tritici* studies, there is an association between a reduction in hyphal growth and reductions in virulence. Limited hyphae describe the most restricted hyphal growth; examples in Figure 3.3 are REMI-2/A, REMI-6/B and REMI-121/L. Reduced hyphal growth refers to mutants that could extend hyphal filaments but were consistently shorter than the wild type (*Z. tritici* L951 strain). Aberrant herein refers to atypical hyphal growth phenotypes compared to the WT strain, examples of those in this category are REMI-67/H and REMI-169/O. Figure 3.3 shows the seven mutants which exhibited either limited or reduced growth, indicating that the mutant's dimorphic switching capacity had been impacted.

Interestingly, one mutant, REMI-23/E, which despite the apparent reduction in hyphal growth, caused WT disease symptoms, as shown in Figure 3.3. However, this was the exception overall, as the remaining hyphal growth mutants also had reduced virulence in previous tests. Of the fifteen, five

mutant hyphal growth phenotypes consistently resembled the WT L951 strain (Figure 3.3, REMI-11, 89, 90, 161 and 166).

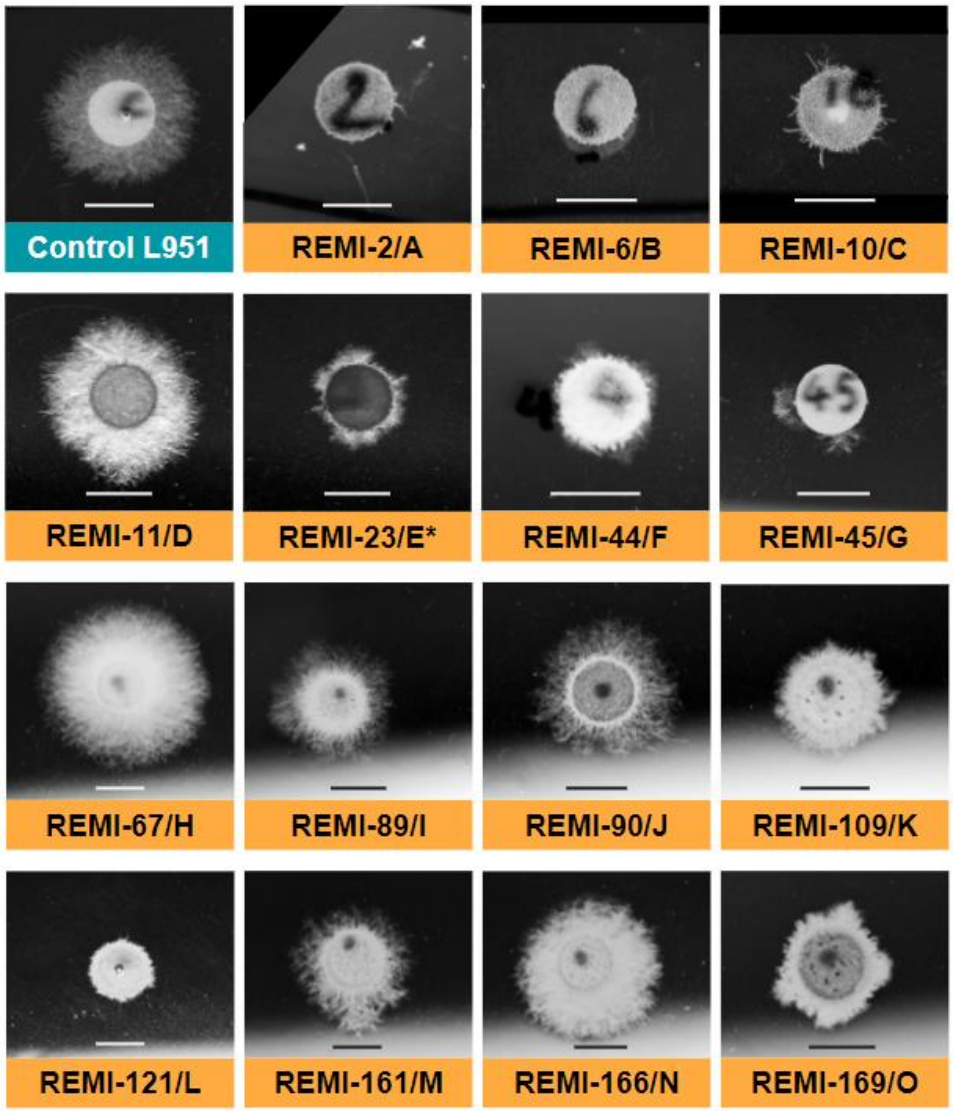

Figure 3.3 The REMI fifteen shows the different hyphal growth phenotypes observed within the 196 screened *Z. tritici* L951 REMI mutant isolates.

Tap water agar is a low nutrient media used to induce hyphal growth, mimicking the low nutrient environment of a leaf surface compared to rich media. For each isolate, 5 µL of 0.01% Tween20-water spore suspensions ($1x10^7$ spores ml^{-1}) were dropped onto solid tap water agar (TWA) at 25˚C. The scale bar on each spot photograph represents 1 cm. The letters (i.e. REMI-2/A) refer to the ID associated with the mutants in sequencing relevant later in Chapter Four. Typical hyphal growth for the parental control strain L951 is shown though there is typically some variation between plates. Limited hyphal growth mutants, such as REMI 2, 6, 10, 23, 44, 45

and 121 are easier to characterise. REMI mutants 67, 109, 166 and 169 have aberrant dense hyphal growth phenotypes. *REMI-23, despite the limited hyphal growth displayed here, is fully virulent *in planta*.

Some mutants with reduced macroscopic radial hyphal growth also exhibited dense or hyper branching filaments that were visually inspected and identified under the microscopic inspection of samples (Figure 3.4). These were already visible four days post-inoculation using a light microscope (Zeiss, West Germany). However, these observations were not consistent across biological replicates in some cases. This is also true for the WT strain L951, which varied in the radial growth pattern and hyphal morphology between replicates. However, Figure 3.4 shows that the branching in REMI-45 was reproducibly and substantially different to WT, manifested in the appearance of multi-conidiated short hyphal filaments.

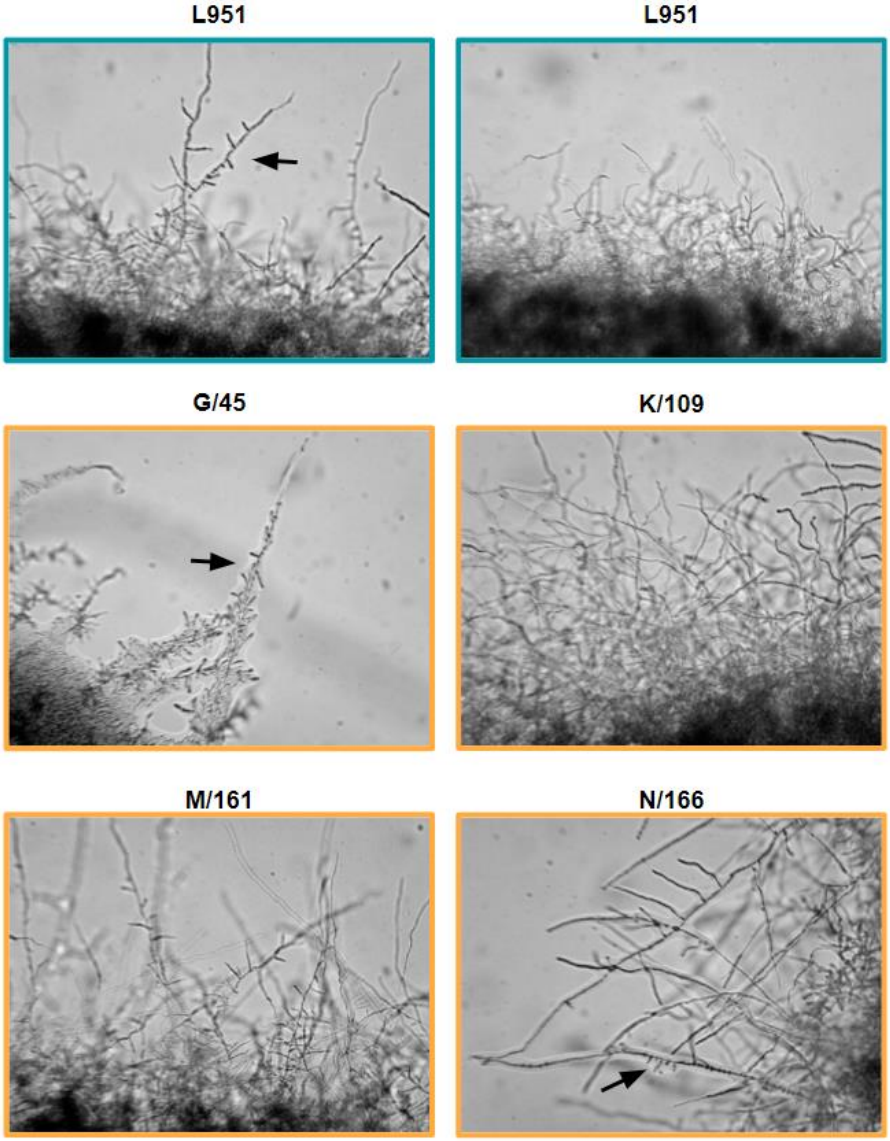

Figure 3.4 Visual inspection of dense/hyperbranched *in vitro* hyphal growth mutants from the REMI fifteen at four dpi.

For each isolate, 5 µL of 0.01% Tween20-water spore suspensions ($1x10^7$ spores ml^{-1}) were dropped onto solid TWA at 25˚C. L951 WT hyphal extension varies spot-to-spot. However, the two photographs outlined in blue are broadly representative of typical growth observed at four dpi. The black arrows point out conidial branching regions. Comparing L951 to REMI-G/45, the mutant only appeared to generate branches with these multi-conidiated short filaments. In REMI-K/109 the filamentous growth is consistently more dense even at this early stage of growth *in vitro*.

3.3.3 Further characterisation of the REMI mutant isolates for *in vitro* growth and stress defects

To further characterise the mutant strains, diluted spore suspensions of ~$1x10^6$ spores ml^{-1} were 'spotted' onto media amended with different fungal growth stressors. The aim was to test whether any previously identified reduced virulence or hyphal growth phenotypes correlated with any altered sensitivity to external stresses (King *et al*., 2017; Yemelin *et al*., 2017). The fifteen L951 *Z. tritici Hin*dIII REMI mutant isolates were spotted on YPD and grown for five days at 16˚C. All displayed similar morphological growth to the L951 parental strain, though some like REMI-2/A grow more slowly in comparison.

The isolates were then tested for altered sensitivity to external stressors by spotting onto amended YPD agar plates. The stress sensitivity tests were performed against cell wall integrity and oxidative and osmotic stresses. The full results for all 15 strains tested for three different stressors are shown in Figure 3.5. The stresses included hydrogen peroxide for the induction of oxidative stress, sorbitol for conditions of osmotic stress, and calcofluor white to induce cell wall integrity stress, each used at concentrations from previous literature, which reported their ability to discriminate sensitive *Z. tritici* mutants from the WT (King *et al*., 2017; Mehrabi *et al*., 2006b; Yemelin *et al*., 2017). Figure 3.5, shows that against these fungal growth stressors, the selected REMI mutants showed no significant alterations in their growth relative to WT. Furthermore, even in the slower-growing REMI-2/A mutant, there appeared to be no negative response to these three stressors. Therefore, no link was identified between altered stress sensitivity with the reduced virulence phenotype for any of the fifteen strains at the concentrations tested.

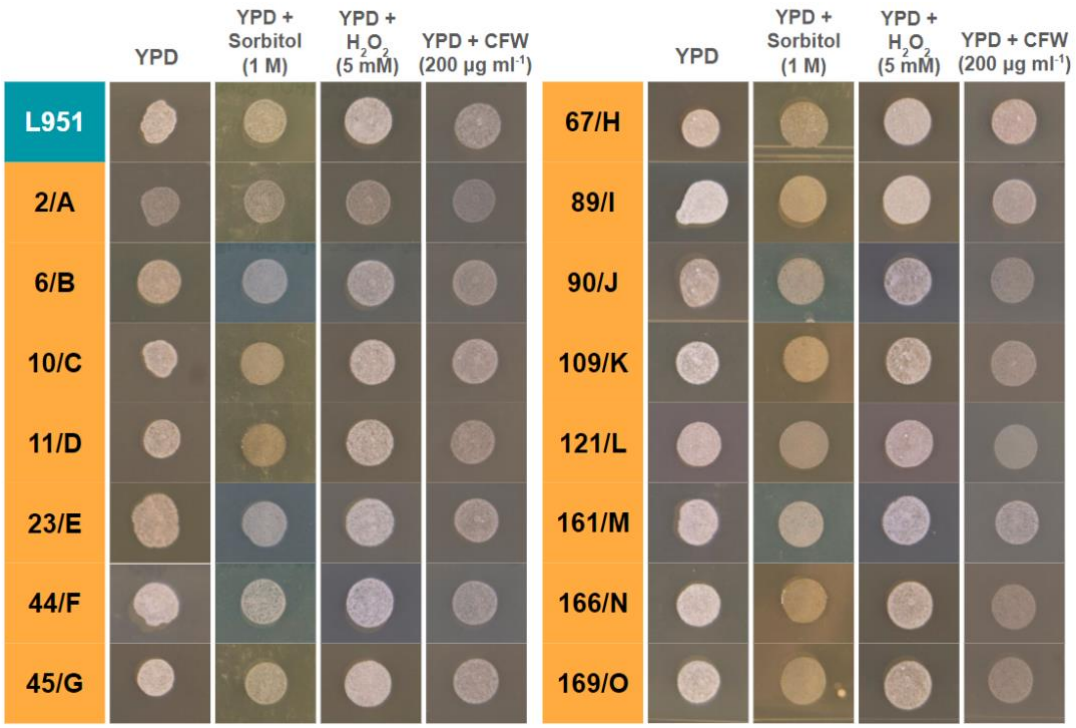

Figure 3.5 *In vitro* 'spotting' REMI mutant screen on YPD agar amended with fungal growth stressors including sorbitol, calcofluor white (CFW) and hydrogen peroxide.

Spores were suspended in 0.01% Tween20 at a concentration of ~1x10^6 spores ml^{-1}, and 5 µl were spotted onto YPD and fungal growth stressor amended YPD, photos all taken at five dpi. Plain YPD, all mutants show typical growth except REMI-2/A appears to be slower, which is true compared to this mutant on the amended plates. Testing the L951 *Z. tritici Hin*dIII REMI mutants' resilience to osmotic stress through spotting on YPD amended with sorbitol (1 M) revealed no reduced growth phenotypes. Spotting on hydrogen peroxide H_2O_2 (5mM) amended plates indicated that none of the fifteen were sensitive oxidative stress. Overall, the REMI mutants including the fifteen shown as representatives here, did not appear to show any reduced growth under cell wall integrity stress using calcofluor white (200 µg ml^{-1}).

Table 3.2 Summary of the *in planta* and *in vitro* filamentous growth phenotypes of the fifteen REMI mutagenised isolates.

L951 Mutant Number	Skinner (2001) Original ID	Sequencing ID (Chapter Four)	Virulence on wheat cv. Riband	Hyphal growth on tap water agar
2	1HR.202	A	Nonpathogenic	Limited
6	1HR.206	B	Nonpathogenic	Limited
10	1HR.210	C	Chlorosis, no pycnidia	Reduced
11	1HR.211	D	Delayed	WT
23	1HR.223	E	WT	Reduced
44	1HR.244	F	Delayed	Reduced
45	1HR.245	G	Delayed	Reduced
67	1HR.117	H	Delayed	Dense
89	1HR.139	I	Delayed	WT
90	1HR.140	J	Delayed	WT
109	1HR.159	K	Chlorosis, no pycnidia	Aberrant
121	1HR.171	L	Nonpathogenic	Limited
161	1HR.261	M	Delayed	WT
166	1HR.266	N	Delayed	WT
169	1HR.269	O	Delayed	Aberrant

3.3.4 *In planta* characterisation of selected *Agrobacterium tumefaciens* mediated (ATMT) transformants

The Rudd group carried an initial high throughput screen on 631 random ATMT mutants with *Z. tritici* IPO323 as the parental strain for reduced *in planta* infection on the wheat cv. Riband (Rudd, unpublished). In this initial screen, fourteen transformants were identified as either non-pathogenic or with reduced virulence. Two from this collection had previously been further analysed and published, describing the impact of mutations detected in the *ZtALG2* (previously published as MgAlg2) and *ZtGT2* genes on *Z. tritici* virulence (King *et al*., 2017; Motteram *et al*., 2011). However, five isolates remained that had not been subjected to further characterisation, including

validation for their apparent reduced virulence. These five mutant isolates were therefore further characterised here.

Each isolate was tested for virulence against the wheat cv. Riband according to the protocols detailed above for the REMI collection. In summary, each mutant was tested for infection against three wheat leaves, and symptom development on wheat was monitored. Photos were taken at 14 days and 21 days post-inoculation. Of the five mutant isolates tested, four had reproducibly reduced virulence on wheat leaves, which manifested as delayed symptom development showing some chlorosis by 21 dpi (Figure 3.6). In contrast, isolate 9-70 showed disease symptom development that did not distinguish significantly from WT strains. The typical levels of disease symptoms for each strain are shown in Figure 3.6. These assays confirmed previous work, which suggested that mutant isolates 4-124, 4-158, 5-51 and 15-120 are reduced virulence mutants of *Z. tritici*.

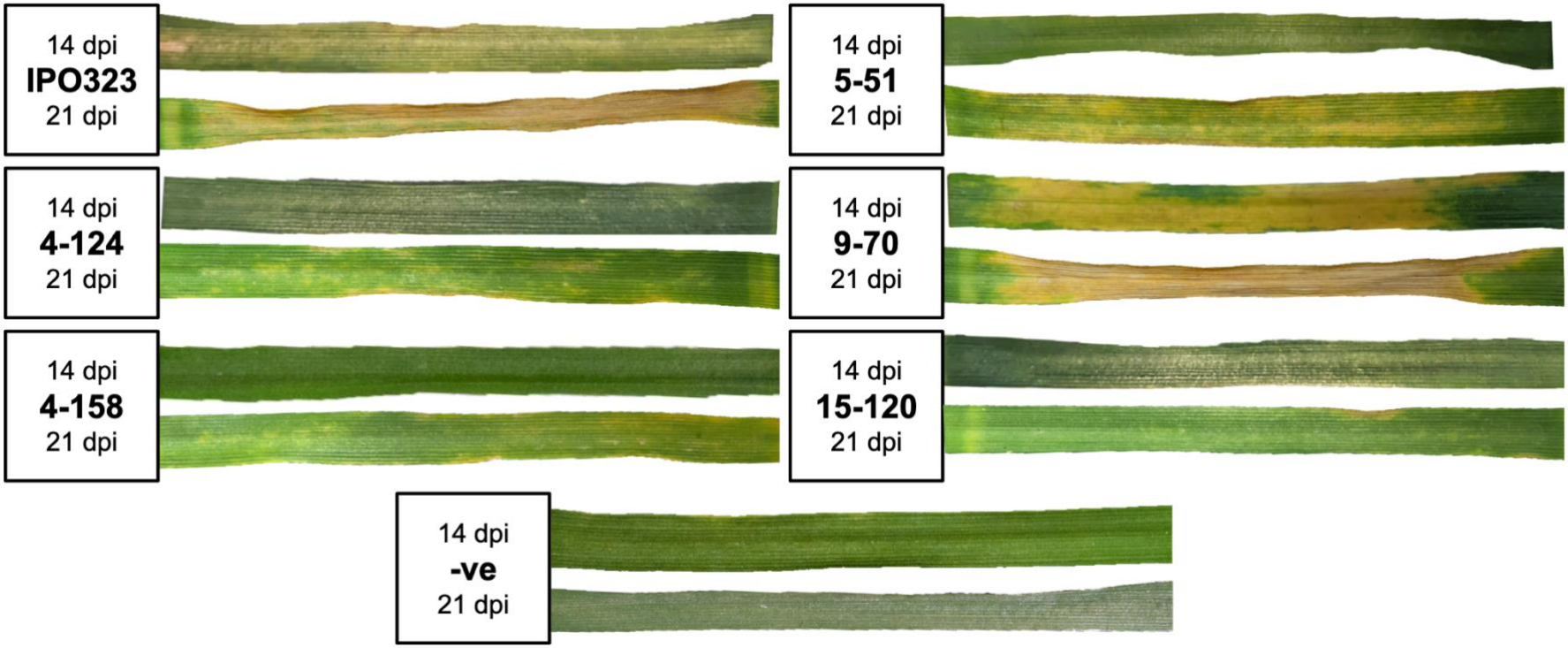

Figure 3.6 *In planta* screening photographs from the *Z. tritici* IPO323 random ATMT mutant isolates on wheat cv. Riband. Images show a representative wheat leaf with typical symptoms from the three replicate inoculated leaves at 14 days post-inoculation (dpi) and 21 dpi. The entire leaf surface displayed was inoculated via cotton swab with $1x10^7$ spores ml^{-1} solution. Each mutant isolate displayed here was tested a minimum of three times *in planta* on wheat cv. Riband.

3.3.5 Further characterisation of the random T-DNA mutant isolates for *in vitro* growth and stress defects

Further phenotyping of the aforementioned random T-DNA mutant isolates *in vitro* was carried out using the different fungal stressors already described and growth on TWA. For stress sensitivity testing, each isolate was tested a minimum of three times against each stress, and final images of fungal growth spotting plates were taken after five days. The typical results of these assays are shown in Figure 3.7. Isolates 4-124 and 4-158 displayed hypersensitivity to osmotic and oxidative stress, whilst 15-120, 5-51 and 9-70 appeared to tolerate all the tested fungal growth stressor conditions.

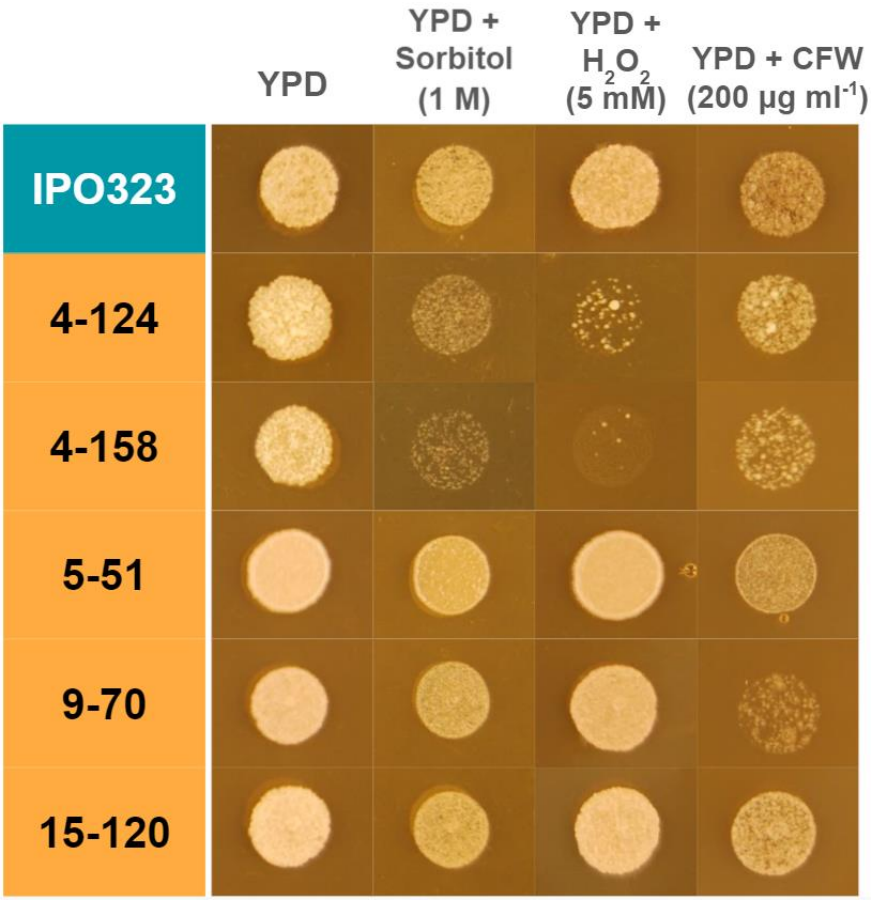

Figure 3.7 *In vitro* 'spotting' stress tests for the five random ATMT *Z. tritici* IPO323 mutants.

Spores were suspended in 0.01% Tween20 at a concentration of 1x10^6 spores ml^{-1}, and 5 µl were spotted onto YPD and fungal growth stressor amended YPD, photos all taken at five dpi. On the plain YPD, all mutants show typical WT growth visually

compared to the parental *Z. tritici* strain IPO323. The IPO323 spot has melanised under cell wall integrity stress using calcofluor white (YPD + CFW, 200 µg ml^{-1}). Mutants 4-124 and 4-158 were sensitive to osmotic (YPD + sorbitol, 1 M) and oxidative (YPD + H_2O_2, 5mM) stressors. In both mutants on CFW, there does appear to be some reduced growth at this spore spotting concentration. Whilst 9-70 was not sensitive to osmotic or oxidative stresses, the mutant showed reduced growth under cell wall integrity stress. 5-51 does not appear susceptible to the fungal growth stressors tested.

In the same process for the REMI mutants, to assess the ability of the isolates to switch to hyphal growth, the five random ATMT IPO323 mutants were also spotted on TWA, Figure 3.8. As the parental strain for this collection was IPO323, an IPO323 spot is used as the WT control comparison. Two of the five mutant isolates in the hyphal growth assays showed a typical WT hyphal growth phenotype, 5-51 and 9-70, compared with the WT IPO323 strain. In contrast, mutant isolate 15-120 displayed the most drastic reduced hyphal growth, compared to the other mutant isolates, with only a few short branches very close to the spot edge. A reduction was also seen for isolates 4-124 and 4-158, exhibiting a similar short, hyperbranched hyphal growth phenotype. This reduction paralleled a similar reduction in virulence and was also associated with hypersensitivity to oxidative and osmotic stress in both strains, suggesting potential functional links between these phenotypes.

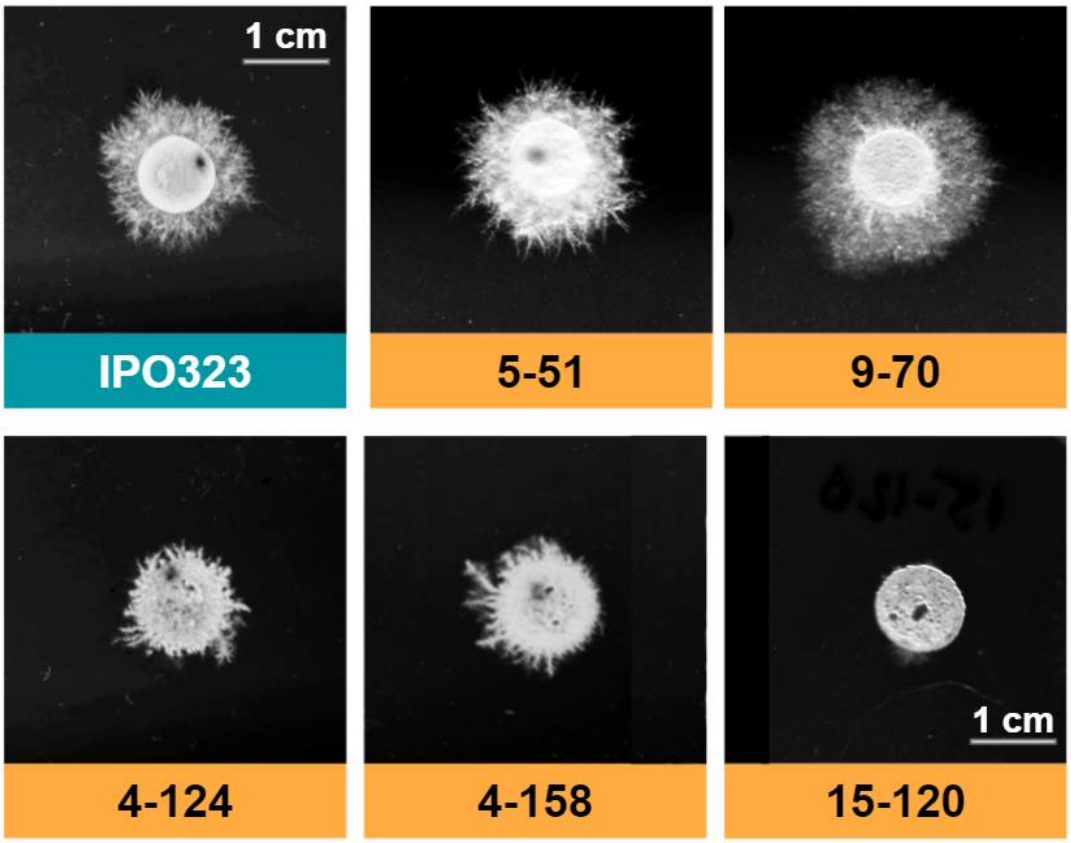

Figure 3.8 *In vitro* hyphal growth assay of random ATMT *Z. tritici* IPO323 mutant isolates on low nutrient tap water agar (TWA).

Spores were suspended in 0.01% Tween20 at a concentration of $1x10^7$ spores ml^{-1}, and 5 µl were spotted onto TWA and photographed after ten days. 5-51 and 9-70 resemble the hyphal growth pattern of the IPO323 WT strain, whilst 15-120 displayed vastly reduced hyphal growth. Isolates 4-124 and 4-158 show a similar short, hyperbranched hyphal growth phenotype.

3.4 Discussion

3.4.1 Twenty years at -80˚C: the viability of fungal mutant libraries in long term storage

Forward genetics studies utilise randomly mutagenised libraries with associated phenotypic observations to identify genes associated with that phenotype (King *et al*., 2017; Urban *et al*., 2015; Yemelin *et al.,* 2017). Though old mutant collections potentially contain a wealth of information, the condition of these mutants after decades in storage is a concern. Likewise, the viability of the L951 REMI mutants to successfully re-grow to bulk stocks

ahead of *in planta* and *in vitro* screening was a concern after 20 years of -80˚C storage. The entire collection was moved from its original home >130 miles to the Rothamsted Research, Harpenden site. A total of 84.8% of the 231 *Z. tritici* L951 REMI mutants could be grown to make stocks that maintained the integration of the hygromycin resistance selectable marker (still stably resistant). Some isolates were reconstituted from effectively single colonies, showing that only a few viable cells are needed to retain and rebuild old collections.

Whilst REMI as a technique is no longer used in *Z. tritici,* it is still in use by some researchers to perform random insertional mutagenesis in other species. These include other pathogenic fungi, slime moulds and even *Xenopus* sp. (Attri *et al*., 2018; Jiang *et al.*, 2017; Bicalho Nogueira *et al*., 2019; Williams *et al.*, 2021; Zlatow *et al.,* 2020). A couple of recent studies utilised pooled genome sequencing in a REMI mutagenised collection of *Dictyostelium discoideum* mutant, described as “REMI-seq” (Gruenheit *et al*., 2021; Stewart *et al*., 2022). This enabled the characterisation of variation in predatory performance in *D. discoideum*, a social amoeba and microbial predator (Stewart *et al*., 2022). Though methods for protoplast–isolation have been recently developed to enable *Z. tritici* transformation using CRISPR/Cas9, the protoplast-based transformation techniques were have been superseded by ATMT (Khan *et al*., 2021). ATMT may prove advantageous for forward genetics screens compared to REMI as it may introduce fewer transgenes. This likely would make identifying strong candidate genes easier and reduce the chances of phenotypes resulting from additive impacts.

3.4.2 *In planta* assay methodologies: spraying, wounded droplet and swab techniques

Groups currently working with *Z. tritici* publish using different inoculation methods; some prefer spray inoculation whilst others use cotton swabs (as here). Skinner (2001) carried out *in planta* assessments of the REMI mutant library using the wounding method of inoculation by gently compressing the

leaf surface with a sterile pipette tip. A droplet of spore suspension of 5 x 10^5 spores ml^{-1} was then applied to the wound site. This method has the caveat of removing natural physical barriers to infection, taking out the random chance of encountering a natural opening in the leaf surface (Steinberg, 2015). Wounding also elicits plant defence responses, including the jasmonic acid (JA) hormone-regulated pathways, which may effectively prime the host to respond to infection (Le Mire *et al*., 2018). Transcriptomic studies showed the wheat response to *Z. tritici* infection up-regulated JA biosynthetic genes at later infection stages (Rudd *et al*., 2015). In Campanaro *et al*., (2021), gene silencing of TaWRKY10, a negative regulator of JA responses in wheat, resulted in an earlier onset necrotic symptom development on leaves inoculated with *Z. tritici* but also observed reduced pycnidiation. In Fones *et al.*, (2017), wounding was reported to encourage pycnidia development, reducing the time taken to pycnidiation across the conditions tested. Furthermore, asynchronous development in *Z. tritici* infection of wheat has been observed (Fantozzi *et al*., 2021). In summary, many conditions can affect the disease progression process. These are likely to have played a role in the discrepancy between the number of non-pathogenic/reduced virulence isolates identified in my *in planta* screens and those previously carried out by Skinner (2001).

3.4.3 Utilising stress screening to help identify and select for mutant isolates of interest

Successful candidate gene identification from forward genetics and mutagenomic studies requires a well-characterised phenotype. In this work, I based my selection of mutants on initial screens for *in planta* and *in vitro* hyphal growth phenotypes. Particularly for the *in planta* results, the delayed virulence mutant phenotypes alone could complicate gene identification in light of the noted asynchronous development of *Z. tritici*. Thus, additional *in planta* screening and a more detailed *in vitro* screen using different fungal growth stressors could be helpful to build on these data and aid in finding interesting candidates from whole-genome resequencing of strains.

Fungal pathogens rely on their ability to detect and respond to biotic and abiotic stresses. When these systems are impacted by mutagenesis, this can result in loss of pathogenicity. Multiple *Z. tritici* mutants with sensitivity to oxidative stress have been linked to reduced pathogenicity (Meherabi *et al.*, 2006b; Yemelin *et al*., 2017; Yemelin *et al*., 2021). The typical example of oxidative stress conditions *in planta* a fungal pathogen may encounter is that upon detection by the host reactive oxygen species (ROS) production is induced. Further examples of infection-related stress events include those imposed on the fungal cell wall by host secreted chitinases and glucanases as part of inducible defence responses. Similarly in the early phases of infection cycles, resistance to desiccation or osmotic stress by fungi germinating hyphae on leaf surfaces and successful transition through the different host tissues (Lo Presti *et al*., 2015; Tian *et al*., 2021).

Amongst the total 18 reduced virulence strains identified in this chapter (REMI and T-DNA combined), only two strains showed an associated hypersensitivity to stress, those being the T-DNA mutants 4-124 and 4-158, which both displayed hypersensitivity to oxidative and osmotic stress, but were WT for cell wall stress. All other tested strains from the T-DNA and REMI collections were WT for responses to these stressors. In the case of the REMI *Z. tritici* library, the lack of sorbitol sensitive mutants is likey explained due to the use of sorbitol in media to recover protoplasts in the transformation process. Hence the method of mutagenesis impact the mutant population produced.

While morphology changes are considered a typical stress response strategy, different forms being ‘better’ suited to differing stresses (Boyce *et al*., 2015; Kiss *et al.*, 2019). The resistance to the fungal growth stressors amongst the fifteen REMI mutants suggests that these severe deficient filamentous growth phenotypes can result from other processes independent of stress responses. Four strains with reduced virulence also have altered hyphal growth re-emphasises the likely link between these processes in many *Zymoseptoria* infections. Furthermore, it highlights the utility of rapid

switching screens to identify mutants likely to have affected virulence. However, the link is not absolute, as demonstrated by REMI mutant 23/E, which was strongly afflicted in its hyphal growth switching on TWA yet still able to cause disease on wheat leaves. This suggests that the TWA screen is not a perfect surrogate for early infection-related morphogenesis, which merits further study.

There are potentially even quicker ways of preselecting stress mutants, which might also display altered virulence in plants. For example, *Z. tritici* mutant libraries could be generated in a phenotype “targeted” manner using rapid mutagenesis methods such as UV applied to fungal colonies, which can then be subjected to replica plating. Such practices were used initially in bacteria and then also applied to yeast. The method enables the direct selection of susceptible isolates to that stressor (Toh-e & Oguchi, 2000) which can then be tested for plant infection. Unpublished work in our lab has applied a similar process in *Z. tritici* to generate and identify a population of cell wall strength defective mutants using replica plating on CFW amended agar. This approach could be further developed to identify mutants with altered responses to other infection-related stressors.

This chapter has identified 15 REMI strains and 5 ATMT strains of *Z. tritici* with ‘interesting’ phenotypes relating to virulence, hyphal growth defects and altered responses to stress. In the following chapter, I describe the bioinformatics and candidate gene discovery pipeline based on whole-genome resequencing of these REMI and random ATMT mutant isolates. Furthermore, I provide detail of the previously unreleased L951 *Z. tritici* genome. Finally, I also describe the “genomic landscapes” of mutation events associated with both methods.

4 Exploring “mutagenomic” landscapes through next-generation genome re-sequencing to identify candidate virulence genes.

4.1 Introduction

The chromosome-scale representative genome of *Z. tritici* is a Dutch isolate, IPO323 (NCBI:txid336722), initially isolated in 1981 from a wheat variety *Triticum aestivum* cv. Arminda (Kema & vanSilfhout, 1997; https://www.ncbi.nlm.nih.gov/assembly/GCF_000219625.1). The 39.7-Mb genome is arranged in 21 chromosomes, of which the smallest eight (chromosomes 14-21) are considered dispensable for asexual plant infection (Goodwin *et al.*, 2011). With the development of faster, more accurate and cheaper sequencing technologies, further isolates of *Z. tritici* have since been fully sequenced. These include strains 1A5, 1E4, 3D1 and 3D7, all isolated in 1999 from infected wheat fields in Switzerland, as well as single isolates of the related *Zymoseptoria* fungi *Z. brevis*, *Z. pseudotritici* and *Z. ardabiliae* (Grandaubert *et al.*, 2015; Lendenmann *et al*., 2014; Plissonneau *et al.*, 2018). The parental strain of the restriction enzyme mediated-integration (REMI) mutant library characterised in Chapter Three is L951, isolated in 1995 from wheat cv. Longbow by Hunter *et al*., (1999) but had not been genome sequenced before this current report.

The *Z. tritici* genome has a high rate of genome plasticity, with regions that contribute to low-level ‘background’ mutations occasionally observable within a single strain (McDonald *et al*., 2016; Möller *et al.*, 2018; Oggernfuss *et al.*, 2021; Plissonneau *et al.*, 2018). This highlights the importance of analysing the genomes of multiple strains and elucidating a pangenome, which should contain all the genes present in the species. Following a pan-genomic approach reveals which parts of a genome are core, unique or dispensable (Plissonneau *et al.*, 2018; Singh *et al*., 2021; Vernikos *et al.*, 2015). The ‘core’ genome should be relatively stable, as this contains genes necessary for essential functions, including growth, primary metabolism, energy etc. Whereas the dispensable or more flexible parts of the genome are less so,

more changeable or occasionally completely lost, and more likely to be involved in environmental interactions (e.g., cultivar sensitivity or interactions with changing temperatures or fungicide regimes).

In *Z. tritici* a significant constituent of the flexible genome is presented by the eight smallest chromosomes (all present in the reference IPO323), which display large presence-absence polymorphism between strains and are not generally considered to encode major components contributing to virulence. This is in contrast to other fungal pathogens, where accessory chromosomes have been shown to harbour virulence and avirulence effectors, such as *Fusarium oxysporum* (Habig *et al.*, 2017). Unique gene clusters or single genes could explain differential virulence or resistance to control chemicals. For *Z. tritici* and other pathogens, a pan-genome prioritises candidate key (universal) pathogenicity determinants by eliminating genes unlikely to be involved in virulence (i.e. absence of a gene in disease-causing field isolates and its widespread presence in the flexible rather than core pan-genome). Similarly, no, or very low, expression of genes might also suggest they could be de-prioritised for further analysis relative to candidates with consistently higher expression. Many groups have developed *Z. tritici* pan-genomes (Plissonneau *et al.*, 2018; Singh *et al*., 2021), and we also have one (unpublished Jason Rudd pers. comm.) constructed from 17 pan-European isolates collected in 2015, with associated *in vitro* culture and *in planta* transcriptomics for 13 of these strains.

Before deploying the methods described above for candidate gene prioritisation, a gene list of all candidates must first be assembled. The haploid genome of *Z. tritici* is amenable to multiple mutagenesis methods, with commonly used and well-established protocols. In the previous chapter, two techniques were described that have been used to transform *Z. tritici*; *Agrobacterium tumefaciens*-mediated transformation (ATMT) and restriction enzyme-mediated integration (REMI). Other mutagenesis methods used include UV light exposure (Gutiérrez-Alonso *et al.*, 2017). The impact of transformation techniques on the genomes of the target organisms has

primarily been unstudied in a genomics context. Before the advent of and advancements in next-generation sequencing (NGS) technologies, researchers used molecular methods to identify the 'tagged' sites of genomic integrations, such as plasmids and T-DNAs. These include plasmid rescue, genome walking and PCR-based methods like TAIL PCR (Urban *et al*., 2015). However, these methods cannot provide information regarding potential 'untagged' mutations during mutagenesis. These untagged mutations may be responsible for the phenotype due to loss of function or missense mutations. As such, the tagged insertion events can be ascribed to a phenotypic impact that an untagged change is causal of. An example in transposon integration where the phenotype was not associated with the *Ds* element, Østergaard & Yanofsky (2004) attributed this to the element jumping more than once in the host genome. Having fully 're-sequenced' genomes from mutant isolates enables detection of any specific 'tagged' integration sites and easier identification of untagged or 'off target' mutations in a mutant isolate. We can identify and filter as many potential candidate genes as possible before beginning the validation process. This approach to detection has been increasingly used due to the reducing costs of NGS technologies. The other benefit of having access to the whole genome of a transformed mutant is the relative ease of checking for structural variation, such as large insertions/deletions and translocations or for the loss of accessory chromosomes (Choi *et al*., 2007; Habig *et al*., 2017; Hodgens *et al*., 2020; Urban *et al*., 2015).

This chapter describes the impact of the REMI transformation procedure on fifteen whole-genome re-sequenced L951 mutants of *Z. tritici*. We similarly use a genome re-sequencing pipeline to investigate T-DNA and untagged effects in the genomes of five IPO323 mutants. I present evidence that suggests an association of REMI mutant plasmid integration sites with the co-inoculated restriction enzyme. This work also identified many additional untagged mutations; some were common amongst the mutant isolates, whereas others were unique to individual isolates. Finally, I present a list of all candidate genes for observed reductions in virulence observed for all

isolates. I then use PHI-base and Zymoseptoria KnetMiner, amongst other tools and databases, and pan-genomic and transcriptomic datasets to prioritise specific genes from within these lists.

4.2 Materials and Methods

4.2.1 Sequencing and assembly of a gapless reference genome assembly for *Z. tritici* strain L951

High molecular weight gDNA was isolated from fungal material grown in YPD broth. DNA was isolated using the Illustra Plant Genomic DNA extraction kit (Cytiva). The resulting DNA was first sequenced using PacBio to generate large contigs, including whole chromosomal scaffolds. Then, sequencing errors were corrected by simultaneously sequencing the gDNA by conventional HiSeq Illumina 100bp paired-end sequencing. Combining both methods led to a finished genome of 39.3 Mb consisting of 20 Chromosomes. To assist in genome annotation and gene calling, two RNAseq libraries were also sequenced (mRNA poly-A based sequencing), a liquid culture sample and an *in planta* infected sample made of a mixture of time points covering both the early symptomless and later symptomatic phases. The L951 genome assembly produced was annotated using InterProScan and BLAST2GO. For mapping, the sequenced mutant L951 isolates OMA (v.2.3.0) was used with default settings to identify genes corresponding to L951 in the reference *Z. tritici* strain IPO323 genome (Altenhoff *et al*., 2019). This work lists these genes under their Rothamsted Research gene annotation IDs and Joint Genome Institute (JGI) MycoCosm protein IDs. Where no initial putative orthologues were found, further BLAT searches in Apollo v1.0.4-RC3 (Dunn *et al*., 2019) Ensembl database to search against the latest community annotated versions of the *Z. tritici* IPO323 genome.

4.2.2 Identifying plasmid integration, T-DNA insertion sites and off-target mutations in mutant strains

As listed in Chapter Two, gDNA was prepared using the Illustra Phytopure DNA extraction kit for all samples. DNA samples were sequenced by

Novogene Ltd (Cambridge UK), and 40M 100 bp paired-end reads were generated from each sample.

The Fastq reads quality was assessed using FastQC and minor Trimmomatic. The location of plasmid insertions was found using a pipeline based on the methodology outlined in (https://github.com/Rothamsted/script-collection/tree/master/FindInsertSeq). First, reads were mapped to the plasmid using Bowtie2 in local alignment mode (v2.3.4.1-intel-2018a; Langmead B. & Salzberg S., 2012) and paired reads that had one of the pairs mapped to the plasmid and one unmapped were exported using SamTools (v1.9-intel-2018b; https://github.com/samtools/samtools) where reads had the bitwise flag set to 8, 'mate unmapped'. The plasmid mapped/unmapped read pairs were then mapped to the L951 genome and SamTools mpileup (http://www.htslib.org/doc/samtools-mpileup.html) was used to export a text file containing the read coverage at each position, locations where the coverage was more than 10 reads were visualised using IGV (Robinson *et al*., 2011).

The position of the T-DNA insertion was determined by mapping paired-end reads to the T-DNA plasmid reference, and where one mate was mapped, and the other mate was unmapped, this unmapped read was from the boundary position of the T-DNA insertion site. Therefore, these unmapped reads were extracted and mapped back to the fungal genome sequence. A stack of forward reads represents the 5' T-DNA insertion boundary loci boundary, and the stack of reverse reads represents the 3' T-DNA insertion boundary loci. The gap between these stacks, therefore, represented any deleted sequence. Copies of T-DNA insertion are determined by the average coverage of mapped reads to the T-DNA versus mapping the raw data to the fungal genome. Detailed instructions on running the FindInsertSeq workflow are available in the previous publication (Urban *et al*., 2015; https://github.com/Rothamsted/AppliedBioinformatics/tree/master/FindInsertSeq). The same workflow was used to identify REMI plasmid integration sites.

4.2.3 Detection of non-plasmid and non-T-DNA insert associated variants in the mutant isolate genomes

Variants were called against the reference L951 or IPO323 genome assemblies, using FreeBayes (v. 1.2.0.4-intel.2019.01) for the REMI and random ATMT mutant isolates, respectively, the likely effects of the mutation on protein functions. Raw variant counts were filtered using SNPsift (v.1.7.0_161) by the depth equal to, or greater than ten, and a quality score of equal to, or greater than, 30. To categorise and assess the likely impacts on annotated genes SNPeff 4.3t (build 2017-11-24 10:18) was used. For high/medium impact variants of interest or concern PROVEAN (Protein Variation Effect Analyzer; http://provean.jcvi.org/index.php) with default settings was also used to predict whether an amino acid substitution or indel impacted the biological function of a protein.

A

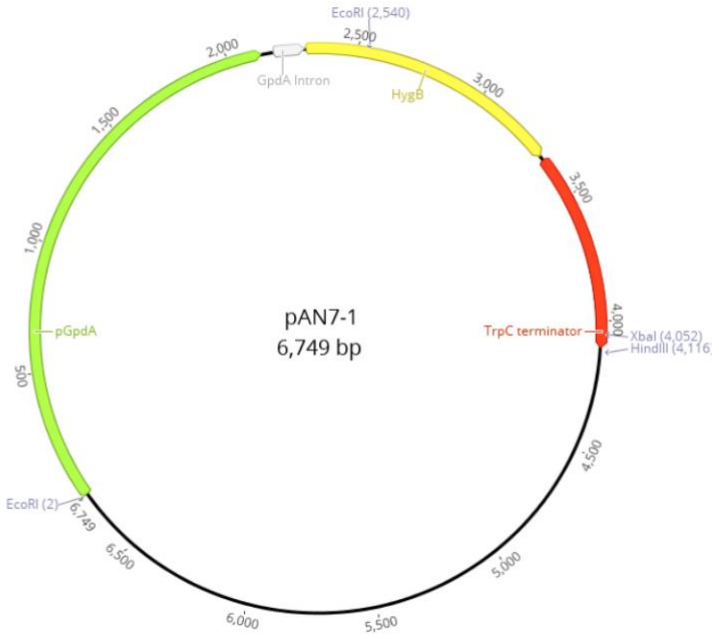

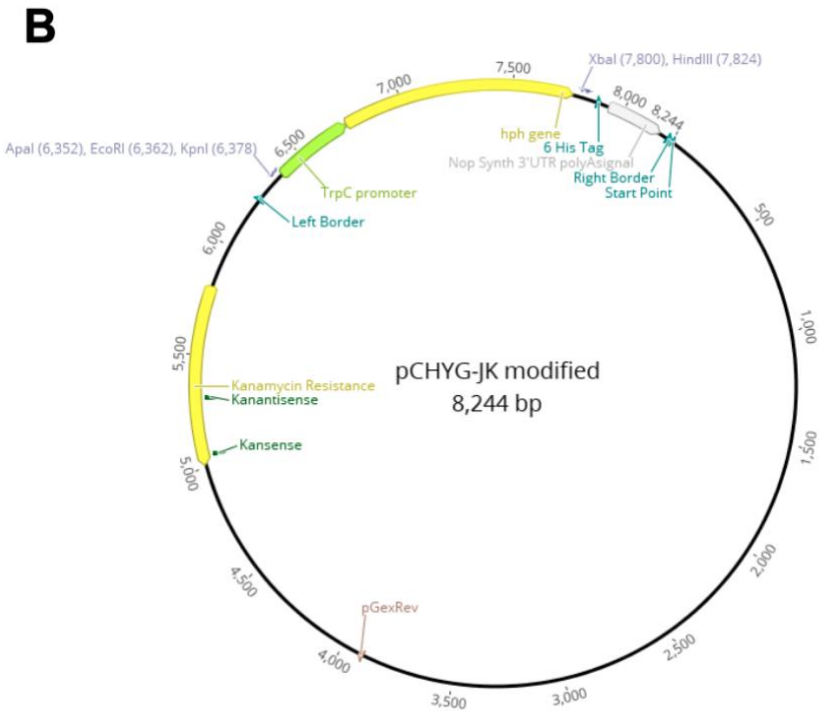

Figure 4.1 Representation of the pAN7-1 and T-DNA plasmids used for transformation by REMI and ATMT, respectively.

[A] pAN7-1 plasmid used by Skinner (2001) in the restriction enzyme-mediated integration (REMI) displaying the *Hin*dIII site present and **[B]** Modified T-DNA plasmid pCHYG used in the generation and the ATMT mutant.

4.3 Results

4.3.1 Assembly and analysis of the genomic sequence for *Z. tritici* strain L951

To enable REMI mutant genome analysis, we first required a high-quality genomic scaffold for the *Z. tritici* L951 strain. I present the basic statistics and comparison of this genome assembly with IPO323 in Table 4.1. While some L951 chromosomes are larger than their IPO323 counterparts, overall, its genome is smaller (39.3Mb vs 39.7Mb). Chromosomes fourteen to twenty are the accessory chromosomes present in L951, as chromosome 21, present in IPO323, is missing. Table 4.1 illustrates that many L951 chromosomes were represented by a single PacBIO sequencing contig, and whole chromosomes assemblies were generated typically from no more than three contigs. The subsequent overlay of the Illumina short reads (150bp

paired-end) resulted in a near gapless final genome assembly with only 26 ambiguous base pair calls. This is less than the current IPO323 genome, with several thousand ambiguous calls highlighted in Table 4.1. Gene annotation pipelines run for the L951 genome subsequently suggested in the region of 13,700 genes to be encoded therein. This high-quality reference scaffold enabled the analysis of REMI integration sites and the identification of any 'untagged' mutations in each of the tested mutant strains (section 4.3.2). Similarly, the "near to" finished genome of IPO323 was also used in the same manner for the four T-DNA mutant strains (section 4.3.6).

Table 4.1 L951 vs. IPO323 genome assembly statistics and chromosome. lengths.

Chromosome	L951 Pacbio Contig no	IPO323 length (bp)	L951 length (bp)	IPO323 unknown (bp)	L951 unknown (bp)
1	2	6,088,797	5,887,365	0	0
2	1	3,860,111	3,755,404	0	0
3	1	3,505,381	3,709,007	0	0
4	2	2,880,011	3,032,853	0	0
5	2	2,861,803	2,772,769	0	0
6	1	2,674,951	2,483,369	1,344	0
7	2	2,665,280	2,773,727**	0	0
8	1	2,443,572	2,393,285	0	0
9	3	2,142,475	2,187,544*	0	0
10	1	1,682,575	1,709,149	0	0
11	1	1,624,292	1,825,690	0	0
12	2	1,462,624	1,540,171	0	0
13	3	1,185,774	1,170,004	0	26
14	2	773,098	599,749	0	0
15	1	639,501	496,284	0	0
16	1	607,044	582,880	0	0
17	1	584,099	511,761	0	0
18	1	573,698	679,330	5,997	0
19	1	549,847	610,380	0	0
20	1	472,105	610,428	0	0

Chromosome	L951 Pacbio Contig no	IPO323 length (bp)	L951 length (bp)	IPO323 unknown (bp)	L951 unknown (bp)
21	NA	409,213*	NA	0	NA
Mitochondria	1	43,964	43,954	0	0
Total***	31	39,686,251	39,331,149	7,341	26

*3' telomere and preceding transposon sequence not assembled. **repeating rRNA sequence from 1,725,000 bp. ***not including the mitochondria.

4.3.2 Identification and analysis of non-plasmid associated 'untagged' sequence variants in the fifteen REMI *Hin*dIII isolates

Whole-genome re-sequencing was performed on fifteen REMI mutagenised L951 *Z. tritici* mutants. Three mutant isolates A, B and L were previously non-pathogenic on susceptible wheat plants. Eleven had defects in virulence, and one (REMI-E/23) had WT virulence (Chapter Three). The rationale for including this isolate, alongside the range in virulence phenotypes, was that it would enable a more straightforward elimination of any shared background mutations in genes as being responsible for the loss of virulence in the other strains.

Raw read data were mapped to the L951 genome to identify all mutations in each strain. To firstly analyse the impact of the REMI mutagenesis method on the genome of L951, common and background changes not directly associated with plasmid integration events were explored. The descriptor 'untagged variants' describes sequence variation identified as not directly associable with a plasmid integration event. This category potentially consists of mutations occurring due to the REMI mutagenesis process and any 'background' variation that may have arisen relative to the "parental" *Z. tritici* L951 strain used in the transformation (Kahmann & Basse, 1999; Maier & Schäfer, 1999). However, as the L951 isolate used by Skinner was not previously sequenced, distinguishing between these possibilities with certainty is not feasible. After filtering for depth and quality, 485 of the identified SNPs were common to all fifteen REMI mutant genomes (in coding and non-coding regions) relative to the fully sequenced L951 source strain,

shown in Table 4.2. This is a relatively small amount of variation when compared to levels of variation seen between distinct *Z. tritici* isolates (Badet *et al*., 2020; McDonald *et al.*, 2016), suggesting that all sequenced REMI strains derived from the same parental isolate and closely resemble the L951 reference strain subsequently sequenced and assembled at project start. But the data also suggests some background mutations had occurred between the REMI strains and the original L951. The raw variant counts before filtering for the isolates are listed in Table 4.2. Of note are the high raw counts in isolates D and F. These raw variant counts were inflated due to the presence of a contaminant. After filtering out these reads, the numbers closely match the isolates without a detectable contaminant.

The variants in predicted, annotated genes in the L951 genome are shown in Tables 4.3 and 4.4 and described in more detail in the next section of this chapter. I categorise the variants by whether they are present in a single L951 REMI mutagenised isolate or are common to multiple isolates. This 'common' variant category is split into 'all strains' and '>1 strain'. Both individual isolate and common variants were assessed for the predicted impact on gene function.

Table 4.2 The total number of variants detected in the fifteen *Z. tritici* L951 *Hin*dIII restriction enzyme-mediated integration mutant isolates.

		Variants filtered by depth ≥10 & variant quality ≥30			
Isolate	**Raw variant count**	**SNP**	**Insertion**	**Deletion**	**Complex**
A/2	40,172	524	28	9	31
B/6	40,706	524	29	8	31
C/10	42,587	576	29	7	39
D/11	**60,151**	522	21	4	41
E/23	38,858	543	30	8	30
F/44	**140,794**	601	22	8	40
G/45	39,454	543	29	7	35
H/67	40,659	566	30	8	35
I/89	40,163	550	28	8	30

Isolate	Raw variant count	Variants filtered by depth ≥10 & variant quality ≥30			
		SNP	Insertion	Deletion	Complex
J/90	43,857	564	27	6	37
K/109	49,078	592	26	5	37
L/121	39,156	538	30	8	29
M/161	39,379	536	33	9	31
N/166	40,553	578	30	8	30
O/169	42,670	595	28	9	40
Common to all strains		**485**	**20**	**6**	**23**

Isolates D and F (in bold) were contaminated which helps explain the much higher raw variant counts as compared to other isolates. After filtering for quality and depth the numbers are in line with the other isolates.

SNPeff 4.3t was used to filter for high, moderate, or low impact changes to annotated L951 genes. High impact variants are classed as having stop or frameshift mutations affecting significant portions of the gene. In contrast, moderate impact variants include missense or in-frame indels, and low impact variants involve synonymous changes or occur outside coding sequences. Figure 4.2 shows that there are a total of eleven ‘high’ impact, eighteen ‘moderate’ impact, and six ‘low’ impact untagged variants when calculating numbers combined from the “All isolate”, “>1 isolate”, and “Individual” isolate groups. We observed more high and moderate variants than low impact changes across all strains (“all isolates”- Figure 4.2). These mutations also occurring in the WT virulence REMI strain E/23 served as a control. It discounted them as a likely source of the reduced virulence phenotype seen in other mutant isolates.

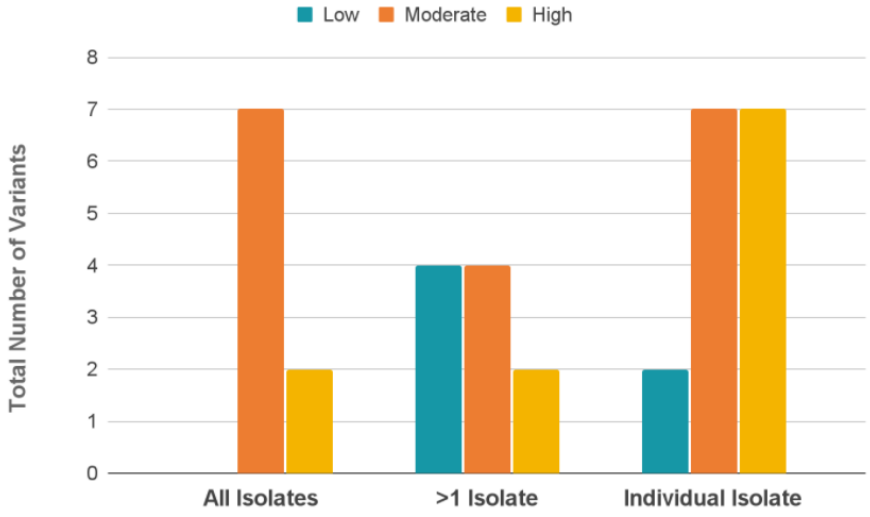

Figure 4.2 The SNPeff assessed impacts in coding sequences of 'non-plasmid' associated variants identified in the *Z. tritici* L951 *Hin*dIII REMI mutant isolates.

A graph displaying the categories of untagged variants by commonality in the isolates and their impacts. SNPeff4.3t was used to filter variants by impact. High impact variants are classed as having stop or frameshift mutations affecting significant portions of the gene, while moderate impact variants include missense or in-frame indels, and low impact variants involve synonymous changes or occur outside coding sequences.

OMA (v.2.3.0) was used with default settings to find the orthologous genes in the reference *Z. tritici* strain IPO323 to enable further analysis. A total of ten genes with untagged variants in L951 had no identifiable IPO323 orthologue suggesting that they are less likely to be essential for core biology. However, for individual strain-specific variants in Table 4.4, only one gene had no orthologue in IPO323, ZtritL951_01g23655. Most variant genes without orthologues are in the common (all strains) category listed in Table 4.3. BLAT nucleotide and protein searches in the Apollo Ensembl database for other user genome annotations identified hits to multiple chromosomes for three low impact predicted variants (ZtritL951_01g09719, ZtritL951_01g09725 & ZtritL951_01g07203). However, each appeared associated with either RIL or RLG element DNA transposons (the BLAT protein searches in Apollo are shown in Appendix Table 4.1).

4.3.2.1 Further detailed analysis of the common 'untagged' mutations identified in the REMI fifteen

To identify potential candidate virulence-associated genes, I started by attempting to determine the effects, if any, of detected 'common' mutations in the mutagenised strains. A total of 35 untagged non-plasmid associated variant genes were identified, indicated in Figure 4.2. Of these, nineteen 'common' variants in predicted protein-encoding genes were identified in several groups of mutant isolates relative to the reference L951 and are listed in Table 4.3. In Figure 4.2, these are represented as nine 'all isolate' and ten untagged variants present in '>1 isolate' detected within predicted genes. The REMI isolates in which each variant is present are listed in Table 4.3. For example, we can see two different variants of the L951 gene, ZtritL951_01g09567, present in different mutant isolates. A missense variant in REMI isolates B,D,E,F,N and an in-frame insertion in REMI isolates C,G,I,K,L,M,O. Both variations were predicted to have a moderate impact on protein function.

The variant common across the fifteen sequenced mutants of most concern was within the predicted orthologue of a cyclin protein ZtritL951_01p02147 (putative orthologue ZtritIPO323_04g01051/Mycgr3G107198), Cln1. Cyclins are a well-conserved protein group that is crucial for the normal progression of cell cycles. Cyclins form complexes with cyclin-dependent kinases (CDK), these cyclin-CDK complexes direct activation of cell cycle progressions. Deletion or other function impacting mutations have consequences that affect typical cell cycle progression (Kelliher & Haase, 2017). In *Z. tritici,* the inactivation of a cyclin-encoding gene, ZtMCC (published as MgMCC), was associated with delayed filamentous growth, hyphal swellings, and increased melanin biosynthesis and reduced pathogenicity (Choi & Goodwin, 2010).

SNPeff categorised this non-synonymous variant as likely to have a moderate impact, whilst PROVEAN using default settings suggested that this was likely to have a deleterious effect (PROVEAN score = -4.328, deleterious; prediction cut off = -2.5). Using NCBI Conserved Domain

Database (CDD, v.3.19) revealed a predicted structure indicating that this variation occurred within a region containing multiple conserved residues and a putative cyclin-dependent kinase (CDK) interface site, see Figure 4.3**.** Due to the presence of this variant in all mutant strains, including an isolate with normal symptom development (REMI E/23) and multiple isolates with typical hyphal growth, there was, however, confidence in the decision that this gene could be excluded as the cause of reduced virulence in other strains.

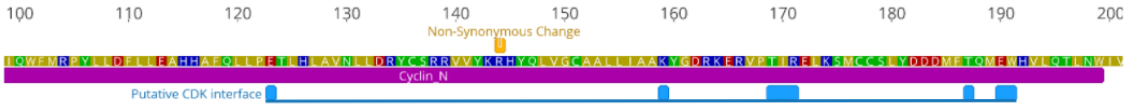

Figure 4.3 SNPeff predicted a moderate impact predicted non-synonymous resulting in an amino acid change near a binding site in a predicted cyclin protein in all REMI mutants, including those with WT pathogenicity.
Here I show a 202 aa portion of ZtritL951_01g02147 (424 aa), a predicted cyclin in *Z. tritici* L951, showing the relevant domains and site of the identified non-synonymous change. The labelled domains were identified using NCBI Conserved Domain Database (CCD, v.3.19) and visualised in Geneious (v.10.2). Labelled in blue are residues indicated to be part of a cyclin-dependent kinase (CDK) interface. The site of variation is labelled "Non-Synonymous Change" in yellow at residue 144, changing the amino acid from arginine (R) to proline (P).

Nine 'all isolate' and ten untagged variants are present in '>1 isolate' detected within annotated genes. Eight were eliminated as unlikely candidates for causing altered fungal virulence, and hyphal growth phenotypes due to either (1) their presence on an accessory chromosome, (2) complete absence in genomes of disease-causing sequenced field isolates of *Z. tritici* (from the flexible pangenome) and (3) expression pattern in other transcriptomic studies and our unpublished pangenome resource. Four low impact variants predicted in almost all mutant strains were ruled out as they were synonymous changes. Seven common variants produced multiple BLAT hits and seemed to associate with various transposable elements. So, in summary, analysis of these 'common' mutations led to no candidate genes being likely responsible for any observed reductions in virulence.

Table 4.3 Common untagged effects in fifteen *Z. tritici* L951 *Hin*dIII restriction enzyme-mediated integration mutant isolates.

L951 Identifier	L951 Chr.	Predicted IPO323 Orthologue	InterPro Name	SNPeff Predicted Impact	Mutation	Present In REMI Isolates…
ZtritL951_01g00775	1	ZtritIPO323_04g11606	N/A	High	stops gained	All
ZtritL951_01g08151	12	CDS:NS.01223-NS.01223	N/A	High	frameshift	A,B,C,E,F,G,H,I,J,K,L,M,N,O
ZtritL951_01g10633	18	ZtritIPO323_04g05274	N/A	High	frameshift	A,B,C,D,E,G,H,I,J,K,L,M,N,O
ZtritL951_01g21125	6	ZtritIPO323_04g10653	N/A	High	frameshift	All
ZtritL951_01g02147	1	ZtritIPO323_04g01051	Cyclin	Moderate	missense variant	All
ZtritL951_01g06577	11	N/A	N/A	Moderate	missense variants	All
ZtritL951_01g06593	11	Mycgr3G96648	N/A	Moderate	missense variant	All
ZtritL951_01g06599	11	ZtritIPO323_04g03262	N/A	Moderate	missense variant	All
ZtritL951_01g09161	14	ZtritIPO323_04g04563	N/A	Moderate	missense variant	A,B,E,F,H,I,K,M,N
ZtritL951_01g09567	15	N/A	N/A	Moderate	missense variant	B,D,E,F,N
ZtritL951_01g09567	15	N/A	N/A	Moderate	conservative inframe insertion	C,G,I,K,L,M,O
ZtritL951_01g09719	15	Multiple BLAT hits (RIL)	N/A	Moderate	missense variant	All
ZtritL951_01g09725	15	Multiple BLAT hits (RIL)	N/A	Moderate	missense variants	All
ZtritL951_01g14011	20	ZtritIPO323_04g06958	N/A	Moderate	conservative inframe deletion	All
ZtritL951_01g22097	6	ZtritIPO323_04g11134	N/A	Moderate	conservative inframe deletion	A,O
ZtritL951_01g06575	11	N/A	N/A	Low	synonymous variant	A,B,C,D,E,F,G,H,I,J,K,M,N,O
ZtritL951_01g06577	11	N/A	N/A	Low	synonymous variant	A,B,C,D,E,F,G,H,I,J,K,M,N,O
ZtritL951_01g06595	11	N/A	N/A	Low	synonymous variant	A,B,C,D,E,F,G,H,I,J,K,M,N,O
ZtritL951_01g07203	11	Multiple BLAT hits (RLG)	N/A	Low	synonymous variants	A,B,C,D,E,F,G,H,I,J,K,M,N,O

4.3.2.2 Analysis of the individual strain (or strain-specific) REMI 'untagged' mutations

As shown previously in Figure 4.2, there are sixteen individual untagged variants unique to single strains, listed in Table 4.4. As with the common untagged variants, each was filtered using SNPeff to categorise which variants have a predicted impact on the function of the genes affected. Five isolates (REMI C, D, F, G and K, see Table 4.4) had more than one individual unique variant present predicted to impact protein function by SNPeff. However, due to their expected low impact, two individual isolate variants in REMI mutants B and C were considered unlikely candidates, see Table 4.4. Greater attention was focused on the seven individual isolates (unique) moderate impact predicted variants and the seven high impact predicted variants. Two independent gene variants immediately appeared to be highly likely candidates for affecting virulence in REMI isolate K and L.

REMI L was previously described as an adenine auxotroph and is the only previously described mutant isolate in Skinner (2001) with this associated information. Table 4.4, shows that a unique gene variant, present only in REMI L, induced a high impact frameshift missense variant in ZtritL951_01g25589, a predicted phosphoribosylformylglycinamidine synthase involved in the *de novo* adenine biosynthesis pathway. This is orthologous to the *S. cerevisiae* ADE6 protein. Yemelin *et al.*, (2017) had previously shown that a mutation in a different gene in this pathway affected virulence. Therefore, I postulated that this mutation would explain adenine auxotrophy and the reduced virulence and hyphal growth phenotype observed for REMI L. There is a more detailed characterisation of this gene and mutant in Chapter Five.

REMI K had a unique moderate impact variant in the L951 gene, ZtritL951_01g24659, encoding a Gti1/Pac2 family protein already described in the literature in *Z. tritici* IPO323 as ZtWor1 (Mirzadi Gohari *et al*., 2014). As the phenotypes of the L951 REMI mutant and the IPO323 defective

ZtWor1 mutant were similar, I de-prioritised the investigation into this already published mutant.

Table 4.4 shows that ZtritL951_01g23655 is the only L951 gene variant in individual strains with no identifiable IPO323 orthologue. BLAT nucleotide searches on the Apollo ENSEMBL database using a 1000 bp region, including the gene, hit two empty regions on IPO323 chromosome seven (1683034-1684467 and 1691507-1691891). BLAT protein top hits also identify this same region of the IPO323 genome. These are within regions known to have repetitive DNA (rDNA) repeats (Schotanus *et al*., 2015).

This analysis identified sixteen individual variants: seven high impact, seven moderate impact and two low impact. Only one L951 individual unique isolate variant without an IPO323 orthologue was detected. This analysis identified that in some strains, the reduced virulence phenotype observed may have arisen from one these mutations (e.g. REMI L/121 L951 variant in predicted *ZtADE6*), though in the many of them were unlikely to be responsible for changes in virulence described for many of the strains characterised in Chapter Three.

Table 4.4 Isolate specific untagged variants present in the fifteen *Z. tritici* L951 *Hin*dIII REMI mutant isolates.

Isolate	L951 Identifier	L951 Chr.	Predicted IPO323 Orthologue	InterPro Name	SNPeff Predicted Impact	Mutation(s)
A	ZtritL951_01g08387	13	ZtritIPO323_04g04292	PA domain;Peptidase M28	Moderate	missense variant
B	ZtritL951_01g13179	2	ZtritIPO323_04g06544	Alcohol dehydrogenase, zinc-type, conserved site	Low	synonymous variant
C	ZtritL951_01g08391	13	ZtritIPO323_04g04290	Zinc finger, RING-type	High	stop gained & missense variant
C	ZtritL951_01g18683	4	ZtritIPO323_04g09410	Amino acid/polyamine transporter I	Low	splice region & intron variant
D	ZtritL951_01g15847	3	Mycgr3G201274.1	N/A	Moderate	missense variants
D	ZtritL951_01g24121	7	ZtritIPO323_04g12130	N/A	Moderate	missense variant
F	ZtritL951_01g23655	7	N/A	N/A	High	frameshift, splice region variant
F	ZtritL951_01g16619	3	ZtritIPO323_04g08387	Major facilitator superfamily	Moderate	missense variant
G	ZtritL951_01g13791*	2	ZtritIPO323_04g06816	Cupin 2, conserved barrel	High	frameshift
G	ZtritL951_01g20915	6	ZtritIPO323_04g10547	Polyketide synthase, phosphopantetheine-binding domain	Moderate	missense variant
I	ZtritL951_01g11383	2	ZtritIPO323_04g05633	FAD/NAD(P)-binding domain superfamily	Moderate	missense variant
J	ZtritL951_01g08385	13	ZtritIPO323_04g04175	N/A	High	frameshift
K	ZtritL951_01g08387	13	ZtritIPO323_04g04292	PA domain;Peptidase M28	High	stop gained
K	ZtritL951_01g24659	8	ZtritIPO323_04g12402	Gti1/Pac2 family	Moderate	missense variant
L	ZtritL951_01g25589	8	ZtritIPO323_04g12872	Phosphoribosylformylglycinamidine synthase	High	frameshift, missense variant
M	ZtritL951_01g04653	1	ZtritIPO323_04g02333	Amino acid permease/ SLC12A domain	High	frameshift

*This gene annotation in the L951 genome requires further resolution as it likely combines genes including cupin domain protein (gene listed in table) and a possible kinase domain protein. For the purposes of my work a BLAT search against the IPO323 genome in Apollo helped putatively place the variation detected occurred in the portion of gene encoding for the cupin domain protein.

As REMI utilises a restriction enzyme to guide plasmid integration into the host genome, the mutagenic process is not entirely random (Maier & Schäfer, 1999). Figure 4.4 shows that untagged variants were detected on thirteen of the twenty chromosomes in the L951 genome. Only two chromosomes had both common and individual variants detected, chromosomes one and six. Thirteen of the twenty L951 chromosomes had untagged variants, though none were detected in four core chromosomes. Figure 4.4, pointed to a possible bias towards chromosome eleven, with seven untagged variants occurring on this chromosome, and to chromosome thirteen, with four individual isolate untagged variants. However, given the number of strains the evidence is limited, particularly as the differences in the number of variants between the chromosomes are marginal.

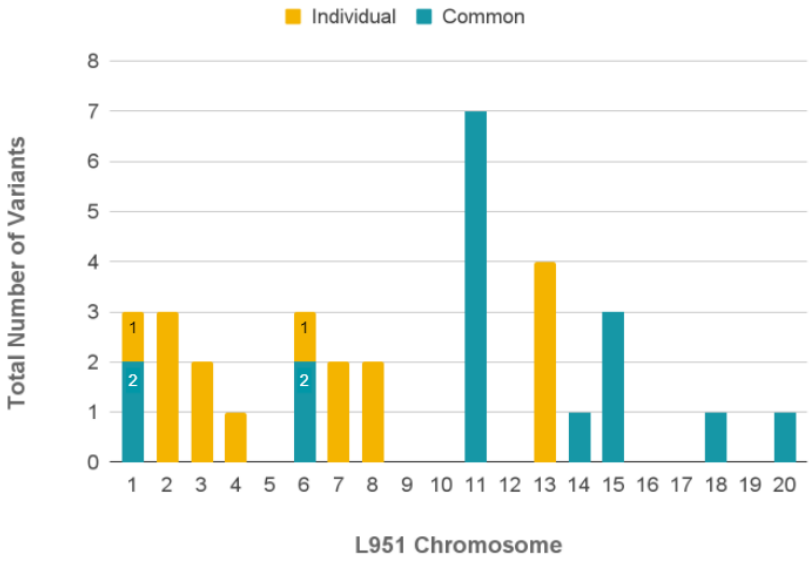

Figure 4.4 Number of untagged variants detected in the fifteen sequenced REMI mutagenised *Z. tritici* L951 isolates by chromosome.

Shows the distribution of untagged variants across the twenty chromosomes present in the L951 genome for the REMI mutagenised isolates. Blue, integrations in 'common' variants (occurring in two or more mutant isolates). Yellow, are the individual isolate identified variants occurring in individual mutant isolates.

Figure 4.5 shows the IPO323 and L951 orthologous chromosomes and the relative positions of both common and individual untagged variant L951 genes with the predicted IPO323 orthologous genes. This also visualises the

chromosomal size differences between the two *Z. tritici* isolates, listed in Table 4.1, and the spread of the variants across each of the chromosomes.

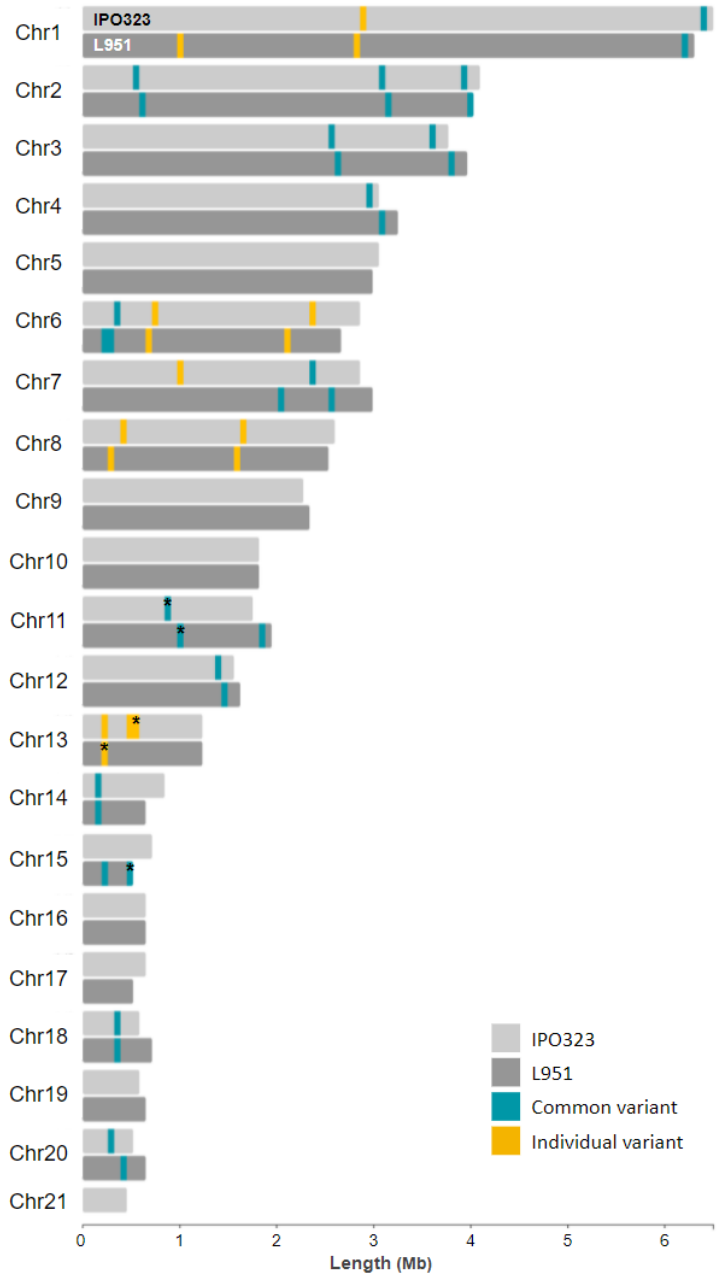

Figure 4.5 Distribution of putative IPO323 orthologues and 'untagged' untagged variants in the L951 genome.

Visualisation of IPO323 (light grey) and L951 (dark grey) chromosomes showing the relative positions of the genes impacted by untagged variants and their putative IPO323 orthologues; blue are common variant locations and yellow individual isolate variant locations, regions marked with an ***** are areas where multiple variants

are collapsed into a single representative bar due scale. Produced in RStudio package chromoMap (v. 0.3.1), Anand & Rodriguez Lopez (2022).

4.3.3 Identification and characterisation of eighteen plasmid integrations identified in the *Z. tritici* L951 *Hin*dIII REMI mutant genomes

We sought to determine the position of the tagged plasmid insertions in the REMI mutant genomes to ascertain whether any of the integrations affected genes that could be considered likely to explain the observed mutant phenotypes. Two depth levels were analysed for mapping read coverage. Integration events from >10x coverage were higher confidence predictions whilst the second cut-off of 5x was also analysed. Twelve mutant isolates had plasmid integrations detected above the higher depth threshold (≥10x coverage), with eighteen plasmid integrations potentially affecting the functions of 28 different genes listed in Tables 4.5 and 4.6. This depth threshold was selected as the minimum acceptable threshold for statistical analyses and had priority in candidate gene determination.

We determined the events position and the number of plasmid integrations per mutant isolate. Figure 4.6 shows the number of integrations in the fifteen REMI mutant isolates, highlighting those with no plasmid integration events, a single event or multiple integration events at both depth thresholds. There are nine isolates with single integration events, and the genes potentially impacted are listed in Table 4.5. In Figure 4.6, I show that REMI isolates A, B and G had multiple integration events, and the genes whose functions may be impacted are listed in Table 4.6. At the lower threshold, ≥5x coverage, four more putative plasmid integrations are putatively identified, listed in Table 4.7. These lower confidence putative integrations are not included in later statistical analyses, and the genes putatively impacted were de-prioritised to reflect the lower certainty in their detection.

At ≥10x coverage, there are three isolates without any identified plasmid integration. All the L951 REMI mutant isolates sent for sequencing were successfully grown on hygromycin amended YPD plates, to which pAN7-1

plasmid should confer resistance; each isolate was predicted to have at least one copy of the plasmid integrated. By including the lower threshold REMI mutant isolates C (peak coverage=5) and M (peak coverage=8) have putative integrations identified. This left only one of the fifteen isolates (O) with no detected plasmid integrations that met either depth threshold.

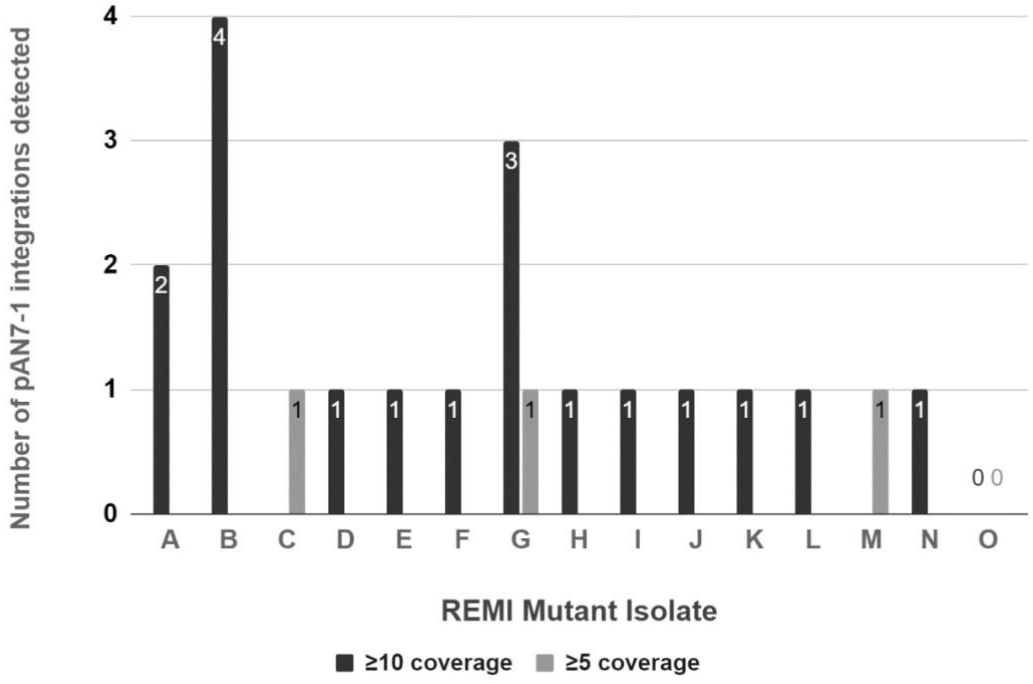

Figure 4.6 Number of detected pAN7-1 plasmid integration events detected in each *Z. tritici* L951 *Hin*dIII REMI mutant isolates above the higher (≥10 coverage) and lower (≥5 coverage) pile-up depth threshold.

REMI mutant B is shown here to have the most plasmid integration events, followed by REMI G. The only mutant isolate without a detected plasmid integration at either coverage depth is REMI O. As all mutant isolates were able to grow on media amended with hygromycin. Though there were multiple lower depth mappings, for reliable detection, those with a pile-up depth of ≥10 coverage were considered and shown here are a few 'putative' cases with ≥5 coverage.

Table 4.5 Nine REMI isolates with single identified pAN7-1 plasmid integration event above the depth threshold (≥10 coverage). The likely impact of the integration event for the listed genes with any known predicted functions are shown.

Isolate	L951 Chr.	Position	Nearest *Hin*dIII site	Peak Coverage	L951 Identifier	Insert location	IPO323 Identifier	InterPro Name
D/11	11	229,712	229,715	20	ZtritL951_01g06093	Upstream	ZtritIPO323_04g03005	Peptide chain release factor class I/class II
E/23	5	2,546,576	2,546,538	14	ZtritL951_01g20577	Intragenic	ZtritIPO323_04g10377	Protein of unknown function DUF3494
F/44	13	975,000	974,956	15	ZtritL951_01g08983	Upstream	ZtritIPO323_04g04480	CPSF6/7 family;RNA-binding domain superfamily
					ZtritL951_01g08985	Downstream	No IPO323 Orthologue	N/A
H/67	10	1,478,522	1,478,522	18	ZtritL951_01g05803	Downstream	ZtritIPO323_04g02889	Sirohaem synthase, N-terminal
					ZtritL951_01g05805	Upstream	ZtritIPO323_04g02890	Phytanoyl-CoA dioxygenase
I/89	9	262,311	262,311	27	ZtritL951_01g26259	Deleted	ZtritIPO323_04g13223	Short-chain dehydrogenase/reductase SDR
					ZtritL951_01g26261	Deleted	ZtritIPO323_04g13224	Ankyrin repeat-containing domain superfamily
					ZtritL951_01g26263	Upstream	ZtritIPO323_04g13226	N/A
J/90	8	1,616,180	1,616,220	17	ZtritL951_01g25689	Intragenic	ZtritIPO323_04g12920	SANT/Myb domain
K/109	8	1,791,779	1,791,706	14	ZtritL951_01g25793	Upstream	ZtritIPO323_04g12979	N/A
L/121	5	1,442,665	1,442,657	20	ZtritL951_01g19831	Intragenic	ZtritIPO323_04g09996	N/A
					ZtritL951_01g19829	Intragenic	ZtritIPO323_04g09997	Cytochrome b5-like heme/steroid binding domain
N/166	1	3,685,209	3,685,204	25	ZtritL951_01g02957	Intragenic	ZtritIPO323_04g01461	Pleckstrin homology domain

Some general observations can be made from the information outlined in Tables 4.5, 4.6 and 4.7. Firstly, no two REMI isolates had plasmid integrations at the same locus, even including the lower depth threshold (≥5 coverage) for plasmid detection. REMI B had the most detected plasmid integration events, whilst REMI O had no detectable integrations. Across the tables describing the genes impacted by the integration of the pAN7-1 plasmid, only two had no detected IPO323 orthologues, ZtritL951_01g22873 and ZtritL951_01g08985. However, eleven genes with IPO323 orthologues had no known protein functional domains detected by InterPro scan.

Most of the plasmid integrations were intergenic in the eighteen detected plasmid integration events above the depth threshold of ≥10 coverage. The plasmid sequence detected between genes could affect the neighbouring genes through interference with the promoter (potentially impacting expression) or the 3'UTR region (potentially impacting efficient translation) (Xu *et al*., 1999; Savinov *et al*., 2021). From Tables 4.5 and 4.6, there were sixteen, including ten upstream and six downstream. However, there were also ten intragenic integrations that directly interrupted a coding sequence. Also noted were the two genes, ZtritL951_01g26259 and ZtritL951_01g26261 on Table 4.5, apparently deleted in REMI mutant isolate 'I' due to the nearby integration of a pAN7-1 plasmid. A larger putative deletion of genes was noted in REMI mutant G on Table 4.7; however, this plasmid integration is below the high confidence depth threshold of ≥10x coverage.

There was no apparent bias for any chromosome having more or less pAN7-1 plasmid integrations in this collection of fifteen sequenced isolates, see Figure 4.7. Even including the lower threshold integrations, the differences between the chromosomes are marginal. Figure 4.7 and 4.8 shows that the only core L951 chromosome not to have a single plasmid integration event detected was chromosome six. Only one insertion was identified on the L951 accessory chromosomes, on chromosome fourteen in REMI isolate 'B' with multiple integrations (see Table 4.6).

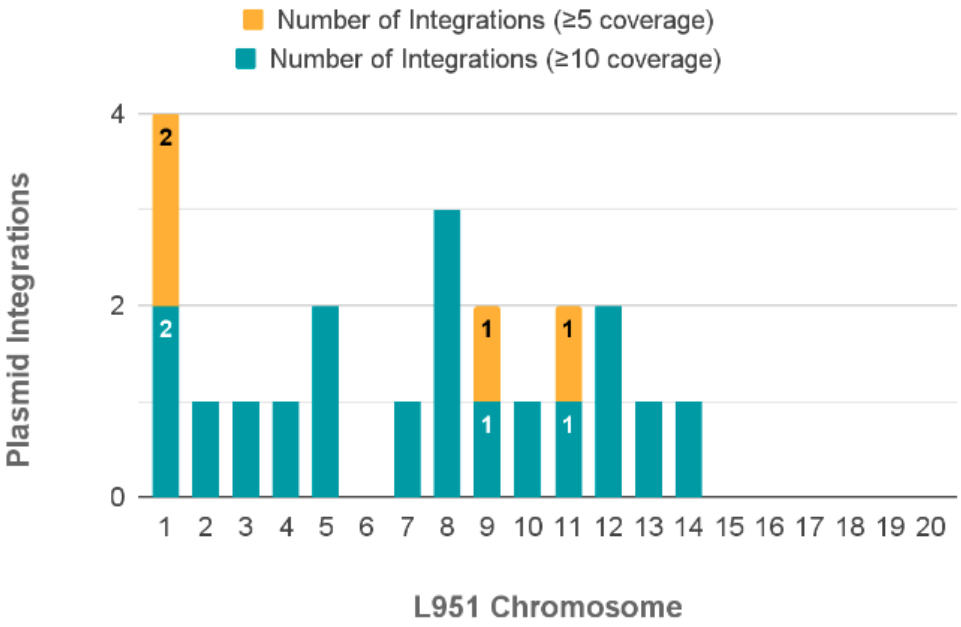

Figure 4.7 Number of plasmid integration events detected in the fifteen sequenced REMI mutagenised *Z. tritici*, L951, isolates by chromosome. Blue, integrations above the confidence depth threshold of ≥10x coverage. Yellow, are potential integration events that meet a lower threshold of ≥5x coverage.

Table 4.6 Three REMI isolates with multiple pAN7-1 plasmid integration events detected above the depth threshold (≥10 coverage).

Isolate	L951 Chr.	Position	Nearest *Hin*dIII site	Peak Coverage	L951 Identifier	Insert location	IPO323 Orthologue Identifier	InterPro Name
A/2	7	718,000	718,043	29	ZtritL951_01g22873	Upstream	No IPO323 Orthologue	N/A
					ZtritL951_01g22875	Downstream	ZtritIPO323_04g11516	N/A
	12	385,500	385,425	15	ZtritL951_01g07443	Upstream	ZtritIPO323_04g03683	PAN/Apple domain
					ZtritL951_01g07445	Upstream	ZtritIPO323_04g03684	Major facilitator superfamily
B/6	1	4,798,660	4,798,640	16	ZtritL951_01g03851	Intragenic	ZtritIPO323_04g01917	HAT (Half-A-TPR) repeat
	4	1,072,675	1,072,830	20	ZtritL951_01g17405	Intragenic	ZtritIPO323_04g08765	Zinc finger, DBF-type
	8	1,733,619	1,733,585	23	ZtritL951_01g25771	Downstream	ZtritIPO323_04g12963	Nucleosome assembly protein (NAP)
	14	551,800	551,826	13	ZtritL951_01g09407	Upstream	ZtritIPO323_04g04704	N/A
					ZtritL951_01g09409	Downstream	ZtritIPO323_04g04688	N/A
G/45	2	3,740,287	3,740,287	12	ZtritL951_01g13791*	Intragenic	ZtritIPO323_04g06816	RmlC-like cupin domain superfamily
	3	435,884	435,884	14	ZtritL951_01g14433	Intragenic	ZtritIPO323_04g07278	Transcription factor TFIIH subunit p52/Tfb2
	12	1,526,200	1,526,289	11	ZtritL951_01g08245	Downstream	ZtritIPO323_04g04098	Septin-type guanine nucleotide-binding domain
					ZtritL951_01g08247	Intragenic	ZtritIPO323_04g04096	Ribosomal protein L32p
					ZtritL951_01g08249	Upstream	ZtritIPO323_04g04097	N/A

*The plasmid integration site detected is 17 bp downstream of the detected untagged variant which is shown in Table 4.4.

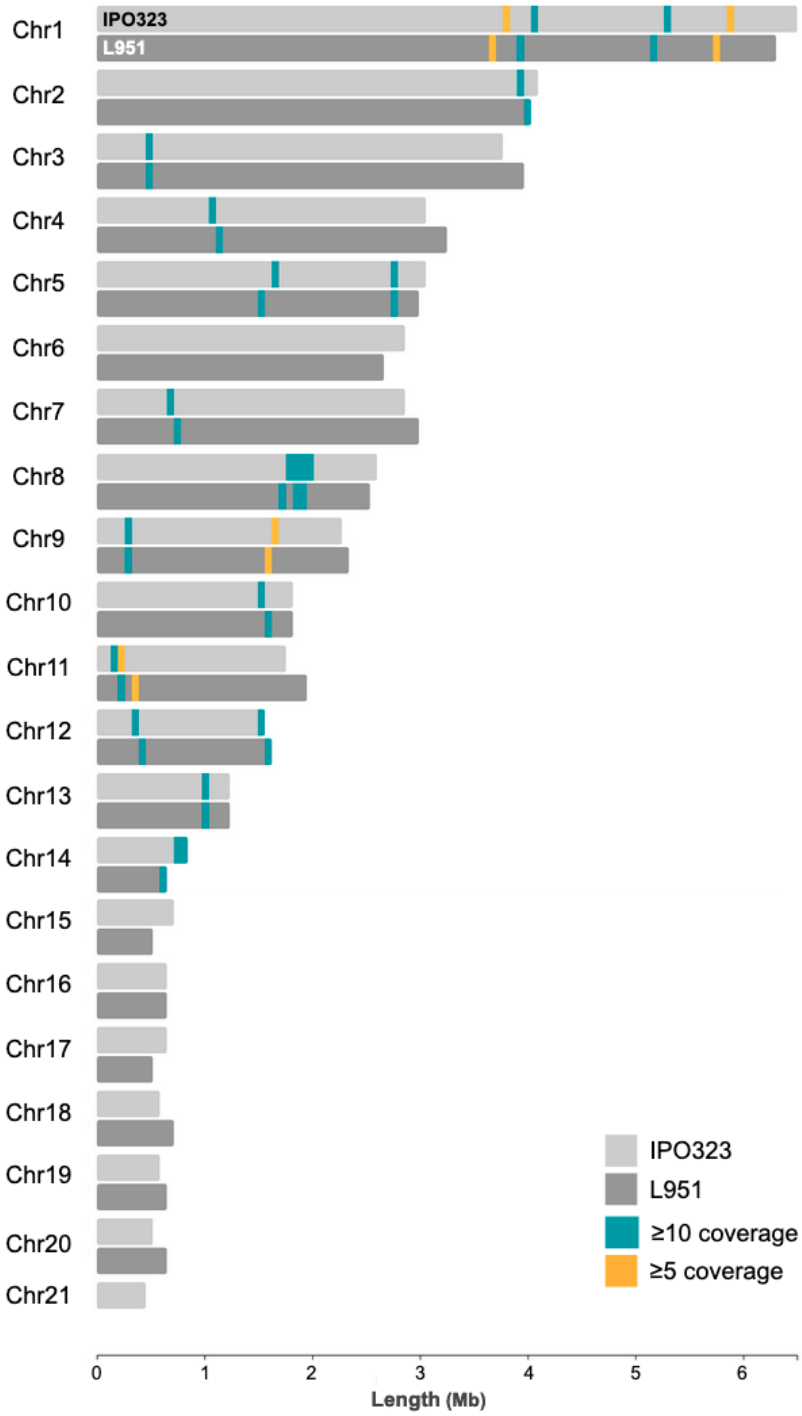

Figure 4.8 Distribution of genes potentially impacted by pAN7-1 plasmid integrations in the L951 REMI mutant isolates genomes showing the relative positions of putative IPO323 orthologues.

Visualisation of IPO323 (light grey) and L951 (dark grey) chromosomes showing relative positions of genes predicted to be impacted by plasmid integration with their putative IPO323 orthologues at both depth thresholds; blue ≥10x coverage and yellow ≥5x coverage. Produced with R package chromoMap (v. 0.3.1), Anand & Rodriguez Lopez (2022)

One gene, ZtritL951_01g13791, appeared in both the untagged variant gene list (Table 4.4) and the genes affected by plasmid integration (Table 4.6). Interestingly the sites of each were less than 20 bp apart on chromosome two in REMI isolate 'G', see Figure 4.9. Furthermore, ZtritL951_01p13791 InterPro and NCBI Conserved Domain Database (CDD, v.3.19) identified in the 544 amino acid sequence were a cupin domain (IPR013096) and a protein kinase domain (IPR000719). From the available information, I cannot determine whether the frameshift directly results from the nearby plasmid integration. However, the genes likely affected in REMI mutant G were de-prioritised given the high number of genes impacted by additional mutations in its genome.

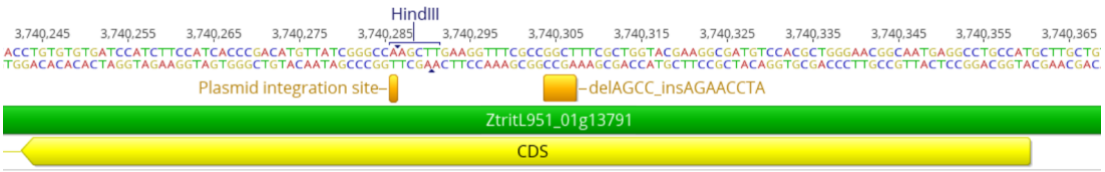

Figure 4.9 pAN7-1 plasmid integration and an untagged variant in the L951 gene, ZtritL951_01g13791, on the reverse strand of chromosome two.
Visualised using Geneious (v.10.2) showing a 120 bp portion of the ZtritL951_01g13791 annotated gene (green) on chromosome two, including the start of the predicted coding sequence (CDS) in yellow. Labelled annotations (orange) indicate the relative positions of the plasmid integration site and the SNpeff predicted high impact frameshift variant.

This analysis identified eighteen plasmid insertion events that met the threshold for confidence in the detection. Eight were intragenic, and the other ten were intergenic, either upstream or downstream of genes. Only two genes impacted by plasmid integration had no detectable orthologues in IPO323. The genes that arose from this list were considered along with those from the untagged mutation analysis to prioritise some for further functional analysis in Chapters Five and Six.

Table 4.7 Putative pAN7-1 integration events detected in four REMI mutant isolates detected above the lower depth threshold (≥5 coverage)

Isolate	L951 Chr.	Position	Nearest *Hin*dIII site	Peak Coverage	L951 Identifier	Insert location	IPO323 Identifier	InterPro Name
C/10	9	1,505,733	1,505,700	5	ZtritL951_01g27137	Downstream	ZtritIPO323_04g13672	Threonine synthase-like
					ZtritL951_01g27139	Upstream	ZtritIPO323_04g13673	Glucose-methanol-choline oxidoreductase
G/45	11	323,909	323,901	9	ZtritL951_01g06159	Deleted	ZtritIPO323_04g03036	Zinc finger, GATA-type;PAS domain
					ZtritL951_01g06161	Deleted	ZtritIPO323_04g03037	Oxidoreductase, molybdopterin-binding domain superfamily
					ZtritL951_01g06163	Deleted	ZtritIPO323_04g03038	N/A
					ZtritL951_01g06165	Upstream	ZtritIPO323_04g03039	Alpha-hydroxy acid dehydrogenase, FMN-dependent
H/67	1	3,427,353	3,427,353	9	ZtritL951_01g02765	Intragenic	ZtritIPO323_04g01362	AhpD-like
M/161	1	5,385,554	5,385,913	8	ZtritL951_01g04313	Downstream	ZtritIPO323_04g02151	N/A
					ZtritL951_01g04315	Upstream	ZtritIPO323_04g02152	Dynamin superfamily

4.3.4 Positional analysis confirms a trend towards REMI plasmid integration "near" *Hin*dIII restriction sites

The REMI mutant collection analysed here was generated in conjunction with the use of the restriction enzyme *Hin*dIII, which cuts the palindromic DNA sequence (5'-A|AGCTT-3') (http://pfam.xfam.org/family/PF09518). The mechanisms of REMI mutation at the genomic level have not been well studied for filamentous fungi, so I sought to determine the proximity of *Hin*dIII sites to plasmid insertion sites to see if there was evidence of the restriction site guiding the integration event. Figure 4.10A shows that for the twelve L951 REMI mutant isolates with eighteen plasmid integration events above our minimum depth threshold (≥10 coverage), the majority are within 50 bp of *Hin*dIII restriction sites, see Figure 4.10A. Examples of a plasmid integration event directly within a *Hin*dIII site, and one with an apparent site nearby, are shown in Figures 4.10B and 4.10C.

To indicate whether REMI mutagenesis using the *Hin*dIII restriction enzyme introduced biased plasmid integration to the vicinity of *Hin*dIII restriction sites within the *Z. tritici* L951 genome, I estimated the relative distance between all predicted *Hin*dIII cut sites identified by Geneious (v.10.2). I divided the length of each chromosome (bp) by the total number of *Hin*dIII cut sites detected on that chromosome; the results are shown in Table 4.8. An important assumption made by this calculation is that the cut sites are equally distributed across the chromosome's length. This gives an average distance per bp between *Hin*dIII sites and provides context for the distance between the cut site and detected plasmid integration sites and variants. For example, on L951 chromosome one, there is one *Hin*dIII site per 3,496 bp. However, as shown in Figure 4.10A, the integrations on chromosome one above the detection threshold in isolates 'B' and 'N' are only 20 and 5 bp away from the nearest *Hin*dIII site. Even including the lower depth threshold integrations on chromosome one, the largest distance to the nearest *Hin*dIII site in REMI isolate 'M' of 360 bp, is still well within the 3,496 bp distance average.

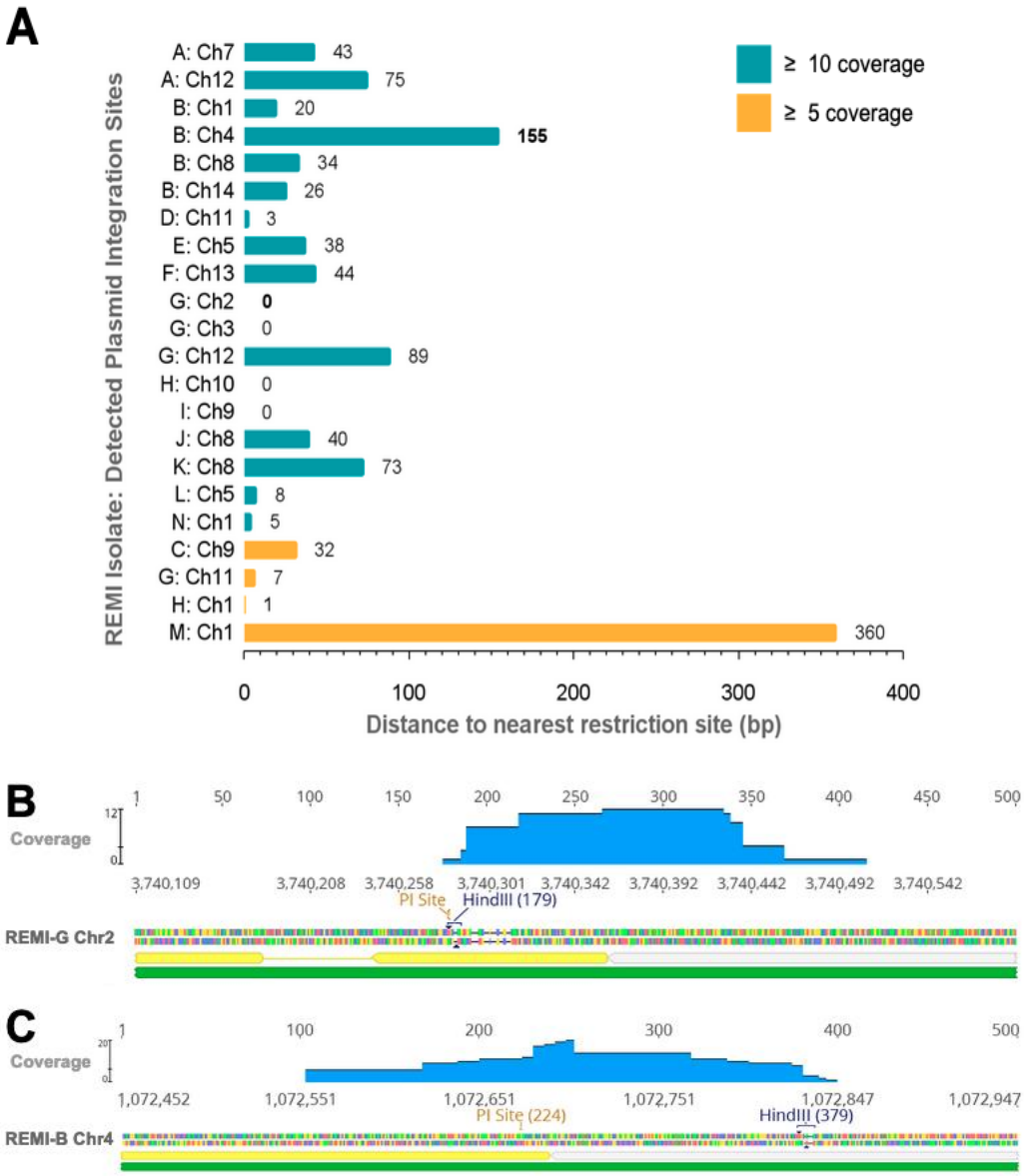

Figure 4.10 Examples of plasmid pile-ups in the *Z. tritici* L951 *Hin*dIII REMI mutant isolates in Geneious.

(A) Distances to nearest *Hin*dIII restriction site in base pairs, all are absolute values meaning they are transformed positive for presentation in this figure for ease of comparison and do not represent whether the cut site is up-/downstream. The numbers in bold relate to Figure 4.10B and C. **(B)** A detected intragenic plasmid integration with ≥10 coverage depth at a *Hin*dIII site in REMI isolate G on chromosome 2. **(B)** A detected intragenic plasmid integration with ≥10 coverage depth 155 bp away from a *Hin*dIII site.

Table 4.8 Estimating the likely distances to the nearest *Hin*dIII site on each chromosome in the L951 genome.

L951 Chromosome	Chromosome Length (bp)	Number of *Hin*dIII sites	One *Hin*dIII restriction site per (bp)*
1	5,887,365	1684	3496
2	3,755,404	1104	3402
3	3,709,007	1153	3217
4	3,032,853	966	3140
5	2,772,769	929	2985
6	2,483,369	774	3208
7	2,773,727	786	3529
8	2,393,285	752	3183
9	2,187,544	709	3085
10	1,709,149	517	3306
11	1,825,690	590	3094
12	1,540,171	450	3423
13	1,170,004	355	3296
14	599,749	197	3044
15	496,284	146	3399
16	582,880	202	2886
17	511,761	170	3010
18	679,330	233	2916
19	610,380	217	2813
20	610,428	177	3449

*Assumes the equal distribution of *Hin*dIII sites across chromosomes.

Combining the information presented in Table 4.8, Figure 4.10A and what is known about the mutagenesis technique from the literature, I had confidence in the presence of a trend towards biased plasmid integration in proximity to the *Hin*dIII restriction site. To explore this more rigorously, a statistical approach was applied to compare the mean distances to the nearest *Hin*dIII sites in untagged variants and plasmid integration sites in the REMI collection. The untagged variants and T-DNA insertions sites from the IPO323 random ATMT collection were combined as an additional

comparison (complete analysis of this collection begins section 4.3.7). I anticipated that there would be limited evidence of bias towards *Hin*dIII cut sites for either T-DNA insert locations or untagged variant sites in the random ATMT mutant isolates. There is no involvement of a restriction enzyme to integrate T-DNA from the Ti plasmid in *A. tumefaciens*. From reports in the literature on untagged variants in REMI mutants, I suspected there might be some association between untagged variants to *Hin*dIII sites. Mullins & Kang (2001) discuss that untagged mutations may result from restriction digest and subsequent inaccurate DNA repair. Some variants may have 'non-randomly' occurred at *Hin*dIII restriction sites. I kept the REMI L951 untagged variants and plasmid integration sites in separate 'mutation' groups. Ahead of analysis, the distances to the nearest *Hin*dIII site were log-transformed with an offset ($\log_{10}(x+1)$) to control for zero values and stabilise within-group variation.

Figure 4.11 shows the mean log10 transformed distances to the nearest *Hin*dIII sites and the spread of the transformed distances in the three mutation groups. A general one-way analysis of variance (ANOVA) revealed that there was a significant effect of the mutation group on the transformed distance to the nearest *Hin*dIII site ($F(2,64)= 51.81$, $p=4.16e^{-14}$). Further investigation of the impact of the mutation group on the distance to the nearest *Hin*dIII site was carried out using planned contrasts; this revealed that untagged REMI variants were associated with a statistically significant difference in mean transformed distance to the nearest *Hin*dIII site compared to plasmid integration, ($F(1,64)= 100.44$, $p=9.68e^{-15}$). The planned contrast between the T-DNA library set and the combined REMI untagged variants and plasmid integrations was non-statistically significant ($F(1,64)= 3.186$, $p=0.079$).

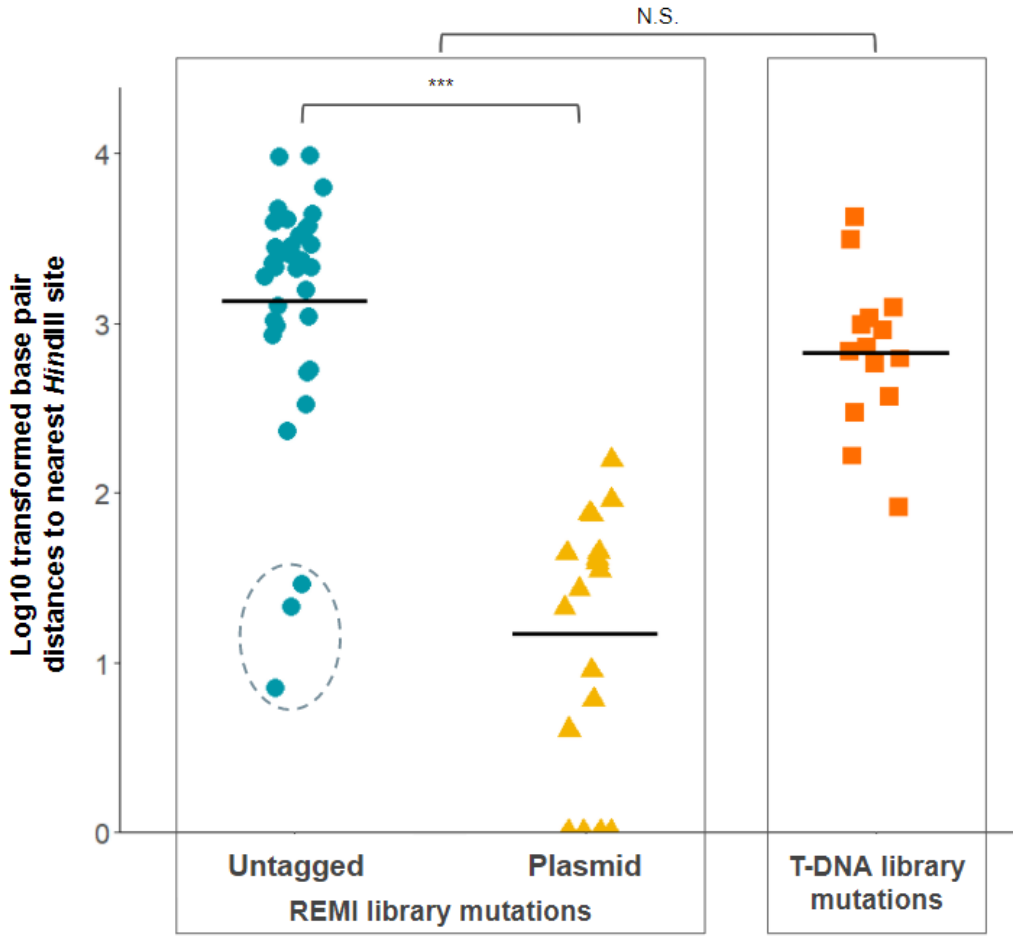

Figure 4.11 Planned contrasts in Log10 transformed base pair distances to the nearest identified *Hin*dIII cut site the sequenced L951 and IPO323 mutants. All values were Log10(x+1) transformed to control for zero values. Untagged REMI variants, including common and individual isolate variants, (blue). REMI plasmid integrations, above the >10 depth threshold, (yellow). The T-DNA library mutations (orange), include inserts and untagged variants for comparison against the REMI mutants. The black bar represents the log10 transformed distance to nearest *Hin*dIII site means, REMI untagged = 3.13, REMI plasmid = 1.17, and T-DNA library mutations = 2.83. Shown are the results of planned contrasts between the REMI untagged variants and plasmid integrations, and the T-DNA library to the REMI library. Circled are three outliers in the REMI untagged variant set that were closer to *Hin*dIII sites. Significance codes: p<0.001 '***', p>0.05 'N.S.'

Whilst we cannot determine whether the REMI untagged variants result from genomic cuts followed by mis-repair or random chance, the three outliers in circled Figure 4.11 are interesting to note. One of these outliers relates to the

individual untagged variant in REMI G in the gene ZtritL951_01g13791, a cupin domain-containing protein (previously described in sections 4.3.5 and shown in Tables 4.4 and 4.6). The next outlier is a common variant, present in almost all strains ZtritL951_01g10633 (Table 4.3). Finally, the outlier with the smallest distance to the nearest a HindIII site, the final outlier, is an individual variant previously mentioned in ZtritL951_01g25589 (REMI-L/121), encoding a predicted phosphoribosylformylglycinamidine synthase.

Overall, this data indicates that the co-incubation with *Hin*dIII has indeed "guided" the subsequent integration of plasmid insertions into the genome of L951. While some of the outliers within the untagged variants may result from mis-repaired cuts at nearby *Hin*dIII sites, there was a statistically significant difference between the transformed means of untagged and 'tagged' plasmid integrations.

4.3.5 Detection of T-DNA insertion sites in the five IPO323 derived random ATMT mutant isolates

Analogous to the analyses on tagged and untagged mutations previously described for the fifteen REMI strains, I now undertook a similar analysis on the ATMT strains characterised in Chapter Three. Whole-genome resequencing was performed on four of the random ATMT IPO323 mutants. All strains were previously shown to have a defect in virulence toward susceptible wheat plants (Chapter Three). Therefore, I sought to perform a comparable analysis on the number and sites of integration of T-DNA sequences for the four reduced virulence strains, with a similar objective of identifying any candidate genes which might be responsible for the phenotypic change.

Unlike what has been shown through previous analysis of the REMI mutant genomes in *Agrobacterium tumefaciens*-mediated transformation (ATMT) on average, a single T-DNA insert on average is expected (Michielse *et al*., 2005). Indeed, for the four IPO323 random ATMT mutant isolates analysed, only one T-DNA insert was detected in each strain. Table 4.9, shows the eight genes that were potentially affected, including six by intergenic insertion

and two by intragenic insertion of the T-DNA. Figure 4.12 shows the positions of the genes impacted by the inserts and the later identified untagged mutation events (section 4.3.7) present in these IPO323 ATMT mutagenised isolates. In addition, an intragenic T-DNA insertion in a putative MAPKKK *ZtSSK2* (ZtritIPO323_04g02061 in 4-124 mutant) was noted to be a component of the Hog1 MAPK signalling pathway. ZtHog1 has already been implicated in the virulence and response to multiple fungal growth stressors in *Z. tritici* (Mehrabi *et al.*, 2006b).

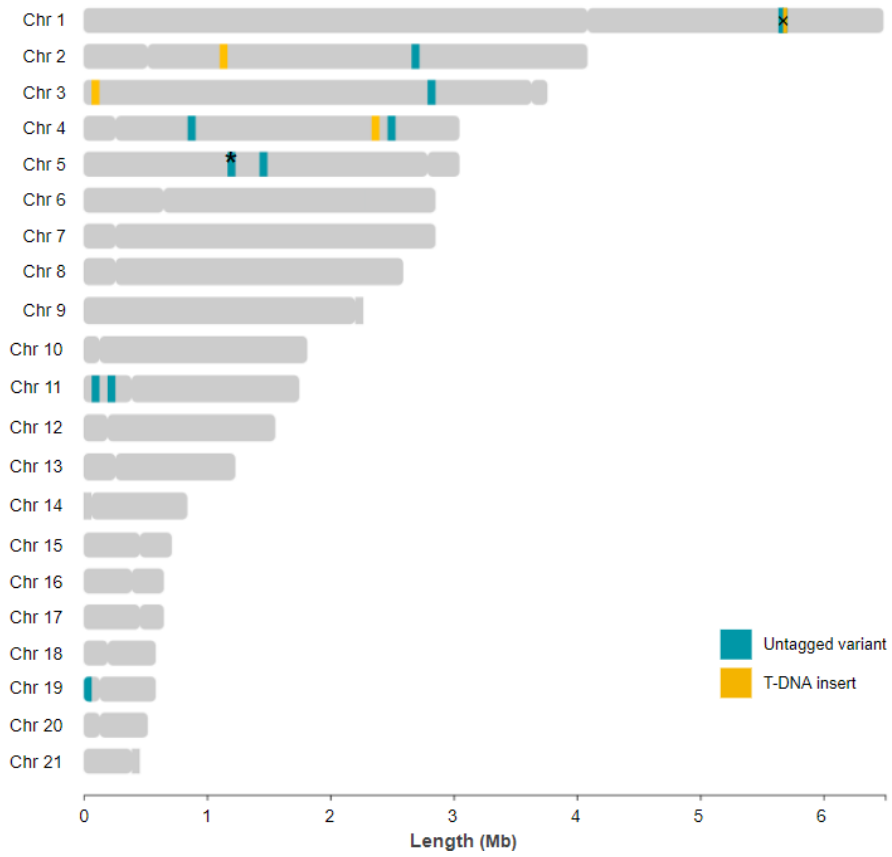

Figure 4.12 Display of the relative chromosomal locations of the T-DNA and untagged variants in the five random ATMT *Z. tritici* IPO323 mutants.

* Indicates a region where two nearby genes with untagged variants were identified on chromosome five. × Indicates ZtritIPO323_04g02061 a gene on chromosome one was impacted in two independent IPO323 random ATMT mutant isolates, 4-124 and 4-158, by a T-DNA insert and an untagged variant caused by a frameshift respectively. Produced with the aid of R package chromoMap (v. 0.3.1).

Table 4.9 The sites of random T-DNA insertion in the four explored IPO323 mutant isolates and the genes with putatively impacted function.

IPO323 Mutant Isolate	IPO323 Chromos -ome	T-DNA Insert Location	Putatively Impacted Genes	Interpro Name	Insert Location
4-124	1	5313974-5315085	ZtritIPO323_04g02061	Mitogen-activated protein (MAP) kinase kinase kinase Ssk2/Ssk22	Intragenic
			ZtritIPO323_04g02062	WD40-repeat-containing domain superfamily	Upstream
4-158	3	99207-99214	ZtritIPO323_04g07162	Gamma-glutamyl cyclotransferase-like	Downstream, 3'UTR
			ZtritIPO323_04g07163	Zn(2)-C6 fungal-type DNA-binding domain	Downstream, 3’UTR
5-51	2	1057013-1057051	ZtritIPO323_04g05837	Major facilitator superfamily	Downstream, 3'UTR
15-120	4	2261923-2261926	ZtritIPO323_04g09207	Molybdenum cofactor sulfurase, C-terminal;MOSC, N-terminal beta barrel	Downstream, 3’UTR
			ZtritIPO323_04g09208	Arf GTPase activating protein	Upstream

4.3.6 Detection of untagged variants in the T-DNA insertion mutants

The investigation of the REMI collection highlighted the importance of checking for ‘untagged’ variation, which can occur and can potentially be responsible for the observed phenotypic changes. So, similarly, I sought to determine the presence and number of additional untagged mutations in the ATMT mutant strains. This analysis identified twelve unique, intragenic untagged mutations, six of which were single isolate specific. In addition, SNpeff identified six genes whose function could be affected by these mutations, including four with predicted function and two without known function. These genes were affected by five frameshifts, and one gained a stop codon mutation, as listed in Table 4.10. Three further moderate impact untagged mutations specific to isolate 15-120 were also identified, see Table 4.10.

Unlike the REMI mutants, there was no high impact common untagged mutations between the isolates, see Table 4.10. However, there was two moderate impact untagged mutations in three of the IPO323 ATMT mutant isolates, and one common low impact mutation listed in Table 4.10. These three variants were the same in 4-124 and 5-51, and two of the same were also in 4-158, but which were missing the moderate missense variant in ZtritIPO323_04g09929. This highlighted a similar issue as with the REMI library, that the specific IPO323 parental isolate cultured for the generation of the random ATMT mutants was not sequenced and that some additional mutations had arisen. Therefore, I cannot determine whether these common, moderate/low untagged variants existed in the ‘background’ before mutagenesis. However, these common variants present in “4-124”; “4-158” and “5-51” are from libraries generated at a similar time, using potentially the same parental IPO323 stock. Irrespective of this, these common moderate and low impact variants were considered unlikely to explain the phenotype observed following the same logic for dismissing the common variants in the REMI library. This was supported by the fact that isolate 5-51 has a different

hyphal growth phenotype compared to 4-124 and 4-158 (Chapter Three). Therefore, these common variants in 4-124, 4-158 and 5-51 are unlikely to explain these isolates' differing hyphal growth phenotypes.

There was one remarkable finding amongst the untagged high impact variants. In the previous analysis of T-DNA insertion sites in mutant 4-124, an intragenic insertion in the promoter and 5' region of a putative MAPKKK, orthologous to *Ssk2/Ssk22* in yeast was detected (Maeda *et al*., 1995: protein ID YNR031C). While analysing the untagged mutations in strain 4-158, I identified a high impact frameshift mutation in the same gene (Mycgr3G67344/ ZtritIPO323_04g02061). This gene is therefore listed in both Tables 4.9 and 4.10. Making this a prioritised candidate gene is explored that was subsequently explored in greater detail (Chapter Six). Incidentally, both 4-124 and 4-158 mutant isolates were shown in Chapter Three to have reduced virulence and similar stress sensitivities and hyphal growth defects. This was an early indication that there may have been a common genetic basis for the shared phenotypes.

Like the analysis of REMI mutations, candidate genes have arisen through both direct insertion events and potentially through untagged mutations. The ability to detect these untagged changes easily by whole genome sequencing highlights the power of this approach. The challenge was to analyse gene lists then and prioritise those whose function might be responsible for the phenotypic changes observed in the parental strains.

Table 4.10 Identified variants in the *Z. tritici* IPO323 random ATMT mutant collection.

ATMT Isolate	IPO323 Chromosome	Putatively Impacted Genes	InterPro Name	SNPeff Predicted Impact	Mutation
4-124	5	ZtritIPO323_04g09806	N/A	High	frameshift
	4	ZtritIPO323_04g08686	N/A	Moderate	conservative inframe deletion[1]
	5	ZtritIPO323_04g09929	P-type ATPase	Moderate	missense variant[2]
	5	ZtritIPO323_04g09809	Alpha/beta hydrolase fold-3	Low	synonymous variant[3]
4-158	1	ZtritIPO323_04g02061	Mitogen-activated protein (MAP) kinase kinase kinase Ssk2/Ssk22	High	frameshift
	4	ZtritIPO323_04g08686	N/A	Moderate	conservative inframe deletion[1]
	5	ZtritIPO323_04g09809	Alpha/beta hydrolase fold-3	Low	synonymous variant[3]
5-51	5	ZtritIPO323_04g09806	N/A	High	frameshift
	11	ZtritIPO323_04g03036	Zinc finger,GATA-type;PAS domain;PAC motif	High	frameshift
	4	ZtritIPO323_04g08686	N/A	Moderate	conservative inframe deletion[1]
	5	ZtritIPO323_04g09929	P-type ATPase	Moderate	missense variant[2]
	5	ZtritIPO323_04g09809	Alpha/beta hydrolase fold-3	Low	synonymous variant[3]
15-120	2	ZtritIPO323_04g06395	Transglutaminase-like	High	stop gained
	11	ZtritIPO323_04g02979	Pyridoxal phosphate-dependent transferase	High	frameshift
	3	ZtritIPO323_04g08085	Piwi domain;PAZ domain; Argonaute, linker 1 domain	Moderate	disruptive inframe deletion
	4	ZtritIPO323_04g09248	ATPase, V0 complex, subunit e1/e2	Moderate	missense variation
	19	ZtritIPO323_04g05318	N/A	Moderate	missense variation

[1] Matching in-frame deletion; [2] Matching missense variant; [3] Matching synonymous variant.

4.3.7 Prioritisation pipeline for best candidate genes affecting virulence in REMI and T-DNA mutant isolates

The previously described analyses of the REMI and ATMT mutant data identified 80 genes affected by the untagged mutation, T-DNA insertion, or plasmid integration. I now sought to define a shortlist from these as most likely to play a role in the virulence phenotype, see Figure 4.13. The first filter for assessing untagged variants was the predicted impact by SNPeff. Predicted “low” impact variants were discarded, whilst those with “moderate” and “high” impact were given more consideration. Intragenic insertions were prioritised over intergenic insertion sites for plasmid and T-DNA insertion events. Subsequently, another simple filter was used, thereby assigning lower priority to candidates present on the accessory chromosomes of L951 and IPO323, as the relevance of their genomic content to virulence and the morphogenic switch to filamentous growth is unlikely.

One of the key resources I could utilise to filter further were pangenomes, including those published in addition to the unpublished pangenome of 18 pan-European strains collected (Rudd, personal communication). The unpublished dataset comprises genomic data for seventeen disease-causing field isolates alongside IPO323, with 13 of the isolates also subjected to replicate *in vitro* and *in planta* RNAseq expression analysis. As some of the mutants exhibited *in vitro* growth defects (including hyphal growth and growth under stress – see Chapter Three), I postulated that the underlying genes were likely to reside in the core pangenome. Therefore, if a gene identified within this pangenome was absent from any strains or present with a knockout (KO) mutation in any strain, it was considered a less likely candidate. Another metric derived from this data was a ‘mutability’ ratio, which is the total number of high and moderate impact SNPs divided by the protein sequence length. I again postulated that important core genes, which affect *Z. tritici* growth and differentiation, would have no high and less moderate impact mutations than those that may confer more flexible

functions. Therefore, this ratio should be relatively low in genes essential for *Z. tritici* virulence if they underpin essential phenotypic changes.

In addition to the pangenome analysis, all genes were checked for relative expression in published datasets and unpublished twelve strain datasets (Rudd, personal communication). This indicated the timing of candidate gene expression, hinting at what point in the *Z. tritici* life or infection cycle stage they are relevant. Finally, I checked the broader literature for all genes where specific functions were inferred and used publicly available databases and online resources (PHI-base, BLAST and Knetminer) to gather more information on their likely roles in fungal growth and virulence. These analyses enabled me to rank all candidate genes identified in each strain for their potential role in the reduced virulence of strains. The complete ranked table with supporting evidence is shown in Table 4.11 and 4.12.

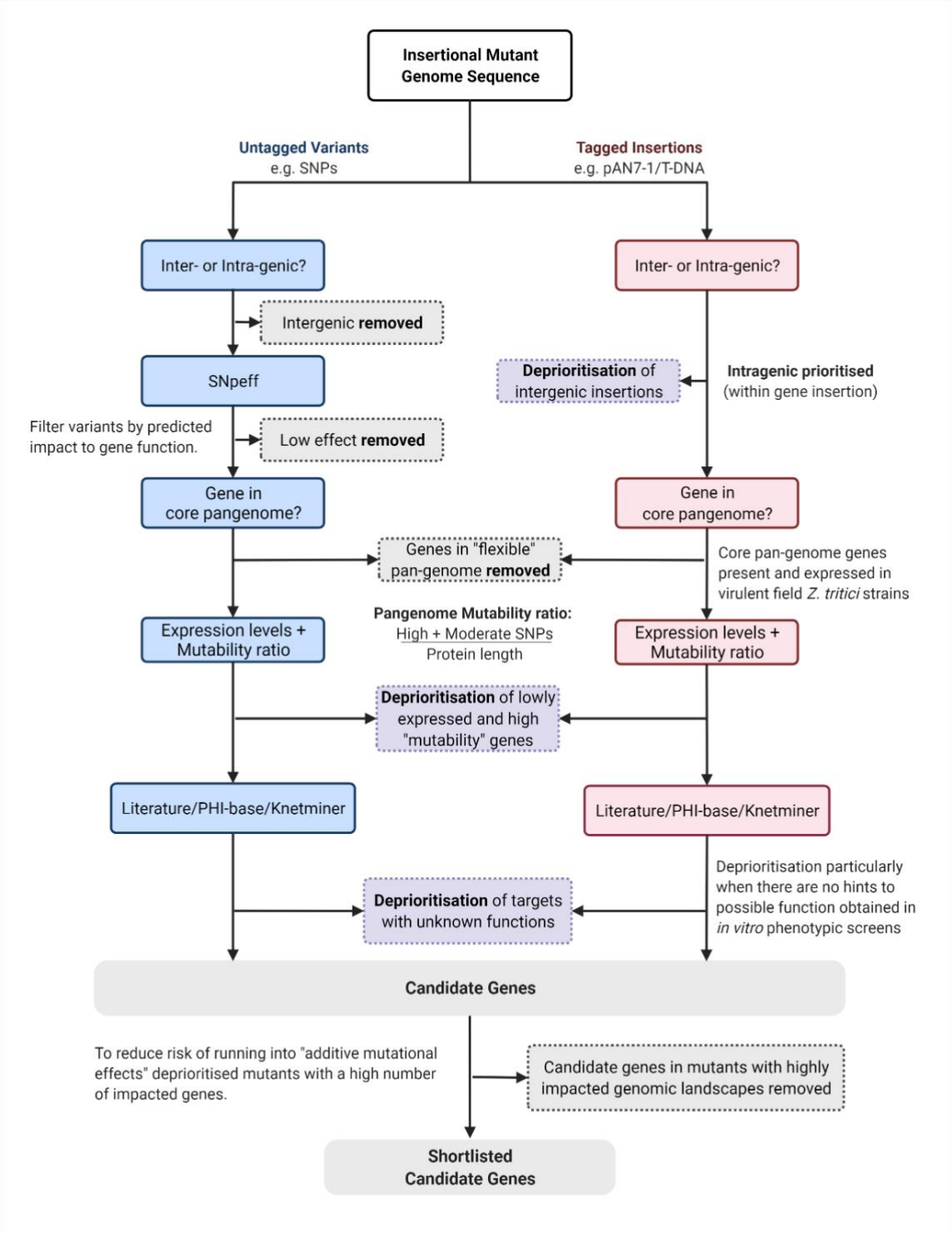

Figure 4.13 Flow diagram showing the stages of the candidate gene elimination process used to arrive at a shortlist of candidates.

Created with BioRender.com/

Another unexpected criterion subsequently considered in prioritisation is that a mutation impacts a single gene in more than a single strain with similar observed phenotypes, as was the case with the putative MAPKKK *Ssk2/Ssk22*. This gene was affected by intragenic T-DNA insertion in strain 4-124 and independently by a frameshift untagged SNP mutation in strain 4-158. As both strains have reduced virulence, it is conceivable that the loss of function of this gene might be responsible for these phenotypes.

Careful consideration was also made ahead of the decision to explore candidates in mutants with multiple high effect mutations (tagged and untagged). For example, REMI mutant G painted the most complicated picture, including untagged variants and genes putatively impacted by plasmid integrations, resulting in 22 genes potentially affected. As a result, the investigation of genes in this mutant was de-prioritised due to the chances that multiple genes may contribute to the overall phenotype. However, a putative plasmid integration affecting the *ZtWCO1* (also published under WC-1) gene was noted. This gene has appeared in previously published literature and is being investigated by other groups (Habig *et al*., 2019; McCorison & Goodwin, 2020).

In summary, this whole-genome resequencing approach applied to reduced virulence mutants led to the final identification of 18 genes, a selection of which were then successfully subjected to functional validation in the forthcoming chapters.

Table 4.11 Final list of prioritised candidate virulence and morphogenic switching associated genes identified in L951 REMI mutant library.

REMI Isolate	L951 Identifier	L951 Chr.	Predicted IPO323 Orthologue	JGI-ID	InterPro Name	Mutation	Mutability Ratio*
M/161	ZtritL951_01g04653	1	ZtritIPO323_04g02333	Mycgr3G67669	Amino acid/polyamine transporter I	NPAV	0.00
L/121	ZtritL951_01g25589	8	ZtritIPO323_04g12872	Mycgr3G61816	Phosphoribosylformylglycinamidine synthase	NPAV	0.02
I/89	ZtritL951_01g26259	9	ZtritIPO323_04g13223	Mycgr3G101134	Short-chain dehydrogenase/reductase SDR	PI, intragenic	0.02
N/166	ZtritL951_01g02957	1	ZtritIPO323_04g01461	Mycgr3G98644	Pleckstrin homology domain	PI, intragenic	0.03
J/90	ZtritL951_01g25689	8	ZtritIPO323_04g12920	Mycgr3G75046	SANT/Myb domain	PI, intragenic	0.03
B/6	ZtritL951_01g03851	1	ZtritIPO323_04g01917	Mycgr3G98811	HAT (Half-A-TPR) repeat	PI, intragenic	0.04
F/44	ZtritL951_01g08983	13	ZtritIPO323_04g04480	Mycgr3G97502	CPSF6/7 family	PI, upstream	0.08
A/2	ZtritL951_01g07445	12	ZtritIPO323_04g03684	Mycgr3G77261	Major facilitator superfamily	PI, upstream	0.08
D/11	ZtritL951_01g06093	11	ZtritIPO323_04g03005	Mycgr3G111162	Peptide chain release factor class I/class II	PI, upstream	0.38
K/109	ZtritL951_01g24659	8	ZtritIPO323_04g12402	Mycgr3G46572	Gti1/Pac2 family	NPAV	0.05

PI = plasmid integration, NPAV = non-plasmid associated variant. *a ratio derived from the unpublished pangenome data set (personal communication, Rudd), taking the number of High and Moderate impact variants detected and dividing by protein length. The highlighted row is a candidate gene identified but not planned to follow up.

Table 4.12 Final list of prioritised candidate virulence and morphogenic switching associated genes identified in the IPO323 random ATMT mutant library.

ATMT isolate	IPO323 Gene Identifier	JGI ID	IPO323 Chr.	InterPro Name	Mutation	Mutability Ratio*
4-124 and 4-158	ZtritIPO323_04g02061	Mycgr3P67344	1	Mitogen-activated protein (MAP) kinase kinase kinase Ssk2/Ssk22	frameshift + T-DNA, intragenic	0.02
15-120	ZtritIPO323_04g06395	Mycgr3P36895	2	Transglutaminase-like	stop gained	0.02
5-51	ZtritIPO323_04g03036	Mycgr3P76651	11	Zinc finger, GATA-type;PAS domain	frameshift	0.03
15-120	ZtritIPO323_04g09208	Mycgr3P71479	4	Arf GTPase activating protein	T-DNA, upstream	0.00
4-158	ZtritIPO323_04g07162	Mycgr3P27346	3	Gamma-glutamyl cyclotransferase-like	T-DNA, 3'UTR	0.01
4-158	ZtritIPO323_04g07163	Mycgr3P28269	3	Zn(2)-C6 fungal-type DNA-binding domain	T-DNA, 3'UTR	0.03
15-120	ZtritIPO323_04g09207	Mycgr3P14486	4	Molybdenum cofactor sulfurase, C-terminal; MOSC, N-terminal beta-barrel	T-DNA, 3'UTR	0.03
15-120	ZtritIPO323_04g02979	Mycgr3P87913	11	Pyridoxal phosphate-dependent transferase	frameshift	0.25
5-51	ZtritIPO323_04g05837	Mycgr3P23761	2	Major facilitator superfamily	T-DNA, 3'UTR	0.62

4.3.8 Whole-genome resequencing confirms the genetic instability of *Z. tritici* genomes

We identified isolates with multiple plasmid integration sites within the fifteen REMI isolates sent for genome re-sequencing. In the set of random ATMT mutants, only single T-DNA inserts in each isolate were observed. It has previously been shown that, on average, ATMT integrates only one copy of a T-DNA insert into the host genome, reducing the analyses' complexity as there should be fewer functionally impacted genes (Michielse *et al.*, 2005). This reduces the chances of multiple affected genes contributing to an observed phenotype. However, both methods here introduce 'untagged' variation, that is, sequence changes not associated with detected pAN7-1 plasmid and T-DNA integration. T-DNA integrations have also been associated with other chromosomal aberrations, including re-arrangements, deletion, duplication, and inversion (Weld *et al*., 2006). Whilst similar large effects have not been described in the process of REMI mutagenesis in the literature, in the fifteen L951 *Z. tritici* mutants, there were some integrations associated with deletions of multiple genes, such as in REMI-I/89.

One of the significant limitations of REMI described in the literature is the high proportions of untagged mutations (Mullins & Kang, 2001). Due to the difference in the size of the two libraries sequenced in my work, it would be challenging to draw any statistically backed conclusions. However, the most complicated L951 mutant, REMI-G/45, has 23 genes putatively impacted by mutations (plus an additional four >5 coverage), including all common variants. However, in comparison, the most 'complicated' IPO323 mutant, 15-120, has seven mutations. From the subset of ATMT mutants that were checked for untagged variant impacts, there appear to be fewer variants than REMI.

As well as the difference in the number of isolates sequenced, the differences between the L951 genome assembly used to map the mutant isolate genomes and the "L951 isolate" that Skinner used in the generation of the REMI collection likely inflate the numbers of untagged variants observed.

Whereas with the random ATMT collection, only a few common untagged variants were observed, suggesting that the parental strain had mutated less in generating the transformants.

A few putative mechanisms explaining how ‘untagged’ variants arise due to the REMI mutagenesis have previously been put forward. A common suggestion is the restriction enzyme digesting of the host genome without a plasmid integration occurring that is then mis-repaired. Additionally, the transformation process itself is mutagenic; ergo, the stress applied to the genome by the transformation, selection, and regeneration process likely generates a number of untagged effects (Kahmann & Basse, 1999; Maier & Schäfer, 1999; Mullins *et al.*, 2001). I argue the latter suggestion fits with the data presented here, particularly for the number of mutations common between all or more than one strain. Even including the outliers in the distance to *Hin*dIII sites to the variants there was a statistically significant difference between untagged and tagged. Alternatively, the L951 strain used by Skinner (2001) for the transformation developed spontaneous low impact ‘background’ mutations before the transformation. REMI and the restriction sites ‘available’ to digest are not entirely random. Therefore, the unlikely option exists for some untagged variants that restriction enzymes ‘targeted’ the same sites (for the list of common untagged), causing the same or similar mutational effects (Maier & Schäfer, 1999). Interestingly, of the three outliers, two were in individual isolates. I postulate that the untagged variant in REMI L/121 and REMI G/45 may result from mis-repair from *Hin*dIII digest without plasmid integration.

4.3.9 The power of casting a genome-wide net in fishing for untagged variants generated by mutagenesis

Z. tritici was the first genome of a filamentous fungus to have a fully sequenced, all chromosomes from telomere to telomere, reference isolate genome (IPO323) (Goodwin *et al.*, 2011). Current knowledge has built on the early studies that identified the presence of dispensable/accessory chromosomes in the variation between strains in chromosome length and

number polymorphisms (McDonald & Martinez, 1991; Kema *et al*., 2002; Wittenberg *et al*., 2009; Testa *et al.,* 2015). However, next-generation sequencing technologies, and a reduction in the cost of using those technologies, have enabled an approach that has more power to identify changes that would have previously gone unseen. By whole-genome sequencing collections of *Z. tritici* field isolated strains, and generated mutant isolates, a lot of information becomes accessible.

Researchers can now explore in-depth chromosome structural changes and presence/absence polymorphism and identify regions with biases to change in *Z. tritici*. In addition, multiple studies now highlight the diversity and instability of some areas of *Z. tritici* chromosomes (McDonald *et al*., 2016; Habig *et al*., 2017). Whilst the variation in mutant isolates is relatively small compared to natural variation between strains in field populations, the fact it occurs points to significant genome instability in this organism, which may also contribute to its rapid evolution rate. For lab generated mutants, identifying tagged events has traditionally used selective techniques, including chromosome/primer walking, plasmid rescue and PCR-based methods. These have also been used to identify T-DNA insertion and REMI integration sites (Michielse *et al*., 2005; Urban *et al*., 2015). By whole-genome sequencing, we identified these untagged effects of mutagenesis. However, to add to the power of this approach in future, the parental strains used in the mutagenesis should also have their gDNA sequenced. This would help identify putative untagged effects due to random ‘background’ mutation from those potentially commonly induced mutations due to the mutagenesis process. Given the propensity *Z. tritici* seemingly has for variation even after a single culture from stock, it may be challenging to have the same “WT” parental strain tested later *in planta* screens and *in vitro* growth characterisations alongside the generated mutants. Of course, with casting such a wide net, careful consideration of the filters applied in the candidate gene identification pathway is necessary.

4.3.10 Prioritisation of candidates: pros and pitfalls of the pipeline

With the sheer volume of data resulting from casting a genome-wide net, having a pipeline to sift and prioritise candidate genes is useful. There is a balance in the filtering approach between applying strict, highly stringent filters that may lose candidates and the number of false candidates that will arise from a less stringent approach. With the current unknowns in understanding the *Z. tritici* genome, cell biology and its infection cycle, applying strict cut-offs is a challenge. Follow single filtering metric is no good, e.g. expression levels would potentially rule out a previously published hyphal growth and virulence-associated gene, *ZtGT2* (Master Mean FPKM: 6.03). However, I would not place this gene in the flexible proponent of the pan-genome (Mutability ratio: 0.00). By ranking and in situations where there are two equally likely genes picking one to start with the experimental phase (using targeted KO or complementation) elimination process can be streamlined.

In the following chapter, I describe experimentation to validate the identified candidate genes in the L951 REMI mutant background through complementation by ATMT of the mutant isolate with a Ti plasmid construct containing a functional copy of the candidate gene to restore the wild-type phenotype.

5 Functional complementation and characterisation of genes arising from the REMI dataset

5.1 Introduction

The previous chapters identified several REMI mutants with reduced virulence on plants and defined the best candidate genes potentially affected in the mutants which could be responsible for the phenotypes described. This chapter details functional validation experiments on two processes: regulation of splicing and purine biosynthesis. Cellular metabolic processes and the progression through the cell cycle phases are highly controlled, and the genes involved tend to be essential.

Previous studies have highlighted the importance of transitioning into a filamentous/hyphal growth state for virulence in various fungal pathosystems, threatening plants, animals, and humans. These include *Z. tritici* and other phytopathogenic fungi, such as *Ustilago maydis*, and human fungal pathogens like *Candida albicans* (Boyce & Andrianopoulos, 2015; Habig *et al*., 2019; Kellner *et al*., 2014; Motteram *et al*., 2011). The general mechanisms of hyphal filament extension have been studied. The extension of hyphal filaments is a tightly controlled process involving multiple cellular processes. Hypha morphogenesis involves cell polarization, exocytic and endocytotic transport machinery, vesicle transport, cell wall generation, and the selection of branching points and septation sites. An essential structure involved with hyphal growth is the Spitzenkörper, which acts as a vesicle distribution centre transporting cell wall materials, extracellular hydrolytic enzymes, and other factors to the hyphal tip. In addition, a microtubule network connects vesicles generated by the endoplasmic reticulum, Golgi, and the Spitzenkörper (Kiss *et al*., 2019; Meyer *et al*, 2021). Given the differences between a unicellular ‘yeast-like’ cell versus the multicellular, filamentous growth forms, it is no surprise that dimorphic switching would be a tightly regulated. The process is better understood in other fungi, much of the genetic circuitry has not been studied in *Z. tritici*.

De novo purine biosynthesis and salvage pathways are critical broadly across the tree of life due to the role of their derivatives in multiple cellular functions. Purines and their derivatives have a variety of roles in cellular biochemistry, including metabolism and producing nucleotides for DNA synthesis and repair and RNA transcription (Pedley & Benkovic, 2017; Yemelin *et al*., 2017). The enzymes which act in the purine biosynthetic pathway are conserved. This synthesis pathway in fungi is best characterised in yeast *Saccharomyces cerevisiae*, though mutants of other species of pathogenic fungi impacted in this biosynthesis pathway have also been investigated. Disruption of genes involved in this biosynthesis pathway in *Candida albicans*, *Cryptococcus neoformans* and *Magnaporthe oryzae* resulted in attenuated or complete loss of virulence towards their respective hosts, and general growth defects. PHI-base BLASTp (http://phi-blast.phi-base.org/) search also identified two bacterial plant pathogens with mutations in *ADE6*, *Dickeya dadantii* and *Erwinia amylovora*, also exhibited reduced virulence phenotypes (Fernandez *et al*., 2013; Jiang *et al*., 2010; Klee *et al*., 2019; Morrow *et al*., 2012; Royet *et al*., 2019).

In *Z. tritici*, Yemelin *et al.*, (2017) identified an adenine auxotrophic mutant with function impacted in the *MYCO4* gene (detected orthologue of *S. cerevisiae* Ade5,7 encoding phosphoribosylglycinamide synthetase) from a collection generated by random ATMT. Their results highlighted the difference in *Z. tritici* purine biosynthesis/salvage pathway to related fungi, as Myco4p and homologs in the Mycosphaerellaceae family were monofunctional proteins, whereas the yeast equivalent is bifunctional. *Z. tritici* is thought to rely on its internal stores during the initial latent phase of symptomless infection. This has been indicated by typical starvation responses determined from *in planta* transcriptomics, which persisted until the onset of necrotrophic symptoms (Keon *et al*., 2007; Rudd *et al*., 2015). In support of this, Derbyshire *et al*., (2018) investigated a different biosynthesis pathway, looking at the role of *ZtPPT* (a post-translational activator phosphopantetheinyl transferase), which produces an essential co-factor for the *de novo* production of lysine. Defective *Ztppt* mutants were auxotrophic

for lysine and non-pathogenic on wheat. Taken together, the *de novo* biosynthesis pathways are likely to be important for early infection when extracellular nutrition is unavailable or limiting.

In REMI mutant B/6, the prioritised candidate gene from Chapter Four is an orthologue of the *S. cerevisiae* Clf1p, a member of the Prp19 complex. The broadly conserved Prp19 complex, also known as the NineTeen protein complex (NTC), plays a key role in the 'spliceosome' complex and is involved in intron removal during pre-mRNA splicing. Splicing of mRNA precursors is an essential part of regulated gene expression and, by extension, important for typical cell cycle progression. In addition, this complex has also been associated with functions in genome maintenance, protein degradation and lipid biogenesis (Borao *et* al., 2021; Chanarat & Sträßer, 2013; Yan *et al*., 2017). The Prp19 complex is broadly conserved with homologues in *Homo sapiens*, *Trypanosoma brucei* (parasitic kinetoplastid belonging to the genus Trypanosoma) and *Arabidopsis thaliana* (Ambrósio *et al*., 2015; Chanarat & Sträßer, 2013; Monaghan *et al*., 2009). Whilst the Prp19 complex has been well studied in yeasts and select human fungal pathogens, there is limited information on the complex in plant pathogenic fungi.

In *S. cerevisiae* Clf1p (also known as Syf3p, YLR117C) is a splicing factor that is involved in several processes of importance for cellular homeostasis. Figure 5.1A shows a simplified representation of the spliceosome assembly and activation in *S. cerevisiae*. Figure 5.1B shows a cryo-EM structure of activated spliceosomal. The predicted yeast orthologue of Zt*CLF1* was identified as the orthologue of the *Drosophila* crooked neck (crn) gene. Significantly, mutations within these two systems are lethal (Chung *et al*., 1999). Whilst there are studies into the origins of spliceosomal introns in the *Zymoseptoria* clade (Wu *et al*., 2017) there are no published studies on the functional analysis of components of the spliceosome complex. However, several putative orthologues in the complex have been identified through sequence similarity and predicted functional protein domains identified in *Z. tritici and* listed in the associated KEGG pathway; Ztr03040.

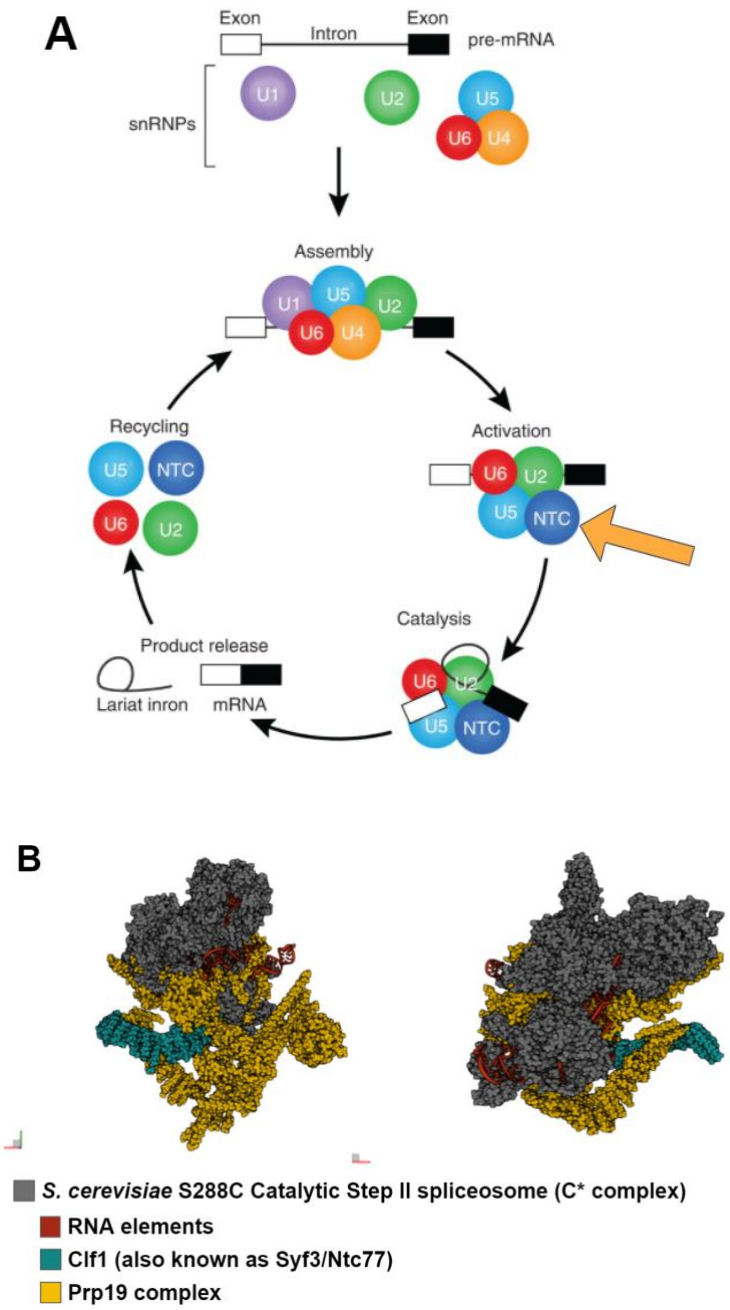

Figure 5.1 *S. cerevisiae* Clf1 and Prp19 C* complex in Catalytic Step II spliceosome complex and functions in the spliceosome.

[A] A representation of the spliceosome adapted from DeHaven *et al*., (2016), a yellow arrow indicates the NTC/Prp19 complex and **[B]** 3D protein structure published Yan *et al*. (2017). The wider complex is grey and the RNA associated elements (U2, U6 and U5) are red. Yellow indicates components indentified as members of the Prp19 complex, and blue is the Clf1 component. The equivalent of this complex is not well studied in *Z. tritici.* Structure accessible: https://www.rcsb.org/structure/5wsq

This chapter adopted a genetic complementation approach to test whether the observed reduced virulence and hyphal growth phenotypes could be rescued. This should be observed upon reintroducing a wild type (WT) copy of the defective candidate gene, driven by native promoters into the candidate mutagenised strain. I demonstrate that for two of the REMI mutagenised isolates, complementation restored *in vitro* growth and *in planta* disease symptom development phenotypes to that of the wild type. In addition, I confirm the gene responsible for reduced virulence in an adenine auxotrophic REMI mutant originally described in Skinner (2001) to be *ZtADE6*. Finally, for the first time, I also show the importance of the spliceosome in the virulence and growth transitions of *Z. tritici*.

5.2 Materials and Methods

5.2.1 Complementation of select candidate genes into the *Z. tritici* REMI mutants

Plasmids were constructed using vector pCGEN, which possesses the geneticin resistance cassette, see Figure 5.2. This plasmid was prepared by linearisation with *KpnI* and *Hin*dIII restriction enzymes and gel purified. For complementation constructs, where the aim is for the whole gene to be 'restored' into the mutant genome, I attempted to ensure the natural promoter and terminator regions were maintained. Therefore, PCR provided an extra 212-1000 bp on the 5' promoter end (avoiding including regions of other annotated genes) and an added 120 bp to the 3' end (to include the 3' UTR). Fragments were ligated into the pCGEN backbone using Gibson Assembly with conditions and primers previously listed in Chapter Two. A restriction digest assay was performed on the mini-prep to check that the plasmid construction was successful before electroporation into *Agrobacterium*. Colony PCR was also performed to confirm the successful introduction of the T-DNA plasmid into the *Agrobacterium*.

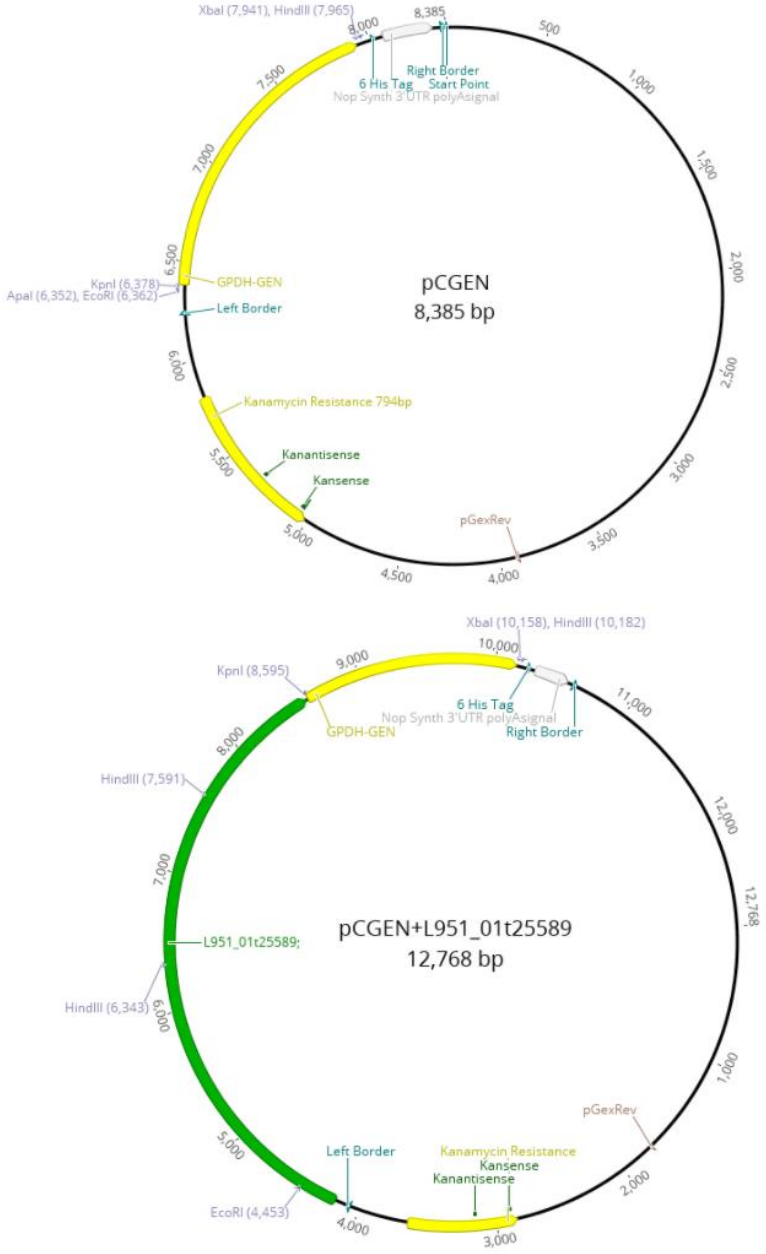

Figure 5.2 pCGEN and an example complementation construct design, *ZtADE6*.

TOP: pCGEN plasmid backbone used to generate complementation constructs, and BOTTOM: representation of an assembled complementation construct for the pCGEN+L951_01t25589 (*ZtADE6* – green annotation) candidate for transformation in REMI mutant isolate 'L/121'. The positions of the selectable resistance markers G418 (Geneticin) and Kanamycin are shown in yellow annotation. Cut sites of select restriction enzymes are represented.

5.2.2 *In planta* and *in vitro* screening

Unless stated otherwise all *in planta* and *in vitro* screening was carried out as described in Chapter Two/Three. An additional *in vitro* assay was carried out in this chapter to show adenine auxotrophy in the REMI L/121 mutant isolate. For this, tap water agar was amended with two concentrations of adenine, 0.01 mM and 1.0 mM. These concentrations are also used in Yemelin *et al*., (2017) investigation of a different *Z. tritici* mutant library isolate with adenine auxotrophy.

5.2.3 Scanning electron microscopy (SEM)

Plants were grown for three weeks under glasshouse conditions listed in Chapter Two. Samples were taken at 24 h post spray inoculation with 1×10^6 spores ml^{-1} 0.1% Tween20-water solution *Z. tritici* L951 and indicated mutant and complemented mutant isolates. The methods used to obtain the images are described in Chapter Two.

5.3 Results

5.3.1 *De novo* purine biosynthesis pathway impacted in REMI L/121 by a frameshift mutation in *ZtADE6*

Both the *de novo* purine biosynthesis and salvage pathways are important for growth, development, and pathogenicity in multiple species (Chua & Fraser, 2020; Fernandez *et al*., 2013; Morrow *et al.*, 2012). Yemelin *et al.* (2017) explored the role of *MYCO4* (Mycgr3G87000), homologous to the *S. cerevisiae* bifunctional *ADE5,7* gene, in the pathway after identifying a reduced virulence ATMT mutant with this gene disrupted. Chapter Four identified an untagged frameshift mutation affecting the candidate gene ZtritL951_01g25589 in REMI L/121. This mutation induced a frameshift which likely renders the protein non-functional. Skinner also demonstrated that this REMI mutant was auxotrophic for purines (for growth on low nutrient media required supplementation with adenine or hypoxanthine).

Figure 5.3 outlines the *de novo* purine biosynthesis pathway in *Z. tritici* adapted from Yemelin *et* al., (2017) with the JGI protein identifiers from the

KEGG pathway entry ztr00230. From this, we can see that the impacted gene in REMI mutant isolate L/121 (*ZtADE6*) functions downstream of the previously described *MYCO4* gene in this pathway. InterPro scan results on Myco4p homologs in the *Mycosphaerellaceae* family showed that only GARS domains were present, enabling only the conversion of 5-phospho-β-D-ribosylamine (PRA) to 5-phosphoribosylglycinamide (GAR). Most other fungi have GARS and AIRS domain-containing proteins that are bifunctional, acting at two points in the biosynthesis/salvage pathways. Yemelin *et* al., (2017) noted an AIRS domain-containing protein identified in the *Z. tritici* genome, Mycgr3P74864, which I have included in Figure 5.3.

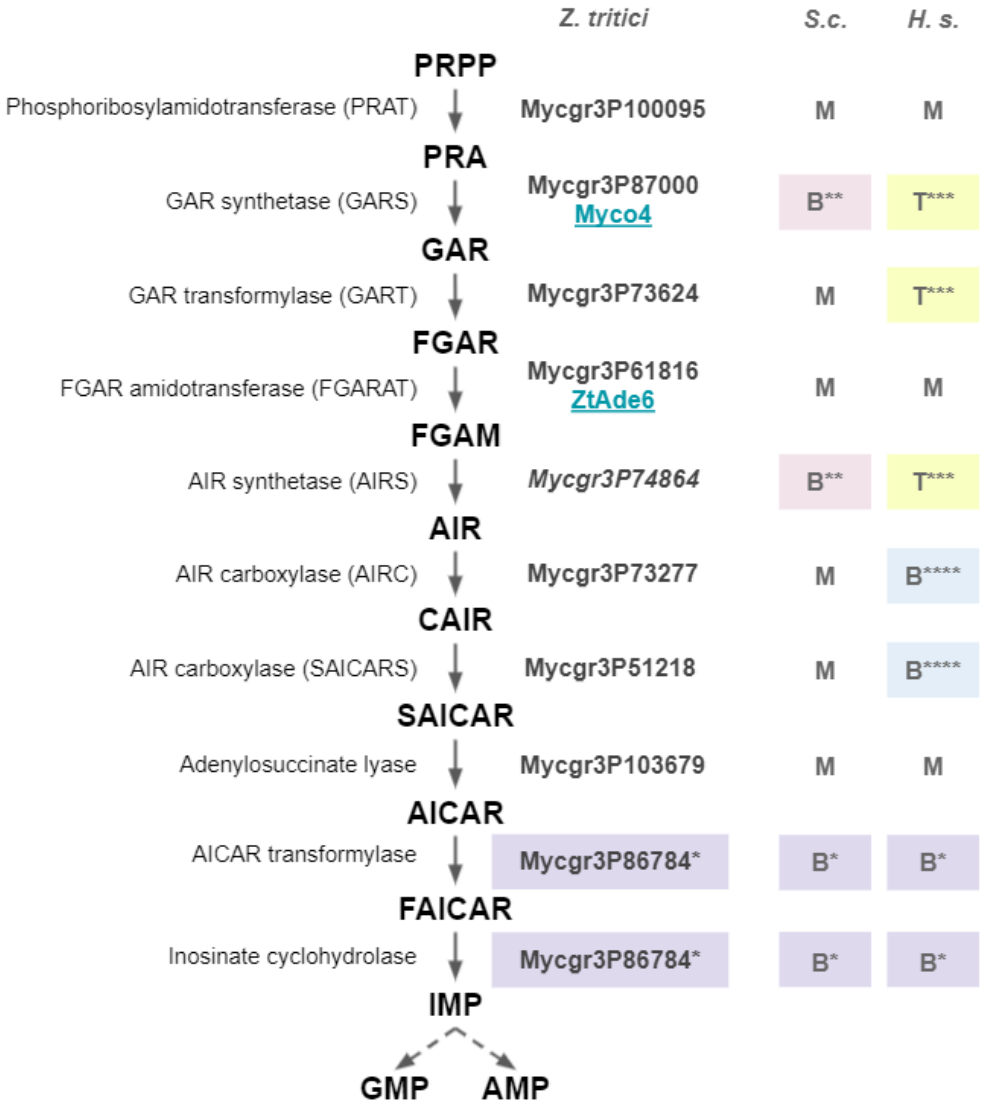

Figure 5.3 A predicted schematic representation of the *de novo* purine biosynthesis pathway in *Z. tritici*.

Based on the *de novo* purine biosynthesis pathway in the yeast *Saccharomyces cerevisiae* (*S.c.*) adapted from Yemelin *et al*., (2017) and information from KEGG (https://www.genome.jp/kegg/pathway.html) *Z. tritici* pathway entry ztr00230, and *Homo sapiens* (*H.s.*) entry hsa00230. Abbreviations: B: Bifunctional, M: monofunctional, T: trifunctional, PRPP: 5-phospho-ribosyl-1α-pyrophosphate, PRA: 5-phospho-β-D-ribosylamine, GAR: 5-phosphoribosylglycinamide, FGAR: 5'-phosphoribosyl-N-formyl glycinamide, FGAM: 5'-phosphoribosyl-N-formylglycinamidine, AIR: 5'-phosphoribosyl-5-aminoimidazole, CAIR: 5'-phosphoribosyl-5-aminoimidazole-4-carboxylate, SAICAR: 5'-phosphoribosyl-4-(N-succinocarboxamide)-5-aminoimidazole, AICAR: 5'-phosphoribosyl-4-carboxamide-5-aminoimidazole, FAICAR: 5'-phosphoribosyl-4-carboxamide-5-formamidoimidazole, IMP: inosine monophosphate, AMP: adenosine monophosphate, GMP: guanosine monophosphate.

BLAST and InterPro results indicated that ZtritL951_01g25589 was the L951 *Z. tritici* orthologue of *S. cerevisiae ADE6*, also represented in strain IPO323 by ZtritIPO323_04g12872/Mycgr3G61816. The NCBI CDD database and InterPro scans were used to identify the domains within the ZtAde6p and check other candidate fungal orthologues for similar domains. Figure 5.4 displays that ZtAde6p shares the domains present in proteins from related fungi, the yeast *S. cerevisiae* and even from *H. sapiens*. This further supports the predicted function and position of *ADE6* in the *Z. tritici de novo* purine biosynthesis and salvage pathways.

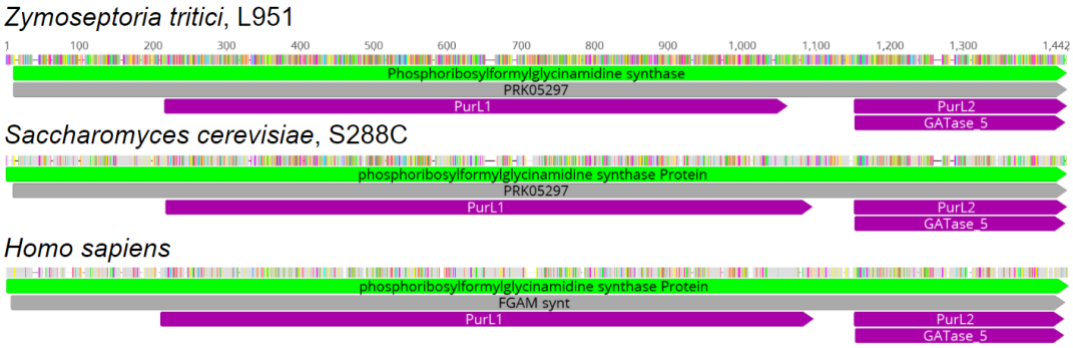

Figure 5.4 *Zymoseptoria tritici* L951 ZtAde6p alignment with *S. cerevisiae* and *Homo sapiens* homologue showing domains.

Highlighting agreements to *Z. tritici* L951 ZtAde6p sequence. Domains lifted from NCBI Conserved Domain Database and InterPro scan results. MUSCLE, 16 iterations, default values on Geneious v.10.2.3.

BLASTp results across 2247 fungal genomes in the JGI MycoCosm (https://mycocosm.jgi.doe.gov/mycocosm/home) database indicated that Ade6p is highly conserved. The only 'fungal' subdivisions without hits even at the lower expect score of $1.0e^{-5}$ are in the lower fungi, specifically in the Microsporidia (taxid:6029) and Cryptomycota (taxid:1031332). Microsporidia are strict obligate intracellular parasites with a wide host range, not including currently known to include plants, that have lost most of the genes necessary for producing primary metabolites (Dean *et al*., 2016). Cryptomycota are similar to Microsporidia, putatively sharing a common endoparasitic ancestor (James *et al*., 2013). The loss of this component of the purine biosynthesis pathway is likely a result of the differing nutrient acquisition and lifestyles of fungi.

A phylogenetic analysis was then performed to assess whether Ade6 protein sequences clustered as anticipated with taxonomic relatedness. Using BLASTp searches, a subset of 36 amino acid sequences was selected as representatives of Basidiomycota, Ascomycota, and the lower fungi, with varied lifestyles with an expected score set at $1.0e^{-100}$. The Neighbour-Joining consensus tree with *Homo sapiens* Ade6 orthologue as an outgroup was generated using Geneious (v.10.2.3) and resampled using the bootstrap method with 100,000 replicates. Figure 5.5 shows that the evolutionary relationship between the protein sequences is similar to the known taxonomic relationship. The Basidiomycota *Puccinia graminis* f. sp. *tritici* being the only outlier. The relationship represented between Ascomycota fungi follows the expected pattern according to current taxonomic assignments of the species, with the closest hits being in other *Zymoseptoria* species, followed by the Mycosphaerella group of the Dothideomycete, other Dothideomycete and back through the Pezizomycetes. This is indicative of a highly conserved sequence of likely functional importance in all the species analysed.

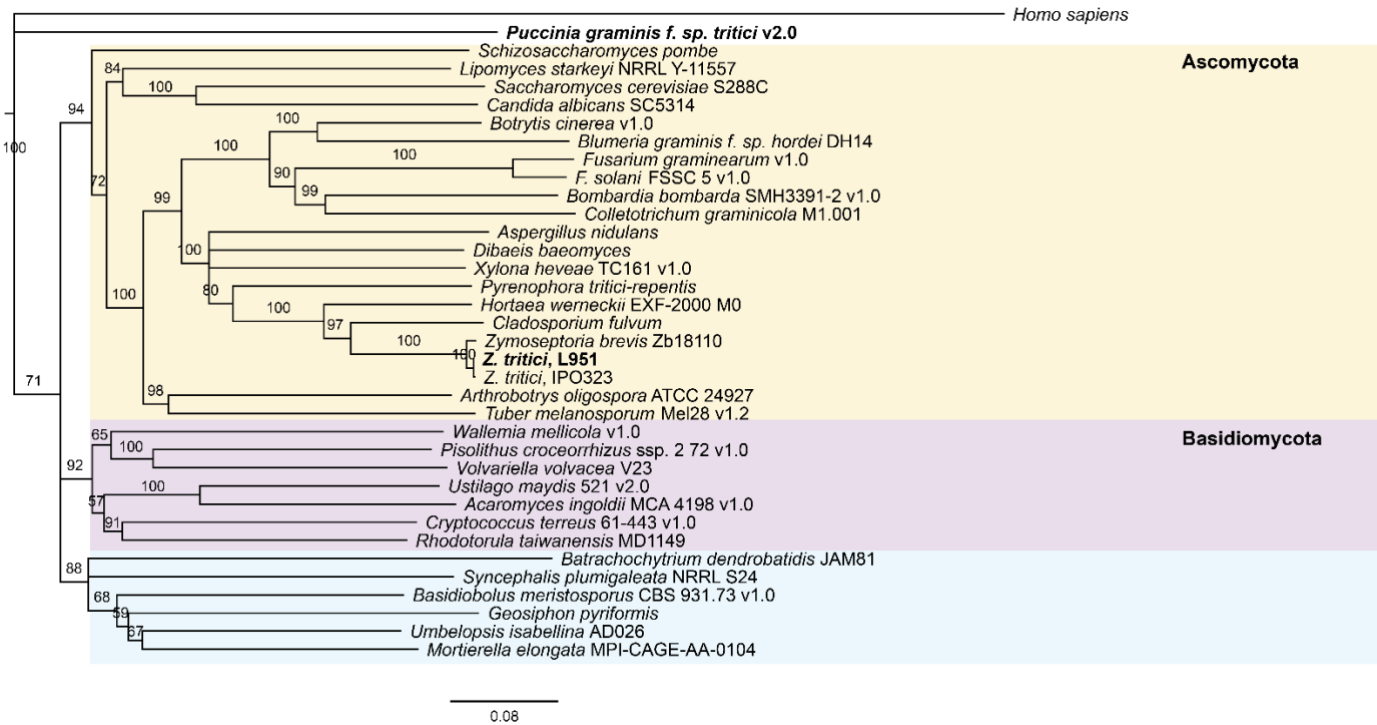

Figure 5.5 Phylogenetic analysis of the L951 *Z. tritici* Ade6p sequence with 35 orthologous proteins.

Neighbour-Joining consensus tree, displaying representative sequence orthologues to ZtAde6p amino acid sequence with *Homo sapiens* as an outgroup, generated using Geneious (v.10.2.3). The consensus tree was resampled using the bootstrap method with 100,000 replicates. Node labels indicate percentage consensus support, only showing those above 50%. *Z. tritici* L951 is in bold, showing the *Zymoseptoria* relationship. Also bold is *Puccinia graminis* f. sp. *tritici*, a Basidiomycte whose sequence is separated from other fungi in its clade. Otherwise the basidiomycota fungi (purple) split from Ascomycota (yellow) and lower fungal groups (blue) as expected.

5.3.2 Complementation with *ZtADE6* restored WT virulence phenotype to REMI L/121

To assess the importance of the *ZtADE6* gene for virulence, complementation strains were generated using ATMT. A construct was assembled with a pCGEN plasmid backbone, with the antibiotic selectable marker geneticin (G418) to allow distinction between successful *Z. tritici* transformants. The plasmid carrying this antibiotic resistance was used as the REMI mutant isolates being complemented were already hygromycin resistant. Three biological replica transformed colonies were cleaned, bulked, and stocked in 50% glycerol ahead of *in planta* testing. Figure 5.6 shows a representative leaf for L951, the original REMI mutant (L/121) and three independent complemented mutant strains from *in planta* screens on cv. Riband at 21 days post-inoculation (dpi). The figure shows that even at 21 dpi, REMI L/121 ("Δ*ZtAde6*") inoculated leaves show little-to-no symptoms of infection, whereas the WT *Z. tritici* L951 strain and complemented Δ*ZtAde6/ZtADE6* show advanced symptom development, including pycnidia, chlorosis and leaf tissue necrosis. These *in planta* screens were repeated a minimum of three times with three inoculated leaves, and the images are representative of all these replicated assays.

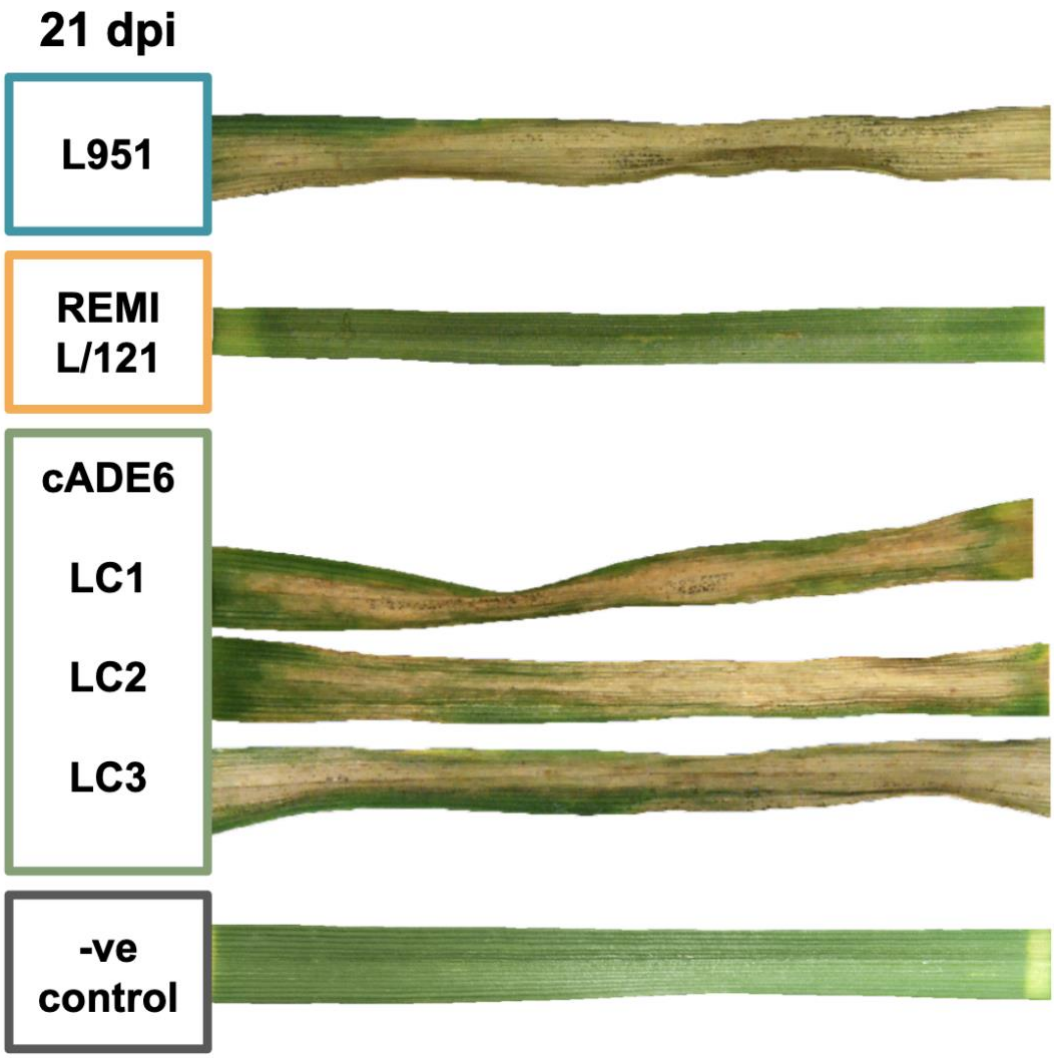

Figure 5.6 *In planta* screening results for the *ZtADE6* complements at 21 days post-inoculation.

Images show a representative wheat leaf with typical symptoms from the three replicate inoculated leaves at 21 dpi. The entire leaf surface displayed was inoculated using a cotton swab with 1×10^7 spores ml^{-1} 0.01% Tween20 solution. A virulent parental strain (L951), an avirulent mutant (REMI-121/L), three biological replica complementation mutants showing restored virulence and a negative control are shown. Each mutant isolate shown here was tested a minimum of three times *in planta* on wheat cv. Riband.

5.3.3 Inactivation of *ZtADE6* resulted in adenine auxotrophy in REMI L/121

To retest the previously identified adenine auxotrophic phenotype in 1HR.171 Skinner (2001) (in my study REMI-L/121), I supplemented minimal nutrient, tap water agar (TWA) with adenine and spot inoculated as previously described. Shown in Figure 5.7 are the results for 0 and 1.0 mM adenine added to the media. In the Δ*ZtAde6* mutant, we see a restoration of hyphal growth compared to the un-amended TWA plate. This further demonstrates the importance of the *de novo* purine biosynthesis and salvage pathway in *Z. tritici* growth, supporting observations made in Yemelin *et al*., (2017). Similar results were observed for 0.01 mM adenine inoculation (data not shown). I also noted that on the adenine amended media, there was a reduction in the hyphal extension in the wild type, L951. This may suggest it can serve as a general nutrient source and thereby suppress the switch to hyphal growth attributed to a limitation on extracellular nutrients.

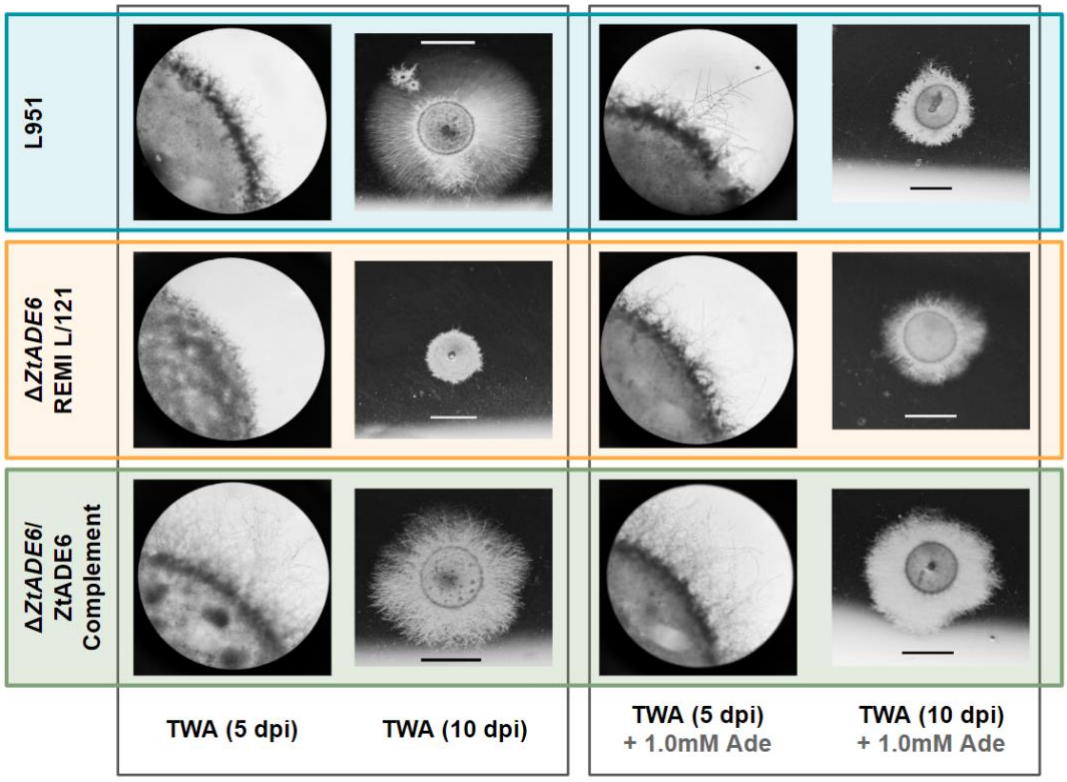

Figure 5.7 *In vitro* spotting of Δ*ZtAde6* mutant and Δ*ZtAde6/ZtADE6* complement on tap water agar under purine auxotrophic conditions.

Spores were suspended in 0.01% Tween20 at a concentration of 1×10^7 spores ml^{-1}, and 5 µl were spotted onto TWA and photographs were taken at five days through a light microscope (Zeiss, West Germany) and ten days. L951 parental strain showed typical growth at 5- and 10-days post-inoculation (dpi), the adenine auxotrophic Δ*ZtAde6* mutant showed restored hyphal growth when media was amended with 1 mM adenine. The representative *ZtADE6* gene complement mutant shown here displays the restoration of hyphal growth observed in three biological replicates. The scales bars on 10 dpi spot photos represent 1 cm.

To investigate the *in planta* spore germination and early filamentous growth of *ZtADE6* defective strains, scanning electron microscopy (SEM) images were obtained at 24 h post-inoculation, Figure 5.8. The parental WT *Z. tritici* L951 and a representative complement mutant isolate were used to compare any differences. However, there did not appear to be much difference in the germination or filament extension between the strains tested at this stage. This opens the possibility that the differences would be seen later, possibly in the fungus' ability to colonise the apoplastic space as effectively.

The analysis presented here confirms the previously described importance of purine biosynthesis for leaf infection by *Z. tritici*. This likely arises from a lack of availability of external purines for uptake, which places pressure on this *de novo* pathway. The data presented indicate that while *in vitro* hyphal growth abnormality is observed, whether and when (at slightly later time point than analysed in the current study) this manifests and causes the impact to virulence *in planta* remains to be uncovered.

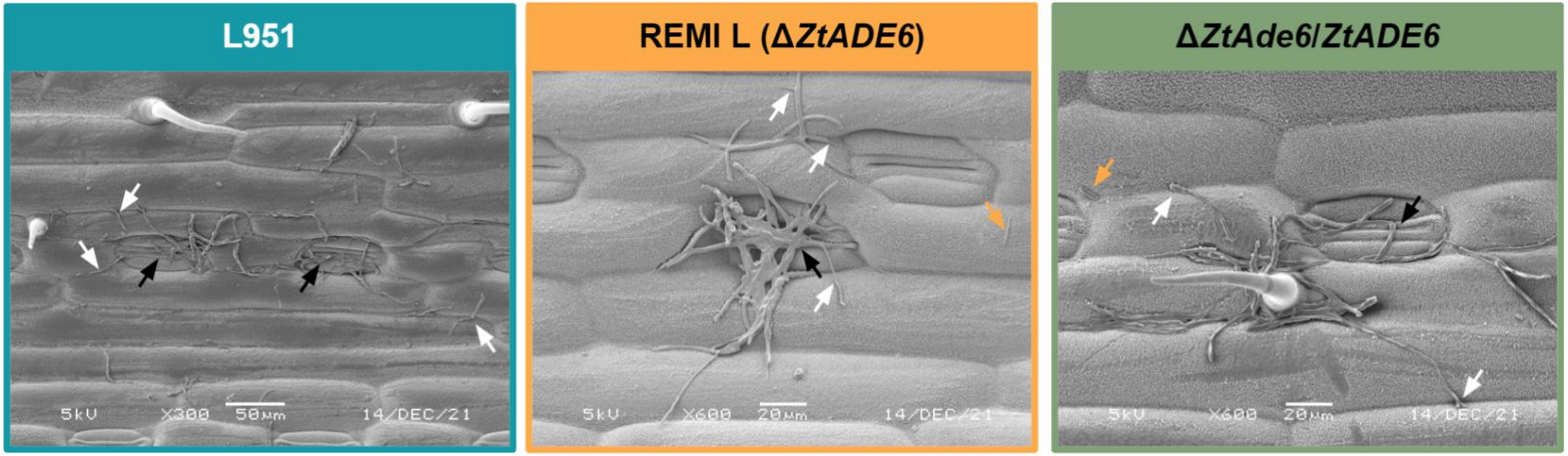

Figure 5.8 Scanning electron microscopy shows little differences at 24 h post-inoculation in spore germination and filament extension in the *ZtADE6* defective strain compared to complements and L951 control.

Spores were suspended in 0. 1% Tween20 at a concentration of 1×10^6 spores ml^{-1} and were gently brushed spotted onto the adaxial surface of wheat cv. Riband leaves were closed into a humidity chamber, and SEM images were taken 24 h post-inoculation. Scale bars are included on the individual photos. There is not much difference between the L951 parental strain, the adenine auxotrophic Δ*ZtAde6* and a representative Δ*ZtAde6/ZtADE6* gene complement mutant. Germination (represented by white arrows) occurred in all three, ungerminated spores were identified (yellow arrows) and attempted to penetrate stomata were observed (black arrows). There was no apparent difference in the germination or hyphal filament extension in WT vs *ZtAde6* defective mutants noted.

5.3.4 *In silico* and phylogenetic analysis of the *Z. tritici* orthologue of the crooked neck-like factor (*ZtCLF1*)

The prioritised gene candidate within the L951 *Z. tritici* REMI mutant 'B/6' was identified due to an intragenic plasmid integration in ZtritL951_01g03851. The *S. cerevisiae* orthologue identified to this gene is *CLF1*, an essential for life gene involved with the Prp19/NineTeen Complex, with deletion mutants having a lethal phenotype (Chung *et al*., 1999). PHI-base BLASTp results also identified a *ZtClf1* orthologue in the opportunistic human pathogen *Cryptococcus neoformans* named Ccn1, which, when mutated rendered the fungus unable to cause systemic infection in mice (Chung *et al*., 2003). This complex component is not well studied in fungal plant pathogens to date. However, an association between the members within Prp19 complex and defects in filamentous growth have been noted in both Δ*num1* deletion strains in *U. maydis* and *MoCwf15* null mutants in *M. oryzae* (Liu *et al*., 2021; Kellner *et al*., 2014).

Zymoseptoria KnetMiner (https://knetminer.com/Zymoseptoria_tritici/) knowledge graphs identify related proteins, genes, domains and more from databases and broader literature. They can be searched with JGI genome identifiers (i.e. information from the literature related to similar genes to *ZtCLF1* can be searched using Mycgr3G98811). Figure 5.10 shows a curated KnetMiner knowledge graph for *ZtCLF1*. The *Z. tritici CLF1* gene is highlighted in yellow and linked to the encoded Clf1p (highlighted in green). The protein is then linked in this knowledge graph to an identified orthologue (*S. cerevisiae*, SGD protein YLR117C) and a protein with a similar sequence (*C. neoformans var. grubii*, uniprot Q9HF03). Observed phenotypes for these two linked proteins are represented by green linked arrows to green boxes. For the yeast predicted orthologue all the associated information is from the *Saccharomyces* Genome Database (SGD). These analyses also suggest that *ZtClf1* may be a functional orthologue of the aforementioned yeast and *Cryptococcus* genes.

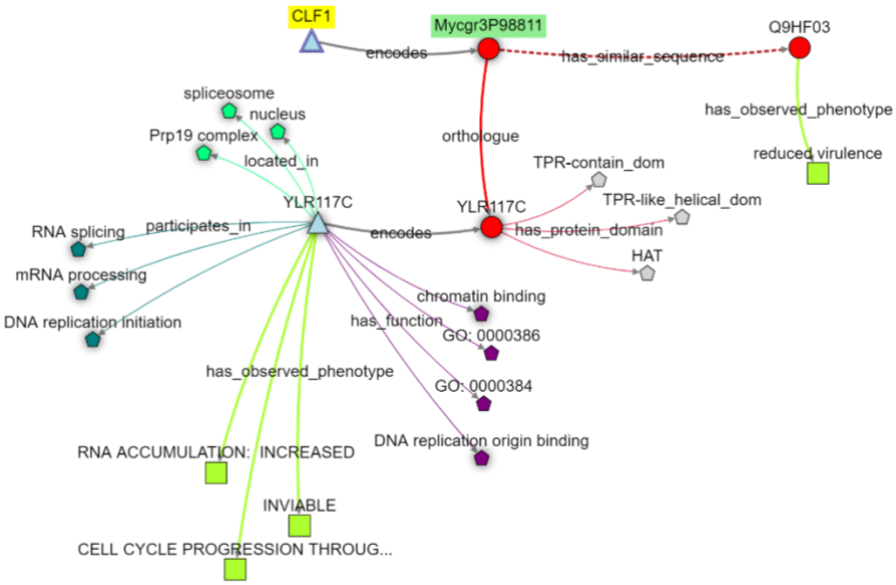

Figure 5.9 Zymoseptoria KnetMiner knowledge graph showing a selection of information on *ZtCLF1*

Accessible online at https://bit.ly/KnetZtCLF1

As there are no apparent studies on *CLF1* in fungi more closely related to *Z. tritici*, I performed BLASTp and phylogenetic analyses to identify how conserved the Clf1 component of the Prp19 complex is. The JGI BLASTp result identified that orthologues were present in all subdivisions of fungi, including the 'lower' fungi, with a single exception being the Microsporidia. From these BLASTp searches, a subset of amino acid sequences were selected as representatives of distinct ascomycete, basidiomycetes and lower fungi, with varied lifestyles with an expected score set at 1.0e-100. Amino acid sequences of 28 Clf1p orthologues across the fungal kingdom were aligned using MUSCLE with 16 iterations and default values in Geneious (v.10.2.3). For phylogenetic reconstruction, the LG+G substitution model was selected by BIC in MEGA 11.0.11. The Maximum Likelihood phylogeny was reconstructed using PhyML, with 1000 bootstraps (Guindon *et al.,* 2010). The analysis shown in Figure 5.11 indicates that the evolutionary relationship between the protein sequences is similar to the known taxonomic relationship, the Ascomycota and Basidiomycota sequences cluster as expected.

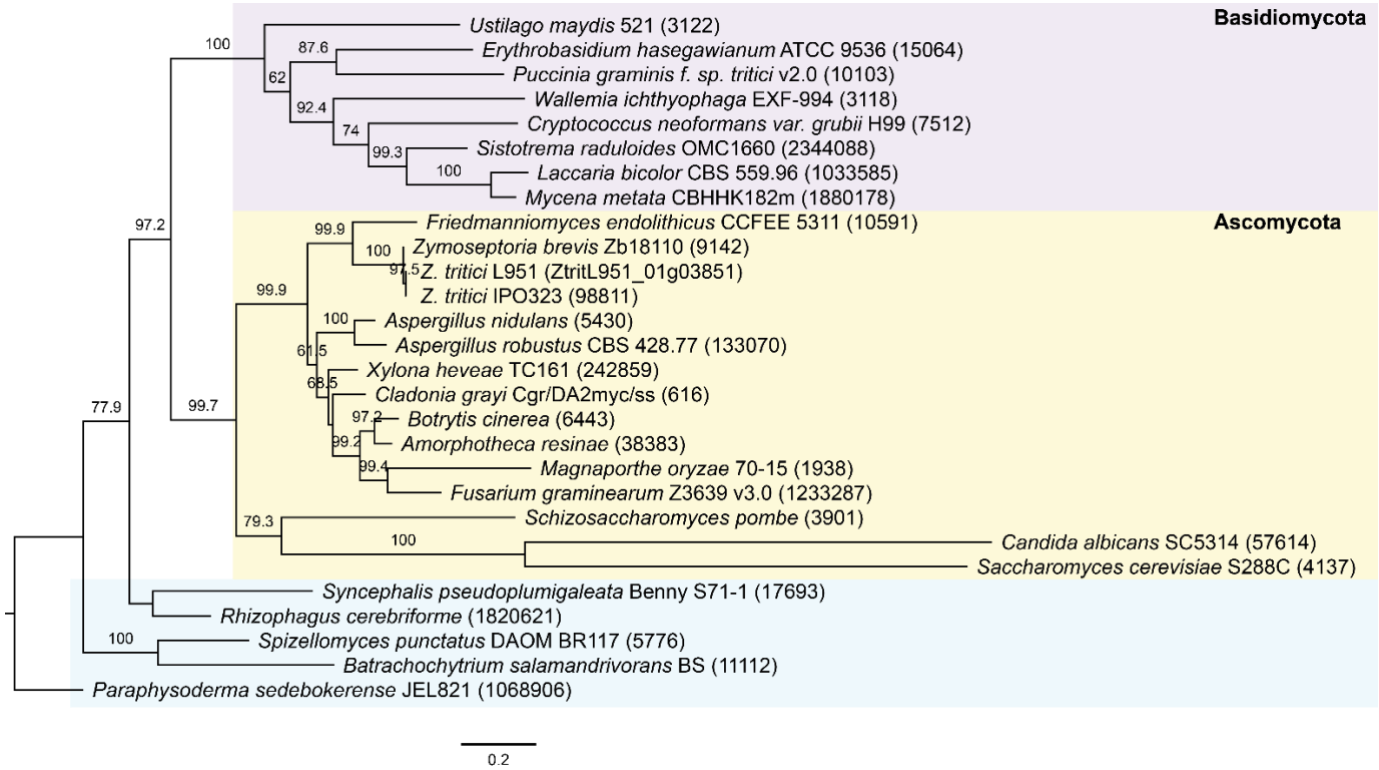

Figure 5.10 *CLF1* phylogenetic analysis reflects the known evolutionary relationship in fungal taxa.

Maximum Likelihood phylogenetic tree (Geneious v.10.2.3) displaying representative sequence orthologues to ZtClf1p from across the fungal tree of life. Basidiomycota fungi (purple) split from Ascomycota (yellow) and lower fungal groups (blue). Node labels indicate percentage bootstrap support (1000 replicates); those below 50 are not shown. Substitution model LG+G identified using MEGA11.

5.3.5 Restoration of virulence to L951 *Z. tritici* REMI B/6 via complementation with *ZtCLF1*

To assess whether the plasmid integration into the *ZtCLF1* gene was responsible for the observed reduction in virulence in REMI B/6, complementation strains were generated as described for the *ZtADE6* study using ATMT with a pCGEN based plasmid construct. Figure 5.12 shows a representative leaf for WT L951, the original REMI mutant (B/6) and three independent complemented mutant strains from *in planta* screens on cv. Riband at 21 days post-inoculation (dpi). Even at 21 dpi REMI B/6 (Δ*ZtClf1*) inoculated leaves only displayed limited chlorotic patches of infection, whereas the WT *Z. tritici* L951 strain and complemented Δ*ZtClf1*/*ZtCLF1* show more advanced symptom development approximately equivalent to WT levels demonstrating the key role for *ZtCLF1* in WT infection.

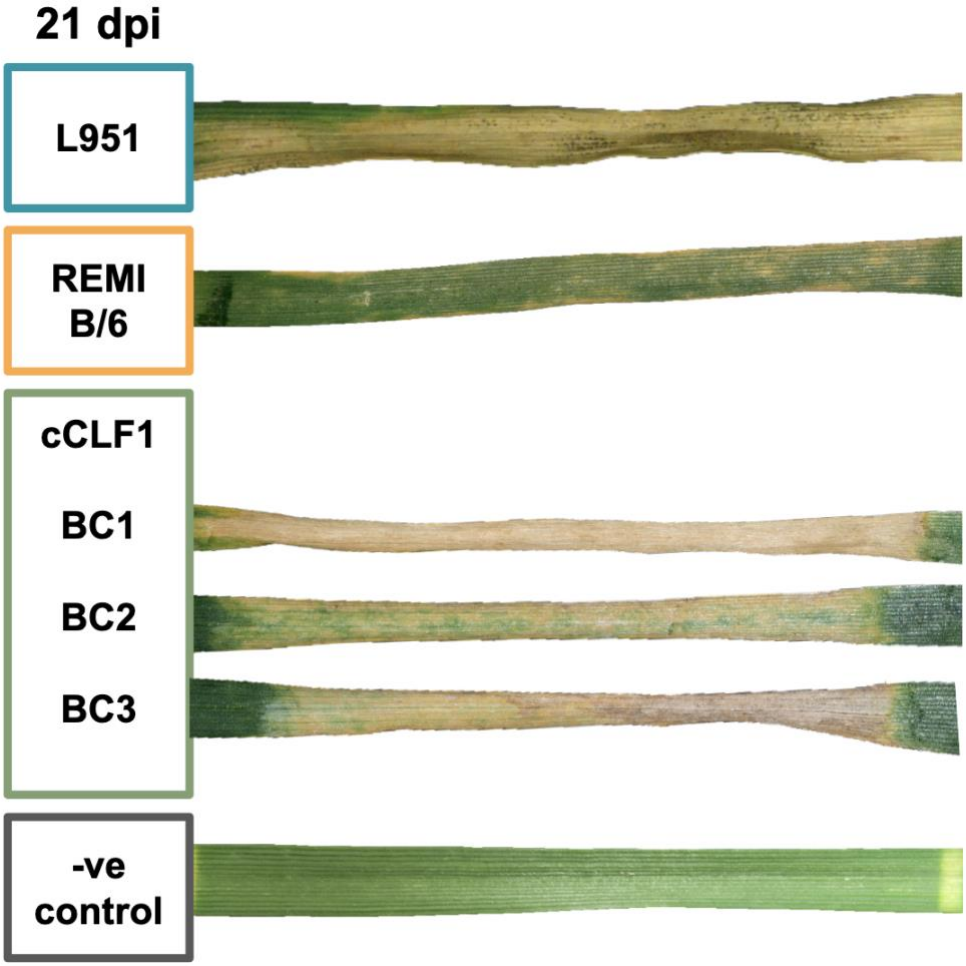

Figure 5.11 *In planta* screening results for the *ZtCLF1* complements at 21 days post-inoculation.

Images show a representative wheat leaf with typical symptoms from the three replicate inoculated leaves at 21 dpi. A virulent parental strain (L951), an reduced virulence mutant (REMI-6/B), three biological replica complementation mutants showing restored virulence and a negative Tween20 solution control are shown. The entire leaf surface shown was inoculated via cotton swab with 1×10^{7} spores ml^{-1} suspended in a 0.01% Tween20-water solution. Each mutant isolate represented here were tested a minimum of three times *in planta* on wheat cv. Riband.

5.3.6 Reintroduction of *ZtCLF1* restores *in vitro* hyphal growth switching

The other phenotype of interest in the *ZtCLF1* defective strains (REMI B/6) discussed in Chapter Three was reduced hyphal growth exhibited *in vitro* on tap water agar (TWA) spotting plates. The mutant strains consistently produced shorter filaments that did not extend compared to the 'parental' strain, L951. Figure 5.13 shows this alongside the complementation results with a functional *ZtCLF1* after ten dpi on tap water agar. The representative complementation strain (one of three tested with identical results) shown displays the restored typical hyphal growth phenotype *in vitro*. The re-introduction of *ZtCLF1* fully restored hyphal growth to REMI mutant B/6 isolate, demonstrating that loss of this gene was responsible for the loss of filamentous growth (Figure 5.13).

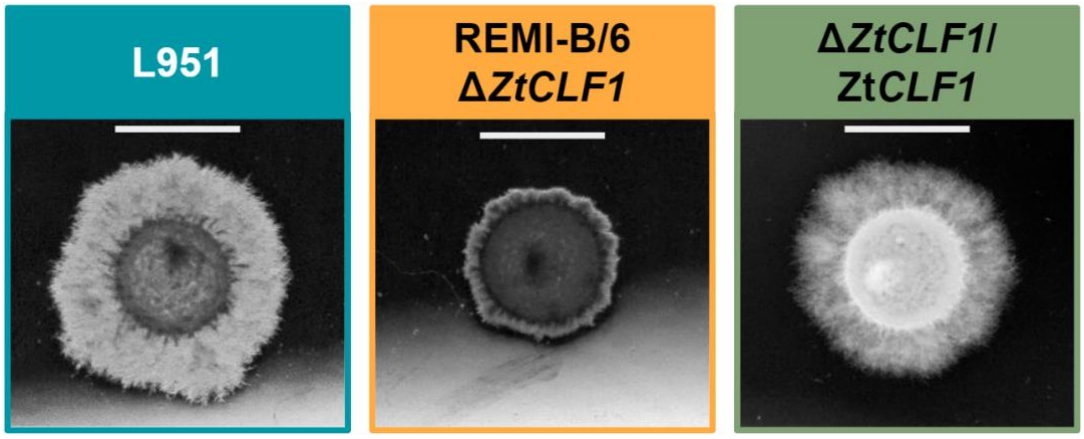

Figure 5.12 Complmentation of *ZtCLF1* restored *in vitro* hyphal growth on TWA.

Spores were suspended in 0.01% Tween20 at a concentration of 1×10^{7} spores ml^{-1}, and 5 µl were spotted onto TWA and photographed after 10 days. A WT L951 *Z. tritici,* REMI B/6 ZtCLF1 defective mutant and a representative ΔZtClf1/ZtCLF1 complement spot. Whilst the REMI mutant's filamentous growth is restricted, complementation with *ZtCLF1* restored of typical WT hyphal growth, the images shown are representatives that reflect all complemented mutant isolates and repeated a minimum of three times. The scale bar represents 1 cm.

To explore the *in planta* leaf surface spore germination and filamentous growth in *ZtCLF1* defective strains, scanning electron microscopy images were obtained at 24 h post inoculation. Figure 5.14 shows *Z. tritici* L951, the Δ*ZtCLF1* mutant and a representative complemented Δ*ZtClf1/ZtCLF1* mutant were inoculated onto the wheat cv. Riband. As per the ADE6 study, there was no obvious difference in spore morphology or very early morphology between WT and mutant strains, potentially due to the early timings investigated. However, a distinction may be seen at later stages that would fit the *in vitro* hyphal growth data. Given the importance of filamentous growth in the *Z. tritici* infection, the defective hyphal development likely limits apoplastic colonisation, which would affect disease progression. Alternatively, if there are other *in planta* impacts (seemingly occurring post-stomatal penetration in the L951 *ZtCLF1* mutant), these could impact pathogenicity. For example, due to splicing inefficiency, transcripts activated in response to the host conditions (such as oxidative stress-related factors),

may result in an ineffective response of the fungus to deal with those stresses (Grützmann *et al*., 2014).

The analysis presented here points to the importance of the spliceosome in the pathogenicity of *Z. tritici*. Given the limited *in vitro* hyphal growth resulting from defective *ZtClf1* I suggest that, as with other fungi, the spliceosome complex is involved with the dimorphic switch and standard filament extension. The data presented indicate that while *in vitro* hyphal growth abnormality is observed, when this manifests and causes its impact to virulence *in planta* remains to be uncovered.

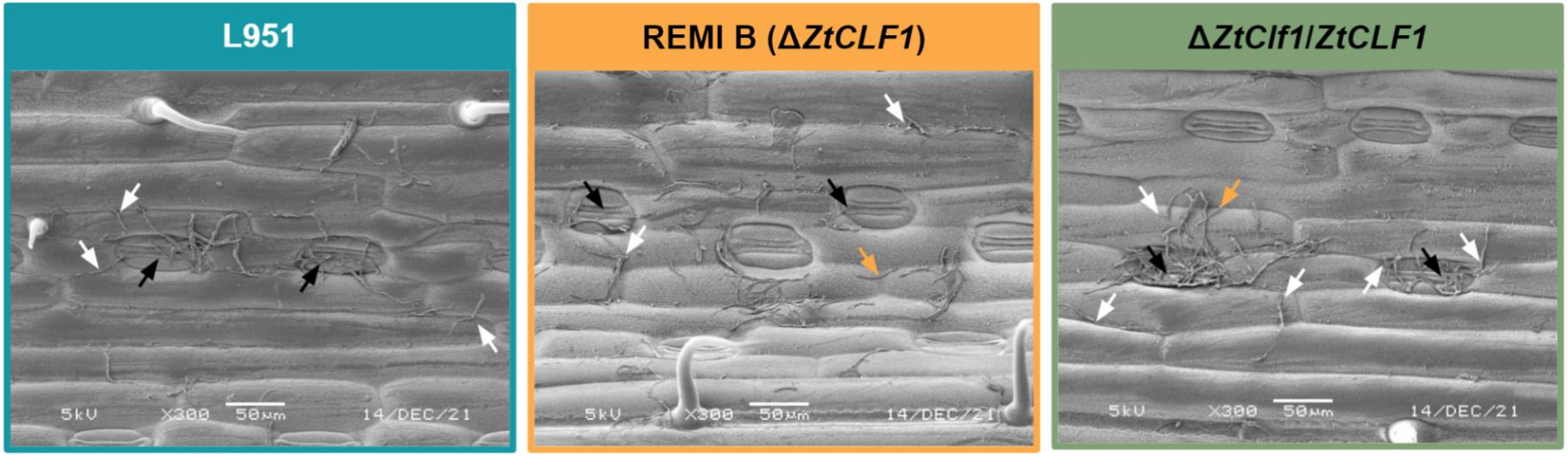

Figure 5.13 Scanning electron microscopy shows no apparent visual differences at 24 h post-inoculation in spore germination and filament extension in the *ZtClf1* defective strain compared to complements and L951 control.

Spores were suspended in 0.1% Tween20 at a concentration of 1×10^6 spores ml^{-1} and were gently brushed spotted onto the adaxial surface of wheat cv. Riband leaves were closed into a humidity chamber, and SEM images were taken 24 h post-inoculation. Scale bars are included on the individual images. There is not much difference between the L951 parental strain, the Δ*ZtClf1* and a representative *ΔZtClf1/ZtCLF1* gene complement mutant shown. Germination (represented by white arrows) occurred in all three, ungerminated spores were identified (yellow arrows) and attempted to penetrate stomata were observed (black arrows). There does not appear to be a difference between the WT and mutants at this early time point.

5.4 Discussion

5.4.1 The diversity of tools now available to explore putative biological function/ pathways affected by gene mutations

In the almost four decades since the first bacterial avirulence gene was cloned, there has been a vast increase in publications identifying virulence-associated genes (Staskawicz *et al*., 1984). Alongside the “data deluge” came the need for improved storage and sharing systems to enable researchers across the globe to make discoveries. As well as the flood of large ‘generalist’ databases (Ensembl, NCBI, UniProt, Pfam, InterPro, etc.) there are several specialist databases (FlyBase, WormBase, *Candida* Genome Database, *Saccharomyces* Genome Database, PomBase, etc.) curated by their respective communities which provide a wealth of information about those systems. Searching through the literature and these databases for relevant information can be time-consuming, particularly with taxonomic classification changes and gene/protein identifiers through the years. In my work, I made use of two tools (as well as BLASTp searching) to help filter and learn more about my candidate genes, PHI-base and KnetMiner.

PHI-base is a curated database of experimentally validated and published mutant phenotypes with the impacted genes (March 2022 PHI-base version 4.12, a total of 8411 genes). The PHI-base blast tool allows a researcher to input their protein sequence of interest and see whether, within the database, there is any information on related sequences. As the curated database grows, the more useful this tool will become to researchers investigating the genomes of their mutant libraries. Zymoseptoria KnetMiner enabled a quick search of candidate genes with JGI identifiers for predicted orthologues and related publications. With access to the PHI-base data, KnetMiner can link phenotypic ontologies alongside GO terms, biological pathways, protein-protein interaction data, and other biological data. Of course, there is still a process of checking the identified connections and supporting literature but utilising these tools streamlined the process of determining what is known, if

anything, about the genes I was looking at. These tools are helpful when something is either known about the protein or a protein of a similar sequence. However, much of what is known about the fundamentals of fungal genetic circuitry and growth is based on (or inferred from) studies in a limited set of fungi, namely *Saccharomyces cerevisiae*, *Candida albicans* and *Aspergillus* species. As such forward and reverse genetics, studies are now filling in some knowledge gaps for a broader picture of the diverse fungal lifestyles.

5.4.2 *De novo* metabolite biosynthesis in fungal pathogenicity

There is an established association between virulence and a variety of *de novo* biosynthetic pathways for pathogenic fungi. Given the diverse spectrum of important biological processes that rely on biosynthesis pathways, defects in these pathways are likely to have knock-on impacts to multiple cellular functions. For example, arginine and lysine biosynthesis have been reported in multiple fungal pathogens to impact germination on the host significantly (Arginine – *M. oryzae*, Aron *et al.*, 2021; Lysine - *Z. tritici,* Derbyshire *et al*., 2018; Lysine - *Metarhizum robertsii,* Giuliano *et al*, 2017; Dietl *et al*., 2020). Between my own study, Yemelin *et al*. (2017), and those carried out in other pathogenic fungi such as *Candida albicans, Fusarium oxysporum*, *Magnaporthe oryzae* and *C. neoformans*, the *de novo* purine biosynthesis and salvage pathways have been linked to virulence (Chitty & Fraser, 2017; Denisov, 2005; Fernadez *et al*., 2013; Jiang *et al*., 2010).

Whilst Fernandez *et al*., (2013) initially identified that deletion of *MoADE1* (SAICAR synthetase) did not cause an effect on the early-penetration phase of the rice blast fungus, *Magnaporthe oryzae.* However, after penetration, it was noted that the switch to invasive hyphal formations was affected. As such *de novo* purine biosynthesis was not required for appressorium formation, a specialised infection structure used to infect its host, but was essential for full virulence. Though *Z. tritici* does not have such structures, similar spore germination and putative stomatal penetration between mutant and wild type parental strain *in planta* SEM images indicate a similar post

penetration effect. Furthermore, Yemelin *et al*. (2017) note that the concentration of adenine amended in TWA needed to restore hyphal growth is lower than what is accessible in the plant apoplast. As such, it is not clear at what stage the defective pathway causes issues for the infecting *Z. tritici*. Given the vast array of roles purines and their derivatives have in the typical cellular function of living organisms, it may not be as straightforward as the reduced filamentous growth leading to inefficient colonisation *in planta* that is the issue for impacted virulence. DNA damage accumulation due to limited purine availability or reduced energy generation in the form of ATP is likely to have severe consequences for a living cell (Chitty & Fraser, 2017; Zhou *et al*., 2020). Outside the lab in the field, adenine auxotrophic *Z. tritici* would not survive to cause infection. Therefore, selective targeting of this pathway could prove helpful in future crop protection.

This study has also re-emphasised the utility of having a yeast-like growth phase of *Z. tritici* on rich, complex nutrients. *ZtADE6* mutants can grow perfectly well on YPD agar suggests they are accessing purines from it. This allows for auxotrophic mutants to be detected when subsequently grown on other media. Whilst auxotrophy was an important screen used initially by Skinner to identify REMI L/121, she could not identify the frameshift mutation in the *ADE6* gene through the methods available (plasmid rescue etc). Hence only the subsequent feasibility of whole-genome re-sequencing enabled the ADE6 mutation to be identified as an untagged mutation. This particular use example further supports the mutagenomics strategy deployed here.

5.4.3 Complex networks integrating spliceosome complex, hyphal growth, and the cell cycle

Extensive cellular structural changes are involved in dimorphic switching, and these must be coordinated to respond to environmental stimuli. Based on this, it was not entirely surprising to see a predicted cell cycle control protein impacted in a defective hyphal growth and reduced virulence mutant as described here. In terms of cell cycle control in *Z. tritici* there is currently only one previous report describing a c-type cyclin, (*MCC1*) which was

described to have a role in filamentous growth and virulence (Choi & Goodwin, 2010). However, the role of the spliceosome in *Z. tritici* has not been investigated thus far.

The spliceosome plays a crucial role in gene expression through pre-mRNA splicing and is necessary for normal cellular functions and development. A direct link between virulence and the spliceosome and prp19 complex was identified in the Basidiomycete corn smut fungus *Ustilago maydis*. The Num1 (orthologue of Spf27/Snt309) interacts with kinesin 1 motor protein, which is involved in vesicle transport, and *num1* defective mutants displayed polarisation of hyphal tip through (Kellner *et al*., 2014). Whilst in *Magnaporthe oryzae* MoCwf15, another component of the Prp19 complex, also showed defective hyphal growth (Liu *et al*., 2021)**.**

Similarly, for the REMI *Z. tritici* L951 *ADE6* mutant, the *CLF1* mutant appeared to grow as wild type on rich nutrient agar as blastospores yet was strongly affected in hyphal growth. Furthermore, I did not observe any difference between the wild type and the *CLF1* mutant even with added pressure of fungal growth stressors indicating that regulated slicing is less important under these conditions. However hyphal growth processes were strongly affected. This could be the result of the mis-splicing, the consequences of which in humans is linked with several diseases including cancers (Pedrotti & Cooper, 2014). Indeed, reducing splicing efficiency in the Ascomycete wheat pathogen *F. graminearum* has recently been linked to reduced virulence though mutations in an RNA-binding protein FgRbp1 (Wang *et al*., 2021). As such it might be possible that, combined with the examples from *M. oryzae* and *U. maydis,* that the Prp19 complex is associated with the splicing of genes particularly involved with hyphal growth as opposed to other stress response processes. Indeed, in the case of MoCwf15, Liu *et al*., (2021) found 19 genes with roles in development and virulence that had defected in splicing in a null *cwf15* mutant.

The spliceosomes of different fungi are composed of differing spliceosome components. For example, the spliceosome model most discussed in this

chapter, *S. cerevisiae*, does not have an orthologue of a spliceosome component found in *F. graminearum FgPRP4*. The *FgPrp4* is a kinase that regulates pre-mRNA splicing, likely by phosphorylation of components in the U4/U6-U5 tri-snRNP (Goa *et al*., 2016). Wang *et al*., (2021) suggest that this may be a consequence of the much lower number of introns in the *S. cerevisiae* genome (376) compared to *F. graminearum* (10,268), making the Prp4 component redundant. Wu *et al*., (2017) indicated that there are 10,192 confirmed intron-containing genes in the *Z. tritici* genome. As such, the elements of the *Z. tritici* spliceosome merit further study.

This study has only begun the functional elucidation of the complete set of REMI mutants, and due to time constraints/lack of complementation, these will require further work in future. Some of the spectra of mutations within a single REMI strain are sometimes complex. In contrast, in the next chapter, I describe a similar exploration of two of the mutants from the random ATMT mutant library with fewer complex mutation events. However, somewhat surprisingly, I reveal that two ATMT strain mutant phenotypes arose from distinct mutations affecting the same gene, which could not have been determined without using the mutagenomics approach.

6 Functional characterisation of the MAPKKK SSK2, impacted in two independent random ATMT *Z. tritici* mutants

6.1 Introduction

The ability to respond to host-imposed environmental stresses is important for virulence in various pathosystems. Though there is a wide array of different environmental factors which may affect fungal pathogens, some key intracellular response pathways are highly conserved. These include the mitogen-activated protein kinase (MAPK) and cyclic adenosine monophosphate(cAMP)-protein kinase A (PKA) pathways (Turrà *et al*., 2014). Indeed, some of the currently implicated genetic factors in the dimorphic switch in *Z. tritici*, are MAPK, G-proteins, transcription factors and cAMP-responsive factors. Three MAPK-encoding genes have been identified as essential for full virulence in *Z. tritici.* These are; *ZtSLT2* (previously published as MgSLT2) linked to cell wall integrity pathway, *ZtFUS3* (previously published as MgFUS3) linked to pheromone response and invasion pathways and *ZtHOG1* linked to osmotic stress response (previously published as MgHog1) (Cousin *et al*., 2006; Mehrabi *et al*., 2006a; Mehrabi *et al*., 2006b).

Investigation into our four random ATMT mutants identified two isolates (4-124 and 4-158), with similar *in planta* and *in vitro* phenotypes. Subsequent genomic re-sequencing of both strains identified a direct T-DNA insertion event in a putative MAPKKK (Ssk2 from yeast nomenclature) in strain 4-124. In contrast, 4-158 had a T-DNA inserted elsewhere in the genome, but we also identified an SNP leading to an inactivating frameshift mutation in Zt*SSK2*. The MAPKKK Ssk2p acts in one of the two phosphorelays of a stress-activated protein kinase (SAPK) pathway in yeast, ultimately activating, through phosphorylation, the high osmolarity glycerol 1 (Hog1) protein kinase, which in turn activates several transcriptional regulators. There is evidence that indicates that the Hog1 pathway is not only activated in response to osmotic stress but also is involved in regulating the stress

adaptation responses induced by oxidative stress, cell wall integrity stress, heat shock and cold shock (Bilsand *et al*., 2004; García-Rodriguez *et al*., 2000; Lawrence *et al*., 2004; Panadero *et al*., 2006). Hog1 has also been associated with tolerance to glucose starvation, methylglyoxal, heavy metals, citric acid, and the bacterial endotoxin lipopolysaccharide (Day & Quinn, 2019). However, the roles and regulation of conserved SAPKs like Hog1 are not always identical across fungi.

The HOG1 pathway is highly conserved and present in other fungi, though it is not essential for pathogenicity in all plant pathogens (Jiang *et al*., 2018). For example, the *HOG1* 'orthologues' in *Magnaporthe oryzae* (*MoOSM1*)*, Colletotrichum orbiculare* and *Bipolaris oryzae* are dispensable for virulence. However, in *Fusarium graminearum*, *Botrytis cinerea, Cochliobolus sativus* and *Z. tritici,* the Hog1 kinase is important for pathogenicity (Li *et al*., 2012; Jiang *et al*., 2018). Interestingly, for the barley (*Hordeum vulgare*) infecting pathogen *C. sativus*, a *CsHOG1* mutant was normal in root infection but against leaves was reduced in virulence (Leng & Zhong, 2015). Jiang *et al*., (2018) speculate that the 'role' of the HOG1 pathway in virulence may be associated with the host tissue that the pathogen infects.

Figure 6.1 shows a simplified representation of the putative *Z. tritici* Hog1 pathway based on the well characterised *S. cerevisiae* pathway. In *S. cerevisiae,* Sln1 auto-phosphorylates, initiating a phosphorelay signalling mechanism. Ypd1p, a histidine phosphate transfer protein, subsequently phosphorylates Ssk1p, a response regulator that represses Ssk2/22p. Ssk2 and Ssk22 are paralog MAPKKKs, though only one 'Ssk2/22' has been identified in *Z. tritici* (herein referred to as ZtSsk2). Osmotic stress releases inhibition of Ssk2/22p, which subsequently binds to Pbs2 that then phosphorylates and activates Hog1 (Brewster & Gustin, 2014). The second phosphorelay branch in *S. cerevisiae* is initiated by Sho1 and converges on Pbs2 through phosphorylation by Ste11. An important note is that there are no known orthologues in *Z. tritici* for three membrane-associated proteins, Msb2, Opy2 and Hkr1, that interact and form a complex with Sho1 or anchor

other proteins to the membrane. These three genes without identified orthologues in *Z. tritici* are not represented in Figure 6.1.

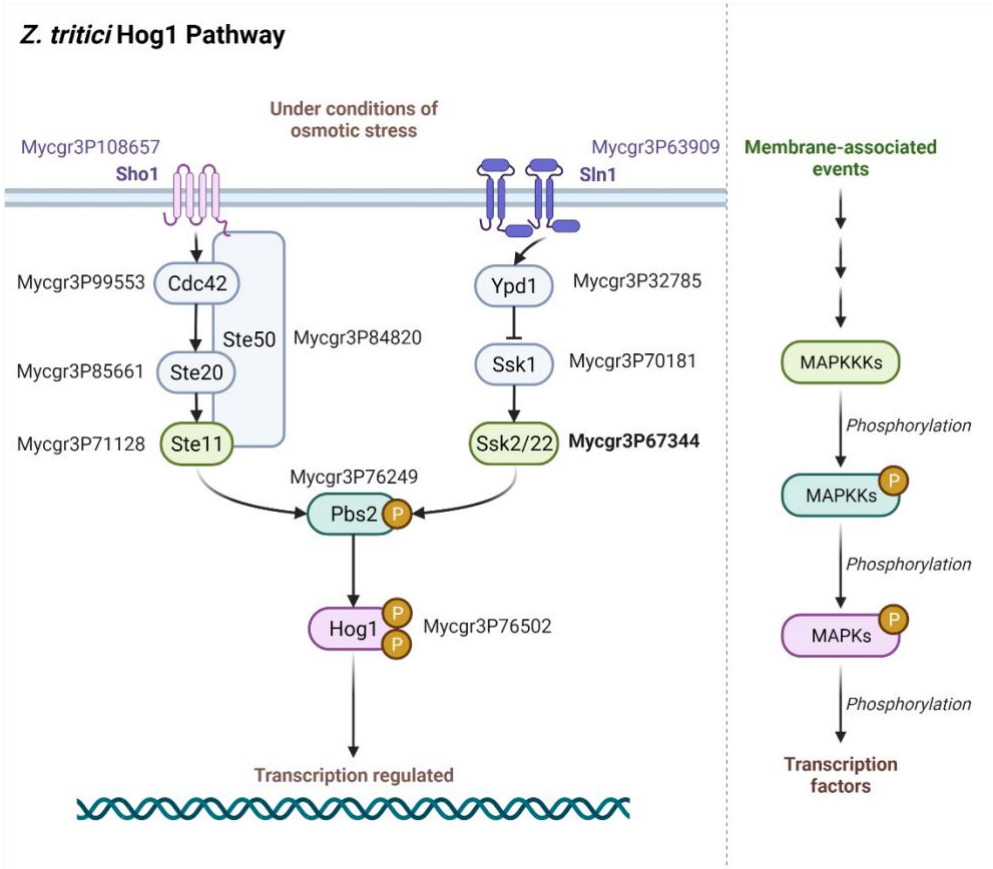

Figure 6.1 The currently known/predicted orthologues in the *Z. tritici* stress-activated protein kinase HOG1 pathway.

A simplified representation of the known components of the Hog1 pathway with predicted orthologues in *Z. tritici*, based on KEGG (ztr04011) and Brewster & Gustin (2014).

Other studies have investigated some of the other participants in the HOG pathway in *Z. tritici*, showing a range of phenotypic consequences to their interruption. Deletion of *ZtHOG1* resulted in sensitivity to multiple environmental stresses, including osmotic and oxidative, inability to switch to filamentous growth, and loss of virulence (Mehrabi *et al*., 2006b). Yemelin *et al*., (2017) studied a random ATMT mutant isolate with an interruption affecting the *ZtSSK1* gene. This interruption resulted in only small chlorotic lesions developing *in planta*, increased sensitivity to osmotic and oxidative stress, reduced sensitivity to phenylpyrrole fungicide fludioxonil and

impacted conidial growth. The putative MAPKKK *ZtSTE11* (previously published as MgSte11) deficient mutants exhibited limited filamentous growth on water agar and were non-pathogenic *in planta* but were not sensitive to the fungal growth stressors tested, including oxidative and osmotic stress (Kramer *et al*., 2009). *ZtSTE20* defective mutants had WT virulence, but their yeast-like growth form was impacted (Kramer *et al.,* 2009). Yeast-two hybrid assays confirmed predicted (from what is known in *S. cerevisiae*) interactions between ZtSte50p-ZtSte11p and ZtSte50p-ZtSte20p. However, as this study looked at the Fus3 MAPK signalling pathway the ZtSte50p-ZtCdc42 (implied in Figure 6.1) interaction has not been experimentally validated (Kramer *et al*., 2009).

In this chapter, I describe the results of the genetic complementation assay of *ZtSSK2* in the two independent Δ*ZtSsk2* ATMT mutants, 4-124 and 4-158, and the subsequent change in *in vitro* growth and *in planta* disease progression phenotypes. Furthermore, I explore the oxidative stress sensitivity and responses of the mutant and complemented strains through Western Blot detection of p38 MAPK protein activation/inactivation and describe changes in the global gene expression of WT and complemented strains using an early time point *in planta* dual RNA-sequencing experiment. The results presented also demonstrates that Hog1 dependent developmental and gene expression responses in *Z. tritici* can be mediated through both Ste11 and Ssk2 MAPKKKs, but that the responses to stresses may be more reliant on the latter.

6.2 Materials and Methods

6.2.1 Constructs

For targeted gene deletion constructs flanking sequences. The complementation construct was designed the same way as the REMI mutant isolate candidates. A representation of the complement construct is shown in Figure 6.2, showing the PCR generated insert *ZtSSK2* gene upstream to include the native promoter and 120 bp downstream to maintain 3' UTR.

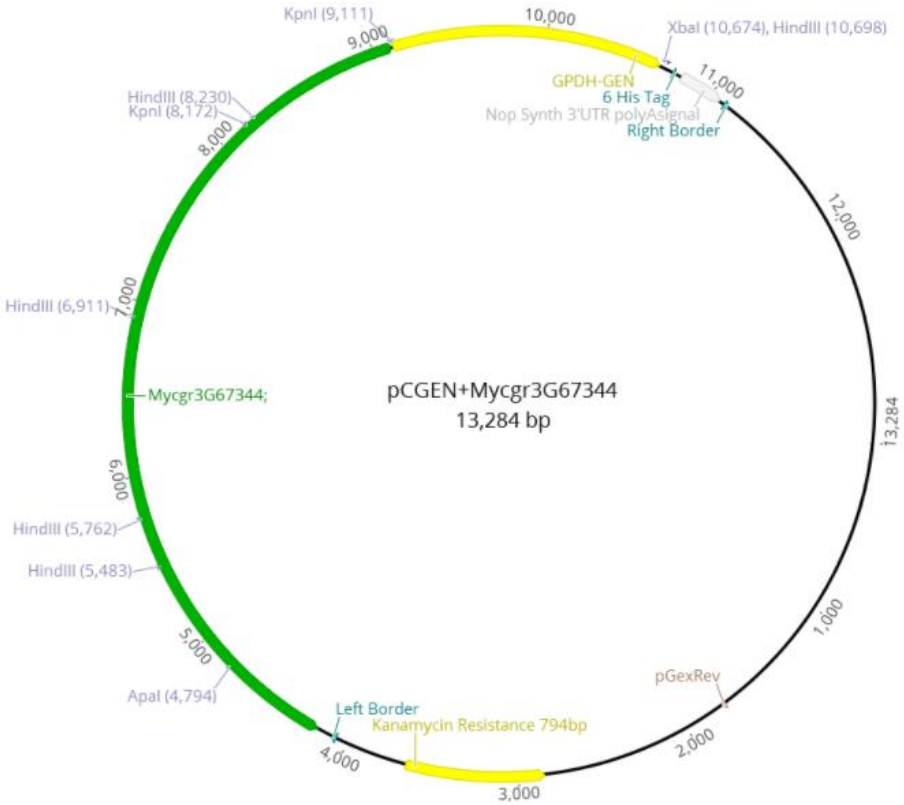

Figure 6.2 pCGEN+ZtSSK2 construct for ATMT for complementation approach to restore functional copy to mutant isolates 4-124 and 4-158.

6.2.2 *In planta* and *in vitro* screening

Unless stated otherwise, all *in planta* and *in vitro* screening was carried out as described in Chapter Three. An additional *in vitro* screen with the anti-fungal Fludioxonil, detailed on concentration, are listed in Chapter Two (and with the relevant Figure in this Chapter).

6.2.3 Protein work

Methods of protein extraction and Western blotting are described in Chapter Two.

6.2.4 RNA Sequencing

Quality control of reads was performed using MultiQC. Sequence trimming of recognised adaptors was performed using Trimmomatic (Bolger *et al*., 2014). Reads were mapped to the *Z. tritici* IPO323 genome using HiSat2 (Kim *et al*., 2019). Principal Component Analysis (PCA) was performed on sample differences of variance stabilising transformed (vsd) gene count data to confirm that the biological replicates clustered together. Count determination was performed using FeatureCounts (Liao *et al*., 2014) on the R Bioconductor. Library normalisation and differential expression (DE) calling were done using the Bioconductor package DESeq2 (Love *et al*., 2014; https://bioconductor.org/packages/release/bioc/html/DESeq2.html) in R studio. Gene expression levels were compared between WT IPO323 and the 4-124 ATMT mutant samples for each time point individually. DEGs were identified by applying a log2 fold change filter of ≥ 1 or ≤ -1, and the DESeq2 implementation of Benjamini-Hochberg (Benjamini & Hochberg, 1995) was used to control for multiple testing (FDR<0.05). Gene Ontology (GO) enrichment analysis was performed for all significantly up-and down-regulated *Z. tritici* genes using OmicsBox to identify overrepresented GO term BLAST2GO Enrichment.

6.3 Results

6.3.1 Further analysis of the T-DNA and SNP mediated mutations in *ZtSSK2* in mutants 4-124 and 4-158

Genome resequencing identified two independent *ZtSSK2* 'defective' mutants within the T-DNA mutant strains, 4-124 and 4-158. In 4-124, a T-DNA insertion resulted in an 1112 bp deletion, including the promoter region and 600 bp into the 5' portion of the gene, resulting in the ATG start codon loss. In 4-158, a frameshift mutation was identified within the protein kinase domain. These areas are shown in Figure 6.3A and B, as well as the regions cloned for the generation of the complementation constructs.

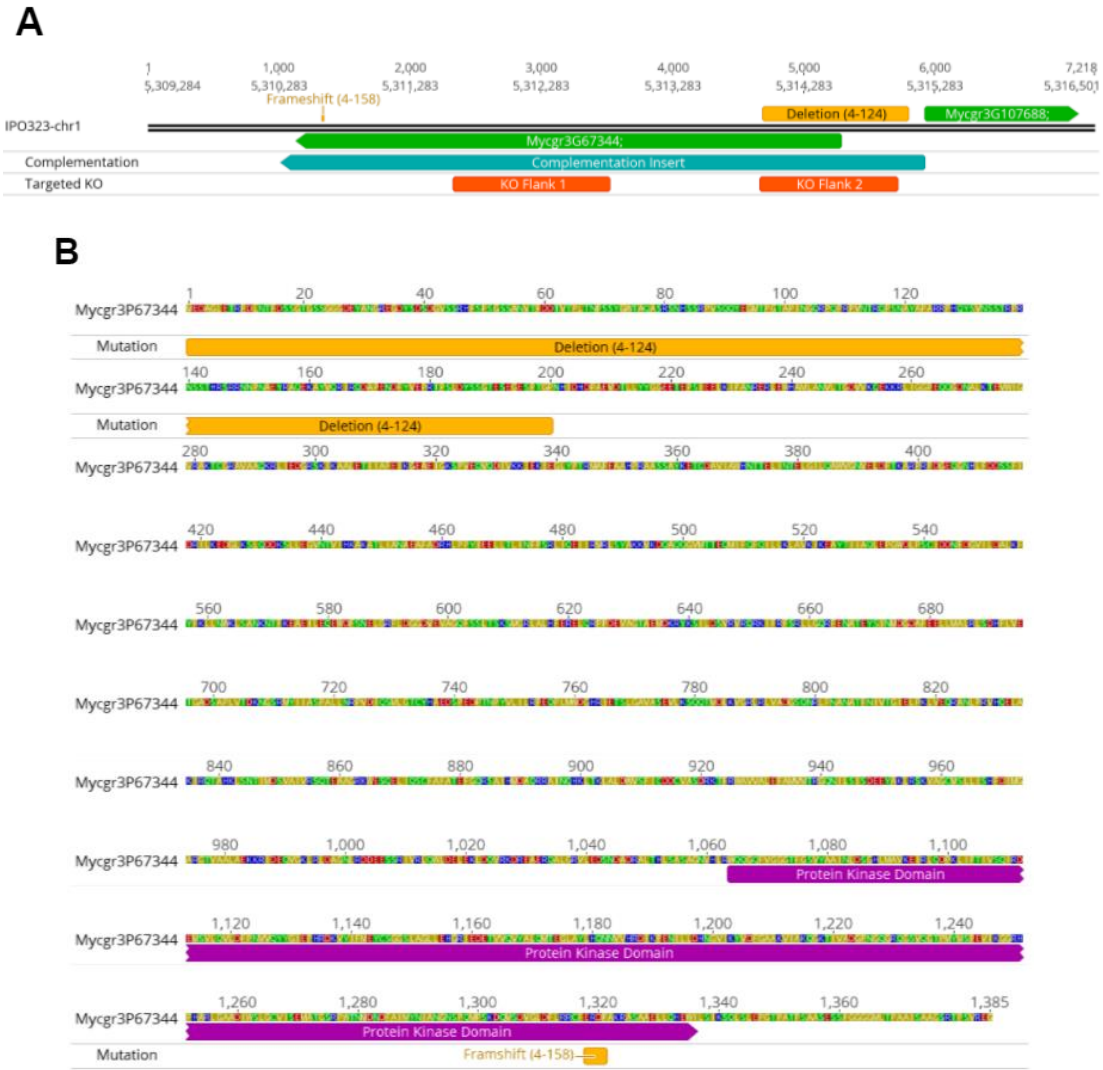

Figure 6.3 Two independent *ZtSsk2* defective strains arising from different mutation events.

Produced in Geneious v10.3. [**A**] Shows a 7200 bp region of *Z. tritici* IPO323 chromosome one, including *ZtSSK2* and a neighbouring gene (annotations in green) in the IPO323 genome, and the relative positions of the mutations in the two isolates (annotations in yellow). The blue 'Complementation Insert' annotation refers to the sequence inserted into a T-DNA plasmid to then transformed into the two independent mutant isolates. [**B**] Shows the amino acid sequence of IPO323 ZtSsk2p. The yellow regions show what residues were affected by the T-DNA insertion in 4-124 and the position of the frameshift in 4-158 within the predicted protein kinase domain (purple annotation). In later phylogenetic analysis, the nucleotide sequence of this protein kinase domain was used.

6.3.2 KnetMiner and phylogenetics analysis confirm *ZtSSK2* as a likely true orthologue of yeast and fungal SSK2 MAPKKKs

Ahead of functional complementation and to seek out further information on the *ZtSSK2* candidate gene, I used a variety of online databases and resources. KnetMiner enables a more visual method for searching predicted orthologues and associated phenotypic information, drawing knowledge graphs across large biological databases and literature. A prototype Zymoseptoria KnetMiner currently draws on data and literature from a few fungi, including Saccharomyces yeast, *Fusarium graminearum*, *Neurospora crassa* and *Aspergillus nidulans*. Figure 6.4 shows the knowledge graph generated for *ZtSSK2* using its JGI identifier Mycgr3G67344. The *Z. tritici* gene (MGSSK2) is highlighted in yellow, linked to the protein it encodes and further linked to orthologues and proteins with similar sequences. KnetMiner identified orthologues in *Fusarium graminearum* (NCBI:txid5518) and *Aspergillus nidulans* FGSC A4 (NCBI:txid227321). The database for the latter has more associated information on cellular activities and functions. For the sequences identified with similar sequences, connected by dotted red lines, the majority share a similar identified phenotype, "reduced virulence", which fits the observed phenotype of 4-124 and 4-158 mutants.

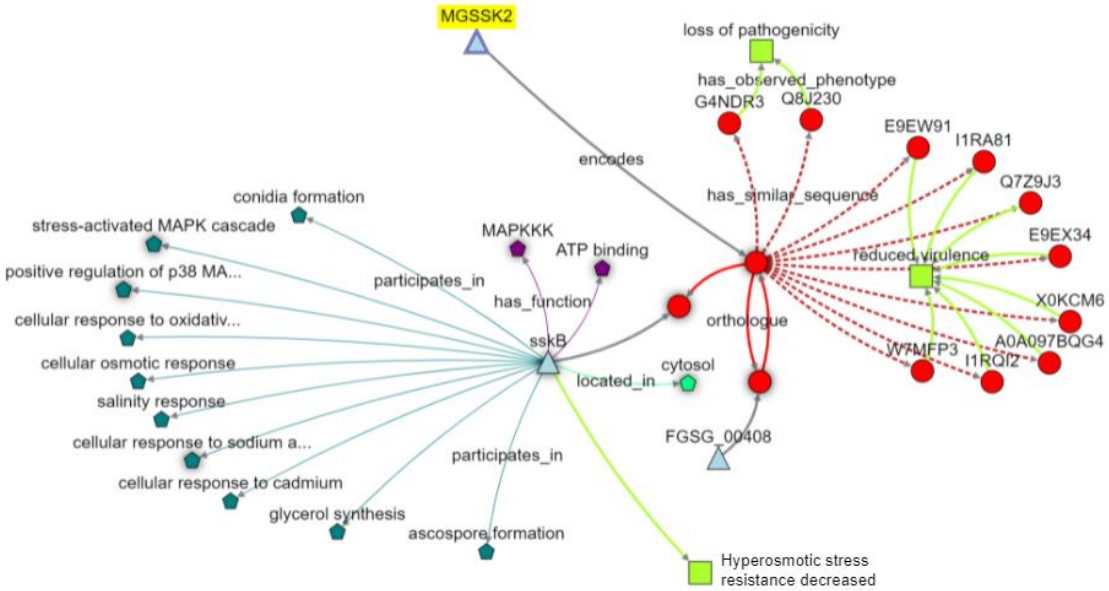

Figure 6.4 KnetMiner knowledge graph on the ZtSsk2 gene.

Link: https://bit.ly/KnetZtSSK2

The Knetminer and other analysis suggest that the *Zymoseptoria SSK2* gene likely functions in the HOG1 MAPK pathway. In fungi the basis for what is known about the HOG pathway and the proteins that function in its phosphorelays, are based on the work initially carried out in *S. cerevisiae*. As such I sought to display the phylogenetic relationship between *Z. tritici* and the orthologs of related taxa. Figure 6.5 shows the results of multiple sequence alignments of fungal *SSK2* protein kinase domain nucleotide sequences and a tree generated by Maximum Likelihood in Geneious. The SYM+I+G nucleotide substitution model was selected using JmodelTest (v. 2.1.10) from the MUSCLE aligned (carried out in Geneious with default values and 16 iterations) sequences of 37 fungal *Ssk2* kinase domains. This analysis highlighted (as anticipated) that the *Z. tritici Ssk2* kinase domain clustered most closely with likely orthologues based on overall taxonomic relatedness, showing it to be a conserved sequence of general importance to fungi.

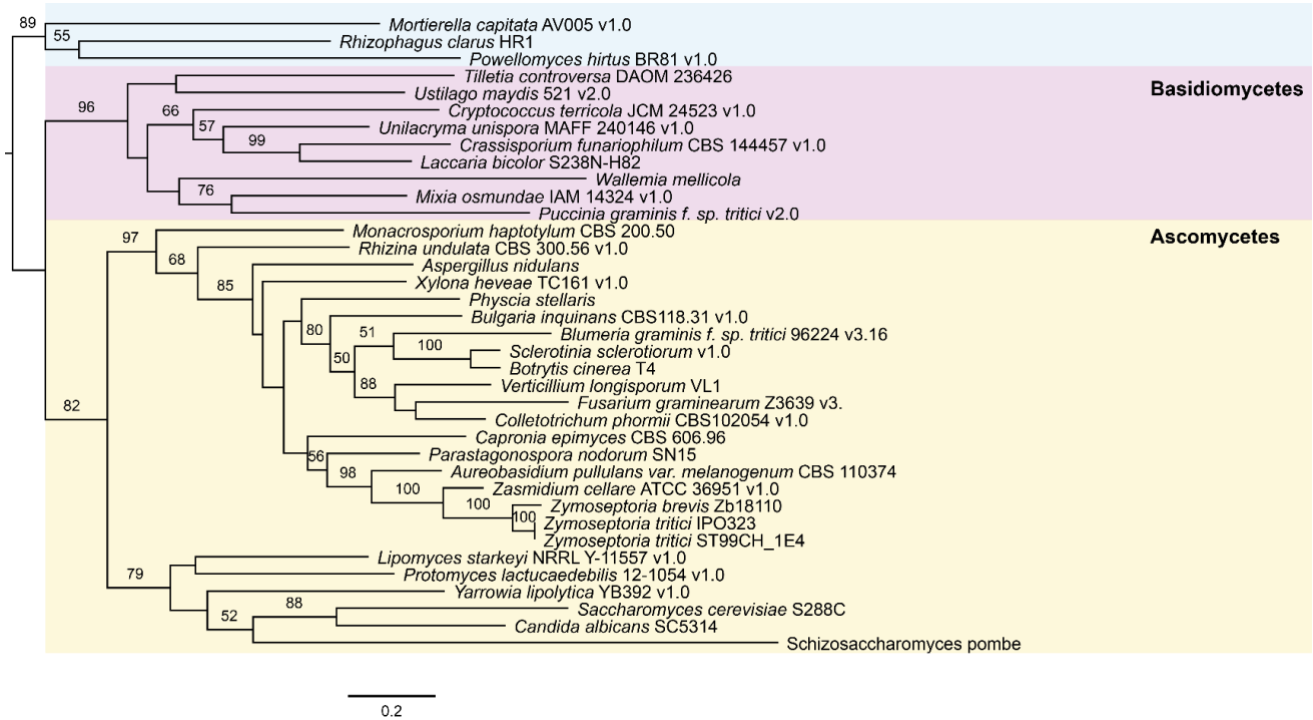

Figure 6.5 Maximum Likelihood *SSK2* kinase domain nucleotide sequence tree.

Maximum Likelihood phylogenetic tree (Geneious v.10.2.3) displaying representative kinase domain nucleotide sequence orthologues to *ZtSSK2* across the fungal tree of life. A total of 37 sequences were aligned by MUSCLE on Geneious with 16 iterations but otherwise default values. Substitution model SYM+I+G was identified using JmodelTest (v. 2.1.10). Basidiomycota fungi (purple) split from Ascomycota (yellow) and lower fungal groups (blue). Node labels indicate percentage bootstrap support (500 replicates); those below 50 are not shown. The scale bar shows phylogenetic distance of 0.2 nucleotide substitutions per site.

6.3.3 Complementation with WT *ZtSSK2* restored full *in planta* disease symptom development

Following the method described for the REMI mutants in Chapter Five, I generated gene complementation constructs from IPO323 gDNA, using primers to amplify a region that included the native promoter, the full coding sequence, and the terminator regions of the gene. These were cloned into vector pCGEN and used in *Agrobacterium*-mediated fungal transformation on both the 4-124 and 4-158 mutants.

The resulting transformants were then tested for increased ability to cause STB disease relative to the original mutants and compared to the WT IPO323 strain. Figure 6.6 shows that multiple independent complemented strains from each parental background were restored for virulence on wheat, supporting the notion that it was the loss of Ssk2 function in both the 4-124 and 4-158 strains which was responsible for the reduction in virulence.

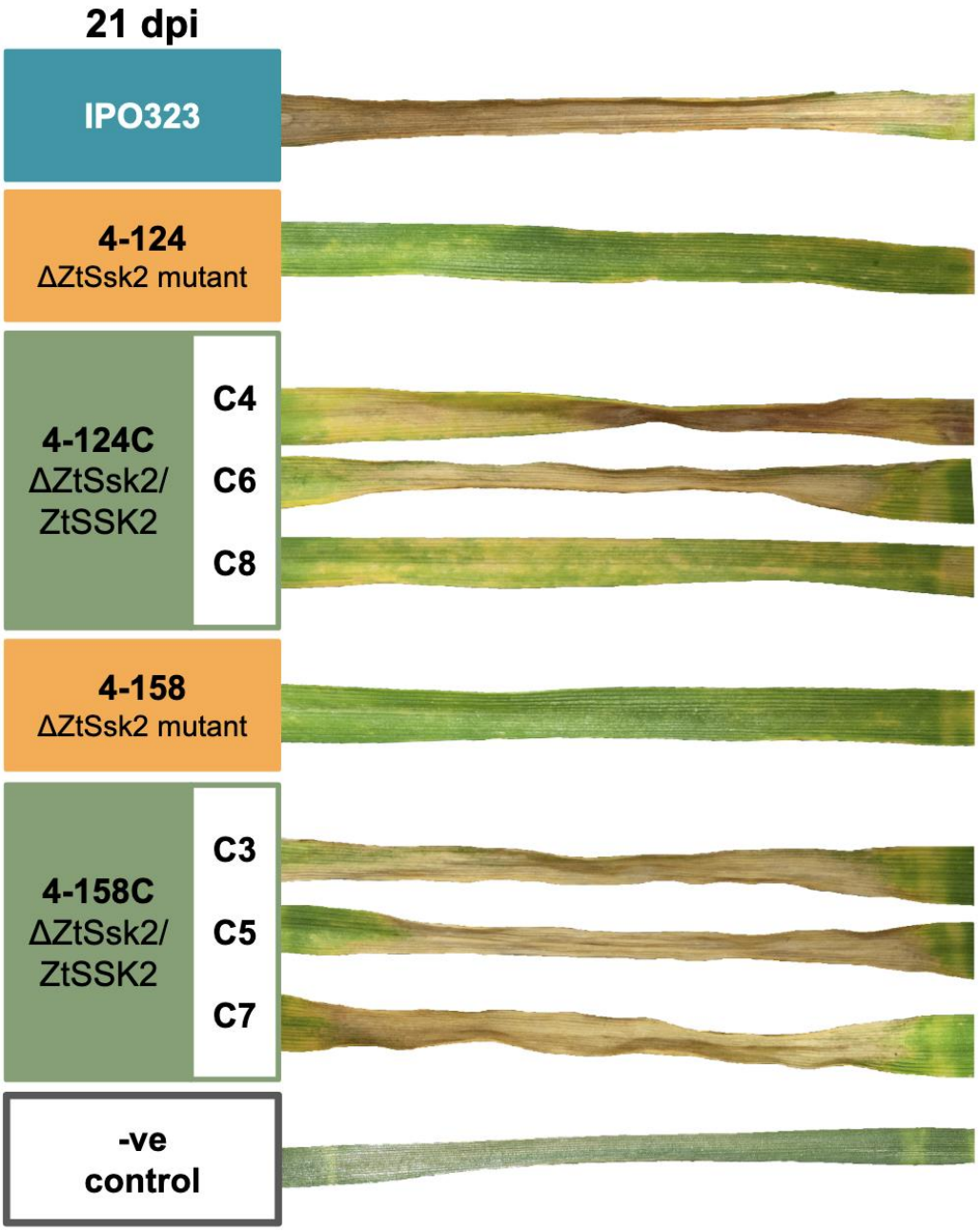

Figure 6.6 *In planta* assessment of disease progression comparing WT IPO323, two *ZtSsk2* defective mutant isolates and *ZtSSK2* complements at 21 dpi.

Images show a representative wheat leaf with typical symptoms from the three replicate inoculated leaves at 21 dpi. The entire leaf surface shown was inoculated via cotton swab with 1×10^{7} spores ml^{-1} 0.01% Tween20 solution. A virulent parental strain (IPO323), the avirulent "*ΔZtSsk2*" mutants (4-124 and 4-158), three biological replica complementation mutants (*ΔZtSsk2*/ZtSSK2) showing restored virulence

and a negative control are shown. Each mutant isolate displayed here were tested a minimum of three times *in planta* on wheat cv. Riband.

6.3.4 Hyphal growth assays on *ZtSsk2* mutants and complemented *ΔZtSsk2*/ZtSSK2 isolates

The other commonly shared phenotype of interest in the *ZtSsk2* defective strains discussed in Chapter Three, was the aberrant hyphal growth exhibited on TWA. The two mutant strains consistently produced less extended filaments, which appeared to be hyper-branched compared to its parental strain, IPO323. Figure 6.8 shows this alongside the complementation results with a functional *ZtSSK2* after 10 dpi on tap water agar. The representative complementation (one of three tested with identical results) mutant shown displays the restored typical hyphal growth phenotype *in vitro*. Figure 6.7 shows that the re-introduction of Ssk2 fully restores hyphal growth to both the 4-124 and 4-158 mutants, again supporting that loss of this gene was responsible for the original phenotypes observed for both strains. The data also confirm a previously suggested link between reduced virulence phenotypes and aberrant growth morphologies for both strains.

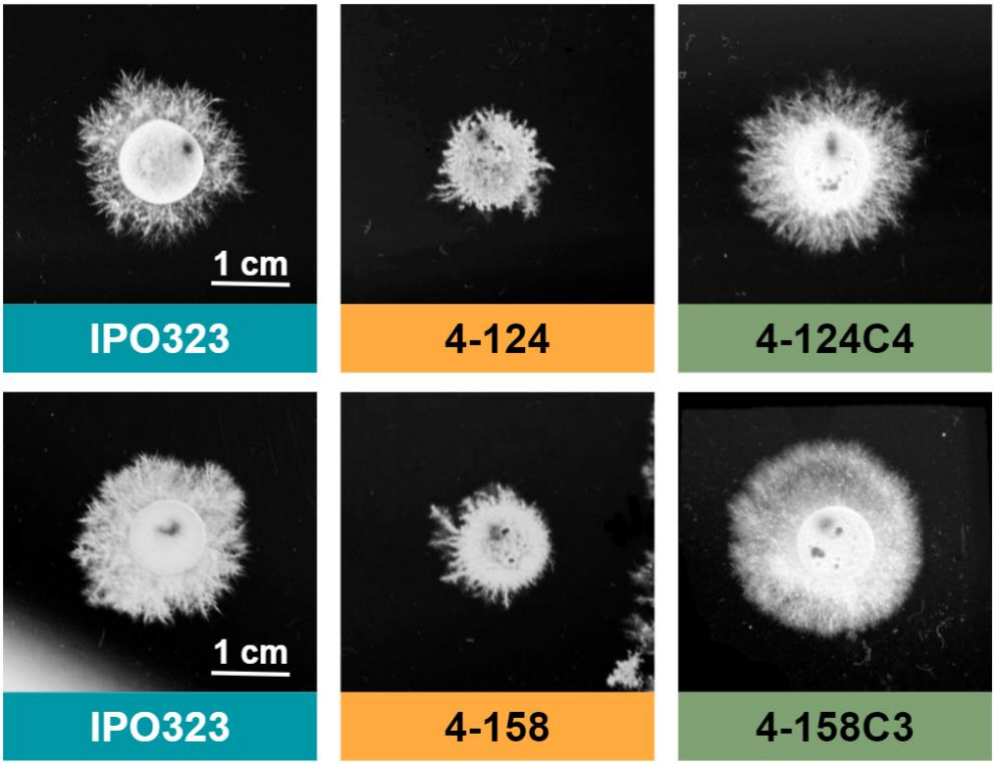

Figure 6.7 *In vitro* spotting on tap water agar (TWA) demonstrates restoration of typical hyphal growth in two independent defective *ZtSsk2* mutant isolates. Spores were suspended in 0.01% Tween20 at a concentration of 1×10^7 spores ml^{-1}, and 5 µl were spotted onto TWA and photographed after ten days. The complemented isolates 4-124 and 4-158 show a restoration of typical WT hyphal growth. The images shown are representatives that reflect all complemented mutant isolates and are repeated a minimum of three times.

6.3.5 Scanning electron microscopy shows germination of hyphae on the wheat leaf surface in the *ZtSsk2* defective mutants

Figure 6.7 indicated that both the *Ssk2* mutants were affected for hyphal growth on water agar. It was, therefore, possible that this defect may also be responsible for the failure of the mutants to cause full disease. To test this, I inoculated wheat leaves with spores of mutants and WT strains and analysed cells for surface germination at 1, 3 and 9 days post-inoculation using SEM. Figure 6.8 shows representative images from 9 dpi. Overall, this analysis revealed no major differences, indicating that the very early germination events are similar in both mutants and WT. The figure also shows some stomatal penetration events do occur as well as some hyphae also growing across stomates without penetration. However, 9 dpi from the surface, no qualitative differences were observed, and a thorough quantitative analysis was not possible. Taken together, this analysis suggests that the hyphal growth (and other) defects likely occur a little later in the infection process and not at the initial point of spore germination.

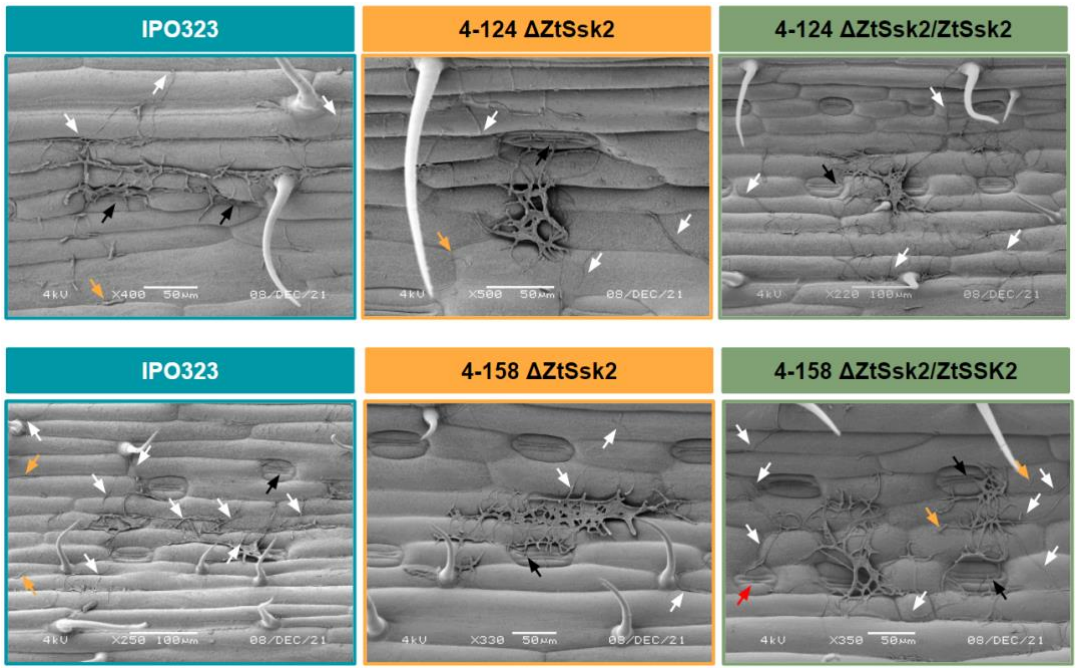

Figure 6.8 Scanning electron microscopy of wheat leaf surface in the *ZtSsk2* defective mutants at nine days post-inoculation.

Spores were suspended in 0.1% Tween20 at a concentration of 1×10^6 spores ml^{-1} and gently brushed onto wheat cv. Riband adaxial surface. Riband leaves closed in a perspex box for three days, and SEM images were taken nine days post-inoculation. Scale bars are included in the individual photos. There is not much difference between the IPO323 parental strain, the two *ΔZtSsk2* mutants (4-124 and 4-158) and the representative *ΔZtSsk2*/*ZtSSK2* gene complement mutants shown. Germination (represented by white arrows) occurred in all three, ungerminated spores were identified (yellow arrows) and attempts to penetrate stomata were observed (black arrows). In the representative image for the complemented 4-158 mutant, a red arrow indicates a filament that has extended over a closed stomata. There was no apparent difference in the germination or hyphal filament extension in WT vs *ZtSsk2* deficient mutants noted.

6.3.6 Stress sensitivity assays on the *ZtSsk2* defective mutants and *ΔZtSsk2/ZtSSK2* complemented strains

The Hog1 pathway is activated in fungi in response to multiple stresses. Chapter Three showed that mutant isolates 4-124 and 4-158 showed increased sensitivity to oxidative (hydrogen peroxide) and osmotic stress (Sorbitol) during blastosporulation on rich nutrient agar. Using the original mutants, the WT strains, and the complemented strains, I next tested whether the re-introduction of functional *ZtSSK2* also restores normal sensitivity (reduced hypersensitivity) to these stressors. Figure 6.9 shows the results of these assays for a complemented strain (representative of three tested with identical results). The figure shows that the re-introduction of Ssk2 into both the 4-124 and 4-158 mutants resulted in a loss of the hypersensitivity to osmotic and oxidative stress seen in both original mutants. In contrast, there was no change in sensitivity to calcofluor white (CFW) which is commonly used to impose cell wall stress and is primarily thought to evoke activation of the cell wall integrity MAPK pathway mediated through Slt2 (Mehrabi *et al.,* 2006a).

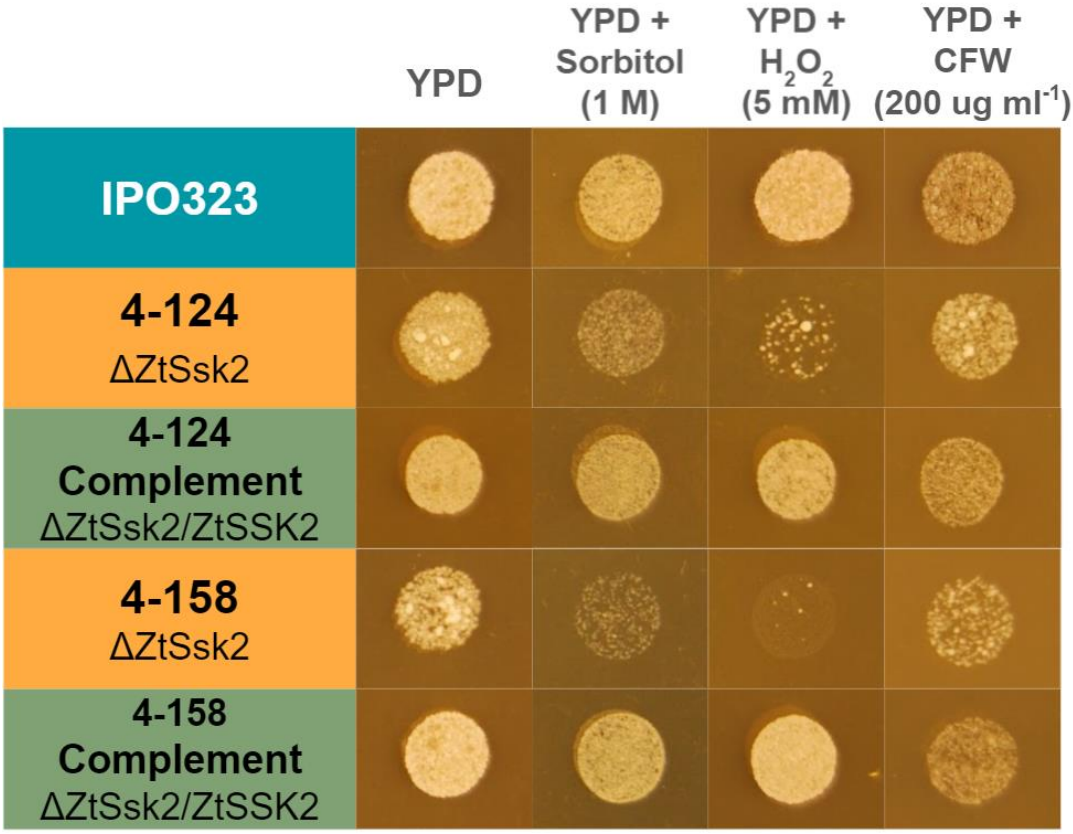

Figure 6.9 *In vitro* fungal growth stressor assays with the *ΔZtSsk2* mutant isolates and *ΔZtSsk2/ZtSSK2* complementation strains.

Spores were suspended in 0.01% Tween20 at a concentration of 1×10^6 spores ml^{-1}, and 5 µl were spotted onto YPD and fungal growth stressor amended YPD, photos all taken at five dpi. On the plain YPD, all mutants show typical WT growth visually compared to the parental *Z. tritici* strain IPO323 (blue). The IPO323 spot has melanised under cell wall integrity stress using calcofluor white (YPD + CFW, 200 µg ml^{-1}). Mutants 4-124 and 4-158 (yellow)) were sensitive to both osmotic (YPD + sorbitol, 1 M) and oxidative (YPD + H_2O_2, 5mM) stressors. However, the representative *ΔZtSsk2/ZtSSK2* complementation strains (green) have restored normal WT stress sensitivity phenotypes.

6.3.7 Fungicide sensitivity assays place ZtSsk2p upstream of ZtHog1p

Two previous studies on *ZtSSK1* and *ZtHOG1* mutants demonstrated increased resistance to a class of fungicides in mutants, as has also been seen for orthologues in other fungal pathogens (Mehrabi *et al*., 2006b; Yemelin *et al*., 2017). To place *ZtSSK2* in this same (Hog1) pathway, I tested whether the original mutants exhibited this increased sensitivity and whether sensitivity was restored by complementation with Ssk2. To this end, I performed a fungicide sensitivity *in vitro* growth assay. This revealed that *ZtSsk2* disrupted mutants 4-124 and 4-158 display increased resistance to the phenylpyrrole fungicide fludioxonil, exhibiting similar enhanced growth phenotypes at higher concentrations (Fig 6.10). This observation supports previous reports by Mehrabi *et al*., (2006b) and Yemelin *et al*., (2017) of *Hog1* and *Ssk1*, respectively. Unlike the disrupted mutant isolates, the IPO323 reference strain and *ΔZtSsk2/ZtSSK2* complementation strain on YPD supplemented with 30 µg ml^{-1} fludioxonil were more sensitive to fludioxonil. Therefore, these data are consistent with the idea that ZtSsk2p also acts upstream of ZtHog1p and contributes to fungicide sensitivity.

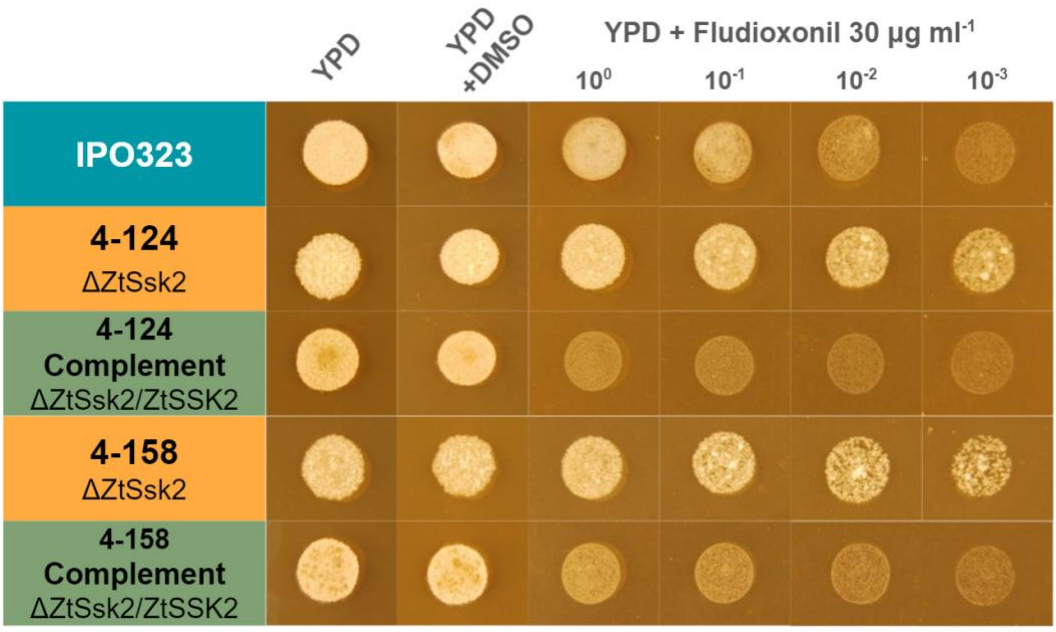

Figure 6.10 *In vitro* fludioxonil sensitivity assay on IPO323, two independent *ZtSsk2* mutant isolates and representative *ΔZtSsk2/ZtSSK2* complementation strains.

Prior to the photographs the *Z. tritici* strains were incubated on YPD amended with fludioxonil (30 µg ml^{-1}, dissolved in DMSO) for 6 days at 16 °C. Three times serial dilutions of the YPD-grown culture (1.0×10^7 spores ml^{-1}) were dropped on the plate. The independent mutant isolates with different mutations impacting the function of ZtSsk2p, 4-124 and 4-158, both display resistance to the phenylpyrrole fungicide fludioxonil. Meanwhile, the wildtype strain IPO323 and the *ΔZtSsk2/ZtSSK2* complementation transformants exhibit diminished growth upon fludioxonil treatment.

6.3.8 Analysis of early gene expression of *ZtSSK2* 'KO' mutant *in planta* through global RNA sequencing

To probe the consequence of defective Ssk2 for impacts on infection-related gene expression, I analysed the transcriptome of the 4-124 mutant isolate through RNA-sequencing with samples taken at two early *in planta* infection time points. This particular mutant *ZtSsk2* isolate was selected because the T-DNA insertion knocks out the promoter and 5' end of the gene. There were no other major effects caused by untagged mutations in the re-sequenced genome. A wild-type *Z. tritici* stain IPO323 was used as a control to compare the expression of the mutant 4-124 against. Strains were inoculated (1.0×10^7

spores ml^{-1}) onto wheat cv. Riband, and grown in a light cabinet prior to RNA isolation, as per conditions described in Chapter Two. RNA extraction was performed at 6 h and 24 h post-inoculation to attempt to capture and compare the early phase of filamentous growth on the leaf surface. Unfortunately, due to a technical error in RNA sequencing, one replicate from the 6 h IPO323 samples was unusable in the analyses. A repeated attempt at sequencing the same sample was successful, but I was unable to incorporate this replicate into my analyses for this thesis due to limited time. Another important observation in my generated RNAseq data is that the “WT” IPO323 strain appeared to have lost chromosome eighteen, as indicated by no read mapping to this template region. Therefore, to identify genes that were differentially expressed elsewhere, all reads mapped to chromosome eighteen in the *Ssk2* mutant were also removed from the subsequent analyses.

Figure 6.11, depicting a principal component analysis (PCA), shows that the biological replicates cluster together (circled) and that principal components split the samples by strain and timepoint. This indicated that the mutant isolate 4-124 and WT IPO323 expression patterns differed more by strain than sampling time.

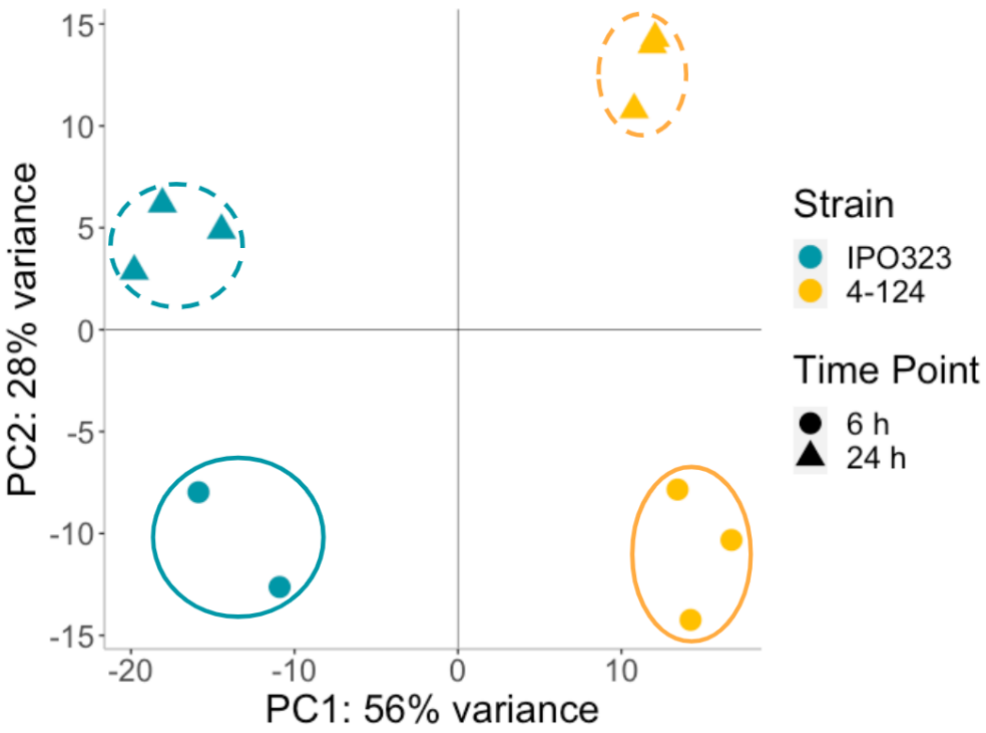

Figure 6.11 Principal component analysis revealed separation of *Z. tritici* IPO323 and *ZtSsk2* defective mutant RNA samples by strain and time.
Principal component analysis (PCA) plot of sample distances based on vsd transformed gene count data of the eleven successfully sequenced RNA samples mapped to the *Z. tritici* transcriptome, excluding the failed replicate IPO323 6 h sample as well as all reads mapped to genes on chromosome eighteen in 4-124. PC1 explains 56% of the sample variance; this splits IPO323 (blue) and 4-124 (yellow) RNA samples. PC2 explains 28% of the variance, and this splits RNA samples by time, 6 h (triangle) and 24 h (spot). Generated using DeSeq2 in R studio.

As the T-DNA insertion occurred upstream and involved the ATG start codon (Figure 6.2), I did not expect to see the expression of *ZtSSK2* in the ATMT *Z. tritici* mutant 4-124. However, in Figure 6.12A I show that low expression levels were still identified for the mapping region of the coding sequence. As time was limited, confirmation of the expression levels using quantitative PCR of the *ZtSsk2* gene in the 4-124 mutant has yet to be carried out. So, it is unclear whether the reads mapping across this region represents intact elements of the *SSK2* gene. Furthermore, as is common to expression studies on fungal MAPK genes, differential expression of *ZtHOG1* itself (downstream kinase) was not expected going into the analysis and was not

observed at a statistically significant level in the mutant versus the 'WT' IPO323, see Figure 6.12B.

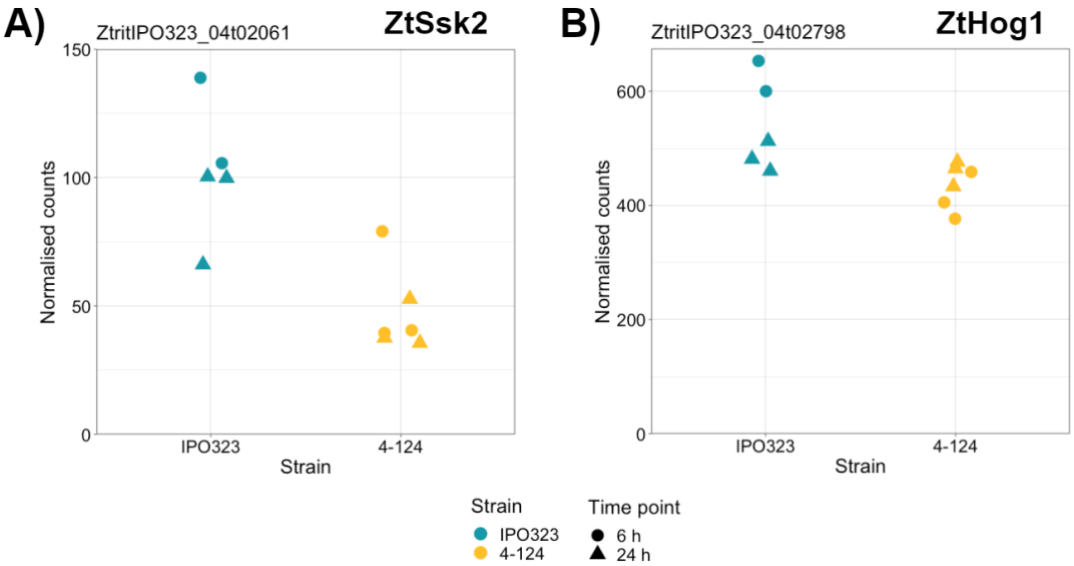

Figure 6.12 Differential expression of *ZtSSK2* and *ZtHOG1* in the *Z. tritici* mutant 4-124 was not statistically significantly different in 4-124 compared to IPO323.

Normalised counts plotted after variance stabilisation through vsd in **A)** *ZtSSK2*, show low expression in the mutant, but not significantly different from IPO323, **B)** *ZtHOG1* expression is comparatively much higher than the *ZtSSK2.*

6.3.8.1 Identifying the differentially expressed genes

Gene expression levels were compared between the *Z. tritici* mutant 4-124 and IPO323 strain at each time point individually. Genes were considered 'differentially expressed' at a cut-off where the average expression was affected by a factor of 1-log2 fold (equates to 2-fold change in expression) and false discovery rate adjusted p-values were less than or equal to 0.05. Due to the failed run of a biological replicate in IPO323 at 6 h the WT expression is based on two replicates, increasing the chance of false positives and negatives. As a result, for this analysis, more focus was applied to investigating differentially expressed genes identified in the strain contrast (4-124 vs WT) at 24 h.

In total, 252 significantly differentially expressed (DE) genes were identified. This included 100 DE genes from 4-124 vs IPO323 strain comparison at 24

h and 74 DE genes at 6 h. Figure 6.134A shows that an additional 78 DE genes overlap (are common) between the different comparisons. An overlap in the number of DE genes was expected given the relatively close time points selected for this study compared to other transcriptomic analyses. Figure 6.13B shows the percentage of genes that are up/down-regulated in 4-124 versus IPO323. From this, we can see that a greater portion of genes were downregulated in the defective *ZtSsk2* mutant compared to IPO323, with 135 unique DE genes across the three comparisons versus 117 upregulated.

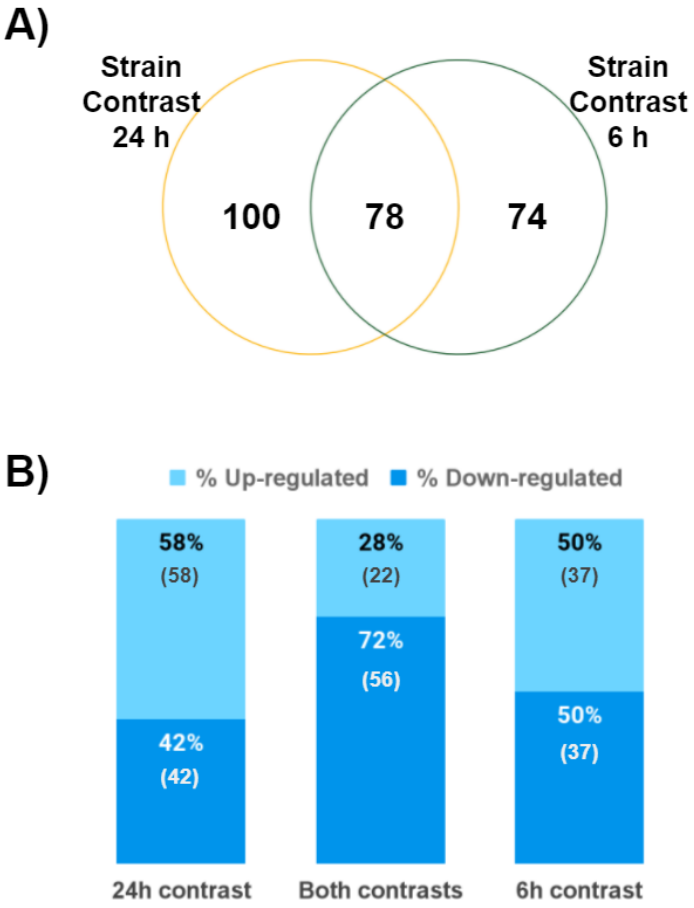

Figure 6.13 Numbers of differentially expressed genes identified in the contrasts between *Z. tritici* Ssk2 mutant and IPO323 (WT).

A) Venn diagram showing the number of differentially expressed (DE) genes shared and unique to these two contrasts of 4-124 versus IPO323 at 24 h and 6 h timepoints. **B)** Stacked percentage bar chart showing the percentage of genes up-regulated (lighter blue) versus down-regulated (darker blue) unique to the 24h and

6h contrast individually as well as overlapping DE genes present in 'Both contrasts' in brackets below the percentage are the actual number of DE genes.

I next visualised the expression patterns of the DE genes using a heatmap generated with 'vsd' normalised and LOG transformed count data, as shown in Figure 6.14. The 'Gene Z-score' represent the number of standard deviations away from the mean, averaging across the samples, i.e. if a gene has a score of zero in a sample (represented black in the figure), its value is the same/similar to the mean expression of that gene (Gu *et al*., 2016). PAM clustering indicated two clusters, in which 'Cluster 1' represents genes "up" in IPO323 (WT) but "down" in the *ZtSsk2* mutant and 'Cluster 2' represents the opposite pattern (Jin & Han, 2011).

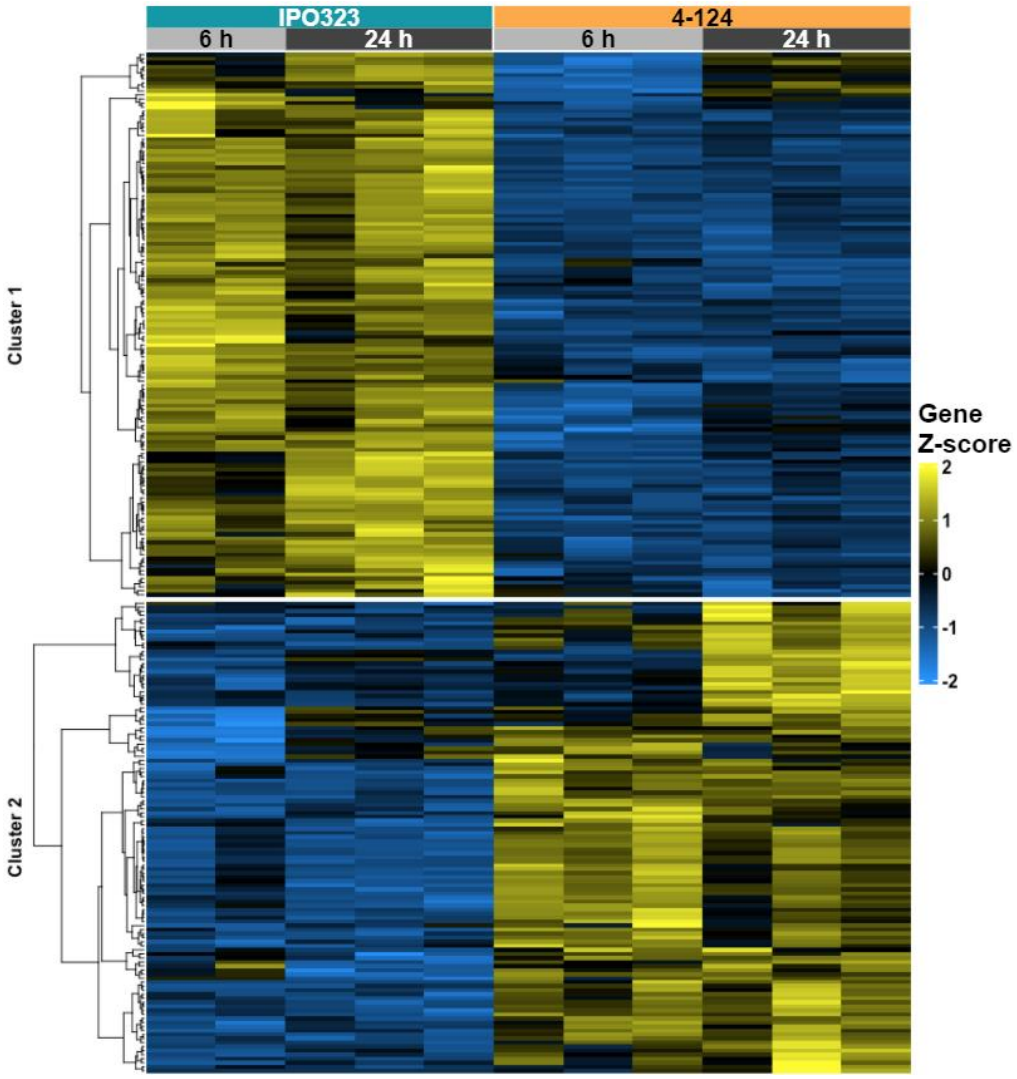

Figure 6.14 Heatmap of the 252 differentially expressed genes in *Z. tritici* IPO323 and *ZtSsk2* deficient strains.

Expression patterns of the differentially expressed genes using a heatmap generated with 'vsd' normalised and log-transformed count data, and clustered using PAM (partition around medoids). Gene Z-score scale represents the number of standard deviations away from the mean, averaging across the samples. Cluster 1 broadly represents the genes down-regulated in the 4-124 mutant (yellow bar) vs *Z. tritici* IPO323 (blue bar), and Cluster 2 represents genes that are up-regulated in the mutant versus the IPO323—generated using DeSeq2 and ComplexHeatmaps in R studio.

6.3.8.2 The characterisation *in silico* of the identified DE genes

Classification of genes into their predicted functions identified 44 functional groups, annotated through GO and Joint Genome Institute data, combined with results retrieved from BLASTp, InterProScan and Blast2GO analyses. This was done similarly to Yemelin *et* al., (2022), who reported a recent *in vitro Z. tritici* transcriptome analysis on isolates with impacted dimorphism and virulence, which included a Δ*ZtHog1* mutant isolate (the downstream transcriptional regulator activated by the MAPKKK ZtSsk2). As shown in Figure 6.15, 175 genes (69.4%) across both six h and 24 h strain contrasts could be classified into functional categories. For ease of representation, the fifteen largest categories are shown. For functional groups with three or less differentially expressed members, these were merged into a 'Three or less representatives' category. Some categories include three genes implicated in the production of some unknown secondary metabolites, protein binding, and ribosome-associated (full list of DEGs shown in Appendix Table 6.2).

To determine whether any functional category was overrepresented in my RNAseq data, I performed a GO enrichment analysis using OmicsBox (v.1.3.11). Fisher's Exact test identified one over-represented GO term that met the false discovery rate (FDR) p-value <0.05, oxidoreductase activity (GO:0016491, FDR p = $4.75E^{-2}$). Fungal enzymes with oxidoreductase activity are involved in various cellular processes and have been linked to pathogenicity and protection against host-defence responses (Singh *et al.*,

2021). Previous transcriptomic studies in *Z. tritici* oxidoreductases, namely secreted chloroperoxidases, displayed up-regulation at one dpi peaking at four dpi (Rudd *et* al., 2015). Similarly, in Palma-Guerro *et* al., (2015), oxidoreductases were identified as the most up-regulated category at seven dpi. Furthermore, oxidoreductases were upregulated in response to UV radiation to reduce the levels of free radicals (McCorison & Goodwin, 2020).

Appendix Table 6.3 shows the numbers of genes in the functional categories shown in Figure 6.15 and for the clusters identified in the heatmap presented in Figure 6.15. To recap, genes in cluster 1 are higher expressed in IPO323 than in 4-124 and genes in cluster 2 show the opposite pattern. Given that the heatmap clustered effectively into which genes were upregulated or downregulated in the mutant vs IPO323 this table indicates that the largest change between these two clusters was the number of genes categorised under 'Metabolic process'. Compared to Cluster 1, more genes categorised under 'Proteolysis activity' and 'Transcription regulators' are in the upregulated Cluster 2. Interestingly, the total number of 'Stress response' associated genes is lower in the upregulated Cluster 2. This may indicate that the reduced activation of Hog1 has downstream consequences for the expression of genes involved in the stress response.

Given the functional disruption of the *ZtSSK2* supported by the results of fungal growth stress and *in planta* virulence assays of the 4-124 mutant, I was interested in identifying the potential effect on the expression of any known Hog1 transcriptionally regulated genes, bringing in literature from other fungi and yeasts. For this, I used the prototype *Zymoseptoria tritici* disease KnetMiner tool (https://knetminer.com/Zymoseptoria_tritici/). The KnetMiner keyword search function was used to identify a list of candidate genes putatively associated with HOG1, oxidative stress and osmotic stress from data from select model fungi and the yeast *S. cerevisiae*. These search terms generated a list of over 2500 genes "linked" to HOG1, oxidative and osmotic stress. A total of 27 of these genes were identified as DE within the 24 h strain comparison.

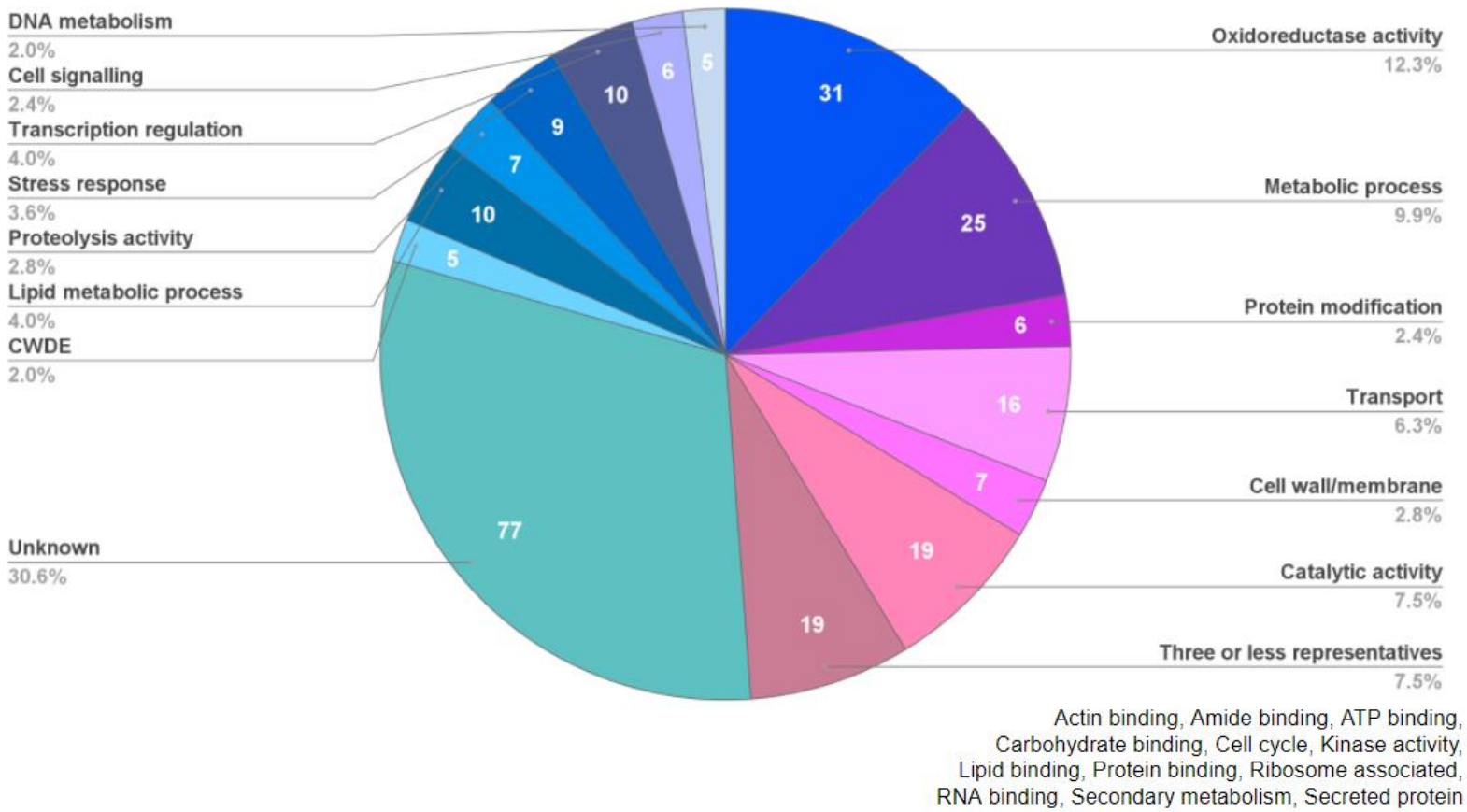

Figure 6.15 Functional categories of the 252 differentially expressed genes across strain contrasts at 6 h and 24 h.

Classification of genes into 44 broad predicted functional groups, done similarly to Yemelin *et al*., (2022). Expressed genes annotated through GO and Joint Genome Institute data, combined with results retrieved from BLASTp, InterProScan and Blast2GO analyses.

Two downregulated DE genes that were present in all three categories, linking them with HOG1, oxidative and osmotic stress, ZtritIPO323_04g01183 (*ZtGLO1*) and ZtritIPO323_04g08156 (*ZtCTT1*). *ZtGLO1* was downregulated compared to the WT IPO323 in the 24 h comparison between strains. *GLO1* encodes predicted monomeric glyoxalase I, which in yeast catalyses the detoxification of a by-product of glycolysis (Morgenstern *et al*., 2020). Glycolysis is a carbon assimilation process, and carbon metabolism is essential for fungal growth and biomass generation (Ene *et al*., 2014). Leuthner *et al*., (2005) identified Glo1 as having a potential role in filamentous growth in *Ustilago maydis*. This study also generated a Glo1 overproducing strain which demonstrated that it functions to also produce H_2O_2. In the yeast *S. cerevisiae, GLO1* expression was induced by osmotic stress conditions but repressed in a disrupted Hog1 background (Inoue *et al*., 1997). This may explain why the gene was downregulated in the *ZtSsk2* mutant (upstream of Hog1 activation) compared to IPO323 in the current data. The *CTT1* gene encodes a putative cytosolic catalase which often functions to destroy H_2O_2 and enable tolerance to ROS. Expression of the *CTT1* gene is induced by a wide variety of stresses, such as osmotic stress and oxidative stress, as well as heat shock. Hog1 is also associated with positive expression regulation of *CTT1* in yeast in response to osmotic stress, and this may again parallel what I have described here for the *ZtSSk2* mutant (Elsztein *et al.*, 2011; Schüller *et al*., 1994; Silva *et al*., 2017).

6.3.9 *ZtSSK2* is required for the post-translational modification and activation of the ZtHog1 MAPK in response to oxidative stress

Much of the previous data has implied that the Ssk2 MAPKKK functions upstream of the Hog1 MAPK. To test this link more directly, I studied the activation of the Hog1 protein using anti-active MAPK antibodies and immunoblotting (western blotting). Activated MAPK proteins can be detected using anti-active antibodies, which only cross-react with MAPKs when dual phosphorylated in the activation loop region. This dual phosphorylation is performed by the upstream MAPKK, which is activated by phosphorylation through MAPKKKs. I performed western blots using MAPK p38 anti active antibodies, which represent the mammalian ortholog of the fungal Hog1. As such (anti-rabbit) p38 MAPK antibodies can also be used to test for the activation of Hog1 in fungi (Han *et al.*, 1994). Western blotting was done on protein extracts from 4-124, 4-124 *SSK2* complemented strains and IPO323 under oxidative stress-induced by H_2O_2. Figure 6.16 shows the activation of Hog1 was impacted in the defective *ZtSsk2* mutant (4-124), whereas the WT IPO323 and representative *ΔZtSsk2*/*ZtSSK2* complementation strain isolate displayed strong activation. These data provide direct supporting evidence that Hog1 activation, through its dual phosphorylation, is an event downstream and requires the function of the Ssk2 MAPKKK in response to oxidative (and potentially) other stresses. The data also suggests that the ZtSte11 MAPKKK cannot compensate for the function of *ZtSSK2* in this response.

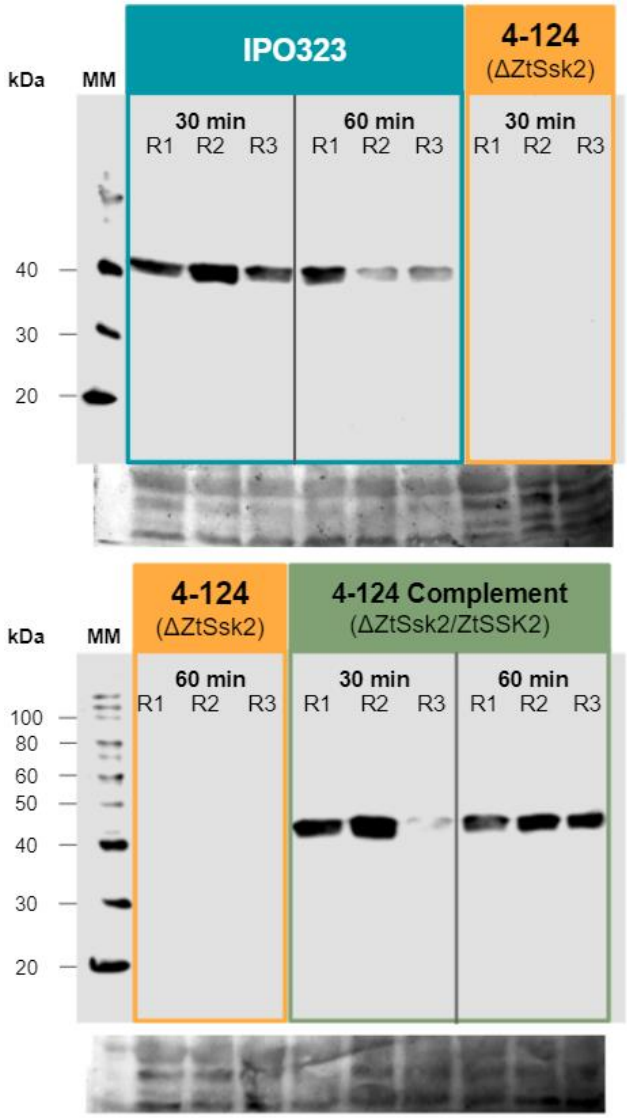

Figure 6.16 Western blot shows oxidative stress activated p38 MAPK Hog1 in a complemented *ΔZtSsk2*/SSK2 mutant isolate.

To test for the activation of p38 MAPK Hog1 in *Z. tritici* IPO323 (blue), 4-124 *ΔZtSsk2* (yellow) and 4-124 *ΔZtSsk2*/*SSK2* (green) following spiking with 25 mM H_2O_2 after 6-days post inoculation YPD culture I performed a Western blot on protein extracted from snap-frozen fungal samples taken 30 and 60 minutes after exposure. In the 4-124 *ΔZtSsk2* mutant, no activation of Hog1p for both time points was observed across three biological replicates ('R'). However, both the wild type *Z. tritici* IPO323 strain and a 4-124 *ΔZtSsk2*/*SSK2* complement isolate have a signal that indicates activation occurred in response to oxidative stress as expected across the replicas to varying strength. 'MM' refers to the MagicMark™ XP Western Protein Standard (Invitrogen), which enables the estimation of protein size.

6.4 Discussion

6.4.1 Efficient stress responses are necessary for fungal virulence and hyphal growth

Like looking left and right to check for cars before crossing the road, fungi continuously sense and respond to environmental cues. There is molecular and genetic circuitry behind those mechanisms that make ‘decisions’ that affect the transitions into lifecycle phases. For example, the invading *Z. tritici* hyphae are exposed to the leaf apoplast environment of the wheat host. Keon *et al*., (2006) reported that this is a low nutrient environment, and upon detection by the host, the fungus is exposed to several stressors. Reactive oxygen species, ions, plant signalling hormones and enzymes attacking major fungal cell wall components, and other microorganisms, are just some examples of elements that an apoplastic fungal pathogen must ‘overcome’ to successfully cause infection (Rodriguez-Moreno *et al*., 2018).

The Hog1 pathway has been described as a conserved and prolific regulator of fungal growth, involved in multiple stress responses, cell cycle progression, morphogenesis, cell wall biogenesis and virulence. Despite this, the control, upstream sensors, activation, and functions of the orthologous Hog1 pathways vary between fungi. The western blot result indicated that in the *ZtSSK2* mutant, the activation of the Hog1 kinase is impacted under the highly oxidative stress conditions. However, the limited activation of Hog1 observed in the defective *Ssk2* mutant could also arise from other aspects. For example, it is possible that the response is either delayed or extremely short-lived in the defective mutant and so would not be seen at the time points tested. Another possibility is that the concentration of H_2O_2 applied overwhelmed the defective *Ssk2* mutant, causing apoptosis and ‘killing’ the fungus. The data also suggests that ZtSte11 cannot compensate for the loss of Ssk2 function as Ste11 is a member of the phosphorelay associated with the sensor Sho1 known to be involved with HOG1 activation (for reference Figure 6.1 shows the known elements in the ZtHog1 pathway). In Kramer *et al*., (2009), it was noted that *ZtSTE11* null mutants were impacted in their

virulence but were not sensitive to the fungal growth stressors tested, including oxidative stress using H_2O_2. Together these data suggest that Ssk2 functions as the major arm in the Hog1 activation pathway in response to oxidative stress. As such osmotic and additional stress associated pathways, such as Slt2 (a functional homolog of human ERK1/2 MAPK p44/42), may attempt to compensate for the loss of Hog1 activity. Western blots could be tested with alternate anti-activated kinase antibodies to determine if the mutant tried to switch to another stress response pathway under stress.

6.4.2 *HOG1*-dependent gene expression

Little is understood about the pre-symptomatic latent phase of *Z. tritici* infection. Previous transcriptomic studies *in planta* typically sample as the earliest time point ~24 h, to capture surface germination and early penetration of the leaf surface. A consideration brought to attention by Fantozzi *et al.*, (2020) is the asynchronous development of *Z. tritici in planta*. In short, invading hyphae follow their developmental program, and expression profiles are likely to reflect this. Under field conditions, where new inoculum can land on the leaf surface and germinate, the impacts would be more prominent than in glasshouse conditions where plants are inoculated at a single time point. The extent to which the asynchrony affects my early timepoint study on gene expression is hard to say, particularly with the added layer of working with a mutant whose expression profile was already likely to be different. However, my data showed a clear separation of overall transcriptomic data between the WT and mutant fungus, indicating that gene loss was a key driver for this and was still showing effects even considering the potentiality of asynchronous development.

Prior to my work, the earliest time point for transcriptomic studies *in planta* found was in Benbow *et al*., (2020). Looking for *in planta* responses to *Z. tritici* against two wheat cultivars, a resistant cultivar (cv. Stigg) and susceptible (cv. Longbow) at four time-points, starting at 6 h. Their focus was on the differing stress responses mounted by wheat against the fungus and identifying disease response genes involved in the early response to *Z. tritici*.

As such, they did not detail any differences in the fungal transcriptome between cultivars. The dual nature of the RNAseq presented here means there is future scope to explore the wheat response to the two different mutants. Whilst Benbow *et al.*, (2020) saw a difference between host responses to infection in susceptible versus resistant cultivars. I postulate that there will be limited difference between the expression profiles of a susceptible cultivar responding to a limited virulence mutant (with a defective *ZtSsk2*) compared to a wild-type virulent strain, particularly at this early time point. However, this must still be analysed. I base this on the observation that only a few germinated spore filaments are likely to have penetrated. Further to this point, the leaf surface SEM imaging indicated little appreciable visual difference between the WT and defective *ZtSsk2* mutant strains. So, unless there is a significant difference in the surface PAMPs presented by the WT and mutant strains, it is difficult to see how the host would respond differently at such early stages. This could, however, change for later stages. It is conceivable that the reduced virulence of Ssk2 mutants could arise from a combination of reduced hyphal growth and greater sensitivity to plant-imposed stresses discussed.

There is a great deal more analysis to undertake with this dataset. For example, Yemelin *et al.,* (2021) recently published the results of a transcriptomic investigation of a ΔZtHog1 mutant *in vitro*. The study identified 354 differentially expressed genes, of which 65 were also differentially expressed in the *ZtSsk2* mutant *in planta*. This provides additional confidence that these genes are in some way associated with expression profiles of defective ZtHOG1 pathway mutants. Furthermore, comparing these two studies may identify different genes related to *in planta* filamentous growth versus *in vitro*.

7 General Discussion

Plant and animal health are threatened by various diseases caused by fungi. While immunity can provide some degree of protection from infection, antifungals are the first line of defence to protect against or combat fungal infections. But antifungal use in agriculture and medicine has driven the emergence of resistance in fungal pathogen populations, this is also true for *Z. tritici*. Farmers and the crop protection industry are very focused on identifying and accessing the next generation of antifungals to combat resistance and protect crops. The discovery pipeline has historically involved screening libraries of small molecule chemistries for their ability to kill fungi. Modes of action and non-target toxicology are then subsequently determined. This “brute force” approach was used to identify many of the antifungals currently in use. However, we are now in a genomics era where thousands of fungal and non-fungal genomes have been sequenced. This should permit more rapid identification of new fungicides based on a more targeted approach. There is also increased precedent for targeting pathogenicity proteins/processes rather than “essential-for-life” processes as these may be, in some cases, unique to pathogenic fungi and thus provide selective targets. The full range of these targets can only arise from a more detailed understanding of the infection processes, which was the aim of the work presented herein.

This project focused on advancing the current understanding of *Zymoseptoria tritici* virulence by deploying a mutagenomic approach to a fungal pathogen to identify key pathogenic determinants in the fungus. The overall course of the work involved testing tools in identifying the entire suite of candidate genes affected by mutation in reduced virulence strains and streamline the decision-making process (prioritisation) for candidate genes arising. Finally, genetic complementation experiments were performed to test whether the prioritised candidate genes were implicated in loss of virulence observed in individual mutants arising from either REMI or ATMT mutagenesis.

7.1 Thawing information in deep freeze: what mysteries at the back of the freezer can we solve today

One of the most rewarding outcomes of these studies is having resolved a 20-year mystery surrounding REMI 1HR.171 (known as L/121 in this study). At the time, based on the available methods, Skinner would (and did) face difficulties in identifying the untagged frameshift mutation. However, even with the genome walking approach to determine untagged mutational effects, the relative ease and depth of information gained from whole-genome re-sequencing are invaluable, as shown here for the ADE6 example. Based on the findings of conserved background mutations being seen in mutagenised strains relative to the WT scaffolds, the optimal application of the mutagenomic approach in *Z. tritici* would be wise to include a re-sequence of the "parental strain" for each mutant batch generated. Whilst I was able to resurrect the glycerol stocks of the Skinner REMI collection, the repeated subcultures to bulk likely resulted in the accumulation of somatic mutations. These could have added complexity to unpicking effects on candidate genes that could affect virulence. However, this was largely mitigated by the decision to also re-sequence a virulent REMI strain which allowed many common background mutations to be discounted as the likely source of reduced virulence in other strains.

Even with whole-genome re-sequencing, assumptions as to which candidate gene is responsible for the observed phenotypes require further testing and validation, either through targeted knockout of the gene in question in an otherwise WT strain, or by complementation (reintroduction of WT allele back into the mutant fungal strain) to either prove or disprove the connection. The power behind the mutagenomic approach to forward genetics studies lies in the potential to determine the functions of many proteins currently of unknown function.

Proteins of unknown function account for approximately ~40% of eukaryotic (including fungal) genomes and represent a substantial untapped resource for selective anti-fungal targets. Some of these may even be fungal kingdom

specific, which in the control of fungal diseases of humans and crops, has relevance for potential lack of toxicity towards the infected host. Despite the number of unknowns in fungal genomes, most mutationally impacted genes identified had predicted functions (or known domains) in my work. This was also a consequence of the prioritisation approach, which used “known” data presented in the KnetMiner tool, PHI-base and related literature to support candidate gene priority. Prioritising genes of currently unknown function would require multiple independent mutations to be observed in the same gene in different reduced virulence strains. This would be somewhat similar to the *ZtSsk2* story described here but lacking the knowledge from a previous annotation. This study covered proteins with predicted functions, but only three of these were investigated in detail, given the limited time available. If there had been no convincing candidates with functional domains or sequence orthology identified by genome re-sequencing, those with unknown functions would have been prioritised.

7.2 Dimorphic switching: An important component of fungal virulence

Given the associations of fungal dimorphic switching to stress responses for invading hosts or evasion of immunity, the impact of defective switching mutants on filamentous pathogenic fungi fitness is no surprise. A number of the fungi capable of causing diseases in immunocompromised humans (or animals) do so by switching morphologies. Some have adapted to tolerating immune responses by changing to a yeast growth form during infection. Examples of this include a basidiomycete *Cryptococcus neoformans* as well as ascomycetes *Histoplasma capsulatum* and *Coccidiodes immitis*. The opposite, a switch to filamentous growth, is not considered common but does occur in the ascomycete yeasts such as *Candida* species, wherein hyphae can facilitate tissue penetration. Additionally, *C. albicans* are thought to revert back into a yeast phase which aids its dissemination through vascular tissues (Boyce & Andrianopoulos, 2015; Lin *et al*., 2015). This is somewhat unlike fungal phytopathogens, where the ‘switch’ to hyphal growth marks the

beginning of irreversible lifestyle change almost universally required for disease.

The importance of the switch to hyphal growth in *Z. tritici* is particularly understandable given its apparent lack of other specialised growth structures. Even if a spore germinates close to open stomata and penetrates, a reduced filamentous or otherwise aberrant hyphal growth phenotype could impact the fungus' subsequent apoplastic colonisation required for full virulence. It is noteworthy that most genes implicated in full virulence of *Z. tritici* to date often also impact the yeast-hyphal switch (Mehrabi *et* al., 2006; Mohammadi *et al*., 2017; Mirzadi Gohari *et al*., 2014; Yemelin *et al*., 2017). Some other examples include *ZtGT2* and *ZtPPT* mutants, where the virulence defect manifests at the pre-penetration/penetration stage (Derbyshire *et* al., 2018; King *et al*., 2015). In the study I present here, all but two mutants, affected in hyphal growth switching *in vitro* were also affected in virulence. The 5-51 mutant showed WT typical hyphal growth, indicating that the candidate's role is not associated with filamentation. As well as REMI-23/E which, despite having a strong defect to *in vitro* switching, was able to cause disease. How this was achieved requires further study. One possibility is that there is something present on the wheat leaf surface that is absent in the *in vitro* tests that could compensate and support morphogenesis followed by successful infection in this mutant. Regardless, the bulk of my work aligned with the established strong association between switching mutants and reduced virulence, which can be further exploited.

The importance of the switching, and the absence of any other specialised infection structures, in *Z. tritici* presents an effectively "stripped down" pathogen to identify genes and processes required for infection. While some of the early genetics required infection by certain foliar phytopathogenic fungi may not be captured in the *Z. tritici* genome (e.g. *U. maydis* or *M. oryzae* appressorium), most have a filamentous and apoplastic stage of infection. It's *in vitro* growth in a yeast-like form and amenability to mutagenesis

methods, combined with a compact haploid genome, make it a very exploitable model system to this end.

7.3 Escaping guilt by sequence similarity: *Z. tritici* as a new model for foliar fungal plant pathogens?

Some of what is known about fungal genetics and the roles of various genetic elements on cellular control come from studies originally in yeast *Saccharomyces cerevisiae* and opportunistic human pathogen *Candida albicans*. Even though these fungi are both Ascomycetes, so they are more closely related to *Z. tritici* than fungi from outside this division, they are distinct from the Pezizomyctes, which represent true filamentous fungi. They are usually diploid in the wild, preferring the yeast growth form, and have only approximately 50% of the genes defined in typical filamentous fungi. In other words, human and plant pathogens have specific adaptations and changes to circuitry behind otherwise conserved pathways. Therefore, it is likely that discovering what makes *Z. tritici* and other plant pathogens successful against their hosts may not always be aided by knowledge from yeasts. Indeed, given the experimental tractability of *Z. tritici* one may argue that it may well become one of the best model systems for dissecting the molecular basis of infection of plants by fungi.

I envisage that the model mutagenomics pipeline established here for *Z. tritici* could lead to the future discovery of “smart” crop protection targets. For example, if a new key virulence gene is identified though this rapid and comprehensive approach, comparison of its sequence in other genomes will reveal the extent to which the target is restricted to pathogenic species, an optimal scenario for minimising other environmental impacts. Alternatively selective chemistry could discriminate only to inhibit the pathogen version if the target protein differs enough in sequence between pathogens and beneficial fungi or other non-target species. This is just one idea of a mutagenomics approach that could lead to smarter future crop protection which is ideally suited to having *Z. tritici* as the model organism for initial discoveries.

7.4 Future work

There are many areas of future work which merit consideration from this initial study, including which metabolic pathways are potentially exploitable for anti-fungal targets and understanding the circuitry behind hyphal morphogenesis in an infection context. Perhaps one of the most interesting is understanding the role of the *Z. tritici* spliceosome. Learning which components of these ribonucleoprotein complexes are present and whether they are required for 'normal' fungal growth and virulence in *Z. tritici* is a logical next step forward based on the findings described in Chapter Five. Generating a 'fresh' targeted knockout of the *CLF1* in IPO323ΔKU70 using ATMT would limit the number of background mutational impacts, and allow for the identification of transcripts affected by the loss of this component of the spliceosome.

There are many implications of a defective malfunctioning spliceosome complex, including mis-splicing and alternative splicing which may affect the infection biology of pathogens. Grützmann *et al*., (2014) highlight the role of alternative splicing (AS), which enables differential production of multiple mRNA and protein isoforms to be produced from one single gene describing the increased rates of AS in pathogenic versus non-pathogenic fungi. This study also indicated putative functions relating to stress responses and dimorphic switching validated in *C. neoformans* studies. But overall, this raises questions about the role of alternative splicing in *Z. tritici* infection. Most notably, *Z. tritici,* like many other plant pathogenic fungi, has a large proportion of its encoding genes possessing introns. This is particularly true of genes encoding secreted and cell wall-associated proteins. In a recent study on *Ustilago maydis* 4,270 AS isoforms were derived from 2,413 genes, 499 of these were labelled infection-specific (Jeon *et al*., 2022). While the extent of alternative splicing in fungi is not yet comprehensively determined, an estimated 6.1% of *Z. tritici* genes have splice variants, compared to 2.3% of *U. maydis* (Chaudhari *et al*., 2019; Grützmann *et al*., 2014). In future, it would be interesting to determine the structure (and expression levels) of

transcripts produced from the *ZtClf1* mutant, in particular those expressed during morphogenetic switching and during leaf infection, by RNAseq.

Beyond these specific examples, I believe the major future work should now be placed upon exploiting the pipeline which I have described here. The future of protecting animal and plant health against fungal diseases requires that we urgently deploy rapid pipelines to identify the full repertoire of pathogen proteins and processes which might be amenable to intervention. The growth habit and experimental tractability of *Z. tritici* should be exploited at scale to this end as a new model for pathogenic fungi.

REFERENCES

Agrios, G. N. (2005). Plant pathology, 5th Edition. *Academic Press*, 922.

Aguilera, J., Rodriguez-Vargas, S., & Prieto, J. A. (2005). The HOG MAP kinase pathway is required for the induction of methylglyoxal-responsive genes and determines methylglyoxal resistance in *Saccharomyces cerevisiae*. *Molecular Microbiology*, *56*(1), 228–239. https://doi.org/10.1111/j.1365-2958.2005.04533.x

Alkan, N., Meng, X., Friedlander, G., Reuveni, E., Sukno, S., Sherman, A., Thon, M., Fluhr, R., & Prusky, D. (2013). Global aspects of pacC regulation of pathogenicity genes in *Colletotrichum gloeosporioides* as revealed by transcriptome analysis. *Molecular Plant-Microbe Interactions*, *26*(11), 1345–1358. https://doi.org/10.1094/MPMI-03-13-0080-R

Almeida, F., Rodrigues, M. L., & Coelho, C. (2019). The Still Underestimated Problem of Fungal Diseases Worldwide. *Frontiers in Microbiology*, *10*(FEB), 1–5. https://doi.org/10.3389/fmicb.2019.00214

Altenhoff, A. M., Levy, J., Zarowiecki, M., Tomiczek, B., Vesztrocy, A. W., Dalquen, D. A., Müller, S., Telford, M. J., Glover, N. M., Dylus, D., & Dessimoz, C. (2019). OMA standalone: Orthology inference among public and custom genomes and transcriptomes. *Genome Research*, *29*(7), 1152–1163. https://doi.org/10.1101/gr.243212.118

Ambrósio, D. L., Badjatia, N., & Günzl, A. (2015). The spliceosomal PRP19 complex of *Trypanosomes*. *Molecular Microbiology*, *95*(5), 885–901. https://doi.org/10.1111/mmi.12910

Aron, O., Wang, M., Mabeche, A. W., Wajjiha, B., Li, M., Yang, S., You, H., Cai, Y., Zhang, T., Li, Y., Wang, B., Zhang, D., Wang, Z., & Tang, W. (2021). MoCpa1-mediated arginine biosynthesis is crucial for fungal growth, conidiation, and plant infection of *Magnaporthe oryzae*. *Applied Microbiology and Biotechnology*, *105*(14–15), 5915–5929. https://doi.org/10.1007/s00253-021-11437-1

Attri, C., Swati, & Kulshrestha, S. (2018). Restriction enzyme-mediated insertional mutagenesis: an efficient method of *Rosellinia necatrix* transformation. *Archives of Microbiology*, *200*(1), 189–194. https://doi.org/10.1007/s00203-017-1466-y

Badet, T., Fouché, S., Hartmann, F. E., Zala, M., & Croll, D. (2021). Machine-learning predicts genomic determinants of meiosis-driven structural variation in a eukaryotic pathogen. *Nature Communications*, *12*(1). https://doi.org/10.1038/s41467-021-23862-x

Badet, T., Oggenfuss, U., Abraham, L., McDonald, B. A., & Croll, D. (2020). A 19-isolate reference-quality global pangenome for the fungal wheat pathogen *Zymoseptoria tritici*. *BMC Biology*, *18*(1), 12. https://doi.org/10.1186/s12915-020-0744-3

Banke, S., & McDonald, B. A. (2005). Migration patterns among global populations of the pathogenic fungus *Mycosphaerella graminicola*. *Molecular Ecology*, *14*(7), 1881–1896. https://doi.org/10.1111/j.1365-294X.2005.02536.x

Bankina, B., Bimšteine, G., Arhipova, I., Kaņeps, J., & Stanka, T. (2018). Importance of agronomic practice on the control of wheat leaf diseases. *Agriculture (Switzerland)*, *8*(4), 1–8. https://doi.org/10.3390/agriculture8040056

Barrett, L. G., Zala, M., Mikaberidze, A., Alassimone, J., Ahmad, M., McDonald, B. A., & Sánchez-Vallet, A. (2021). Mixed infections alter transmission potential in a fungal plant pathogen. *Environmental Microbiology*, *23*(4), 2315–2330. https://doi.org/10.1111/1462-2920.15417

Baum, J. A., Bogaert, T., Clinton, W., Heck, G. R., Feldmann, P., Ilagan, O., Johnson, S., Plaetinck, G., Munyikwa, T., Pleau, M., Vaughn, T., & Roberts, J. (2007). Control of coleopteran insect pests through RNA interference. *Nature Biotechnology*, *25*(11), 1322–1326. https://doi.org/10.1038/nbt1359

Ben M'Barek, S., Cordewener, J. H. G., Tabib Ghaffary, S. M., van der Lee, T. A. J., Liu, Z., Mirzadi Gohari, A., Mehrabi, R., America, A. H. P., Robert, O., Friesen, T. L., Hamza, S., Stergiopoulos, I., de Wit, P. J. G. M., & Kema, G. H. J. (2015). FPLC and liquid-chromatography mass spectrometry identify candidate necrosis-inducing proteins from culture filtrates of the fungal wheat pathogen *Zymoseptoria tritici*. *Fungal Genetics and Biology*, *79*, 54–62. https://doi.org/10.1016/j.fgb.2015.03.015

Benbow, H. R., Brennan, C. J., Zhou, B., Christodoulou, T., Berry, S., Uauy, C., Mullins, E., & Doohan, F. M. (2020). Insights into the resistance of a synthetically-derived wheat to Septoria tritici blotch disease: Less is more. *BMC Plant Biology*, *20*(1), 1–23. https://doi.org/10.1186/s12870-020-02612-z

Bhadauria, V., Banniza, S., Wei, Y., & Peng, Y. L. (2009). Reverse genetics for functional genomics of phytopathogenic fungi and oomycetes. *Comparative and Functional Genomics*, *2009*. https://doi.org/10.1155/2009/380719

Bicalho Nogueira, G., dos Santos, L. V., de Queiroz, C. B., Ribeiro Corrêa, T. L., Pedrozo Menicucci, R., Soares Bazzolli, D. M., de Araújo, E. F., & de Queiroz, M. V. (2019). The histidine kinase slnCl1 of *Colletotrichum lindemuthianum* as a pathogenicity factor against Phaseolus vulgaris L. *Microbiological Research*, *219*(October 2018), 110–122. https://doi.org/10.1016/j.micres.2018.10.005

Bolger, A. M., Lohse, M., & Usadel, B. (2014). Trimmomatic: A flexible trimmer for Illumina sequence data. *Bioinformatics*, *30*(15), 2114–2120. https://doi.org/10.1093/bioinformatics/btu170

Boller, T., & Felix, G. (2009). A Renaissance of Elicitors: Perception of Microbe-Associated Molecular Patterns and Danger Signals by Pattern-Recognition Receptors. *Annual Review of Plant Biology*, *60*(1), 379–406. https://doi.org/10.1146/annurev.arplant.57.032905.105346

Borao, S., Ayté, J., & Hümmer, S. (2021). Evolution of the Early Spliceosomal Complex—From Constitutive to Regulated Splicing. *International Journal of Molecular Sciences*, *22*(22), 12444. https://doi.org/10.3390/ijms222212444

Boyce, K. J., & Andrianopoulos, A. (2015). Fungal dimorphism: the switch from hyphae to yeast is a specialized morphogenetic adaptation allowing colonization of a host. *FEMS Microbiology Reviews*, *39*(6), 797–811. https://doi.org/10.1093/femsre/fuv035

Brefort, T., Doehlemann, G., Mendoza-Mendoza, A., Reissmann, S., Djamei, A., & Kahmann, R. (2009). *Ustilago maydis* as a Pathogen. *Annual Review of Phytopathology*, *47*(1), 423–445. https://doi.org/10.1146/annurev-phyto-080508-081923

Brennan, C. J., Benbow, H. R., Mullins, E., & Doohan, F. M. (2019). A review of the known unknowns in the early stages of septoria tritici blotch disease of wheat. *Plant Pathology*, *68*(8), 1427–1438. https://doi.org/10.1111/ppa.13077

Brewster, J. L., & Gustin, M. C. (2014). Hog1: 20 years of discovery and impact. *Science Signaling*, *7*(343). https://doi.org/10.1126/scisignal.2005458

Brown, J. K. M., Chartrain, L., Lasserre-Zuber, P., & Saintenac, C. (2015). Genetics of resistance to *Zymoseptoria tritici* and applications to wheat breeding. *Fungal Genetics and Biology*, *79*, 33–41. https://doi.org/10.1016/j.fgb.2015.04.017

Brunner, P. C., & McDonald, B. A. (2018). Evolutionary analyses of the avirulence effector AvrStb6 in global populations of *Zymoseptoria tritici* identify candidate amino acids involved in recognition. *Molecular Plant Pathology*, *19*(8), 1836–1846. https://doi.org/10.1111/mpp.12662

Brunner, P. C., Torriani, S. F. F., Croll, D., Stukenbrock, E. H., & McDonald, B. A. (2013). Coevolution and life cycle specialization of plant cell wall degrading enzymes in a hemibiotrophic pathogen. *Molecular Biology and Evolution*, *30*(6), 1337–1347. https://doi.org/10.1093/molbev/mst041

Cairns, T. C., Zheng, X., Zheng, P., Sun, J., & Meyer, V. (2019). Moulding the mould: Understanding and reprogramming filamentous fungal growth and morphogenesis for next generation cell factories. *Biotechnology for Biofuels*, *12*(1), 1–18. https://doi.org/10.1186/s13068-019-1400-4

Cairns, T., & Meyer, V. (2017). *In silico* prediction and characterization of secondary metabolite biosynthetic gene clusters in the wheat pathogen *Zymoseptoria tritici*. *BMC Genomics*, *18*(1). https://doi.org/10.1186/s12864-017-3969-y

Campanaro, A., Srivastava, A. K., Zhang, C., Lee, J., Millyard, L., Gatehouse, A. M. R., Byrne, E., & Sadanandom, A. (2021). TaWRKY10 transcription factor is a novel jasmonic acid signalling regulator involved in immunity against Septoria tritici blotch disease in wheat. *Plant Pathology*, *70*(6), 1397–1408. https://doi.org/10.1111/ppa.13388

Cavalheiro, M., Pais, P., Galocha, M., & Teixeira, M. C. (2018). Host-pathogen interactions mediated by MDR transporters in fungi: As pleiotropic as it gets! *Genes*, *9*(7). https://doi.org/10.3390/genes9070332

Chanarat, S., & Sträßer, K. (2013). Splicing and beyond: The many faces of the Prp19 complex. *Biochimica et Biophysica Acta (BBA) - Molecular Cell Research*, *1833*(10), 2126–2134. https://doi.org/10.1016/j.bbamcr.2013.05.023

Chaudhari, Y., Cairns, T. C., Sidhu, Y., Attah, V., Thomas, G., Csukai, M., Talbot, N. J., Studholme, D. J., & Haynes, K. (2019). The *Zymoseptoria tritici* ORFeome: A functional genomics community resource. *Molecular Plant-Microbe Interactions*, *32*(12), 1564–1570. https://doi.org/10.1094/MPMI-05-19-0123-A

Chen, L.-H., Tsai, H.-C., Yu, P.-L., & Chung, K.-R. (2017). A Major Facilitator Superfamily Transporter-Mediated Resistance to Oxidative Stress and Fungicides Requires Yap1, Skn7, and MAP Kinases in the Citrus Fungal Pathogen Alternaria alternata. *PLOS ONE*, *12*(1), e0169103. https://doi.org/10.1371/journal.pone.0169103

Chen, R. S., & McDonald, B. a. (1996). Sexual reproduction plays a major role in the genetic structure of populations of the fungus *Mycosphaerella graminicola*. *Genetics*, *142*(4), 1119–1127.

Chitty, J., & Fraser, J. (2017). Purine Acquisition and Synthesis by Human Fungal Pathogens. *Microorganisms*, *5*(2), 33. https://doi.org/10.3390/microorganisms5020033

Choi, J., Park, J., Jeon, J., Chi, M. H., Goh, J., Yoo, S. Y., Park, J., Jung, K., Kim, H., Park, S. Y., Rho, H. S., Kim, S., Kim, B. R., Han, S. S., Kang, S., & Lee, Y. H. (2007). Genome-wide analysis of T-DNA integration into the chromosomes of *Magnaporthe oryzae*. *Molecular Microbiology*, *66*(2), 371–382. https://doi.org/10.1111/j.1365-2958.2007.05918.x

Choi, Y.-E., & Goodwin, S. B. (2011). Gene Encoding a c-Type Cyclin in *Mycosphaerella graminicola* Is Involved in Aerial Mycelium Formation, Filamentous Growth, Hyphal Swelling, Melanin Biosynthesis, Stress Response, and Pathogenicity. *Molecular Plant-Microbe Interactions*, *24*(4), 469–477. https://doi.org/10.1094/MPMI-04-10-0090

Chua, S. M. H., Wizrah, M. S. I., Luo, Z., Lim, B. Y. J., Kappler, U., Kobe, B., & Fraser, J. A. (2021). Structural features of *Cryptococcus neoformans* bifunctional GAR/AIR synthetase may present novel antifungal drug targets. *Journal of Biological Chemistry*, *297*(4), 101091. https://doi.org/10.1016/j.jbc.2021.101091

Chung, S., McLean, M. R., & Rymond, B. C. (1999). Yeast ortholog of the Drosophila crooked neck protein promotes spliceosome assembly through stable U4/U6.U5 snRNP addition. *Rna*, *5*(8), 1042–1054. https://doi.org/10.1017/S1355838299990635

Chung, S., Mondon, P., Chang, Y. C., & Kwon-Chung, K. J. (2003). *Cryptococcus neoformans* with a mutation in the tetratricopeptide repeat-containing gene, CCN1, causes subcutaneous lesions but fails to cause systemic infection. *Infection and Immunity*, *71*(4), 1988–1994. https://doi.org/10.1128/IAI.71.4.1988-1994.2003

Cook, D. E., Mesarich, C. H., & Thomma, B. P. H. J. (2015). Understanding Plant Immunity as a Surveillance System to Detect Invasion. *Annual Review of Phytopathology*, *53*(1), 541–563. https://doi.org/10.1146/annurev-phyto-080614-120114

Cousin, A., Mehrabi, R., Guilleroux, M., Dufresne, M., Van Der Lee, T., Waalwijk, C., Langin, T., & Kema, G. H. J. (2006). The MAP kinase-encoding gene MgFus3 of the non-appressorium phytopathogen *Mycosphaerella graminicola* is required for penetration and *in vitro* pycnidia formation. *Molecular Plant Pathology*, *7*(4), 269–278. https://doi.org/10.1111/j.1364-3703.2006.00337.x

Croll, D., Zala, M., & McDonald, B. A. (2013). Breakage-fusion-bridge Cycles and Large Insertions Contribute to the Rapid Evolution of Accessory Chromosomes in a Fungal Pathogen. *PLoS Genetics*, *9*(6), e1003567. https://doi.org/10.1371/journal.pgen.1003567

Crous, P. W., Videira, S. I. R., & Quaedvlieg, W. (2012). *Zymoseptoria* verkleyi. *Persoonia*, *29*, 178–179. http://www.fungalplanet.org/content/pdf-files/FungalPlanet143.pdf

Crous, P. W., Shivas, R. G., Wingfield, M. J., Summerell, B. A., Rossman, A. Y., Alves, J. L., Adams, G. C., Barreto, R. W., Bell, A., Coutinho, M. L., Flory, S. L., Gates, G., Grice, K. R., Hardy, G. E. S. J., Kleczewski, N. M., Lombard, L., Longa, C. M. O., Louis-Seize, G., Macedo, F., … Groenewald, J. Z. (2012). Fungal Planet description sheets: 128–153. *Persoonia - Molecular Phylogeny and Evolution of Fungi*, *29*(1), 146–201. https://doi.org/10.3767/003158512X661589

Curran, E., & Tiley, Anna M. M., Freechan, Angela, Burke, J. I. (2019). Pangenome analysis of the wheat pathogen *Zymoseptoria tritici* from the UK. *In: 2019 IS-MPMI XVIII Congress. ISMPMI.* https://ismpmi.confex.com/ismpmi/2019/meetingapp.cgi/Paper/3313

Day, A. M., & Quinn, J. (2019). Stress-activated protein kinases in human fungal pathogens. *Frontiers in Cellular and Infection Microbiology*, *9*(JUL), 1–15. https://doi.org/10.3389/fcimb.2019.00261

de Jonge, R., Peter van Esse, H., Kombrink, A., Shinya, T., Desaki, Y., Bours, R., van der Krol, S., Shibuya, N., Joosten, M. H. a J., & Thomma, B. P. H. J. (2010). Conserved Fungal LysM Effector Ecp6 Prevents Chitin-Triggered Immunity in Plants. *Science*, *329*(5994), 953–955. https://doi.org/10.1126/science.1190859

Dean, P., Hirt, R. P., & Embley, T. M. (2016). Microsporidia: Why Make Nucleotides if You Can Steal Them? *PLoS Pathogens*, *12*(11), 1–13. https://doi.org/10.1371/journal.ppat.1005870

Dean, R., Van Kan, J. A. L., Pretorius, Z. A., Hammond-Kosack, K. E., Di Pietro, A., Spanu, P. D., Rudd, J. J., Dickman, M., Kahmann, R., Ellis, J., & Foster, G. D. (2012). The Top 10 fungal pathogens in molecular plant pathology. *Molecular Plant Pathology*, *13*(4), 414–430. https://doi.org/10.1111/j.1364-3703.2011.00783.x

DeHaven, A. C., Norden, I. S., & Hoskins, A. A. (2016). Lights, camera, action! Capturing the spliceosome and pre-mRNA splicing with single-molecule fluorescence microscopy. *Wiley Interdisciplinary Reviews: RNA*, *7*(5), 683–701. https://doi.org/10.1002/wrna.1358

Del Sorbo, G., Schoonbeek, H., & De Waard, M. A. (2000). Fungal Transporters Involved in Efflux of Natural Toxic Compounds and Fungicides. *Fungal Genetics and Biology*, *30*(1), 1–15. https://doi.org/10.1006/fgbi.2000.1206

Deller, S., Hammond-Kosack, K. E., & Rudd, J. J. (2011). The complex interactions between host immunity and non-biotrophic fungal pathogens of wheat leaves. *Journal of Plant Physiology*, *168*(1), 63–71. https://doi.org/10.1016/j.jplph.2010.05.024

Deng, S., Sun, W., Dong, L., Cui, G., & Deng, Y. Z. (2019). MoGT2 Is Essential for Morphogenesis and Pathogenicity of *Magnaporthe oryzae*. *MSphere*, *4*(5), 1–14. https://doi.org/10.1128/mSphere.00309-19

Derbyshire, M. C., Gohari, A. M., Mehrabi, R., Kilaru, S., Steinberg, G., Ali, S., Bailey, A., Hammond-Kosack, K., Kema, G. H. J. J., & Rudd, J. J. (2018). Phosphopantetheinyl transferase (Ppt)-mediated biosynthesis of lysine, but not siderophores or DHN melanin, is required for virulence of *Zymoseptoria tritici* on wheat. *Scientific Reports*, *8*(1), 1–11. https://doi.org/10.1038/s41598-018-35223-8

Dietl, A., Binder, U., Bauer, I., Shadkchan, Y., Osherov, N., & Haas, H. (2020). Arginine Auxotrophy Affects Siderophore Biosynthesis and Attenuates Virulence of Aspergillus fumigatus. *Genes*, *11*(4), 423. https://doi.org/10.3390/genes11040423

Domazakis, E., Lin, X., Aguilera-Galvez, C., Wouters, D., Bijsterbosch, G., Wolters, P. J., & Vleeshouwers, V. G. A. A. (2017). Effectoromics-based identification of cell surface receptors in potato. *Methods in Molecular Biology*, *1578*, 337–353. https://doi.org/10.1007/978-1-4939-6859-6_29

Dooley, H. (2015). Fungicide resistance management tactics: impacts on *Zymoseptoria tritici* populations. *Thesis*.

Duba, A., Goriewa-Duba, K., & Wachowska, U. (2018). A review of the interactions between wheat and wheat pathogens: *Zymoseptoria tritici*, fusarium spp. and parastagonospora nodorum. In *International Journal of Molecular Sciences* (Vol. 19, Issue 4). https://doi.org/10.3390/ijms19041138

Duncan, K. E., & Howard, R. J. (2000). Cytological analysis of wheat infection by the leaf blotch pathogen *Mycosphaerella graminicola*. *Mycological Research*, *104*(9), 1074–1082. https://doi.org/10.1017/S0953756299002294

Dunn, N. A., Unni, D. R., Diesh, C., Munoz-Torres, M., Harris, N. L., Yao, E., Rasche, H., Holmes, I. H., Elsik, C. G., & Lewis, S. E. (2019). Apollo: Democratizing genome annotation. *PLoS Computational Biology*, *15*(2), 1–14. https://doi.org/10.1371/journal.pcbi.1006790

Elsztein, C., de Lucena, R. M., & de Morais, M. A. (2011). The resistance of the yeast *Saccharomyces cerevisiae* to the biocide polyhexamethylene biguanide: Involvement of cell wall integrity pathway and emerging role for YAP1. *BMC Molecular Biology*, *12*. https://doi.org/10.1186/1471-2199-12-38

Ene, I. V., Brunke, S., Brown, A. J. P., & Hube, B. (2014). Metabolism in fungal pathogenesis. *Cold Spring Harbor Perspectives in Medicine*, *4*(12), 1–22. https://doi.org/10.1101/cshperspect.a019695

Enjalbert, B., Smith, D. A., Cornell, M. J., Alam, I., Nicholls, S., Brown, A. J. P., & Quinn, J. (2006). Role of the Hog1 Stress-activated Protein Kinase in the Global Transcriptional Response to Stress in the Fungal Pathogen *Candida albicans*. *Molecular Biology of the Cell*, *17*(2), 1018–1032. https://doi.org/10.1091/mbc.e05-06-0501

Eriksen, L., Shaw, M. W., & Ostergård, H. (2001). A Model of the Effect of Pseudothecia on Genetic Recombination and Epidemic Development in Populations of *Mycosphaerella graminicola*. *Phytopathology*, *91*(3), 240–248. https://doi.org/10.1094/PHYTO.2001.91.3.240

Eyal, A. (1981). Integrated control of Septoria diseases of wheat. *Plant Disease*, *65*, 763–768.

Eyal, Z. ., Scharen, A. L. ., Prescott, J. M. ., and Ginkel, M. Van. (1987). The Septoria diseases of wheat: concepts and methods of disease management. *Mexico: CIMMYT Available at: Https://Repository.Cimmyt.Org/Xmlui/Handle/10883/1113.*

Fantozzi, E., Kilaru, S., Gurr, S. J., & Steinberg, G. (2021). Asynchronous development of *Zymoseptoria tritici* infection in wheat. *Fungal Genetics and Biology*, *146*, 103504. https://doi.org/10.1016/j.fgb.2020.103504

FAO. (2009). How to Feed the World in 2050. *Insights from an Expert Meeting at FAO*.

FAO. (2021). In Brief to The State of Food Security and Nutrition in the World 2021. In *In Brief to The State of Food Security and Nutrition in the World 2021*. FAO, IFAD, UNICEF, WFP and WHO. https://doi.org/10.4060/cb5409en

Fell, V. L., & Schild-Poulter, C. (2012). Ku Regulates Signaling to DNA Damage Response Pathways through the Ku70 von Willebrand A Domain. *Molecular and Cellular Biology*, *32*(1), 76–87. https://doi.org/10.1128/MCB.05661-11

Fernandez, J., & Orth, K. (2018). Rise of a Cereal Killer: The Biology of *Magnaporthe oryzae* Biotrophic Growth. *Trends in Microbiology*, *26*(7), 582–597. https://doi.org/10.1016/j.tim.2017.12.007

Fernandez, J., Yang, K. T., Cornwell, K. M., Wright, J. D., & Wilson, R. A. (2013). Growth in rice cells requires *de novo* purine biosynthesis by the blast fungus *Magnaporthe oryzae*. *Scientific Reports*, *3*, 1–9. https://doi.org/10.1038/srep02398

Figueroa, M., Hammond-Kosack, K. E., & Solomon, P. S. (2018). A review of wheat diseases-a field perspective. *Molecular Plant Pathology*, *19*(6), 1523–1536. https://doi.org/10.1111/mpp.12618

Fones, H. N., Bebber, D. P., Chaloner, T. M., Kay, W. T., Steinberg, G., & Gurr, S. J. (2020). Threats to global food security from emerging fungal and oomycete crop pathogens. In *Nature Food*. https://doi.org/10.1038/s43016-020-0075-0

Fones, H. N., Eyles, C. J., Kay, W., Cowper, J., & Gurr, S. J. (2017). A role for random, humidity-dependent epiphytic growth prior to invasion of wheat by *Zymoseptoria tritici*. *Fungal Genetics and Biology*, *106*(May), 51–60. https://doi.org/10.1016/j.fgb.2017.07.002

Fones, H. N., Steinberg, G., & Gurr, S. J. (2015). Measurement of virulence in *Zymoseptoria tritici* through low inoculum-density assays. *Fungal Genetics and Biology*, *79*, 89–93. https://doi.org/10.1016/j.fgb.2015.03.020

Fones, H., & Gurr, S. (2015). The impact of Septoria tritici Blotch disease on wheat: An EU perspective. *Fungal Genetics and Biology*, *79*, 3–7. https://doi.org/10.1016/j.fgb.2015.04.004

Fraaije, B. A., Bayon, C., Atkins, S., Cools, H. J., Lucas, J. A., & Fraaije, M. W. (2012). Risk assessment studies on succinate dehydrogenase inhibitors, the new weapons in the battle to control Septoria leaf blotch in wheat. *Molecular Plant Pathology*, *13*(3), 263–275. https://doi.org/10.1111/j.1364-3703.2011.00746.x

Francisco, C. S., Ma, X., Zwyssig, M. M., McDonald, B. A., & Palma-Guerrero, J. (2019). Morphological changes in response to environmental stresses in the fungal plant pathogen *Zymoseptoria tritici*. *Scientific Reports*, *9*(1), 9642. https://doi.org/10.1038/s41598-019-45994-3

Gao, X., Jin, Q., Jiang, C., Li, Y., Li, C., Liu, H., Kang, Z., & Xu, J.-R. (2016). FgPrp4 Kinase Is Important for Spliceosome B-Complex Activation and Splicing Efficiency in *Fusarium graminearum*. *PLOS Genetics*, *12*(4), e1005973. https://doi.org/10.1371/journal.pgen.1005973

García-Rodriguez, L. J., Durán, A., & Roncero, C. (2000). Calcofluor antifungal action depends on chitin and a functional high- osmolarity glycerol response (HOG) pathway: Evidence for a physiological role of the *Saccharomyces cerevisiae* HOG pathway under noninducing conditions. *Journal of Bacteriology*, *182*(9), 2428–2437. https://doi.org/10.1128/JB.182.9.2428-2437.2000

Ghaffary, S. M. T. (2011). Efficacy and mapping of resistance to *Mycosphaerella graminicola* in wheat. In *Thesis*.

Gijzen, M., & Nürnberger, T. (2006). Nep1-like proteins from plant pathogens: Recruitment and diversification of the NPP1 domain across taxa. *Phytochemistry*, *67*(16), 1800–1807. https://doi.org/10.1016/j.phytochem.2005.12.008

Gilbert, G. S. (2002). Evolutionary ecology of plant diseases in natural ecosystems. *Annual Review of Phytopathology*, *40*(1), 13–43. https://doi.org/10.1146/annurev.phyto.40.021202.110417

Goodwin, S. B., M'Barek, S. Ben, Dhillon, B., Wittenberg, A. H. J., Crane, C. F., Hane, J. K., Foster, A. J., van der Lee, T. A. J., Grimwood, J., Aerts, A., Antoniw, J., Bailey, A., Bluhm, B., Bowler, J., Bristow, J., van der Burgt, A., Canto-Canché, B., Churchill, A. C. L., Conde-Ferràez, L., … Kema, G. H. J. (2011). Finished genome of the fungal wheat pathogen *Mycosphaerella graminicola* reveals dispensome structure, chromosome plasticity, and stealth pathogenesis. *PLoS Genetics*, *7*(6). https://doi.org/10.1371/journal.pgen.1002070

Grandaubert, J., Bhattacharyya, A., & Stukenbrock, E. H. (2015). RNA-seq-Based Gene Annotation and Comparative Genomics of Four Fungal Grass Pathogens in the Genus *Zymoseptoria* Identify Novel Orphan Genes and Species-Specific Invasions of Transposable Elements. *G3 Genes|Genomes|Genetics*, *5*(7), 1323–1333. https://doi.org/10.1534/g3.115.017731

Green, C., & Ivins, J. (1985). Time of sowing and the yield of winter wheat. *Journal of Agricultural Science*, *104*, 235–238.

Gruenheit, N., Baldwin, A., Stewart, B., Jaques, S., Keller, T., Parkinson, K., Salvidge, W., Baines, R., Brimson, C., Wolf, J. B., Chisholm, R., Harwood, A. J., & Thompson, C. R. L. (2021). Mutant resources for functional genomics in Dictyostelium discoideum using REMI-seq technology. *BMC Biology*, *19*(1), 172. https://doi.org/10.1186/s12915-021-01108-y

Grützmann, K., Szafranski, K., Pohl, M., Voigt, K., Petzold, A., & Schuster, S. (2014). Fungal alternative splicing is associated with multicellular complexity and virulence: A genome-wide multi-species study. *DNA Research*, *21*(1), 27–39. https://doi.org/10.1093/dnares/dst038

Guerin, N. A., & Larochelle, D. A. (2002). A user's guide to restriction enzyme-mediated integration in Dictyostelium. *Journal of Muscle Research and Cell Motility*, *23*(7–8), 597–604. https://doi.org/10.1023/A:1024494704863

Guindon, S., Dufayard, J. F., Lefort, V., Anisimova, M., Hordijk, W., & Gascuel, O. (2010). New algorithms and methods to estimate maximum-likelihood phylogenies: Assessing the performance of PhyML 3.0. *Systematic Biology*, *59*(3), 307–321. https://doi.org/10.1093/sysbio/syq010

Habig, M., Bahena-Garrido, S. M., Barkmann, F., Haueisen, J., & Stukenbrock, E. H. (2020). The transcription factor Zt107320 affects the dimorphic switch, growth and virulence of the fungal wheat pathogen *Zymoseptoria tritici*. *Molecular Plant Pathology*, *21*(1), 124–138. https://doi.org/10.1111/mpp.12886

Habig, M., Quade, J., & Stukenbrock, E. H. (2017). Forward Genetics Approach Reveals Host Genotype-Dependent Importance of Accessory Chromosomes in the Fungal Wheat Pathogen *Zymoseptoria tritici*. *MBio*, *8*(6). https://doi.org/10.1128/mBio.01919-17

Habig, M., Schotanus, K., Hufnagel, K., Happel, P., & Stukenbrock, E. H. (2021). Ago1 Affects the Virulence of the Fungal Plant Pathogen *Zymoseptoria tritici*. *Genes*, *12*(7). https://doi.org/10.3390/genes12071011

Hamel, L. P., Nicole, M. C., Duplessis, S., & Ellis, B. E. (2012). Mitogen-activated protein kinase signaling in plant-interacting fungi: Distinct messages from conserved messengers. *Plant Cell*, *24*(4), 1327–1351. https://doi.org/10.1105/tpc.112.096156

Han, Y., Liu, X., Benny, U., Corby Kistler, H., & VanEtten, H. D. (2001). Genes determining pathogenicity to pea are clustered on a supernumerary chromosome in the fungal plant pathogen Nectria haematococca. *Plant Journal*, *25*(3), 305–314. https://doi.org/10.1046/j.1365-313X.2001.00969.x

Haseena, Khan, Mcdonald, Megan, Solomon, P. (2021). Protoplast Isolation from *Zymoseptoria tritici*. *Protocols.Io*. https://doi.org/dx.doi.org/10.17504/protocols.io.k8gcztw

Hatta, R., Ito, K., Hosaki, Y., Tanaka, T., Tanaka, A., Yamamoto, M., Akimitsu, K., & Tsuge, T. (2002). A conditionally dispensable chromosome controls host-specific pathogenicity in the fungal plant pathogen Alternaria alternata. *Genetics*, *161*(1), 59–70.

Head, G. P., Carroll, M. W., Evans, S. P., Rule, D. M., Willse, A. R., Clark, T. L., Storer, N. P., Flannagan, R. D., Samuel, L. W., & Meinke, L. J. (2017). Evaluation of SmartStax and SmartStax PRO maize against western corn rootworm and northern corn rootworm: efficacy and resistance management. *Pest Management Science*, *73*(9), 1883–1899. https://doi.org/10.1002/ps.4554

Heun, M., Schäfer-Pregl, R., Klawan, D., Castagna, R., Accerbi, M., Borghi, B., & Salamini, F. (1997). Site of Einkorn Wheat Domestication Identified by DNA Fingerprinting. *Science*, *278*(5341), 1312–1314. https://doi.org/10.1126/science.278.5341.1312

Hodgens, C., Chang, N., Eric Schaller, G., & Kieber, J. J. (2020). Mutagenomics: A rapid, high-throughput method to identify causative mutations from a genetic screen. *Plant Physiology*, *184*(4), 1658–1673. https://doi.org/10.1104/pp.20.00609

Holmes, S. J. I., & Colhoun, J. (1974). Infection of wheat by Septoria nodorum and S. tritici in relation to plant age, air temperature and relative humidity. *Transactions of the British Mycological Society*, *63*(2), 329–338. https://doi.org/10.1016/S0007-1536(74)80178-6

Holoch, D., & Moazed, D. (2015). RNA-mediated epigenetic regulation of gene expression. *Nature Reviews Genetics*, *16*(2), 71–84. https://doi.org/10.1038/nrg3863

Hunter, Coker, & Royle. (1999). The teleomorph stage, *Mycosphaerella graminicola*, in epidemics of septoria tritici blotch on winter wheat in the UK. *Plant Pathology*, *48*(1), 51–57. https://doi.org/10.1046/j.1365-3059.1999.00310.x

Ibrahim, H. M. M., Kusch, S., Didelon, M., & Raffaele, S. (2021). Genome-wide alternative splicing profiling in the fungal plant pathogen *Sclerotinia sclerotiorum* during the colonization of diverse host families. *Molecular Plant Pathology*, *22*(1), 31–47. https://doi.org/10.1111/mpp.13006

Idrissou, M., & Maréchal, A. (2022). The PRP19 Ubiquitin Ligase, Standing at the Cross-Roads of mRNA Processing and Genome Stability. *Cancers*, *14*(4), 878. https://doi.org/10.3390/cancers14040878

Inoue, Y., Tsujimoto, Y., & Kimura, A. (1998). Expression of the glyoxalase I gene of *Saccharomyces cerevisiae* is regulated by high osmolarity glycerol mitogen-activated protein kinase pathway in osmotic stress response. *Journal of Biological Chemistry*, *273*(5), 2977–2983. https://doi.org/10.1074/jbc.273.5.2977

Jacobson, E. S. (2000). Pathogenic roles for fungal melanins. *Clinical Microbiology Reviews*, *13*(4), 708–717. https://doi.org/10.1128/CMR.13.4.708-717.2000

James, T. Y., Pelin, A., Bonen, L., Ahrendt, S., Sain, D., Corradi, N., & Stajich, J. E. (2013). Shared signatures of parasitism and phylogenomics unite cryptomycota and microsporidia. *Current Biology*, *23*(16), 1548–1553. https://doi.org/10.1016/j.cub.2013.06.057

Jeon, J., Kim, K. T., Choi, J., Cheong, K., Ko, J., Choi, G., Lee, H., Lee, G. W., Park, S. Y., Kim, S., Kim, S. T., Min, C. W., Kang, S., & Lee, Y. H. (2022). Alternative splicing diversifies the transcriptome and proteome of the rice blast fungus during host infection. *RNA Biology*, *19*(1), 373–385. https://doi.org/10.1080/15476286.2022.2043040

Jiang, C., Zhang, X., Liu, H., & Xu, J.-R. (2018). Mitogen-activated protein kinase signaling in plant pathogenic fungi. *PLOS Pathogens*, *14*(3), e1006875. https://doi.org/10.1371/journal.ppat.1006875

Jiang, D., Zhou, J., Bai, G., Xing, X., Tang, L., Yang, X., Li, J., Zhang, K.-Q., & Yang, J. (2017). Random mutagenesis analysis and identification of a novel C2H2-type transcription factor from the nematode-trapping fungus Arthrobotrys oligospora. *Scientific Reports*, *7*(1), 5640. https://doi.org/10.1038/s41598-017-06075-5

Jiang, D., Zhu, W., Wang, Y., Sun, C., Zhang, K.-Q., & Yang, J. (2013). Molecular tools for functional genomics in filamentous fungi: Recent advances and new strategies. *Biotechnology Advances*, *31*(8), 1562–1574. https://doi.org/10.1016/j.biotechadv.2013.08.005

Jiang, L., Zhao, J., Guo, R., Li, J., Yu, L., & Xu, D. (2010). Functional characterization and virulence study of ADE8 and GUA1 genes involved in the *de novo* purine biosynthesis in *Candida albicans*. *FEMS Yeast Research*, *10*(2), 199–208. https://doi.org/10.1111/j.1567-1364.2009.00600.x

Jianping, Z., Guifang, D., Kai, Z., Yongjun, Z., Yongliang, L., & Liuqing, Y. (2012). Screening and identification of insertion mutants from Bipolaris eleusines by mutagenesis based on restriction enzyme-mediated integration. *FEMS Microbiology Letters*, *330*(2), 90–97. https://doi.org/10.1111/j.1574-6968.2012.02537.x

Jin, X., & Han, J. (2010). K-Medoids Clustering. In C. Sammut & G. I. Webb (Eds.), *Encyclopedia of Machine Learning* (pp. 564–565). Springer US. https://doi.org/10.1007/978-0-387-30164-8_426

Jones, J. D. G. G., & Dangl, J. L. (2006). The plant immune system. *Nature*, *444*(7117), 323–329. https://doi.org/10.1038/nature05286

Kahmann, R., & Basse, C. (1999). REMI (Restriction Enzyme Mediated Integration) and its impact on the isolation of pathogenicity genes in fungi attacking plants. *European Journal of Plant Pathology*, *105*(3), 221–229. https://doi.org/10.1023/A:1008757414036

Kanyuka, K., & Rudd, J. J. (2019). Cell surface immune receptors: the guardians of the plant's extracellular spaces. *Current Opinion in Plant Biology*, *50*, 1–8. https://doi.org/10.1016/j.pbi.2019.02.005

Kelliher, C. M., & Haase, S. B. (2017). Connecting virulence pathways to cell-cycle progression in the fungal pathogen *Cryptococcus neoformans*. *Current Genetics*, *63*(5), 803–811. https://doi.org/10.1007/s00294-017-0688-5

Kellner, N., Heimel, K., Obhof, T., Finkernagel, F., & Kämper, J. (2014). The SPF27 Homologue Num1 Connects Splicing and Kinesin 1-Dependent Cytoplasmic Trafficking in Ustilago maydis. *PLoS Genetics*, *10*(1), e1004046. https://doi.org/10.1371/journal.pgen.1004046

Kellner, R., Bhattacharyya, A., Poppe, S., Hsu, T. Y., Brem, R. B., & Stukenbrock, E. H. (2014). Expression profiling of the wheat pathogen *Zymoseptoria tritici* reveals genomic patterns of transcription and host-specific regulatory programs. *Genome Biology and Evolution*, *6*(6), 1353–1365. https://doi.org/10.1093/gbe/evu101

Kema, G. H. J., Annone, J. G., Sayoud, R., Van Silfhout, C. H., & de Bree, J. (1996). Genetic Variation for Virulence and Resistance in the Wheat-*Mycosphaerella graminicola* Pathosystem II. Analysis of Interactions Between Pathogen Isolates and Host Cultivars. In *Phytopathology* (Vol. 86, Issue 2, p. 213). https://doi.org/10.1094/Phyto-86-213

Kema, G. H. J., Mirzadi Gohari, A., Aouini, L., Gibriel, H. A. Y., Ware, S. B., Van Den Bosch, F., Manning-Smith, R., Alonso-Chavez, V., Helps, J., Ben M'Barek, S., Mehrabi, R., Diaz-Trujillo, C., Zamani, E., Schouten, H. J., Van Der Lee, T. A. J., Waalwijk, C., De Waard, M. A., De Wit, P. J. G. M., Verstappen, E. C. P., … Seidl, M. F. (2018). Stress and sexual reproduction affect the dynamics of the wheat pathogen effector AvrStb6 and strobilurin resistance. *Nature Genetics*, *50*(3), 375–380. https://doi.org/10.1038/s41588-018-0052-9

Kema, G. H. J., Yu, D., Rijkenberg, F. H. J., Shaw, M. W., & Baayen, R. P. (1996). Histology of pathogenesis of *Mycosphaerella graminicola* in wheat. In *Phytopathology* (Vol. 7, pp. 777–786). https://doi.org/10.1094/Phyto-86-777

Kema, G. H. J., & van Silfhout, C. H. (1997). Genetic Variation for Virulence and Resistance in the Wheat- *Mycosphaerella graminicola* Pathosystem III. Comparative Seedling and Adult Plant Experiments. *Phytopathology*, *87*(3), 266–272. https://doi.org/10.1094/PHYTO.1997.87.3.266

Kema, G. H. J., Verstappen, E. C. P., & Waalwijk, C. (2000). Avirulence in the Wheat Septoria tritici Leaf Blotch Fungus *Mycosphaerella graminicola* Is Controlled by a Single Locus. *Molecular Plant-Microbe Interactions*, *13*(12), 1375–1379. https://doi.org/10.1094/MPMI.2000.13.12.1375

Kemppainen, M., Duplessis, S., Martin, F., & Pardo, A. G. (2008). T-DNA insertion, plasmid rescue and integration analysis in the model mycorrhizal fungus *Laccaria bicolor*. Microbial Biotechnology, 1(3), 258–269. https://doi.org/10.1111/j.1751-7915.2008.00029.x

Keon, J., Antoniw, J., Carzaniga, R., Deller, S., Ward, J. L., Baker, J. M., Beale, M. H., Hammond-Kosack, K., & Rudd, J. J. (2007). Transcriptional Adaptation of *Mycosphaerella graminicola* to Programmed Cell Death (PCD) of Its Susceptible Wheat Host. *Molecular Plant-Microbe Interactions*®, *20*(2), 178–193. https://doi.org/10.1094/MPMI-20-2-0178

Keon, J., Antoniw, J., Rudd, J., Skinner, W., Hargreaves, J., & Hammond-Kosack, K. (2005). Analysis of expressed sequence tags from the wheat leaf blotch pathogen *Mycosphaerella graminicola* (anamorph Septoria tritici). *Fungal Genetics and Biology*, *42*(5), 376–389. https://doi.org/10.1016/j.fgb.2004.12.005

Kettles, G. J., Bayon, C., Sparks, C. A., Canning, G., Kanyuka, K., & Rudd, J. J. (2018). Characterization of an antimicrobial and phytotoxic ribonuclease secreted by the fungal wheat pathogen *Zymoseptoria tritici*. *New Phytologist*, *217*(1), 320–331. https://doi.org/10.1111/nph.14786

Kettles, G. J., & Kanyuka, K. (2016). Dissecting the Molecular Interactions between Wheat and the Fungal Pathogen *Zymoseptoria tritici*. *Frontiers in Plant Science*, *7*. https://doi.org/10.3389/fpls.2016.00508

Khan, H., Solomon, P., McDonald, M., & Williams, S. (2019). Development and Application of a novel genome editing technique using CRISPR/Cas9 in necrotrophic pathogens. *International Symposium on Cereal Leaf Blights*

2019, University College Dublin, Ireland, 22-24 May 2019. https://www.isclb2019.com/portal/public/abstracts/ABS67224/

Kim, D., Paggi, J. M., Park, C., Bennett, C., & Salzberg, S. L. (2019). Graph-based genome alignment and genotyping with HISAT2 and HISAT-genotype. *Nature Biotechnology*, *37*(8), 907–915. https://doi.org/10.1038/s41587-019-0201-4

King, R., Urban, M., Lauder, R. P., Hawkins, N., Evans, M., Plummer, A., Halsey, K., Lovegrove, A., Hammond-Kosack, K., & Rudd, J. J. (2017). A conserved fungal glycosyltransferase facilitates pathogenesis of plants by enabling hyphal growth on solid surfaces. *PLOS Pathogens*, *13*(10), e1006672. https://doi.org/10.1371/journal.ppat.1006672

Kiss, E., Hegedüs, B., Virágh, M., Varga, T., Merényi, Z., Kószó, T., Bálint, B., Prasanna, A. N., Krizsán, K., Kocsubé, S., Riquelme, M., Takeshita, N., & Nagy, L. G. (2019). Comparative genomics reveals the origin of fungal hyphae and multicellularity. *Nature Communications*, *10*(1). https://doi.org/10.1038/s41467-019-12085-w

Klee, S. M., Sinn, J. P., Finley, M., Allman, E. L., Smith, P. B., Aimufua, O., Sitther, V., Lehman, B. L., Krawczyk, T., Peter, K. A., & McNellis, T. W. (2019). Erwinia amylovora Auxotrophic Mutant Exometabolomics and Virulence on Apples. *Applied and Environmental Microbiology*, *85*(15). https://doi.org/10.1128/AEM.00935-19

Kohler, J. R., Casadevall, A., & Perfect, J. (2015). The Spectrum of Fungi That Infects Humans. *Cold Spring Harbor Perspectives in Medicine*, *5*(1), a019273–a019273. https://doi.org/10.1101/cshperspect.a019273

Kornitzer, D. (2019). Regulation of *Candida albicans* Hyphal Morphogenesis by Endogenous Signals. *Journal of Fungi*, *5*(1), 21. https://doi.org/10.3390/jof5010021

Kramer, B., Thines, E., & Foster, A. J. (2009). MAP kinase signalling pathway components and targets conserved between the distantly related plant pathogenic fungi *Mycosphaerella graminicola* and *Magnaporthe grisea*. *Fungal Genetics and Biology*, *46*(9), 667–681. https://doi.org/10.1016/j.fgb.2009.06.001

Krishnan, P., Meile, L., Plissonneau, C., Ma, X., Hartmann, F. E., Croll, D., McDonald, B. A., & Sánchez-Vallet, A. (2018). Transposable element insertions shape gene regulation and melanin production in a fungal pathogen of wheat. *BMC Biology*, *16*(1), 1–18. https://doi.org/10.1186/s12915-018-0543-2

Kushalappa, A. C., Yogendra, K. N., & Karre, S. (2016). Plant Innate Immune Response: Qualitative and Quantitative Resistance. *Critical Reviews in Plant Sciences*, *35*(1), 38–55. https://doi.org/10.1080/07352689.2016.1148980

Langmead, B., & Salzberg, S. L. (2012). Fast gapped-read alignment with Bowtie 2. *Nature Methods*, *9*(4), 357–359. https://doi.org/10.1038/nmeth.1923

Law, C. J., Maloney, P. C., & Wang, D.-N. (2008). Ins and Outs of Major Facilitator Superfamily Antiporters. *Annual Review of Microbiology*, *62*(1), 289–305. https://doi.org/10.1146/annurev.micro.61.080706.093329

Lawrence, C. L., Botting, C. H., Antrobus, R., & Coote, P. J. (2004). Evidence of a New Role for the High-Osmolarity Glycerol Mitogen-Activated Protein Kinase Pathway in Yeast: Regulating Adaptation to Citric Acid Stress. *Molecular and Cellular Biology*, *24*(8), 3307–3323. https://doi.org/10.1128/mcb.24.8.3307-3323.2004

Le Mire, G., Siah, A., Brisset, M.-N., Gaucher, M., Deleu, M., & Jijakli, M. (2018). Surfactin Protects Wheat against *Zymoseptoria tritici* and Activates Both Salicylic Acid- and Jasmonic Acid-Dependent Defense Responses. *Agriculture*, *8*(1), 11. https://doi.org/10.3390/agriculture8010011

Lee, S. C., Ni, M., Li, W., Shertz, C., & Heitman, J. (2010). The Evolution of Sex: a Perspective from the Fungal Kingdom. *Microbiology and Molecular Biology Reviews*, *74*(2), 298–340. https://doi.org/10.1128/MMBR.00005-10

Lee, S. J., Lee, M. R., Kim, S., Kim, J. C., Park, S. E., Shin, T. Y., & Kim, J. S. (2018). Conidiogenesis-related DNA photolyase gene in *Beauveria bassiana*. *Journal of Invertebrate Pathology*, *153*, 85–91. https://doi.org/10.1016/j.jip.2018.02.013

Lee, W.-S., Rudd, J. J., Hammond-Kosack, K. E., & Kanyuka, K. (2014). *Mycosphaerella graminicola* LysM Effector-Mediated Stealth Pathogenesis Subverts Recognition Through Both CERK1 and CEBiP Homologues in Wheat. *Molecular Plant-Microbe Interactions*, *27*(3), 236–243. https://doi.org/10.1094/MPMI-07-13-0201-R

Lendenmann, M. H., Croll, D., Stewart, E. L., & McDonald, B. A. (2014). Quantitative Trait Locus Mapping of Melanization in the Plant Pathogenic Fungus *Zymoseptoria tritici*. *Genes|Genomes|Genetics*, *4*(12), 2519–2533. https://doi.org/10.1534/g3.114.015289

Leng, Y., & Zhong, S. (2015). The Role of Mitogen-Activated Protein (MAP) Kinase Signaling Components in the Fungal Development, Stress Response and Virulence of the Fungal Cereal Pathogen *Bipolaris sorokiniana*. *PLOS ONE*, *10*(5), e0128291. https://doi.org/10.1371/journal.pone.0128291

Leuthner, B., Aichinger, C., Oehmen, E., Koopmann, E., Müller, O., Müller, P., Kahmann, R., Bölker, M., & Schreier, P. H. (2005). A H_2O_2-producing glyoxal oxidase is required for filamentous growth and pathogenicity in *Ustilago maydis*. *Molecular Genetics and Genomics*, *272*(6), 639–650. https://doi.org/10.1007/s00438-004-1085-6

Li, G., Zhou, X., & Xu, J. R. (2012). Genetic control of infection-related development in *Magnaporthe oryzae*. *Current Opinion in Microbiology*, *15*(6), 678–684. https://doi.org/10.1016/j.mib.2012.09.004

Li, Q., Wang, C., & Mou, Z. (2020). Perception of Damaged Self in Plants. *Plant Physiology*, *182*(4), 1545–1565. https://doi.org/10.1104/pp.19.01242

Linde, C. C., Zhan, J., & McDonald, B. A. (2002). Population Structure of *Mycosphaerella graminicola* : From Lesions to Continents. *Phytopathology*, *92*(9), 946–955. https://doi.org/10.1094/PHYTO.2002.92.9.946

Liu, X., Pan, X., Chen, D., Yin, C., Peng, J., Shi, W., Qi, L., Wang, R., Zhao, W., Zhang, Z., Yang, J., & Peng, Y. (2021). Prp19-associated splicing factor Cwf15 regulates fungal virulence and development in the rice blast fungus. *Environmental Microbiology*, *23*(10), 5901–5916. https://doi.org/10.1111/1462-2920.15616

Lo Presti, L., Lanver, D., Schweizer, G., Tanaka, S., Liang, L., Tollot, M., Zuccaro, A., Reissmann, S., & Kahmann, R. (2015). Fungal Effectors and Plant Susceptibility. *Annual Review of Plant Biology*, *66*(1), 513–545. https://doi.org/10.1146/annurev-arplant-043014-114623

Lohse, M. B., Zordan, R. E., Cain, C. W., & Johnson, A. D. (2010). Distinct class of DNA-binding domains is exemplified by a master regulator of phenotypic switching in *Candida albicans*. *Proceedings of the National Academy of Sciences*, *107*(32), 14105–14110. https://doi.org/10.1073/pnas.1005911107

Love, M. I., Huber, W., & Anders, S. (2014). Moderated estimation of fold change and dispersion for RNA-seq data with DESeq2. *Genome Biology*, *15*(12), 1–21. https://doi.org/10.1186/s13059-014-0550-8

Ma, L.J., van der Does, H. C., Borkovich, K. A., Coleman, J. J., Daboussi, M.-J., Di Pietro, A., Dufresne, M., Freitag, M., Grabherr, M., Henrissat, B., Houterman, P. M., Kang, S., Shim, W.-B., Woloshuk, C., Xie, X., Xu, J.-R., Antoniw, J., Baker, S. E., Bluhm, B. H., … Rep, M. (2010). Comparative genomics reveals mobile pathogenicity chromosomes in *Fusarium*. *Nature*, *464*(7287), 367–373. https://doi.org/10.1038/nature08850

Madhani, H. D., & Fink, G. R. (1998). The control of filamentous differentiation and virulence in fungi. *Trends in Cell Biology*, *8*(9), 348–353. https://doi.org/10.1016/S0962-8924(98)01298-7

Maeda, T., Takekawa, M., & Saito, H. (1995). Activation of yeast PBS2 MAPKK by MAPKKKs or by binding of an SH3-containing osmosensor. *Science*, *269*(5223), 554–558. https://doi.org/10.1126/science.7624781

Maier, F. J., & Schäfer, W. (1999). Mutagenesis via Insertional or Restriction Enzyme-Mediated Integration (REMI) as a Tool to Tag Pathogenicity Related Genes in Plant Pathogenic Fungi. *Biological Chemistry*, *380*(7–8), 855–864. https://doi.org/10.1515/BC.1999.105

Manivasakam, P., & Schiestl, R. H. (1998). Nonhomologous End Joining during Restriction Enzyme-Mediated DNA Integration in *Saccharomyces cerevisiae*. *Molecular and Cellular Biology*, *18*(3), 1736–1745. https://doi.org/10.1128/MCB.18.3.1736

Marcel, T. C., Audeon, C., Bouchet, S., Saintenac, C., Lapalu, N., & Croll, D. (2019). Cloning of AvrStb9, a gene of *Zymoseptoria tritici* conferring avirulence on wheat cultivars carrying the Stb9 resistance gene. *International*

Symposium on Cereal Leaf Blights 2019, University College Dublin, Ireland, 22-24 May 2019. https://www.isclb2019.com/portal/public/abstracts/ABS74674/

Marques, J. M., Rodrigues, R. J., De Magalhães-Sant'Ana, A. C., & Gonçalves, T. (2006). *Saccharomyces cerevisiae* Hog1 protein phosphorylation upon exposure to bacterial endotoxin. *Journal of Biological Chemistry*, *281*(34), 24687–24694. https://doi.org/10.1074/jbc.M603753200

Marshall, R., Kombrink, A., Motteram, J., Loza-Reyes, E., Lucas, J., Hammond-Kosack, K. E., Thomma, B. P. H. J., & Rudd, J. J. (2011). Analysis of Two *in planta* Expressed LysM Effector Homologs from the Fungus *Mycosphaerella graminicola* Reveals Novel Functional Properties and Varying Contributions to Virulence on Wheat. *Plant Physiology*, *156*(2), 756–769. https://doi.org/10.1104/pp.111.176347

McCarthy, C. G. P., & Fitzpatrick, D. A. (2019). Pan-genome analyses of model fungal species. *Microbial Genomics*, *5*(2). https://doi.org/10.1099/mgen.0.000243

McCarthy, U., Uysal, I., Badia-Melis, R., Mercier, S., O'Donnell, C., & Ktenioudaki, A. (2018). Global food security – Issues, challenges and technological solutions. In *Trends in Food Science and Technology*. https://doi.org/10.1016/j.tifs.2018.05.002

McCorison, C. B., & Goodwin, S. B. (2020). The wheat pathogen *Zymoseptoria tritici* senses and responds to different wavelengths of light. *BMC Genomics*, *21*(1), 1–15. https://doi.org/10.1186/s12864-020-06899-y

McDonald, B. A., & Mundt, C. C. (2016). How Knowledge of Pathogen Population Biology Informs Management of Septoria Tritici Blotch. *Phytopathology*, *106*(9), 948–955. https://doi.org/10.1094/PHYTO-03-16-0131-RVW

McDonald, M. C., McGinness, L., Hane, J. K., Williams, A. H., Milgate, A., & Solomon, P. S. (2016). Utilizing gene tree variation to identify candidate effector genes in *Zymoseptoria tritici*. *G3: Genes, Genomes, Genetics*, *6*(4), 779–791. https://doi.org/10.1534/g3.115.025197

McLoughlin, A. G., Wytinck, N., Walker, P. L., Girard, I. J., Rashid, K. Y., de Kievit, T., Fernando, W. G. D., Whyard, S., & Belmonte, M. F. (2018). Identification and application of exogenous dsRNA confers plant protection against *Sclerotinia sclerotiorum* and *Botrytis cinerea*. *Scientific Reports*, *8*(1), 7320. https://doi.org/10.1038/s41598-018-25434-4

Mehrabi, R., & Kema, G. H. J. (2006). Protein kinase A subunits of the ascomycete pathogen *Mycosphaerella graminicola* regulate asexual fructification, filamentation, melanization and osmosensing. *Molecular Plant Pathology*, *7*(6), 565–577. https://doi.org/10.1111/j.1364-3703.2006.00361.x

Mehrabi, R., M'Barek, S. B., van der Lee, T. A. J., Waalwijk, C., de Wit, P. J. G. M., & Kema, G. H. J. (2009). G-alpha and G-beta Proteins Regulate the Cyclic AMP Pathway That Is Required for Development and Pathogenicity of

the Phytopathogen *Mycosphaerella graminicola*. *Eukaryotic Cell*, *8*(7), 1001–1013. https://doi.org/10.1128/EC.00258-08

Mehrabi, R., Van der Lee, T., Waalwijk, C., & Gert, H. J. K. (2006a). MgSlt2, a cellular integrity MAP kinase gene of the fungal wheat pathogen *Mycosphaerella graminicola*, is dispensable for penetration but essential for invasive growth. *Molecular Plant-Microbe Interactions : MPMI*, *19*(4), 389–398. https://doi.org/10.1094/MPMI-19-0389

Mehrabi, R., Zwiers, L.-H., de Waard, M. A., & Kema, G. H. J. (2006b). MgHog1 regulates dimorphism and pathogenicity in the fungal wheat pathogen *Mycosphaerella graminicola*. *Molecular Plant-Microbe Interactions : MPMI*, *19*(11), 1262–1269. https://doi.org/10.1094/MPMI-19-1262

Meile, L., Croll, D., Brunner, P. C., Plissonneau, C., Hartmann, F. E., McDonald, B. A., & Sánchez-Vallet, A. (2018). A fungal avirulence factor encoded in a highly plastic genomic region triggers partial resistance to septoria tritici blotch. *New Phytologist*, *219*(3), 1048–1061. https://doi.org/10.1111/nph.15180

Mentlak, T. A., Kombrink, A., Shinya, T., Ryder, L. S., Otomo, I., Saitoh, H., Terauchi, R., Nishizawa, Y., Shibuya, N., Thomma, B. P. H. J., & Talbot, N. J. (2012). Effector-Mediated Suppression of Chitin-Triggered Immunity by *Magnaporthe oryzae* Is Necessary for Rice Blast Disease. *The Plant Cell*, *24*(1), 322–335. https://doi.org/10.1105/tpc.111.092957

Meyer, V., Andersen, M. R., Brakhage, A. A., Braus, G. H., Caddick, M. X., Cairns, T. C., de Vries, R. P., Haarmann, T., Hansen, K., Hertz-Fowler, C., Krappmann, S., Mortensen, U. H., Peñalva, M. A., Ram, A. F. J. J., & Head, R. M. (2016). Current challenges of research on filamentous fungi in relation to human welfare and a sustainable bio-economy: a white paper. *Fungal Biology and Biotechnology*, *3*(1), 6. https://doi.org/10.1186/s40694-016-0024-8

Michielse, C. B., Hooykaas, P. J. J., van den Hondel, C. A. M. J. J., & Ram, A. F. J. (2005). *Agrobacterium*-mediated transformation as a tool for functional genomics in fungi. *Current Genetics*, *48*(1), 1–17. https://doi.org/10.1007/s00294-005-0578-0

Mirzadi Gohari, A., Mehrabi, R., Robert, O., Ince, I. A., Boeren, S., Schuster, M., Steinberg, G., de Wit, P. J. G. M., & Kema, G. H. J. (2014). Molecular characterization and functional analyses of ZtWor1 , a transcriptional regulator of the fungal wheat pathogen *Zymoseptoria tritici*. *Molecular Plant Pathology*, *15*(4), 394–405. https://doi.org/10.1111/mpp.12102

Mirzadi Gohari, A., Ware, S. B., Wittenberg, A. H. J., Mehrabi, R., Ben M'Barek, S., Verstappen, E. C. P., van der Lee, T. A. J., Robert, O., Schouten, H. J., de Wit, P. P. J. G. M., & Kema, G. H. J. (2015). Effector discovery in the fungal wheat pathogen *Zymoseptoria tritici*. *Molecular Plant Pathology*, *16*(9), 931–945. https://doi.org/10.1111/mpp.12251

Mohammadi, N., Mehrabi, R., Mirzadi Gohari, A., Mohammadi Goltapeh, E., Safaie, N., & Kema, G. H. J. (2017). The ZtVf1 transcription factor regulates development and virulence in the foliar wheat pathogen *Zymoseptoria tritici*. *Fungal Genetics and Biology*, *109*, 26–35. https://doi.org/10.1016/j.fgb.2017.10.003

Mohammadi, N., Mehrabi, R., Mirzadi Gohari, A., Roostaei, M., Mohammadi Goltapeh, E., Safaie, N., & Kema, G. H. J. (2020). MADS-Box Transcription Factor ZtRlm1 Is Responsible for Virulence and Development of the Fungal Wheat Pathogen *Zymoseptoria tritici*. *Frontiers in Microbiology*, *11*(August), 1–13. https://doi.org/10.3389/fmicb.2020.01976

Möller, M., Habig, M., Freitag, M., & Stukenbrock, E. H. (2018). Extraordinary Genome Instability and Widespread Chromosome Rearrangements During Vegetative Growth. *Genetics*, *210*(2), 517–529. https://doi.org/10.1534/genetics.118.301050

Möller, M., & Stukenbrock, E. H. (2017). Evolution and genome architecture in fungal plant pathogens. In *Nature Reviews Microbiology* (Vol. 15, Issue 12, pp. 756–771). https://doi.org/10.1038/nrmicro.2017.76

Monaghan, J., Xu, F., Gao, M., Zhao, Q., Palma, K., Long, C., Chen, S., Zhang, Y., & Li, X. (2009). Two Prp19-Like U-Box Proteins in the MOS4-Associated Complex Play Redundant Roles in Plant Innate Immunity. *PLoS Pathogens*, *5*(7), e1000526. https://doi.org/10.1371/journal.ppat.1000526

Morgenstern, J., Campos, M. C., Nawroth, P., & Fleming, T. (2020). The glyoxalase system—new insights into an ancient metabolism. *Antioxidants*, *9*(10), 1–15. https://doi.org/10.3390/antiox9100939

Morrow, C. A., Valkov, E., Stamp, A., Chow, E. W. L., Lee, I. R., Wronski, A., Williams, S. J., Hill, J. M., Djordjevic, J. T., Kappler, U., Kobe, B., & Fraser, J. A. (2012). *De novo* GTP Biosynthesis Is Critical for Virulence of the Fungal Pathogen *Cryptococcus neoformans*. *PLoS Pathogens*, *8*(10). https://doi.org/10.1371/journal.ppat.1002957

Motteram, J., Küfner, I., Deller, S., Brunner, F., Hammond-Kosack, K. E., Nürnberger, T., & Rudd, J. J. (2009). Molecular characterization and functional analysis of MgNLP, the sole NPP1 domain-containing protein, from the fungal wheat leaf pathogen *Mycosphaerella graminicola*. *Molecular Plant-Microbe Interactions : MPMI*, *22*(7), 790–799. https://doi.org/10.1094/MPMI-22-7-0790

Motteram, J., Lovegrove, A., Pirie, E., Marsh, J., Devonshire, J., van de Meene, A., Hammond-Kosack, K., & Rudd, J. J. (2011). Aberrant protein N-glycosylation impacts upon infection-related growth transitions of the haploid plant-pathogenic fungus *Mycosphaerella graminicola*. *Molecular Microbiology*, *81*(2), 415–433. https://doi.org/10.1111/j.1365-2958.2011.07701.x

Mullins, E. D., & Kang, S. (2001). Transformation: a tool for studying fungal pathogens of plants. *Cellular and Molecular Life Sciences*, *58*(14), 2043–2052. https://doi.org/10.1007/PL00000835

Muria-Gonzalez, M. J., Chooi, Y.-H., Breen, S., & Solomon, P. S. (2015). The past, present and future of secondary metabolite research in the Dothideomycetes. *Molecular Plant Pathology*, *16*(1), 92–107. https://doi.org/10.1111/mpp.12162

Nødvig, C. S., Nielsen, J. B., Kogle, M. E., & Mortensen, U. H. (2015). A CRISPR-Cas9 System for Genetic Engineering of Filamentous Fungi. *PLOS ONE*, *10*(7), e0133085. https://doi.org/10.1371/journal.pone.0133085

Nurse, P., & Hayles, J. (2019). Using genetics to understand biology. *Heredity*, *123*(1), 4–13. https://doi.org/10.1038/s41437-019-0209-z

Nygren, J., Shad, N., Kvarnheden, A., & Westerbergh, A. (2015). Variation in Susceptibility to Wheat dwarf virus among Wild and Domesticated Wheat. *PLOS ONE*, *10*(4), e0121580. https://doi.org/10.1371/journal.pone.0121580

O'Rourke, S. M., & Herskowitz, I. (2004). Unique and Redundant Roles for HOG MAPK Pathway Components as Revealed by Whole-Genome Expression Analysis. *Molecular Biology of the Cell*, *15*(2), 532–542. https://doi.org/10.1091/mbc.e03-07-0521

Orton, E. (2012). Responses of wheat to infection by *Mycosphaerella graminicola*. *Thesis*. https://ueaeprints.uea.ac.uk/id/eprint/40585

Orton, E. S., Rudd, J. J., & Brown, J. K. M. M. (2017). Early molecular signatures of responses of wheat to *Zymoseptoria tritici* in compatible and incompatible interactions. *Plant Pathology*, *66*(3), 450–459. https://doi.org/10.1111/ppa.12633

Østergaard, L., & Yanofsky, M. F. (2004). Establishing gene function by mutagenesis in Arabidopsis thaliana. *The Plant Journal*, *39*(5), 682–696. https://doi.org/10.1111/j.1365-313X.2004.02149.x

Palma-Guerrero, J., Torriani, S. F. F., Zala, M., Carter, D., Courbot, M., Rudd, J. J., McDonald, B. A., & Croll, D. (2016). Comparative transcriptomic analyses of Z ymoseptoria tritici strains show complex lifestyle transitions and intraspecific variability in transcription profiles. *Molecular Plant Pathology*, *17*(6), 845–859. https://doi.org/10.1111/mpp.12333

Palmer, C.-L., & Skinner, W. (2002). *Mycosphaerella graminicola* : latent infection, crop devastation and genomics. *Molecular Plant Pathology*, *3*(2), 63–70. https://doi.org/10.1046/j.1464-6722.2002.00100.x

Panadero, J., Pallotti, C., Rodríguez-Vargas, S., Randez-Gil, F., & Prieto, J. A. (2006). A downshift in temperature activates the high osmolarity glycerol (HOG) pathway, which determines freeze tolerance in *Saccharomyces cerevisiae*. *Journal of Biological Chemistry*, *281*(8), 4638–4645. https://doi.org/10.1074/jbc.M512736200

Pedley, A. M., & Benkovic, S. J. (2017). A New View into the Regulation of Purine Metabolism: The Purinosome. *Trends in Biochemical Sciences*, *42*(2), 141–154. https://doi.org/10.1016/j.tibs.2016.09.009

Pedrotti, S., & Cooper, T. A. (2014). In Brief: (Mis)splicing in disease. *The Journal of Pathology*, *233*(1), 1–3. https://doi.org/10.1002/path.4337

Penna, S., & Jain, S. M. (2017). Mutant resources and mutagenomics in crop plants. In *Emirates Journal of Food and Agriculture* (Vol. 29, Issue 9, pp. 651–657). https://doi.org/10.9755/ejfa.2017.v29.i9.86

Plaumann, P. L., Schmidpeter, J., Dahl, M., Taher, L., & Koch, C. (2018). A dispensable chromosome is required for virulence in the hemibiotrophic plant pathogen Colletotrichum higginsianum. *Frontiers in Microbiology*, *9*(MAY). https://doi.org/10.3389/fmicb.2018.01005

Plissonneau, C., Hartmann, F. E., & Croll, D. (2018). Pangenome analyses of the wheat pathogen *Zymoseptoria tritici* reveal the structural basis of a highly plastic eukaryotic genome. *BMC Biology*, *16*(1), 5. https://doi.org/10.1186/s12915-017-0457-4

Ponomarenko, A., Goodwin, S. B., & Kema, G. (2011). *Septoria Tritici Blotch (STB)*. The Plant Health Instructor. https://doi.org/10.1094/PHI-I-2011-0407-01

Pontiggia, D., Benedetti, M., Costantini, S., De Lorenzo, G., & Cervone, F. (2020). Dampening the DAMPs: How Plants Maintain the Homeostasis of Cell Wall Molecular Patterns and Avoid Hyper-Immunity. *Frontiers in Plant Science*, *11*. https://doi.org/10.3389/fpls.2020.613259

Pour-Aboughadareh, A., Kianersi, F., Poczai, P., & Moradkhani, H. (2021). Potential of wild relatives of wheat: Ideal genetic resources for future breeding programs. *Agronomy*, *11*(8), 1–31. https://doi.org/10.3390/agronomy11081656

Quaedvlieg, W., Kema, G. H. J., Groenewald, J. Z., Verkley, G. J. M., Seifbarghi, S., Razavi, M., Mirzadi Gohari, A., Mehrabi, R., & Crous, P. W. (2011). *Zymoseptoria* gen. nov.: A new genus to accommodate Septoria-like species occurring on graminicolous hosts. *Persoonia: Molecular Phylogeny and Evolution of Fungi*, *26*, 57–69. https://doi.org/10.3767/003158511X571841

Ramirez-Prado, J. S., Abulfaraj, A. A., Rayapuram, N., Benhamed, M., & Hirt, H. (2018). Plant Immunity: From Signaling to Epigenetic Control of Defense. *Trends in Plant Science*, *23*(9), 833–844. https://doi.org/10.1016/j.tplants.2018.06.004

Robinson, J. T., Thorvaldsdóttir, H., Winckler, W., Guttman, M., Lander, E. S., Getz, G., & Mesirov, J. P. (2011). Integrative genomics viewer. *Nature Biotechnology*, *29*(1), 24–26. https://doi.org/10.1038/nbt.1754

Rodriguez-Moreno, L., Ebert, M. K., Bolton, M. D., & Thomma, B. P. H. J. (2018). Tools of the crook- infection strategies of fungal plant pathogens. *Plant Journal*, *93*(4), 664–674. https://doi.org/10.1111/tpj.13810

Roohparvar, R., De Waard, M. A., Kema, G. H. J., & Zwiers, L.-H. (2007). MgMfs1, a major facilitator superfamily transporter from the fungal wheat pathogen *Mycosphaerella graminicola*, is a strong protectant against natural toxic compounds and fungicides. *Fungal Genetics and Biology*, *44*(5), 378–388. https://doi.org/10.1016/j.fgb.2006.09.007

Roohparvar, R., Mehrabi, R., Van Nistelrooy, J. G., Zwiers, L.-H., & De Waard, M. A. (2008). The drug transporter MgMfs1 can modulate sensitivity of field strains of the fungal wheat pathogen *Mycosphaerella graminicola* to the strobilurin fungicide trifloxystrobin. *Pest Management Science*, *64*(7), 685–693. https://doi.org/10.1002/ps.1569

Rossman, A. Y., Crous, P. W., Hyde, K. D., Hawksworth, D. L., Aptroot, A., Bezerra, J. L., Bhat, J. D., Boehm, E., Braun, U., Boonmee, S., Camporesi, E., Chomnunti, P., Dai, D.-Q., D'souza, M. J., Dissanayake, A., Gareth Jones, E. B., Groenewald, J. Z., Hernández-Restrepo, M., Hongsanan, S., … Zhang, Y. (2015). Recommended names for pleomorphic genera in Dothideomycetes. *IMA Fungus*, *6*(2), 507–523. https://doi.org/10.5598/imafungus.2015.06.02.14

Royet, K., Parisot, N., Rodrigue, A., Gueguen, E., & Condemine, G. (2019). Identification by Tn-seq of *Dickeya dadantii* genes required for survival in chicory plants. *Molecular Plant Pathology*, *20*(2), 287–306. https://doi.org/10.1111/mpp.12754

Rudd, J. (2015). Previous bottlenecks and future solutions to dissecting the *Zymoseptoria tritici* –wheat host-pathogen interaction. *Fungal Genetics and Biology*, *79*, 24–28. https://doi.org/10.1016/j.fgb.2015.04.005

Rudd, J. J., Kanyuka, K., Hassani-Pak, K., Derbyshire, M., Andongabo, A., Devonshire, J., Lysenko, A., Saqi, M., Desai, N. M., Powers, S. J., Hooper, J., Ambroso, L., Bharti, A., Farmer, A., Hammond-Kosack, K. E., Dietrich, R. A., & Courbot, M. (2015). Transcriptome and Metabolite Profiling of the Infection Cycle of *Zymoseptoria tritici* on Wheat Reveals a Biphasic Interaction with Plant Immunity Involving Differential Pathogen Chromosomal Contributions and a Variation on the Hemibiotrophic Lifestyle Def. *Plant Physiology*, *167*(3), 1158–1185. https://doi.org/10.1104/pp.114.255927

Saintenac, C., Lee, W.-S., Cambon, F., Rudd, J. J., King, R. C., Marande, W., Powers, S. J., Bergès, H., Phillips, A. L., Uauy, C., Hammond-Kosack, K. E., Langin, T., & Kanyuka, K. (2018). Wheat receptor-kinase-like protein Stb6 controls gene-for-gene resistance to fungal pathogen *Zymoseptoria tritici*. *Nature Genetics*, *50*(3), 368–374. https://doi.org/10.1038/s41588-018-0051-x

Sánchez-Vallet, A., McDonald, M. C., Solomon, P. S., & McDonald, B. A. (2015). Is *Zymoseptoria tritici* a hemibiotroph? *Fungal Genetics and Biology*, *79*, 29–32. https://doi.org/10.1016/j.fgb.2015.04.001

Sarde, S. J., Kempken, F., & Kumar, A. (2018). Spliceosomal proteins encoded by fungal genomes. *Current Science*, *114*(8), 1677–1686. https://doi.org/10.18520/cs/v114/i08/1677-1686

Saunders, D. G. O., Pretorius, Z. A., & Hovmøller, M. S. (2019). Tackling the re-emergence of wheat stem rust in Western Europe. *Communications Biology*, *2*(1), 51. https://doi.org/10.1038/s42003-019-0294-9

Savinov, A., Brandsen, B. M., Angell, B. E., Cuperus, J. T., & Fields, S. (2021). Effects of sequence motifs in the yeast 3′ untranslated region determined from massively parallel assays of random sequences. *Genome Biology*, *22*(1), 1–27. https://doi.org/10.1186/s13059-021-02509-6

Scheele, B. C., Foster, C. N., Hunter, D. A., Lindenmayer, D. B., Schmidt, B. R., & Heard, G. W. (2019). Living with the enemy: Facilitating amphibian coexistence with disease. *Biological Conservation*, *236*, 52–59. https://doi.org/10.1016/j.biocon.2019.05.032

Schiestl, R. H., & Petes, T. D. (1991). Integration of DNA fragments by illegitimate recombination in *Saccharomyces cerevisiae*. *Proceedings of the National Academy of Sciences*, *88*(17), 7585–7589. https://doi.org/10.1073/pnas.88.17.7585

Schoonbeek, H.-J., Raaijmakers, J. M., & De Waard, M. A. (2002). Fungal ABC Transporters and Microbial Interactions in Natural Environments. *Molecular Plant-Microbe Interactions*, *15*(11), 1165–1172. https://doi.org/10.1094/MPMI.2002.15.11.1165

Schotanus, K., Soyer, J. L., Connolly, L. R., Grandaubert, J., Happel, P., Smith, K. M., Freitag, M., & Stukenbrock, E. H. (2015). Histone modifications rather than the novel regional centromeres of *Zymoseptoria tritici* distinguish core and accessory chromosomes. *Epigenetics and Chromatin*, *8*(1), 1–18. https://doi.org/10.1186/s13072-015-0033-5

Schüller, C., Brewster, J. L., Alexander, M. R., Gustin, M. C., & Ruis, H. (1994). The HOG pathway controls osmotic regulation of transcription via the stress response element (STRE) of the *Saccharomyces cerevisiae* CTT1 gene. *EMBO Journal*, *13*(18), 4382–4389. https://doi.org/10.1002/j.1460-2075.1994.tb06758.x

Schuster, M., Schweizer, G., Reissmann, S., & Kahmann, R. (2016). Genome editing in *Ustilago maydis* using the CRISPR–Cas system. *Fungal Genetics and Biology*, *89*, 3–9. https://doi.org/10.1016/j.fgb.2015.09.001

Shaw, M. W., & Royle, D. J. (1993). Factors determining the severity of epidemics of *Mycosphaerella graminicola* (Septoria tritici) on winter wheat in the UK. *Plant Pathology*, *42*(6), 882–899. https://doi.org/10.1111/j.1365-3059.1993.tb02674.x

Shetty, N. P., Kristensen, B. K., Newmana, M. A., Møller, K., Gregersen, P. L., & Jørgensen, H. J. L. (2003). Association of hydrogen peroxide with restriction of Septoria tritici in resistant wheat. *Physiological and Molecular Plant Pathology*, *62*(6), 333–346. https://doi.org/10.1016/S0885-5765(03)00079-1

Shetty, N. P., Jensen, J. D., Knudsen, A., Finnie, C., Geshi, N., Blennow, A., Collinge, D. B., & Jorgensen, H. J. L. (2009). Effects of -1,3-glucan from

Septoria tritici on structural defence responses in wheat. *Journal of Experimental Botany*, *60*(15), 4287–4300. https://doi.org/10.1093/jxb/erp269

Shewry, P. R. (2009). Wheat. *Journal of Experimental Botany*, *60*(6), 1537–1553. https://doi.org/10.1093/jxb/erp058

Shiferaw, B., Smale, M., Braun, H.-J., Duveiller, E., Reynolds, M., & Muricho, G. (2013). Crops that feed the world 10. Past successes and future challenges to the role played by wheat in global food security. *Food Security*, *5*(3), 291–317. https://doi.org/10.1007/s12571-013-0263-y

Shipton, W. A., Boyd, W. R. J., Rosielle, A. A., & Shearer, B. I. (1971). The common Septoria diseases of wheat. *The Botanical Review*, *37*(2), 231–262. https://doi.org/10.1007/BF02858957

Siah, A., Deweer, C., Duyme, F., Sanssené, J., Durand, R., Halama, P., & Reignault, P. (2010). Correlation of *in planta* endo-beta-1,4-xylanase activity with the necrotrophic phase of the hemibiotrophic fungus *Mycosphaerella graminicola*. *Plant Pathology*, *59*(4), 661–670. https://doi.org/10.1111/j.1365-3059.2010.02303.x

Silva, A., Cavero, S., Sarah, V., Solé, C., Böttcher, R., Chávez, S., Posas, F., & de Nadal, E. (2017). Regulation of transcription elongation in response to osmostress. *PLoS Genetics*, *13*(11), 1–24. https://doi.org/10.1371/journal.pgen.1007090

Simaan, H., Lev, S., & Horwitz, B. A. (2019). Oxidant-Sensing Pathways in the Responses of Fungal Pathogens to Chemical Stress Signals. *Frontiers in Microbiology*, *10*(MAR), 1–12. https://doi.org/10.3389/fmicb.2019.00567

Singh, Y., Nair, A. M., & Verma, P. K. (2021). Surviving the odds: From perception to survival of fungal phytopathogens under host-generated oxidative burst. *Plant Communications*, *2*(3), 100142. https://doi.org/10.1016/j.xplc.2021.100142

Skinner, W. S. (2001). Non-pathogenic mutants of *Mycosphaerella graminicola*. Thesis.

Spanu, P. D. (2012). The genomics of obligate (and non-obligate) biotroph. *Annual Review of Phytopathology*, *50*, 91–109. https://doi.org/10.1146/annurev-phyto-081211-173024

Staskawicz, B. J., Dahlbeck, D., & Keen, N. T. (1984). Cloned avirulence gene of *Pseudomonas syringae* pv. *glycinea* determines race-specific incompatibility on Glycine max (L.) Merr. *Proceedings of the National Academy of Sciences*, *81*(19), 6024–6028. https://doi.org/10.1073/pnas.81.19.6024

Steinberg, G. (2015). Cell biology of *Zymoseptoria tritici*: Pathogen cell organization and wheat infection. *Fungal Genetics and Biology*, *79*, 17–23. https://doi.org/10.1016/j.fgb.2015.04.002

Stergiopoulos, I., Zwiers, L.-H., & De Waard, M. A. (2003). The ABC Transporter MgAtr4 Is a Virulence Factor of *Mycosphaerella graminicola* that Affects Colonization of Substomatal Cavities in Wheat Leaves. *Molecular Plant-Microbe Interactions*, *16*(8), 689–698. https://doi.org/10.1094/MPMI.2003.16.8.689

Stewart, B., Gruenheit, N., Baldwin, A., Chisholm, R., Rozen, D., Harwood, A., Wolf, J. B., & Thompson, C. R. L. (2022). The genetic architecture underlying prey-dependent performance in a microbial predator. *Nature Communications*, *13*(1), 319. https://doi.org/10.1038/s41467-021-27844-x

Stewart, E. L., Croll, D., Lendenmann, M. H., Sanchez-Vallet, A., Hartmann, F. E., Palma-Guerrero, J., Ma, X., & Mcdonald, B. A. (2018). Quantitative trait locus mapping reveals complex genetic architecture of quantitative virulence in the wheat pathogen *Zymoseptoria tritici*. *Molecular Plant Pathology*, *19*(1), 201–216. https://doi.org/10.1111/mpp.12515

Stotz, H. U., Mitrousia, G. K., de Wit, P. J. G. M., & Fitt, B. D. L. (2014). Effector-triggered defence against apoplastic fungal pathogens. *Trends in Plant Science*, *19*(8), 491–500. https://doi.org/10.1016/j.tplants.2014.04.009

Stukenbrock, E. H., Jørgensen, F. G., Zala, M., Hansen, T. T., McDonald, B. A., & Schierup, M. H. (2010). Whole-Genome and Chromosome Evolution Associated with Host Adaptation and Speciation of the Wheat Pathogen *Mycosphaerella graminicola*. *PLoS Genetics*, *6*(12), e1001189. https://doi.org/10.1371/journal.pgen.1001189

Stukenbrock, E. H., & Dutheil, J. Y. (2018). Fine-Scale Recombination Maps of Fungal Plant Pathogens Reveal Dynamic Recombination Landscapes and Intragenic Hotspots. *Genetics*, *208*(March), 1209–1229. https://doi.org/10.1534/genetics.117.300502/-/DC1.1

Sweigard, J. A., Carroll, A. M., Farrall, L., Chumley, F. G., & Valent, B. (1998). *Magnaporthe grisea* Pathogenicity Genes Obtained Through Insertional Mutagenesis. *Molecular Plant-Microbe Interactions®*, *11*(5), 404–412. https://doi.org/10.1094/MPMI.1998.11.5.404

Tan, K.-C., Phan, H. T. T., Rybak, K., John, E., Chooi, Y. H., Solomon, P. S., & Oliver, R. P. (2015). Functional redundancy of necrotrophic effectors – consequences for exploitation for breeding. *Frontiers in Plant Science*, *6*(July), 1–9. https://doi.org/10.3389/fpls.2015.00501

Tettelin, H., Masignani, V., Cieslewicz, M. J., Donati, C., Medini, D., Ward, N. L., Angiuoli, S. V., Crabtree, J., Jones, A. L., Durkin, A. S., Deboy, R. T., Davidsen, T. M., Mora, M., Scarselli, M., Margarit Y Ros, I., Peterson, J. D., Hauser, C. R., Sundaram, J. P., Nelson, W. C., … Fraser, C. M. (2005). Genome analysis of multiple pathogenic isolates of *Streptococcus agalactiae*: Implications for the microbial "'pan-genome.'" *Proceedings of the National Academy of Sciences*, *102*(45), 16530–16530. https://doi.org/10.1073/pnas.0508532102

Thon, M. R., Nuckles, E. M., & Vaillancourt, L. J. (2000). Restriction Enzyme-Mediated Integration Used to Produce Pathogenicity Mutants of *Colletotrichum graminicola*. *Molecular Plant-Microbe Interactions*, *13*(12), 1356–1365. https://doi.org/10.1094/MPMI.2000.13.12.1356

Thrall, P. H., Oakeshott, J. G., Fitt, G., Southerton, S., Burdon, J. J., Sheppard, A., Russell, R. J., Zalucki, M., Heino, M., & Ford Denison, R. (2011). Evolution in agriculture: The application of evolutionary approaches to the management of biotic interactions in agro-ecosystems. *Evolutionary Applications*, *4*(2), 200–215. https://doi.org/10.1111/j.1752-4571.2010.00179.x

Tian, H., MacKenzie, C. I., Rodriguez-Moreno, L., Berg, G. C. M., Chen, H., Rudd, J. J., Mesters, J. R., & Thomma, B. P. H. J. (2021). Three LysM effectors of *Zymoseptoria tritici* collectively disarm chitin-triggered plant immunity. *Molecular Plant Pathology*, *22*(6), 683–693. https://doi.org/10.1111/mpp.13055

Tiley, A., Bailey, A., & Foster, G. (2018). Exploring the genetic regulation of asexual sporulation in *Zymoseptoria tritici*. *Frontiers in Microbiology*, *9*(August), 1859. https://doi.org/10.3389/FMICB.2018.01859

Toh-E, A., & Oguchi, T. (2000). An improved integration replacement/disruption method for mutagenesis of yeast essential genes. *Genes and Genetic Systems*, *75*(1), 33–39. https://doi.org/10.1266/ggs.75.33

Torres-Martínez, S., & Ruiz-Vázquez, R. M. (2017). The RNAi Universe in Fungi: A Varied Landscape of Small RNAs and Biological Functions. *Annual Review of Microbiology*, *71*, 371–391. https://doi.org/10.1146/annurev-micro-090816-093352

Torriani, S. F. F., Brunner, P. C., & McDonald, B. A. (2011). Evolutionary history of the mitochondrial genome in *Mycosphaerella* populations infecting bread wheat, durum wheat and wild grasses. *Molecular Phylogenetics and Evolution*, *58*(2), 192–197. https://doi.org/10.1016/j.ympev.2010.12.002

Torriani, S. F. F., Melichar, J. P. E., Mills, C., Pain, N., Sierotzki, H., & Courbot, M. (2015). *Zymoseptoria tritici*: A major threat to wheat production, integrated approaches to control. *Fungal Genetics and Biology*, *79*, 8–12. https://doi.org/10.1016/j.fgb.2015.04.010

Turner, T. R., James, E. K., & Poole, P. S. (2013). The plant microbiome. *Genome Biology*, *14*(6), 209. https://doi.org/10.1186/gb-2013-14-6-209

Turrà, D., Segorbe, D., & Di Pietro, A. (2014). Protein kinases in plant-pathogenic Fungi: Conserved regulators of infection. *Annual Review of Phytopathology*, *52*, 267–288. https://doi.org/10.1146/annurev-phyto-102313-050143

Urban, M., Bhargava, T., & Hamer, J. E. (1999). An ATP-driven efflux pump is a novel pathogenicity factor in rice blast disease. *The EMBO Journal*, *18*(3), 512–521. https://doi.org/10.1093/emboj/18.3.512

Urban, M., King, R., Hassani-Pak, K., & Hammond-Kosack, K. E. (2015). Whole-genome analysis of *Fusarium graminearum* insertional mutants identifies virulence associated genes and unmasks untagged chromosomal deletions. *BMC Genomics*, *16*(1), 261. https://doi.org/10.1186/s12864-015-1412-9

Vela-Corcía, D., Aditya Srivastava, D., Dafa-Berger, A., Rotem, N., Barda, O., & Levy, M. (2019). MFS transporter from *Botrytis cinerea* provides tolerance to glucosinolate-breakdown products and is required for pathogenicity. *Nature Communications*, *10*(1), 1–11. https://doi.org/10.1038/s41467-019-10860-3

Vernikos, G., Medini, D., Riley, D. R., & Tettelin, H. (2015). Ten years of pan-genome analyses. *Current Opinion in Microbiology*, *23*, 148–154. https://doi.org/10.1016/j.mib.2014.11.016

Wang, C., Skrobek, A., & Butt, T. M. (2003). Concurrence of losing a chromosome and the ability to produce destruxins in a mutant of *Metarhizium anisopliae*. *FEMS Microbiology Letters*, *226*(2), 373–378. https://doi.org/10.1016/S0378-1097(03)00640-2

Wang, L., & Lin, X. (2012). Morphogenesis in Fungal Pathogenicity: Shape, Size, and Surface. *PLoS Pathogens*, *8*(12), e1003027. https://doi.org/10.1371/journal.ppat.1003027

Wang, M., Ma, T., Wang, H., Liu, J., Chen, Y., Shim, W. B., & Ma, Z. (2021). The RNA binding protein FgRbp1 regulates specific pre-mRNA splicing via interacting with U2AF23 in *Fusarium*. *Nature Communications*, *12*(1), 1–15. https://doi.org/10.1038/s41467-021-22917-3

Wang, Q., Chen, D., Wu, M., Zhu, J., Jiang, C., Xu, J. R., & Liu, H. (2018). MFS transporters and GABA metabolism are involved in the self-defense against DON in *Fusarium graminearum*. *Frontiers in Plant Science*, *9*(April), 1–10. https://doi.org/10.3389/fpls.2018.00438

Wang, S., Chen, H., Tang, X., Zhang, H., Chen, W., & Chen, Y. Q. (2017). Molecular tools for gene manipulation in filamentous fungi. *Applied Microbiology and Biotechnology*, *101*(22), 8063–8075. https://doi.org/10.1007/s00253-017-8486-z

Wassenaar, T., & Gaastra, W. (2001). Bacterial virulence: can we draw the line? *FEMS Microbiology Letters*, *201*(August), 1–7. http://www3.interscience.wiley.com/journal/119020569/abstract

Weld, R. J., Plummer, K. M., Carpenter, M. A., & Ridgway, H. J. (2006). Approaches to functional genomics in filamentous fungi. *Cell Research*, *16*(1), 31–44. https://doi.org/10.1038/sj.cr.7310006

Williams, F. N., Wu, Y., & Scaglione, K. M. (2021). Development of a Positive Selection High Throughput Genetic Screen in *Dictyostelium discoideum*. *Frontiers in Cell and Developmental Biology*, *9*. https://doi.org/10.3389/fcell.2021.725678

Winkler, A., Arkind, C., Mattison, C. P., Burkholder, A., Knoche, K., & Ota, I. (2002). Heat stress activates the yeast high-osmolarity glycerol mitogen-activated protein kinase pathway, and protein tyrosine phosphatases are essential under heat stress. *Eukaryotic Cell*, *1*(2), 163–173. https://doi.org/10.1128/EC.1.2.163-173.2002

Wittenberg, A. H. J., van der Lee, T. A. J., M'Barek, S. Ben, Ware, S. B., Goodwin, S. B., Kilian, A., Visser, R. G. F., Kema, G. H. J., & Schouten, H. J. (2009). Meiosis drives extraordinary genome plasticity in the haploid fungal plant pathogen *Mycosphaerella graminicola*. *PLoS ONE*, *4*(6). https://doi.org/10.1371/journal.pone.0005863

Wu, B., Macielog, A. I., & Hao, W. (2017). Origin and spread of spliceosomal introns: Insights from the fungal clade *Zymoseptoria*. *Genome Biology and Evolution*, *9*(10), 2658–2667. https://doi.org/10.1093/gbe/evx211

Xu, J.-R. (2000). MAP Kinases in Fungal Pathogens. *Fungal Genetics and Biology*, *31*(3), 137–152. https://doi.org/10.1006/fgbi.2000.1237

Xu, Y., Krishnan, A., Wan, X. S., Majima, H., Yeh, C. C., Ludewig, G., Kasarskis, E. J., & St.Clair, D. K. (1999). Mutations in the promoter reveal a cause for the reduced expression of the human manganese superoxide dismutase gene in cancer cells. *Oncogene*, *18*(1), 93–102. https://doi.org/10.1038/sj.onc.1202265

Yan, C., Wan, R., Bai, R., Huang, G., & Shi, Y. (2017). Structure of a yeast step II catalytically activated spliceosome. *Science (New York, N.Y.)*, *355*(6321), 149–155. https://doi.org/10.1126/science.aak9979

Yang, F., Melo-Braga, M. N., Larsen, M. R., Jørgensen, H. J. L., & Palmisano, G. (2013). Battle through Signaling between Wheat and the Fungal Pathogen Septoria tritici Revealed by Proteomics and Phosphoproteomics. *Molecular & Cellular Proteomics*, *12*(9), 2497–2508. https://doi.org/10.1074/mcp.M113.027532

Yemelin, A., Brauchler, A., Jacob, S., Foster, A. J., Laufer, J., Heck, L., Antelo, L., Andresen, K., & Thines, E. (2021). Two Novel Dimorphism-Related Virulence Factors of *Zymoseptoria tritici* Identified Using *Agrobacterium*-Mediated Insertional Mutagenesis. *International Journal of Molecular Sciences*, *23*(1), 400. https://doi.org/10.3390/ijms23010400

Yemelin, A., Brauchler, A., Jacob, S., Laufer, J., Heck, L., Foster, A. J., Antelo, L., Andresen, K., & Thines, E. (2017). Identification of factors involved in dimorphism and pathogenicity of *Zymoseptoria tritici*. *PLOS ONE*, *12*(8), e0183065. https://doi.org/10.1371/journal.pone.0183065

Yoder, O. C. (1980). Toxins in pathogenesis. *Annual Review of Phytopathology*, *18*(1), 103–129. https://doi.org/10.1146/annurev.py.18.090180.000535

Yu, J.-H., & Keller, N. (2005). Regulation of Secondary Metabolism in Filamentous Fungi. *Annual Review of Phytopathology*, *43*(1), 437–458. https://doi.org/10.1146/annurev.phyto.43.040204.140214

Zhan, J., Kema, G. H. ., Waalwijk, C., & McDonald, B. . (2002). Distribution of mating type alleles in the wheat pathogen *Mycosphaerella graminicola* over spatial scales from lesions to continents. *Fungal Genetics and Biology*, *36*(2), 128–136. https://doi.org/10.1016/S1087-1845(02)00013-0

Zhang, Z., Hua, L., Gupta, A., Tricoli, D., Edwards, K. J., Yang, B., & Li, W. (2019). Development of an *Agrobacterium* -delivered CRISPR/Cas9 system for wheat genome editing. *Plant Biotechnology Journal*, *17*(8), 1623–1635. https://doi.org/10.1111/pbi.13088

Zhong, Z., Marcel, T. C., Hartmann, F. E., Ma, X., Plissonneau, C., Zala, M., Ducasse, A., Confais, J., Compain, J., Lapalu, N., Amselem, J., McDonald, B. A., Croll, D., & Palma-Guerrero, J. (2017). A small secreted protein in *Zymoseptoria tritici* is responsible for avirulence on wheat cultivars carrying the Stb6 resistance gene. *New Phytologist*, *214*(2), 619–631. https://doi.org/10.1111/nph.14434

Zhou, L., Obhof, T., Schneider, K., Feldbrügge, M., Ulrich Nienhaus, G., & Kämper, J. (2018). Cytoplasmic Transport Machinery of the SPF27 Homologue Num1 in *Ustilago maydis*. *Scientific Reports*, *8*(1), 1–12. https://doi.org/10.1038/s41598-018-21628-y

Zhou, W., Yao, Y., Scott, A. J., Wilder-Romans, K., Dresser, J. J., Werner, C. K., Sun, H., Pratt, D., Sajjakulnukit, P., Zhao, S. G., Davis, M., Nelson, B. S., Halbrook, C. J., Zhang, L., Gatto, F., Umemura, Y., Walker, A. K., Kachman, M., Sarkaria, J. N., … Wahl, D. R. (2020). Purine metabolism regulates DNA repair and therapy resistance in glioblastoma. *Nature Communications*, *11*(1), 1–14. https://doi.org/10.1038/s41467-020-17512-x

Zlatow, A. L., Wilson, S. S., Bouley, D. M., Tetens-Woodring, J., Buchholz, D. R., & Green, S. L. (2020). Axial skeletal malformations in genetically modified *Xenopus laevis* and *Xenopus tropicalis*. *Comparative Medicine*, *70*(6), 532–541. https://doi.org/10.30802/AALAS-CM-20-000069

Zwiers, L. H., & De Waard, M. A. (2001). Efficient *Agrobacterium tumefaciens*-mediated gene disruption in the phytopathogen *Mycosphaerella graminicola*. *Current Genetics*, *39*(5–6), 388–393. https://doi.org/10.1007/s002940100216

Professional Internships for PhD Students reflection form.

For three months, I remotely became a part of the TU Delft Open Science Programme, working within the 'Digital Competence Centre' team. My personal goals to achieve during the placement were to develop my interpersonal, networking, writing and communication skills. As a result of the placement, I was also able to gain experience with the real world of Open Science and practical application of FAIR principles, as well as insights into the diversity of research support roles. Due to the COVID-19 pandemic, I was unable to be physically present on the TU Delft campus in the Netherlands and meet in person with those I was working with. In spite of this, and additional challenges of working remotely, I enjoyed my time working with the very newly established Digital Competence Centre support team.

Open Science/Research is a movement that encourages making scientific research accessible to all levels of society. Enabling anyone from keen amateurs to professional researchers, whether academic or industry-based to access scientifically obtained information. The goals of open science are to make research more collaborative, transparent, efficient, replicable, and robust. Whether or not 'Open Science' achieves its idealised outcomes will depend on whether researchers feel the system effectively benefits, rewards, and recognises those who partake. The movement would benefit from changes to the 'just the way it is' facets of being a researcher today, including 'publish or perish' and issues surrounding how research is funded. Irrespective of any personal views of Open Science, I believe that most researchers would agree with the FAIR principles. The FAIR guiding principles can be applied to both research data and software, and whilst uptake of FAIR would strengthen Open Science, the two are separate concepts. In other words, FAIR does not necessarily mean open. Originally published in 2016, the acronym stands for findable (F), accessible (A), interoperable (I), and reusable (R). In terms of research data, applying the FAIR principles involves careful planning of the creation and then storage of

data. How/where/what format are the data and metadata stored, how long will data be stored, how will the data be accessed and users authenticated, what access levels are appropriate, this list goes on. However, researchers typically have highly specialised skillsets that sometimes lack ways to (or the time to learn how) make their research data or software easily FAIR. That is exactly what TU Delft aims to achieve with the setting up of a 'Digital Competence Centre'.

The TU Delft 'Digital Competence Centre' was set up in September 2020 to support its researchers and help achieve the goals of the institute's Open Science Programme, by encouraging and enabling research that is FAIR. It is an interdepartmental support team, combining Library and IT departmental expertise, made of 'Data Managers' and 'Research Software Engineers' that are available to any researchers at any level within the university to help them make their work FAIR (whether that is research data or software). My role within the team was to develop case studies surrounding the initial phase and pilot run of the programme to enable future case studies to build on the insights I gained. My knowledge of the world of research software development was very limited at the beginning of my placement, being something that I only experienced using imaging and statistical analysis software. However, data management was more familiar, my work involves processing and storing lots of image files, but the advanced levels of working with large, complicated datasets were harder for me to visualise. I developed my knowledge of what both these roles entail and an understanding of the skills necessary to perform those roles.

First, I had to decide on the direction I wanted to take the case studies and how I was going to communicate what I found. I wanted to learn more about the open science community at TU Delft, and how it was previously cultivated and supported. To get to know the team, as well as the researchers on the pilot and their projects, I sat in on the first post-acceptance meetings and took detailed notes. I considered it essential to gain the perspective of the team members as well as the researchers who successfully signed on for the pilot

from different departments, to learn how they hoped the programme would be able to help TU Delft researchers. I conducted interviews with the data managers, research software engineers, team management, and some of the researchers on the pilot run. The steps after the interview, checking transcripts and synthesising the things covered, was more of a challenge. In part, I think due to being exclusively desk-based for so long due to the pandemic and away from the university. Still, I developed the skills necessary for case study development, and learned a lot about the role of the Library in a research institution function to facilitate multi-department requiring research across their institutes that I had not fully appreciated prior to my placement.

During the placement, I had the opportunity to attend a few networking and conference events surrounding 'Open Working' and the implementation of FAIR principles in research. This gave me insights into other institutions' practices, introduced me to other interested groups, and to the real-world application of FAIR. Further putting context to the challenges that researchers face when managing big data sets, maintaining their research software and working more openly in general. I did struggle listening back to the interviews to get the full transcripts, particularly when I perceived that I had not given my best interview, but in a time of lockdown, it was so wonderful to hear from people I otherwise would never have met. One of the most rewarding aspects of this placement is knowing that whatever direction this support programme develops, I was a part of the team in the beginning, looking into its pilot run. As someone who wholeheartedly believes in the benefits of applying the FAIR principles to scientific research (and hopes for a more open future), it was incredibly rewarding and interesting to get the perspectives of the TU Delft researchers themselves.

FAIR principles: https://www.go-fair.org/fair-principles/.

APPENDICES

Appendix Chapter 4

Table A4.1 Top five BLAT hits for the low impact common mutations linked to transposable elements.

L951 Identifier	Chromosome	Start	End	Score	Significance	Identity	Element Hit
ZtritL951_01g09719	1	24360	24477	76	4.10E-14	94.87	RIL
	4	2872521	2872398	74	2.10E-13	90.24	RIL
	15	20507	20627	73	3.60E-13	92.5	RIL
	16	22001	22124	73	3.60E-13	87.8	RIL
	17	68248	68362	72	4.70E-13	94.74	RIL
ZtritL951_01g09725	5	2811507	2811279	137	2.10E-32	90.79	RIL
	2	3828838	3828616	136	2.70E-32	91.89	RIL
	2	3806187	3805965	136	2.70E-32	91.89	RIL
	8	2407942	2407714	134	1.80E-31	89.47	RIL
	1	23383	23611	133	2.40E-31	88.16	RIL
ZtritL951_01g07203	18	295723	295876	96	4.30E-20	98.04	RLG
	7	2518003	2518156	96	4.30E-20	98.04	RLG
	13	1082158	1082005	95	5.60E-20	96.08	RLG
	18	280603	280756	94	1.70E-19	96.08	RLG
	5	1084198	1084045	94	1.70E-19	94.12	RLG

Table A4.2 Planned contrast distances to *Hin*dIII Summary Statistics

Summary statistics and ANOVA analysis of the average transformed $\log_{10}(x+1)$ distances to nearest *Hin*dIII site and significant differences as calculated through ANOVA planned contrasts ($p<0.05$).

Group	n	Transformed Mean	Standard deviation	Standard Error
REMI Untagged	35	3.13	0.70	0.12
REMI Plasmid	18	1.17	0.76	0.18
T-DNA	14	2.83	0.45	0.12

ANOVA	Df	s.s.	m.s.	F-value	P-vaue
Log transformed distance to nearest *Hin*dIII site	2	47.35	23.67	51.811	4.16E-14
Contrast 1: REMI vs. T-DNA	1	1.46	1.46	3.186	0.079
Contrast 2: REMI untagged vs. tagged	1	45.89	45.89	100.437	9.68E-15
Residuals	64	29.24	0.46		

Appendix Chapter 6

Table A6.1 RNA and RNA sequencing quality control measures.

Sample	Strain	Timepoint (h)	Replicate	RIN value	Effective (%)	Error (%)	Q20%	Q30%	GC%
A	IPO323	6	r1	6.8	99.34	0.03	96.95	91.9	56.45
B	IPO323	6	r2	7.5	98.06	0.03	97.85	94.08	60.05
C	IPO323	6	r3	6.6	99.47	0.03	96.77	91.44	55.76
D	4-124	6	r1	6.9	99.53	0.03	97.27	92.47	55.72
E	4-124	6	r2	6.8	99.02	0.03	97.44	92.8	56.31
F	4-124	6	r3	6.5	98.53	0.03	97.36	92.71	56.19
G	IPO323	24	r1	6.2	99.00	0.03	97.33	92.58	54.55
H	IPO323	24	r2	6.6	98.87	0.03	97.34	92.63	55.54
I	IPO323	24	r3	6.4	98.70	0.03	97.04	92.08	55.48
J	4-124	24	r1	6.4	98.98	0.03	97.48	93.28	55.34
K	4-124	24	r2	6.0	99.10	0.03	97.22	92.39	55.53
L	4-124	24	r3	6.5	99.15	0.03	96.79	91.51	55.48

Highlighted unsuccessful RNA sequencing run.

Table A6.2 DE genes identified in the individually carried out contrasts between strains at 6 h and 24 h.

RRes GeneID	JGI Protein ID	DESeq2 Contrast	Log2 Fold Change	FC	FDR (adjust p-value)	Heatmap Cluster	Chr.	Top BLAST hit description	BLAST e-value	Broad functional category	Functional sub-category
ZtritIPO323_04g09786	Mycgr3P104452	both	-4.09	17.03	1.13E-32	C1	5	F-box/WD repeat-containing protein 1A	0.00E+00	Cell signalling	Signal transduction
ZtritIPO323_04g03766	Mycgr3P77354	both	-4.04	16.45	5.32E-20	C1	12	class I glutamine amidotransferase-like protein	3.05E-173	Catalytic activity	Transferase activity
ZtritIPO323_04g10011	Mycgr3P104571	both	-4.44	21.71	8.55E-20	C1	5	phosphatidylethanolamine-binding-like protein	2.92E-145	Metabolic process	Metabolic process
ZtritIPO323_04g00943	Mycgr3P89280	both	-5.7	51.98	3.12E-19	C1	1	putative tartrate dehydrogenase/decarboxylase TtuC	1.97E-99	Unknown	Unknown
ZtritIPO323_04g13811	Mycgr3P110887	both	-4.21	18.51	8.68E-19	C1	9	uncharacterized protein MYCGRDRAFT_110887	0.00E+00	Unknown	Unknown
ZtritIPO323_04g03884	Mycgr3P111505	both	-5.92	60.55	2.70E-18	C1	12	uncharacterized protein MYCGRDRAFT_111505	9.92E-108	Unknown	Unknown
ZtritIPO323_04g09283	Mycgr3P71559	both	-6.34	81.01	7.06E-18	C1	4	short-chain dehydrogenase like protein	0.00E+00	Oxidoreductase activity	Oxidoreductase activity
ZtritIPO323_04g10527	#N/A	both	4.82	28.25	3.69E-16	C2	6	unnamed protein product	4.80E-47	Unknown	Unknown
ZtritIPO323_04g00449	Mycgr3P106897	24 h	4.69	25.81	1.12E-12	C2	1	Linoleate 9S-lipoxygenase 2	0.00E+00	Three or less representatives	Secondary metabolism
ZtritIPO323_04g09762	Mycgr3P104437	both	4.24	18.9	1.92E-12	C2	5	sam-dependent methyltransferase like protein	0.00E+00	Catalytic activity	Transferase activity
ZtritIPO323_04g00341	Mycgr3P106843	both	-6.43	86.22	7.73E-12	C1	1	uncharacterized protein MYCGRDRAFT_106843	4.37E-76	Unknown	Unknown
ZtritIPO323_04g07140	Mycgr3P79738	both	-4.54	23.26	1.21E-11	C1	3	Dual specificity protein kinase	1.12E-32	Unknown	Unknown
ZtritIPO323_04g02669	Mycgr3P96234	24 h	3.9	14.93	4.01E-11	C2	10	glutathione s-transferase like protein	0.00E+00	Protein modification	Transferase activity
ZtritIPO323_04g07327	Mycgr3P103578	both	3.5	11.31	9.62E-11	C2	3	ABC transporter domain-containing protein	0.00E+00	Transport	Transport

RRes GeneID	JGI Protein ID	DESeq2 Contrast	Log2 Fold Change	FC	FDR (adjust p-value)	Heatmap Cluster	Chr.	Top BLAST hit description	BLAST e-value	Broad functional category	Functional sub-category
ZtritIPO323_04g09576	Mycgr3P104366	both	-4.17	18	9.62E-11	C1	5	Proline utilization trans-activator	1.07E-121	Transcription regulation	Transcription regulation
ZtritIPO323_04g04526	Mycgr3P106573	6 h	-4.84	28.64	1.11E-10	C1	13	related to HSP30 heat shock protein Yro1p	0.00E+00	Cell signalling	Cell signalling
ZtritIPO323_04g03303	Mycgr3P96677	6 h	-4.09	17.03	1.57E-10	C1	11	related to oxidase	0.00E+00	Stress response	Oxidative stress
ZtritIPO323_04g12173	Mycgr3P74298	both	-2.71	6.54	3.32E-10	C1	7	Aromatic peroxygenase	0.00E+00	Stress response	Oxidative stress
ZtritIPO323_04g08375	Mycgr3P99750	both	-3.52	11.47	3.32E-10	C1	3	acyltransferase like protein	0.00E+00	Catalytic activity	Transferase activity
ZtritIPO323_04g01615	Mycgr3P102725	both	3.29	9.78	4.03E-10	C2	1	uncharacterized protein MYCGRDRAFT_102725	1.46E-166	Transcription regulation	Transcription regulation
ZtritIPO323_04g01193	Mycgr3P102508	24 h	3.3	9.85	5.79E-10	C2	1	unnamed protein product	1.25E-112	Three or less representatives	Cell cycle
ZtritIPO323_04g05895	Mycgr3P107968	both	4.78	27.47	5.79E-10	C2	2	uncharacterized protein MYCGRDRAFT_107968	6.69E-123	Unknown	Unknown
ZtritIPO323_04g01749	Mycgr3P34332	both	-3.51	11.39	1.78E-09	C1	1	NHL repeat-containing protein	0.00E+00	Three or less representatives	Carbohydrate binding
ZtritIPO323_04g09607	Mycgr3P58686	both	-2.88	7.36	1.96E-09	C1	5	putative AIM2 family protein	0.00E+00	Metabolic process	Metabolic process
ZtritIPO323_04g11454	Mycgr3P105080	both	4.75	26.91	3.12E-09	C2	7	triacylglycerol hydrolase	0.00E+00	Lipid metabolic process	Lipid metabolic process
ZtritIPO323_04g08424	Mycgr3P108912	6 h	-3.3	9.85	3.49E-09	C1	3	uncharacterized protein MYCGRDRAFT_108912	7.79E-146	Unknown	Unknown
ZtritIPO323_04g01555	Mycgr3P66753	both	-5.74	53.45	4.60E-09	C1	1	probable alcohol dehydrogenase homolog Bli-4	0.00E+00	Oxidoreductase activity	Oxidoreductase activity
ZtritIPO323_04g09597	Mycgr3P104372	24 h	2.53	5.78	5.97E-09	C2	5	uncharacterized protein MYCGRDRAFT_104372	1.02E-99	Transcription regulation	Transcription regulation
ZtritIPO323_04g07298	Mycgr3P69330	both	-3.2	9.19	8.29E-09	C1	3	putative acid trehalase	0.00E+00	CWDE	CWDE

RRes GeneID	JGI Protein ID	DESeq2 Contrast	Log2 Fold Change	FC	FDR (adjust p-value)	Heatmap Cluster	Chr.	Top BLAST hit description	BLAST e-value	Broad functional category	Functional sub-category
ZtritIPO323_04g11855	Mycgr3P94594	24 h	-3.09	8.51	9.36E-09	C1	7	Xenotropic and polytropic retrovirus receptor 1-like protein	0.00E+00	Unknown	Unknown
ZtritIPO323_04g03427	Mycgr3P50051	6 h	-4.18	18.13	5.58E-08	C1	11	unnamed protein product	2.21E-149	Cell wall/membrane	Membrane component
ZtritIPO323_04g02689	#N/A	both	6.46	88.03	7.46E-08	C2	10	---NA---		Unknown	Unknown
ZtritIPO323_04g13285	Mycgr3P105661	both	-3.12	8.69	8.12E-08	C1	9	unnamed protein product	0.00E+00	Unknown	Unknown
ZtritIPO323_04g08151	Mycgr3P103891	both	-4.01	16.11	9.80E-08	C1	3	related to URE2-nitrogen catabolite repression regulator	2.38E-180	Protein modification	Transferase activity
ZtritIPO323_04g12886	Mycgr3P74996	both	2.4	5.28	9.80E-08	C2	8	related to bile acid ABC transport protein	0.00E+00	Transport	Transport
ZtritIPO323_04g03110	Mycgr3P76728	both	-3.85	14.42	1.01E-07	C1	11	3-dehydroquinate synthase	0.00E+00	Metabolic process	Metabolic process
ZtritIPO323_04g07579	Mycgr3P69689	24 h	3.87	14.62	1.18E-07	C2	3	haloacid dehalogenase-like hydrolase	2.72E-145	Catalytic activity	Catalytic activity
ZtritIPO323_04g04349	Mycgr3P111657	6 h	-3.74	13.36	1.84E-07	C1	13	Satratoxin biosynthesis SC1 cluster protein 4	0.00E+00	Cell wall/membrane	Cell wall
ZtritIPO323_04g07232	Mycgr3P38624	both	-3.82	14.12	2.14E-07	C1	3	short chain dehydrogenase/reductase family oxidoreductase like protein	0.00E+00	Oxidoreductase activity	Oxidoreductase activity
ZtritIPO323_04g00796	Mycgr3P98377	both	-7.21	148.06	2.62E-07	C1	1	mannose-6-phosphate isomerase like protein	0.00E+00	Metabolic process	Metabolic process
ZtritIPO323_04g00114	Mycgr3P64923	both	-2.47	5.54	3.20E-07	C1	1	putative NADP-dependent mannitol dehydrogenase	0.00E+00	Oxidoreductase activity	Oxidoreductase activity
ZtritIPO323_04g05590	Mycgr3P103030	both	-3.67	12.73	5.81E-07	C1	2	uncharacterized protein MYCGRDRAFT_103030	1.02E-20	Unknown	Unknown
ZtritIPO323_04g11551	#N/A	both	-4.37	20.68	5.92E-07	C1	7	unnamed protein product	3.35E-22	Unknown	Unknown

RRes GeneID	JGI Protein ID	DESeq2 Contrast	Log2 Fold Change	FC	FDR (adjust p-value)	Heatmap Cluster	Chr.	Top BLAST hit description	BLAST e-value	Broad functional category	Functional sub-category
ZtritIPO323_04g04086	Mycgr3P106430	both	2.81	7.01	8.48E-07	C2	12	class I glutamine amidotransferase-like protein	0.00E+00	Catalytic activity	Transferase activity
ZtritIPO323_04g06680	Mycgr3P103459	both	-2.77	6.82	1.57E-06	C1	2	peroxiredoxin like protein	2.44E-122	Stress response	Oxidative stress
ZtritIPO323_04g02303	Mycgr3P102996	24 h	-2.94	7.67	1.69E-06	C1	1	uncharacterized protein MYCGRDRAFT_102996	1.96E-104	Unknown	Unknown
ZtritIPO323_04g03984	Mycgr3P97167	24 h	4.15	17.75	1.77E-06	C2	12	lipase 3-like protein	1.38E-153	Lipid metabolic process	Lipid Metabolic process
ZtritIPO323_04g03400	Mycgr3P82659	24 h	-2.76	6.77	2.10E-06	C1	11	unnamed protein product	5.43E-95	Catalytic activity	Peptidase activity
ZtritIPO323_04g00480	Mycgr3P102136	6 h	4.44	21.71	2.47E-06	C2	1	unnamed protein product	0.00E+00	Unknown	Unknown
ZtritIPO323_04g06586	Mycgr3P103423	both	-6.18	72.5	3.17E-06	C1	2	uncharacterized protein MYCGRDRAFT_103423	1.93E-108	Unknown	Unknown
ZtritIPO323_04g11344	Mycgr3P100643	6 h	-2.86	7.26	3.84E-06	C1	7	Glutathione S-transferase 2	2.64E-167	Protein modification	Transferase activity
ZtritIPO323_04g08384	Mycgr3P103968	24 h	-2.83	7.11	5.85E-06	C1	3	hard surface induced protein	0.00E+00	Catalytic activity	Transferase activity
ZtritIPO323_04g07520	Mycgr3P108534	24 h	3.84	14.32	7.19E-06	C2	3	uncharacterized protein MYCGRDRAFT_108534	2.93E-133	Unknown	Unknown
ZtritIPO323_04g00457	Mycgr3P32802	both	3.25	9.51	7.19E-06	C2	1	related to oxidase	0.00E+00	Stress response	Cellular oxidant detoxification
ZtritIPO323_04g02831	Mycgr3P87870	both	4.76	27.1	7.19E-06	C2	10	unnamed protein product	0.00E+00	Cell signalling	Nuclear structure
ZtritIPO323_04g09797	Mycgr3P104459	24 h	2.33	5.03	7.20E-06	C2	5	acyl-CoA dehydrogenase NM domain-like protein	0.00E+00	Oxidoreductase activity	Oxidoreductase activity
ZtritIPO323_04g10603	Mycgr3P100421	both	-2.59	6.02	8.24E-06	C1	6	linoleate diol synthase	0.00E+00	Metabolic process	Metabolic process
ZtritIPO323_04g03230	Mycgr3P63646	6 h	-3.31	9.92	8.31E-06	C1	11	chaperone/heat shock protein	5.33E-52	Stress response	Stress response

RRes GeneID	JGI Protein ID	DESeq2 Contrast	Log2 Fold Change	FC	FDR (adjust p-value)	Heatmap Cluster	Chr.	Top BLAST hit description	BLAST e-value	Broad functional category	Functional sub-category
ZtritIPO323_04g12840	Mycgr3P110524	24 h	3.44	10.85	1.07E-05	C2	8	putative mitochondrial chaperone bcs1	0.00E+00	Stress response	Stress response
ZtritIPO323_04g06695	Mycgr3P103460	24 h	2.74	6.68	1.28E-05	C2	2	Protein rds1	0.00E+00	Metabolic process	Metabolic process
ZtritIPO323_04g02339	Mycgr3P95996	24 h	-9.1	548.75	1.28E-05	C1	10	uncharacterized protein MYCGRDRAFT_95996	1.80E-85	Transcription regulation	Transcription regulation
ZtritIPO323_04g10337	Mycgr3P109668	6 h	-4.15	17.75	1.34E-05	C1	5	putative 3-oxo-5-alpha-steroid 4-dehydrogenase protein	0.00E+00	Lipid metabolic process	Lipid metabolic process
ZtritIPO323_04g11623	Mycgr3P105173	both	-2.92	7.57	1.55E-05	C1	7	Zinc finger protein with KRAB and SCAN domains 5	0.00E+00	Unknown	Unknown
ZtritIPO323_04g02177	Mycgr3P67486	both	4.53	23.1	2.00E-05	C2	1	related to tRNA ligase	0.00E+00	Three or less representatives	RNA binding
ZtritIPO323_04g11589	Mycgr3P60749	both	-3.5	11.31	2.53E-05	C1	7	related to alcohol dehydrogenase	0.00E+00	Oxidoreductase activity	Oxidoreductase activity
ZtritIPO323_04g11269	Mycgr3P43593	24 h	3.06	8.34	2.81E-05	C2	6	unnamed protein product	3.13E-132	Catalytic activity	Transferase activity
ZtritIPO323_04g00770	Mycgr3P98369	both	-2.69	6.45	2.81E-05	C1	1	probable phosphoketolase	0.00E+00	Metabolic process	Metabolic process
ZtritIPO323_04g02111	Mycgr3P107708	both	-7.03	130.69	3.68E-05	C1	1	---NA---		Unknown	Unknown
ZtritIPO323_04g12731	Mycgr3P100990	both	-5.63	49.52	3.74E-05	C1	8	uncharacterized protein MYCGRDRAFT_100990	2.08E-165	Metabolic process	Metabolic process
ZtritIPO323_04g02136	Mycgr3P84263	both	-6.75	107.63	4.44E-05	C1	1	uncharacterized protein MYCGRDRAFT_84263	1.06E-18	Unknown	Unknown
ZtritIPO323_04g01223	Mycgr3P102520	both	5.4	42.22	4.47E-05	C2	1	uncharacterized protein MYCGRDRAFT_102520	0.00E+00	Transport	Transport
ZtritIPO323_04g12676	Mycgr3P46866	6 h	-2.54	5.82	4.66E-05	C1	8	related to spore coat protein SP96 precursor	0.00E+00	CWDE	CWDE
ZtritIPO323_04g13632	Mycgr3P62547	24 h	5.34	40.5	5.07E-05	C2	9	unnamed protein product	4.44E-102	Unknown	Unknown

RRes GeneID	JGI Protein ID	DESeq2 Contrast	Log2 Fold Change	FC	FDR (adjust p-value)	Heatmap Cluster	Chr.	Top BLAST hit description	BLAST e-value	Broad functional category	Functional sub-category
ZtritIPO323_04g04380	Mycgr3P97431	both	5.61	48.84	5.11E-05	C2	13	unnamed protein product	0.00E+00	Unknown	Unknown
ZtritIPO323_04g06252	Mycgr3P99166	both	-4.31	19.84	7.11E-05	C1	2	aldehyde reductase like protein	0.00E+00	Catalytic activity	Catalytic activity
ZtritIPO323_04g01464	Mycgr3P102658	24 h	-3.03	8.17	7.32E-05	C1	1	uncharacterized protein MYCGRDRAFT_102658	5.64E-74	Protein modification	Protein modification
ZtritIPO323_04g01136	Mycgr3P107242	24 h	2.41	5.31	7.97E-05	C2	1	uncharacterized protein MYCGRDRAFT_107242	4.88E-98	Cell wall/membrane	Cell wall
ZtritIPO323_04g02407	Mycgr3P105844	both	-2.69	6.45	8.00E-05	C1	10	probable aryl-alcohol dehydrogenase Aad14	0.00E+00	Oxidoreductase activity	Oxidoreductase activity
ZtritIPO323_04g10500	Mycgr3P109710	24 h	-2.99	7.94	9.27E-05	C1	6	PR-1-like protein	1.93E-136	Three or less representatives	Pathogenicity related protein
ZtritIPO323_04g08391	Mycgr3P70547	6 h	-6.48	89.26	9.36E-05	C1	3	probable fluconazole resistance protein	0.00E+00	Transport	Transport
ZtritIPO323_04g13103	Mycgr3P46257	6 h	-3.75	13.45	1.19E-04	C1	8	uncharacterized protein MYCGRDRAFT_46257	1.18E-22	Unknown	Unknown
ZtritIPO323_04g10297	Mycgr3P93498	6 h	-3.78	13.74	1.29E-04	C1	5	unnamed protein product	0.00E+00	Unknown	Unknown
ZtritIPO323_04g13305	Mycgr3P105672	24 h	-2.46	5.5	1.34E-04	C1	9	uncharacterized protein MYCGRDRAFT_105672	3.10E-79	Unknown	Unknown
ZtritIPO323_04g01715	Mycgr3P32500	6 h	-5.5	45.25	1.43E-04	C1	1	putative alpha beta-hydrolase protein	0.00E+00	Metabolic process	Metabolic process
ZtritIPO323_04g03592	#N/A	24 h	2.49	5.62	1.47E-04	C2	12	unnamed protein product	3.89E-114	Unknown	Unknown
ZtritIPO323_04g02258	Mycgr3P33514	both	-3.16	8.94	1.70E-04	C1	1	uncharacterized protein MYCGRDRAFT_33514	1.90E-47	Unknown	Unknown
ZtritIPO323_04g09061	Mycgr3P58200	6 h	2.48	5.58	1.70E-04	C2	4	putative ABC transporter	0.00E+00	Transport	Transport
ZtritIPO323_04g01318	Mycgr3P33493	6 h	-5.4	42.22	1.79E-04	C1	1	unnamed protein product	0.00E+00	Unknown	Unknown

RRes GeneID	JGI Protein ID	DESeq2 Contrast	Log2 Fold Change	FC	FDR (adjust p-value)	Heatmap Cluster	Chr.	Top BLAST hit description	BLAST e-value	Broad functional category	Functional sub-category
ZtritIPO323_04g13502	Mycgr3P47621	both	2.8	6.96	2.00E-04	C2	9	Zinc finger protein	0.00E+00	Transcription regulation	Transcription regulation
ZtritIPO323_04g12868	Mycgr3P74970	both	2.87	7.31	2.02E-04	C2	8	ABC transporter	0.00E+00	Transport	Transport
ZtritIPO323_04g04326	Mycgr3P30788	24 h	7.57	190.02	2.04E-04	C2	13	DUF1768-domain-containing protein	9.58E-131	Unknown	Unknown
ZtritIPO323_04g07871	#N/A	24 h	-3.22	9.32	2.16E-04	C1	3	GYF domain-containing protein mpd2	1.13E-104	Unknown	Unknown
ZtritIPO323_04g05497	Mycgr3P90329	24 h	3.17	9	2.91E-04	C2	2	uncharacterized protein MYCGRDRAFT_90329	0.00E+00	Proteolysis activity	Proteolysis activity
ZtritIPO323_04g09490	Mycgr3P18625	6 h	3.24	9.45	2.95E-04	C2	5	unnamed protein product	8.71E-136	Catalytic activity	Transferase activity
ZtritIPO323_04g07462	#N/A	24 h	5.58	47.84	3.00E-04	C2	3	---NA---		Unknown	Unknown
ZtritIPO323_04g10627	Mycgr3P109761	both	-4.61	24.42	3.00E-04	C1	6	uncharacterized protein MYCGRDRAFT_109761	0.00E+00	Unknown	Unknown
ZtritIPO323_04g11596	#N/A	both	7.86	232.32	3.00E-04	C2	7	---NA---		Unknown	Unknown
ZtritIPO323_04g02938	Mycgr3P27196	24 h	4.68	25.63	3.00E-04	C2	10	UMTA methyltransferase family protein	0.00E+00	Catalytic activity	Transferase activity
ZtritIPO323_04g11561	#N/A	24 h	6.07	67.18	3.16E-04	C2	7	kinase-like domain-containing protein	7.55E-131	Catalytic activity	Transferase activity
ZtritIPO323_04g05633	Mycgr3P67804	both	3.5	11.31	3.20E-04	C2	2	related to monooxigenase	0.00E+00	Metabolic process	Metabolic process
ZtritIPO323_04g10208	Mycgr3P86225	24 h	-3.19	9.13	3.29E-04	C1	5	zinc-binding alcohol dehydrogenase	0.00E+00	Oxidoreductase activity	Oxidoreductase activity
ZtritIPO323_04g01894	Mycgr3P34715	24 h	2.96	7.78	3.93E-04	C2	1	choline-sulfatase like protein	0.00E+00	DNA metabolism	Nucleic acid binding
ZtritIPO323_04g06248	Mycgr3P55428	6 h	2.67	6.36	4.73E-04	C2	2	related to NACHT domain protein	0.00E+00	Three or less representatives	Protein binding

RRes GeneID	JGI Protein ID	DESeq2 Contrast	Log2 Fold Change	FC	FDR (adjust p-value)	Heatmap Cluster	Chr.	Top BLAST hit description	BLAST e-value	Broad functional category	Functional sub-category
ZtritIPO323_04g02416	Mycgr3P49129	24 h	4.99	31.78	4.97E-04	C2	10	probable thermophilic desulfurizing enzyme family protein	0.00E+00	Oxidoreductase activity	Oxidoreductase activity
ZtritIPO323_04g13466	Mycgr3P75537	6 h	8.64	398.93	5.18E-04	C2	9	related to extracellular lipase	0.00E+00	Lipid metabolic process	Lipid metabolic process
ZtritIPO323_04g00123	Mycgr3P88664	24 h	3.75	13.45	7.69E-04	C2	1	uncharacterized protein MYCGRDRAFT_88664	9.59E-105	Three or less representatives	Protein binding
ZtritIPO323_04g02319	Mycgr3P67654	24 h	-2.17	4.5	7.77E-04	C1	1	unnamed protein product	0.00E+00	Unknown	Unknown
ZtritIPO323_04g07283	Mycgr3P103564	both	-4.38	20.82	7.80E-04	C1	3	related to stress response protein (Rds1)	0.00E+00	Stress response	Stress response
ZtritIPO323_04g05700	Mycgr3P107889	24 h	2.62	6.15	8.93E-04	C2	2	unnamed protein product	5.10E-106	Unknown	Unknown
ZtritIPO323_04g01750	Mycgr3P102792	24 h	3.03	8.17	1.10E-03	C2	1	uncharacterized protein MYCGRDRAFT_102792	2.58E-79	Unknown	Unknown
ZtritIPO323_04g00714	Mycgr3P89110	24 h	5.22	37.27	1.10E-03	C2	1	uncharacterized protein MYCGRDRAFT_89110	0.00E+00	Cell signalling	Nuclear structure
ZtritIPO323_04g08711	Mycgr3P40062	both	-2.26	4.79	1.12E-03	C1	4	shwachman-bodian-diamond syndrome protein	1.55E-62	Proteolysis activity	Proteolysis activity
ZtritIPO323_04g09483	Mycgr3P109332	24 h	2.86	7.26	1.19E-03	C2	5	uncharacterized protein MYCGRDRAFT_109332	0.00E+00	Unknown	Unknown
ZtritIPO323_04g07195	#N/A	24 h	8.41	340.14	1.26E-03	C2	3	unnamed protein product	5.16E-18	Unknown	Unknown
ZtritIPO323_04g02632	Mycgr3P76289	24 h	-3.14	8.82	1.33E-03	C1	10	MFS general substrate transporter	0.00E+00	Transport	Transport
ZtritIPO323_04g07342	Mycgr3P22994	6 h	9.33	643.59	1.44E-03	C2	3	ubiquitin-conjugating enzyme family protein	0.00E+00	Protein modification	Protein modification
ZtritIPO323_04g00729	Mycgr3P17477	6 h	8.42	342.51	1.44E-03	C2	1	unnamed protein product	0.00E+00	Transcription regulation	Hydrolase activity

RRes GeneID	JGI Protein ID	DESeq2 Contrast	Log2 Fold Change	FC	FDR (adjust p-value)	Heatmap Cluster	Chr.	Top BLAST hit description	BLAST e-value	Broad functional category	Functional sub-category
ZtritIPO323_04g00700	Mycgr3P102228	24 h	-2.04	4.11	1.48E-03	C1	1	4-amino-5-hydroxymethyl-2-methylpyrimidine phosphate synthase	2.58E-115	Metabolic process	Metabolic process
ZtritIPO323_04g13116	Mycgr3P110633	24 h	3.37	10.34	1.48E-03	C2	8	uncharacterized protein MYCGRDRAFT_110633	0.00E+00	Unknown	Unknown
ZtritIPO323_04g00208	Mycgr3P28684	6 h	-4.27	19.29	1.48E-03	C1	1	unnamed protein product	0.00E+00	DNA metabolism	DNA binding
ZtritIPO323_04g00819	Mycgr3P102276	both	-2.72	6.59	1.51E-03	C1	1	nadp-dependent alcohol dehydrogenase like protein	0.00E+00	Oxidoreductase activity	Oxidoreductase activity
ZtritIPO323_04g02517	Mycgr3P105887	24 h	-2.43	5.39	1.51E-03	C1	10	glutathione-s-transferase like protein	5.44E-167	Protein modification	Transferase activity
ZtritIPO323_04g10587	#N/A	24 h	-3.69	12.91	1.52E-03	C1	6	unnamed protein product	2.50E-35	Unknown	Unknown
ZtritIPO323_04g05555	#N/A	both	4.52	22.94	1.55E-03	C2	2	hypothetical protein TI39_contig5865g00012, partial	1.46E-09	Unknown	Unknown
ZtritIPO323_04g12312	Mycgr3P74334	6 h	-3.85	14.42	1.55E-03	C1	8	CYP-42 P450 monooxygenase	0.00E+00	Oxidoreductase activity	Oxidoreductase activity
ZtritIPO323_04g13080	Mycgr3P105604	24 h	-3.65	12.55	1.62E-03	C1	8	uncharacterized protein MYCGRDRAFT_105604	3.90E-44	Unknown	Unknown
ZtritIPO323_04g01836	Mycgr3P107598	24 h	2.4	5.28	1.75E-03	C2	1	Zinc finger transcription factor ace1	0.00E+00	Transcription regulation	Transcription regulation
ZtritIPO323_04g07223	Mycgr3P39691	6 h	-8.04	263.2	1.75E-03	C1	3	uncharacterized protein MYCGRDRAFT_39691	2.43E-64	Unknown	Unknown
ZtritIPO323_04g08936	Mycgr3P109129	24 h	-3.48	11.16	1.79E-03	C1	4	uncharacterized protein MYCGRDRAFT_109129	6.70E-115	Cell wall/membrane	Membrane component
ZtritIPO323_04g08156	Mycgr3P85387	both	-2.51	5.7	1.79E-03	C1	3	CAT1 catalase	0.00E+00	Stress response	Oxidative stress
ZtritIPO323_04g09063	Mycgr3P58203	6 h	3.37	10.34	2.10E-03	C2	4	related to hxB protein	0.00E+00	Metabolic process	Metabolic process

RRes GeneID	JGI Protein ID	DESeq2 Contrast	Log2 Fold Change	FC	FDR (adjust p-value)	Heatmap Cluster	Chr.	Top BLAST hit description	BLAST e-value	Broad functional category	Functional sub-category
ZtritIPO323_04g03785	#N/A	6 h	5.44	43.41	2.17E-03	C2	12	unnamed protein product	3.06E-21	Unknown	Unknown
ZtritIPO323_04g00059	Mycgr3P14095	6 h	2.94	7.67	2.80E-03	C2	1	proline oxidase PrnD like protein	0.00E+00	Oxidoreductase activity	Oxidoreductase activity
ZtritIPO323_04g08996	Mycgr3P39898	6 h	-2.96	7.78	2.87E-03	C1	4	related to channel proteins	0.00E+00	Transport	Transport
ZtritIPO323_04g01183	Mycgr3P102499	24 h	-2.26	4.79	2.88E-03	C1	1	monomeric glyoxalase I	0.00E+00	Metabolic process	Metabolic process
ZtritIPO323_04g03452	Mycgr3P96782	6 h	9.6	776.05	2.91E-03	C2	11	unnamed protein product	2.36E-145	Proteolysis activity	Proteolysis activity
ZtritIPO323_04g09440	Mycgr3P92924	both	3.9	14.93	3.03E-03	C2	4	uncharacterized protein MYCGRDRAFT_92924	7.15E-153	Unknown	Unknown
ZtritIPO323_04g01594	Mycgr3P107473	both	-2.83	7.11	3.14E-03	C1	1	oxidoreductase like protein	1.15E-171	Oxidoreductase activity	Oxidoreductase activity
ZtritIPO323_04g09472	Mycgr3P41969	24 h	3.37	10.34	3.14E-03	C2	5	uncharacterized protein MYCGRDRAFT_41969	0.00E+00	Lipid metabolic process	Lipid metabolic process
ZtritIPO323_04g06403	Mycgr3P35394	6 h	-4.75	26.91	3.66E-03	C1	2	related to UPF0659 protein C216.03	1.13E-175	Metabolic process	Metabolic process
ZtritIPO323_04g00098	Mycgr3P34808	24 h	2.79	6.92	3.92E-03	C2	1	FMNH(2)-dependent dimethylsulfone monooxygenase	0.00E+00	Oxidoreductase activity	Oxidoreductase activity
ZtritIPO323_04g03802	Mycgr3P111470	6 h	4.44	21.71	3.97E-03	C2	12	mediator of RNA polymerase II transcription subunit 18 like protein	8.64E-160	Transcription regulation	Transcription regulation
ZtritIPO323_04g09401	#N/A	24 h	-4.1	17.15	4.34E-03	C1	4	unnamed protein product	2.15E-156	Unknown	Actin binding?
ZtritIPO323_04g11895	Mycgr3P110270	both	-3.04	8.22	4.71E-03	C1	7	related to multidrug resistant protein	0.00E+00	Transport	Transport
ZtritIPO323_04g00655	Mycgr3P14647	24 h	3.12	8.69	4.87E-03	C2	1	unnamed protein product	0.00E+00	Three or less representatives	Cell cycle

RRes GeneID	JGI Protein ID	DESeq2 Contrast	Log2 Fold Change	FC	FDR (adjust p-value)	Heatmap Cluster	Chr.	Top BLAST hit description	BLAST e-value	Broad functional category	Functional sub-category
ZtritIPO323_04g04088	Mycgr3P97233	24 h	2.75	6.73	5.44E-03	C2	12	putative oxidoreductase yanE	1.70E-167	Oxidoreductase activity	Oxidoreductase activity
ZtritIPO323_04g08359	Mycgr3P38880	both	-2.38	5.21	5.62E-03	C1	3	putative cell agglutination protein	0.00E+00	Three or less representatives	Ribosome associated
ZtritIPO323_04g04239	Mycgr3P97328	24 h	3.25	9.51	6.73E-03	C2	13	related to DEAD/DEAH box RNA helicase	0.00E+00	DNA metabolism	Nucleic acid binding
ZtritIPO323_04g03152	Mycgr3P49735	6 h	-4.47	22.16	7.04E-03	C1	11	putative P450 monooxygenase	0.00E+00	Oxidoreductase activity	Oxidoreductase activity
ZtritIPO323_04g01335	#N/A	6 h	-2.67	6.36	7.79E-03	C1	1	hypothetical protein TI39_contig481g00021	4.90E-116	Three or less representatives	Secondary metabolism
ZtritIPO323_04g11408	Mycgr3P100666	6 h	4.61	24.42	8.02E-03	C2	7	unnamed protein product	0.00E+00	Unknown	Unknown
ZtritIPO323_04g08522	Mycgr3P70646	both	-2.92	7.57	8.27E-03	C1	4	glutamate decarboxylase	0.00E+00	Catalytic activity	Lyase activity
ZtritIPO323_04g01859	#N/A	24 h	3.16	8.94	8.37E-03	C2	1	---NA---		Unknown	Unknown
ZtritIPO323_04g11679	Mycgr3P73993	both	-2.21	4.63	8.37E-03	C1	7	probable catechol O-methyltransferase	0.00E+00	Catalytic activity	Transferase activity
ZtritIPO323_04g00311	Mycgr3P35016	6 h	8.01	257.78	8.40E-03	C2	1	alpha/beta-hydrolase like protein	8.73E-179	Metabolic process	Metabolic process
ZtritIPO323_04g11240	Mycgr3P94167	6 h	3.93	15.24	8.41E-03	C2	6	unnamed protein product	0.00E+00	Catalytic activity	Transferase activity
ZtritIPO323_04g11632	Mycgr3P105182	6 h	-2.71	6.54	8.64E-03	C1	7	extracellular protein 20-2	2.63E-92	Unknown	Unknown
ZtritIPO323_04g13289	Mycgr3P75353	6 h	2.84	7.16	8.79E-03	C2	9	kinase-like protein	0.00E+00	Three or less representatives	Kinase activity
ZtritIPO323_04g01182	Mycgr3P89478	24 h	-2.24	4.72	9.17E-03	C1	1	short-chain dehydrogenase like protein	4.04E-133	Oxidoreductase activity	Oxidoreductase activity
ZtritIPO323_04g01444	Mycgr3P35346	6 h	6.32	79.89	9.21E-03	C2	1	uncharacterized protein MYCGRDRAFT_35346	0.00E+00	Unknown	Unknown

RRes GeneID	JGI Protein ID	DESeq2 Contrast	Log2 Fold Change	FC	FDR (adjust p-value)	Heatmap Cluster	Chr.	Top BLAST hit description	BLAST e-value	Broad functional category	Functional sub-category
ZtritIPO323_04g08957	Mycgr3P92595	24 h	-4.36	20.53	9.30E-03	C1	4	uncharacterized protein MYCGRDRAFT_92595	0.00E+00	Three or less representatives	Lipid binding
ZtritIPO323_04g01463	Mycgr3P102657	both	-3.51	11.39	9.30E-03	C1	1	uncharacterized protein MYCGRDRAFT_102657	1.36E-106	Unknown	Unknown
ZtritIPO323_04g08185	Mycgr3P70343	24 h	2.13	4.38	9.46E-03	C2	3	putative P450 monooxygenase	0.00E+00	Oxidoreductase activity	Oxidoreductase activity
ZtritIPO323_04g13370	Mycgr3P95637	both	-2.93	7.62	9.67E-03	C1	9	3-ketoacyl-ACP reductase like protein	0.00E+00	Oxidoreductase activity	Oxidoreductase activity
ZtritIPO323_04g13203	Mycgr3P75286	24 h	-3.02	8.11	9.69E-03	C1	9	uncharacterized protein MYCGRDRAFT_75286	0.00E+00	Oxidoreductase activity	Oxidoreductase activity
ZtritIPO323_04g03638	Mycgr3P50425	24 h	-4.43	21.56	9.69E-03	C1	12	related to tropinone reductase	0.00E+00	Oxidoreductase activity	Oxidoreductase activity
ZtritIPO323_04g05630	Mycgr3P11143	24 h	3.07	8.4	9.69E-03	C2	2	unnamed protein product	0.00E+00	Proteolysis activity	Proteolysis activity
ZtritIPO323_04g07281	#N/A	6 h	-7.13	140.07	1.10E-02	C1	3	---NA---		Unknown	Unknown
ZtritIPO323_04g09809	Mycgr3P109455	6 h	-3.72	13.18	1.10E-02	C1	5	alpha/beta-hydrolase like protein	0.00E+00	Metabolic process	Metabolic process
ZtritIPO323_04g09215	#N/A	24 h	6.82	112.99	1.11E-02	C2	4	DNA-binding protein HEXBP	0.00E+00	Unknown	Unknown
ZtritIPO323_04g04099	Mycgr3P82936	6 h	2.51	5.7	1.15E-02	C2	12	unnamed protein product	7.32E-104	Metabolic process	Metabolic process
ZtritIPO323_04g00687	#N/A	24 h	-2.27	4.82	1.18E-02	C1	1	Baeyer-Villiger monooxygenase	0.00E+00	Unknown	Unknown
ZtritIPO323_04g12729	#N/A	6 h	7.03	130.69	1.18E-02	C2	8	Vascular endothelial zinc finger 1	3.77E-29	Transcription regulation	Transcription regulation
ZtritIPO323_04g10687	Mycgr3P44206	24 h	-2.76	6.77	1.18E-02	C1	6	unnamed protein product	1.24E-58	Catalytic activity	Catalytic activity
ZtritIPO323_04g03325	Mycgr3P101603	6 h	-5.51	45.57	1.20E-02	C1	11	uncharacterized protein MYCGRDRAFT_101603	0.00E+00	Transport	Transport

RRes GeneID	JGI Protein ID	DESeq2 Contrast	Log2 Fold Change	FC	FDR (adjust p-value)	Heatmap Cluster	Chr.	Top BLAST hit description	BLAST e-value	Broad functional category	Functional sub-category
ZtritIPO323_04g07619	#N/A	24 h	-4.97	31.34	1.22E-02	C1	3	unnamed protein product	8.09E-20	Three or less representatives	Actin binding
ZtritIPO323_04g09072	#N/A	24 h	2.33	5.03	1.22E-02	C2	4	unnamed protein product	1.16E-89	Unknown	Unknown
ZtritIPO323_04g00181	Mycgr3P106779	6 h	-2.57	5.94	1.27E-02	C1	1	putative Exo-beta-1,3-glucanase	0.00E+00	CWDE	CWDE
ZtritIPO323_04g02688	Mycgr3P111056	6 h	3.22	9.32	1.27E-02	C2	10	ATP-dependent DNA helicase PIF1	0.00E+00	DNA metabolism	DNA repair
ZtritIPO323_04g04503	Mycgr3P51562	24 h	-2.84	7.16	1.31E-02	C1	13	MFS general substrate transporter	0.00E+00	Transport	Transport
ZtritIPO323_04g02469	Mycgr3P76101	6 h	7.48	178.53	1.42E-02	C2	10	short chain dehydrogenase/ reductase like protein	0.00E+00	Oxidoreductase activity	Oxidoreductase activity
ZtritIPO323_04g00308	Mycgr3P52069	24 h	3	8	1.46E-02	C2	1	related to lipase 1	0.00E+00	Lipid metabolic process	Lipid metabolic process
ZtritIPO323_04g03684	Mycgr3P77261	both	-2.86	7.26	1.46E-02	C1	12	polyamine transporter protein	0.00E+00	Transport	Transport
ZtritIPO323_04g10092	Mycgr3P93368	6 h	6.81	112.21	1.52E-02	C2	5	peptidase S8/S53 domain-containing protein	0.00E+00	Proteolysis activity	Proteolysis activity
ZtritIPO323_04g08808	Mycgr3P57881	both	-3.56	11.79	1.65E-02	C1	4	S-(hydroxymethyl)glutathione dehydrogenase/alcohol dehydrogenase like protein	0.00E+00	Oxidoreductase activity	Oxidoreductase activity
ZtritIPO323_04g03111	Mycgr3P106091	6 h	-2.72	6.59	1.68E-02	C1	11	unnamed protein product	0.00E+00	Three or less representatives	ATP binding
ZtritIPO323_04g10724	Mycgr3P109795	24 h	2.98	7.89	1.73E-02	C2	6	uncharacterized protein MYCGRDRAFT_109795	0.00E+00	Lipid metabolic process	Lipid metabolic process
ZtritIPO323_04g00071	Mycgr3P64902	24 h	-3.56	11.79	1.74E-02	C1	1	uncharacterized protein MYCGRDRAFT_64902	0.00E+00	Metabolic process	Metabolic process
ZtritIPO323_04g12774	Mycgr3P61690	both	-2.91	7.52	1.74E-02	C1	8	methyltransferase domain-containing protein	0.00E+00	Metabolic process	Metabolic process
ZtritIPO323_04g09454	Mycgr3P71676	both	2.1	4.29	1.74E-02	C2	5	uncharacterized protein MYCGRDRAFT_71676	0.00E+00	Catalytic activity	Catalytic activity

RRes GeneID	JGI Protein ID	DESeq2 Contrast	Log2 Fold Change	FC	FDR (adjust p-value)	Heatmap Cluster	Chr.	Top BLAST hit description	BLAST e-value	Broad functional category	Functional sub-category
ZtritIPO323_04g03039	Mycgr3P76652	24 h	-4.26	19.16	1.76E-02	C1	11	FMN-dependent alpha-hydroxy acid dehydrogenase	0.00E+00	Oxidoreductase activity	Oxidoreductase activity
ZtritIPO323_04g11630	#N/A	both	-2.35	5.1	1.77E-02	C1	7	Dimeric alpha+beta barrel like protein	5.48E-74	Metabolic process	Metabolic process
ZtritIPO323_04g01372	Mycgr3P78728	6 h	-2.37	5.17	1.88E-02	C1	1	UPF0057-domain-containing protein	1.97E-13	Stress response	Stress response
ZtritIPO323_04g04241	Mycgr3P97330	24 h	4.75	26.91	1.90E-02	C2	13	related to Y.lipolytica GPR1 protein and Fun34p	0.00E+00	Transport	Transport
ZtritIPO323_04g11560	Mycgr3P44640	24 h	2.46	5.5	1.95E-02	C2	7	putative P450 monooxygenase	0.00E+00	Oxidoreductase activity	Oxidoreductase activity
ZtritIPO323_04g12558	#N/A	6 h	6.91	120.26	1.99E-02	C2	8	unnamed protein product	1.44E-40	Unknown	Unknown
ZtritIPO323_04g01180	Mycgr3P89476	6 h	-4.45	21.86	1.99E-02	C1	1	uncharacterized protein MYCGRDRAFT_89476	0.00E+00	Cell signalling	Cytoskeleton?
ZtritIPO323_04g12862	Mycgr3P101035	6 h	-2.5	5.66	2.05E-02	C1	8	related to glyoxal oxidase precursor	0.00E+00	Unknown	Unknown
ZtritIPO323_04g01892	Mycgr3P90001	24 h	2.07	4.2	2.06E-02	C2	1	covalently-linked cell wall protein	1.09E-172	Cell wall/membrane	Cell wall
ZtritIPO323_04g08708	Mycgr3P39970	both	-2.35	5.1	2.07E-02	C1	4	unnamed protein product	2.55E-104	Unknown	Unknown
ZtritIPO323_04g06038	Mycgr3P68282	24 h	3.9	14.93	2.14E-02	C2	2	(R,R)-butanediol dehydrogenase	0.00E+00	Three or less representatives	Secondary metabolism
ZtritIPO323_04g02648	Mycgr3P48706	24 h	-2.59	6.02	2.30E-02	C1	10	related to phospholipase D	0.00E+00	Lipid metabolic process	Metabolic process
ZtritIPO323_04g11225	#N/A	both	-2.7	6.5	2.31E-02	C1	6	unnamed protein product	3.74E-162	Unknown	Unknown
ZtritIPO323_04g10608	Mycgr3P29873	24 h	-2.43	5.39	2.59E-02	C1	6	putative precursor lipase	0.00E+00	Lipid metabolic process	Lipid metabolic process
ZtritIPO323_04g10055	Mycgr3P59219	both	-2.46	5.5	2.63E-02	C1	5	gamma-carboxymuconolactone decarboxylase like protein	0.00E+00	Metabolic process	Metabolic process

RRes GeneID	JGI Protein ID	DESeq2 Contrast	Log2 Fold Change	FC	FDR (adjust p-value)	Heatmap Cluster	Chr.	Top BLAST hit description	BLAST e-value	Broad functional category	Functional sub-category
ZtritIPO323_04g02641	#N/A	6 h	6.95	123.64	2.64E-02	C2	10	unnamed protein product	1.68E-96	Unknown	Unknown
ZtritIPO323_04g04039	Mycgr3P50597	6 h	2.26	4.79	2.68E-02	C2	12	uncharacterized protein MYCGRDRAFT_50597	0.00E+00	Catalytic activity	Transferase activity
ZtritIPO323_04g00432	Mycgr3P88895	6 h	-2.67	6.36	2.70E-02	C1	1	uncharacterized protein MYCGRDRAFT_88895	2.67E-101	Unknown	Unknown?
ZtritIPO323_04g02493	Mycgr3P76119	24 h	-3.55	11.71	2.77E-02	C1	10	DUF1264-domain-containing protein	1.98E-165	Three or less representatives	Protein binding
ZtritIPO323_04g11562	Mycgr3P94391	24 h	4.19	18.25	3.13E-02	C2	7	unnamed protein product	1.64E-168	Proteolysis activity	Proteolysis activity
ZtritIPO323_04g13407	Mycgr3P87461	6 h	2.66	6.32	3.15E-02	C2	9	sh3 domain-containing protein	0.00E+00	Cell wall/membrane	Membrane component
ZtritIPO323_04g13266	Mycgr3P83225	6 h	7.17	144.01	3.15E-02	C2	9	---NA---		Unknown	Unknown
ZtritIPO323_04g12252	Mycgr3P45128	6 h	2.93	7.62	3.16E-02	C2	7	Membrane-associated proteins in eicosanoid and glutathione metabolism	2.13E-103	Metabolic process	Metabolic process
ZtritIPO323_04g07152	Mycgr3P108392	6 h	6.3	78.79	3.39E-02	C2	3	uncharacterized protein MYCGRDRAFT_108392	0.00E+00	Oxidoreductase activity	Oxidoreductase activity
ZtritIPO323_04g13249	Mycgr3P26564	6 h	-2.66	6.32	3.45E-02	C1	9	unnamed protein product	0.00E+00	Unknown	Unknown
ZtritIPO323_04g08442	Mycgr3P99766	6 h	2.37	5.17	3.49E-02	C2	4	MFS1 putative major facilitator superfamily transporter	0.00E+00	Transport	Transport
ZtritIPO323_04g03663	#N/A	24 h	3.19	9.13	3.60E-02	C2	12	DNA recombination/repair protein Rad52	0.00E+00	DNA metabolism	DNA repair
ZtritIPO323_04g08516	#N/A	both	-2.47	5.54	3.60E-02	C1	4	hypothetical protein TI39_contig4216g00004	4.39E-64	Unknown	Unknown
ZtritIPO323_04g04373	Mycgr3P101885	24 h	-2.17	4.5	3.72E-02	C1	13	putative P450 monooxygenase	0.00E+00	Oxidoreductase activity	Oxidoreductase activity
ZtritIPO323_04g04405	Mycgr3P97449	6 h	4.33	20.11	3.80E-02	C2	13	uncharacterized protein MYCGRDRAFT_97449	4.19E-60	Unknown	Unknown

RRes GeneID	JGI Protein ID	DESeq2 Contrast	Log2 Fold Change	FC	FDR (adjust p-value)	Heatmap Cluster	Chr.	Top BLAST hit description	BLAST e-value	Broad functional category	Functional sub-category
ZtritIPO323_04g11226	Mycgr3P110020	24 h	-2.25	4.76	3.88E-02	C1	6	unnamed protein product	0.00E+00	Cell wall/membrane	Membrane component
ZtritIPO323_04g03151	Mycgr3P96571	24 h	4.31	19.84	3.97E-02	C2	11	uncharacterized protein MYCGRDRAFT_96571	9.75E-92	Unknown	Unknown
ZtritIPO323_04g11557	#N/A	24 h	4.16	17.88	3.98E-02	C2	7	unnamed protein product	1.19E-115	Unknown	Unknown
ZtritIPO323_04g03676	Mycgr3P82765	6 h	6.79	110.66	3.98E-02	C2	12	uncharacterized protein MYCGRDRAFT_82765, partial	0.00E+00	Oxidoreductase activity	Oxidoreductase activity
ZtritIPO323_04g08184	Mycgr3P108814	6 h	2.75	6.73	4.02E-02	C2	3	2,4-dienoyl-CoA reductase like protein	0.00E+00	Oxidoreductase activity	Oxidoreductase activity
ZtritIPO323_04g00863	Mycgr3P65793	24 h	-2.69	6.45	4.11E-02	C1	1	UPF0261 protein	0.00E+00	Unknown	Unknown
ZtritIPO323_04g03079	Mycgr3P87954	24 h	4.11	17.27	4.11E-02	C2	11	uncharacterized protein MYCGRDRAFT_87954	0.00E+00	Oxidoreductase activity	Oxidoreductase activity
ZtritIPO323_04g02810	Mycgr3P101477	24 h	1.87	3.66	4.11E-02	C2	10	MFS general substrate transporter	0.00E+00	Transport	Transport
ZtritIPO323_04g09988	Mycgr3P72253	24 h	4.73	26.54	4.18E-02	C2	5	methyltransferase type 11	4.03E-171	Catalytic activity	Transferase activity
ZtritIPO323_04g07726	Mycgr3P103731	24 h	1.99	3.97	4.33E-02	C2	3	unnamed protein product	0.00E+00	Three or less representatives	Ribosome associated
ZtritIPO323_04g08304	Mycgr3P70454	6 h	-4.39	20.97	4.37E-02	C1	3	histidine acid phosphatase like protein	0.00E+00	Metabolic process	Metabolic process
ZtritIPO323_04g10685	Mycgr3P72918	24 h	3.53	11.55	4.40E-02	C2	6	alternative oxidase like protein	0.00E+00	Oxidoreductase activity	Oxidoreductase activity
ZtritIPO323_04g03830	Mycgr3P14586	6 h	-2.68	6.41	4.52E-02	C1	12	tat pathway signal sequence like protein	0.00E+00	Lipid metabolic process	Lipid metabolic process
ZtritIPO323_04g11159	Mycgr3P94107	6 h	6.76	108.38	4.61E-02	C2	6	uncharacterized protein MYCGRDRAFT_94107	1.84E-76	Unknown	Unknown
ZtritIPO323_04g10309	Mycgr3P104658	24 h	2.08	4.23	4.68E-02	C2	5	putative glucan 1,3-beta-glucosidase	0.00E+00	CWDE	Hydrolase activity

RRes GeneID	JGI Protein ID	DESeq2 Contrast	Log2 Fold Change	FC	FDR (adjust p-value)	Heatmap Cluster	Chr.	Top BLAST hit description	BLAST e-value	Broad functional category	Functional sub-category
ZtritIPO323_04g10341	Mycgr3P28946	24 h	-2.76	6.77	4.70E-02	C1	5	Condensin complex subunit 1	5.49E-136	Unknown	Unknown
ZtritIPO323_04g06356	#N/A	24 h	9.1	548.75	4.70E-02	C2	2	unnamed protein product	1.16E-69	Unknown	Unknown
ZtritIPO323_04g11352	Mycgr3P100647	24 h	-2.05	4.14	4.70E-02	C1	7	glycoside hydrolase family 17 protein	0.00E+00	CWDE	Hydrolase activity
ZtritIPO323_04g09768	Mycgr3P109435	24 h	-2.41	5.31	4.71E-02	C1	5	proteoglycan-like protein	0.00E+00	Unknown	Unknown
ZtritIPO323_04g07618	#N/A	24 h	2.44	5.43	4.84E-02	C2	3	unnamed protein product	0.00E+00	Unknown	Unknown
ZtritIPO323_04g00397	Mycgr3P35302	6 h	-2.04	4.11	4.84E-02	C1	1	Histidine protein kinase NIK1	0.00E+00	Cell signalling	Signal transduction
ZtritIPO323_04g13232	Mycgr3P95537	6 h	-6.17	72	4.90E-02	C1	9	uncharacterized protein MYCGRDRAFT_95537	2.89E-110	Unknown	Unknown
ZtritIPO323_04g07546	Mycgr3P91583	24 h	3.25	9.51	4.93E-02	C2	3	uncharacterized protein MYCGRDRAFT_91583	2.32E-72	Unknown	Unknown
ZtritIPO323_04g11040	Mycgr3P73347	6 h	2.47	5.54	4.93E-02	C2	6	related to peroxisomal amine oxidase (copper-containing)	0.00E+00	Metabolic process	Metabolic process
ZtritIPO323_04g12781	Mycgr3P74861	24 h	-2.42	5.35	4.95E-02	C1	8	uncharacterized protein MYCGRDRAFT_74861	0.00E+00	Unknown	Unknown
ZtritIPO323_04g06454	Mycgr3P68784	both	2.06	4.17	4.95E-02	C2	2	eukaryotic translation initiation factor 6	1.74E-180	Three or less representatives	Ribosome associated
ZtritIPO323_04g02338	Mycgr3P95995	24 h	-4.94	30.7	4.95E-02	C1	10	uncharacterized protein MYCGRDRAFT_95995	6.53E-96	Transcription regulation	Transcription regulation
ZtritIPO323_04g13735	Mycgr3P110861	24 h	-1.79	3.46	4.98E-02	C1	9	putative G protein-coupled receptor	0.00E+00	Transport	Transport
ZtritIPO323_04g03109	Mycgr3P49555	24 h	-2.5	5.66	4.99E-02	C1	11	related to nonribosomal peptide synthetase MxcG	0.00E+00	Three or less representatives	Amide binding
ZtritIPO323_04g08743	#N/A	6 h	6.77	109.14	4.99E-02	C2	4	unnamed protein product	1.68E-69	Unknown	Unknown

RRes GeneID	JGI Protein ID	DESeq2 Contrast	Log2 Fold Change	FC	FDR (adjust p-value)	Heatmap Cluster	Chr.	Top BLAST hit description	BLAST e-value	Broad functional category	Functional sub-category
ZtritIPO323_04g09300	Mycgr3P109293	6 h	-1.87	3.66	4.99E-02	C1	4	alpha/beta hydrolase fold family protein	0.00E+00	Metabolic process	Metabolic process
ZtritIPO323_04g12647	Mycgr3P110435	6 h	3	8	4.99E-02	C2	8	putative acylamino-acid-releasing enzyme	0.00E+00	Proteolysis activity	Proteolysis activity

C1: cluster 1 (down regulated in mutant compared to wild type), C2: cluster 2 (up regulated in mutant compared to wild type)

Table A6.3 Number of differentially expressed genes present in the functional categories in this study.

Functional Category	DE genes Cluster 1 (Upregulated in IPO323)	DE genes Cluster 2 (Upregulated in 4-124)
Catalytic activity	8	11
Cell signalling	4	2
Cell wall/membrane	4	3
CWDE	4	1
Lipid metabolic process	4	6
Metabolic process	18	7
Oxidoreductase activity	18	13
Protein modification	4	2
Proteolysis activity	1	6
Stress response	7	2
Three or less representatives	9	10
Transcription regulation	3	7
Transport	8	8
Unknown	42	35